SHALLOW SHEAR WAVE VELOCITY MODEL FOR THE KUMAON AND GARHWAL HIMALAYAS

Ph. D. THESIS

by

PARUL

DEPARTMENT OF EARTH SCIENCES
INDIAN INSTITUTE OF TECHNOLOGY ROORKEE
ROORKEE-247 667 (INDIA)
MAY, 2018

SHALLOW SHEAR WAVE VELOCITY MODEL FOR THE KUMAON AND GARHWAL HIMALAYAS

A THESIS

Submitted in partial fulfilment of the requirements for the award of the degree

of

DOCTOR OF PHILOSOPHY

in

Earth Sciences

by

PARUL

DEPARTMENT OF EARTH SCIENCES
INDIAN INSTITUTE OF TECHNOLOGY ROORKEE
ROORKEE-247 667 (INDIA)
MAY, 2018

INDIAN INSTITUE OF TECHNOLGY ROORKEE
ROORKEE

CANDIDATE'S DECLARATION

I hereby certify that the work, which is being presented in this thesis entitled **"SHALLOW SHEAR WAVE VELOCITY MODEL FOR THE KUMAON AND GARHWAL HIMALAYAS"** in partial fulfilment of the requirements for the award of the Degree of Doctor of Philosophy and submitted in the Department of Earth Sciences of the Indian Institute of Technology Roorkee, Roorkee is an authentic record of my own work carried out during a period from December, 2010 to May, 2018 under the supervision of Dr. Anand Joshi, Professor, Department of Earth Sciences, Indian Institute of Technology Roorkee, Roorkee and Mr. S.K. Das, Ex. Executive Director, ONGC (22, Nilgiri Apartments, Alaknanda, New Delhi-110019).

The matter presented in the thesis has not been submitted by me for the award of any other degree of this or any other Institute.

(PARUL)

This is to certify that the above statement made by the candidate is correct to the best of our knowledge.

(Anand Joshi) (S.K. Das)
Supervisor Supervisor

The Ph.D. Viva-Voce Examination of **Parul**, Research Scholar, has been held on September ,2018.

Chairman, SRC Signature of External Examiner

This is to certify that the student has made all the corrections in the thesis.

Signature of Supervisor (s) Head of the Department

Dated: September ,2018

ABSTRACT

The region of Kumaon and Garhwal Himalayas that has been used for the present research work falls in central Himalayan seismic gap. Despite of high seismicity in the Himalayas, the quantitative study of the amplification of seismic waves is still lacking. Limited database available in the rough and inaccessible terrain of Kumaon and Garhwal region have resulted in limited research work related to the estimation of site amplification. The work presented in the thesis includes several locations in Kumaon and Garhwal Himalayas.

In the present analysis, the site amplification functions have been estimated for Kumaon and Garhwal Himalayas using earthquakes and ambient noise data recorded locally at 27 sites from Kumaon and Garhwal region. Various methods have been applied on the records to generate shallow shear wave velocity models in Kumaon and Garhwal Himalayas. Later, the results derived from various methods are compared. No such in-depth study has been done in India yet, primarily because data acquisition in the terrains of Kumaon and Garhwal Himalayas is very tough. Following are the sections and methods used in the present research work:

Multi- channel Surface Wave Analysis (MASW): The data has been acquired at nine fields of the Kumaon and Garhwal Himalayas. The data acquisition, processing and interpretation of recorded data in the Kumaon and Garhwal Himalaya using MASW have been discussed in detail in the research. The final outcomes of the method are 2D shear wave velocity profiles (V_{S30}) and the approximate bedrock thickness 30 m beneath the surface. Geology of the stations considered in the present work has been correlated with the results obtained.

Later in this study, the records are analyzed using three different methods: (a) Non-Reference site method : the horizontal to vertical (H/V) spectral ratio on ambient noise records, (b) Non- Reference site method : the horizontal to vertical (H/V) spectral ratio on strong ground motion records, and (c) Reference site dependent method : Standard Spectral ratio,

Non- Reference site method: the horizontal to vertical (H/V) spectral ratio on ambient noise records (Nakamura's Technique): The data has been regularly recorded and collected every year. The present study is done using the data from twenty seven locations of the Kumaon and Garhwal Himalayas. The recorded data at 27 stations has been processed for the research purpose i.e. ambient noise. Whenever the density of the data is more, best twenty records are selected considering good data quality at each station. The amplification functions

i.e. predominant frequency of various sites and amplification levels are estimated using Horizontal to Vertical Spectral Ratio (HVSR) technique. The inversion of shear wave velocity model using global optimization technique was carried out. The shear wave velocity models up to 500 m have been estimated using ambient noise records. These shear wave velocity models after many genetic algorithm (GA) runs at individual stations can be used for seismic hazard studies in the area.

Non- Reference site method: the horizontal to vertical (H/V) spectral ratio on strong ground motion records: Total 248 strong ground motion records at 22 stations has been processed for the research purpose. The shear wave velocity models up to 500 m have been estimated using strong ground motion records. The amplification functions i.e. predominant frequency of various sites and amplification levels are estimated using HVSR technique. The comparison between ambient noise data and strong ground motion data has been done. The inversion of shear wave velocity model using global optimization technique was carried out. The shear wave velocity models up to 500 m have been estimated using strong ground motion records and then compared with ambient noise records.

The two dimensional shear wave velocity profiles at nineteen stations of Kumaon Himalaya and eight stations of Garhwal Himalaya respectively are generated after inverting H/V curves using genetic algorithm for both ambient noise records as well as strong ground motion records. Shear wave velocity of Kumaon and Garhwal Himalayas i.e. V_{S500} varies from 462 ms^{-1} to 1348 ms^{-1} and V_{s500} vary from 557 ms^{-1} to 1651 ms^{-1} respectively. These velocity values can be employed in various studies related to seismic hazard of the region. Velocity information is also important for simulation of earthquake strong ground motions.

Reference site dependent method: Standard Spectral ratio (SSR): Such analysis has been carried out for total ten stations using strong ground motion data. Sediment to bedrock spectral ratio estimates between pairs of stations are compared with the ratio obtained using non- reference site estimate i.e. horizontal to vertical component spectral ratio of strong ground motion records and ambient noise.

The site amplification factor for the region varies between 0.23 and 7.91 using HVSR (strong ground motion records) and between 0.3 and 6.01 using HVSR (ambient noise records). The estimated predominant frequency using ambient noise records and using strong ground motion data are found to be varying from 8.7 Hz to 11.6 Hz and from 9.8 Hz to 14.5 Hz, respectively.

ACKNOWLEDGEMENTS

I feel deeply indebted to Ph.D. supervisor **Dr. Anand Joshi,** Professor, Department of Earth Sciences, and would like to express my sincere gratitude for the guidance and the support; he has given me during this research work and throughout my stay at the institute. Apart from the technical inputs, I would also like to thank him for the motivation and encouragement he has provided to make the work an invaluable learning experience.

I am equally grateful to my co-guide **Mr. S.K. Das,** Ex- Executive Director, Oil and Natural Gas Corporation (ONGC) for his wise pieces of advice in my Ph.D. work. I highly appreciate all his contributions of time, ideas, persistence in high quality results, and make my Ph.D. experience productive and stimulating.

I am sincerely thankful to Director (Exploration), ONGC, for his kind permission for doing the research. I am thankful to Dr. R.P. Gupta (former Head of the Department of Earth Sciences), Dr. P.K. Gupta (former Head of the Department of Earth Sciences), Dr. A.K. Saraf (former Head of the Department of Earth Sciences), and Dr. D.K. Srivastava, Head of the Department of Earth Sciences, Indian Institute of Technology Roorkee, for providing departmental facilities for carrying out my research work.

I am thankful to Dr. Dinesh Kumar, Professor, Department of Geophysics, Kurukshetra University, Kurukshetra for his valuable suggestions and constructive comments. I sincerely thank Mr. A. Bhardwaj, Executive Director, ONGC, Dehradun and Mr. S. Banerjee, DGM, ONGC, Dehradun for their valuable recommendations and observations.

I sincerely thank Indian Institute of Technology Roorkee and ONGC for supporting this work. I wish to thank Department of Science and Technology (DST), Government of India for sponsoring project reference no. SR/S4/ES-596/2011.The strong ground motion data for a few Garhwal stations obtained from http://www.pesmos.in are thankfully acknowledged. Sincere thanks to Che-Min Lin, National Center for Research on Earthquake Engineering, Taipei, Taiwan for the genetic algorithm coding used in the present work.

I am also indebted to Dr. Sandeep Singh, SRC Chairman, and Dr. J.P. Narayana, SRC External Member, Indian Institute of Technology Roorkee, Roorkee, for their motivational comments and positive inputs during the progressive seminars. I am thankful to my friends Ms.

Vinay Kundu, Geologist and Dr. Dinesh Chauhan, Senior Geologist from Geological Survey of India, Dehradun for their valuable suggestions during the work.

I would also like to thank all other members of IIT Roorkee (Parveen Kumar, Sumedha, Ashvini Kumar, Pushpa, Sandeep Arora, Anita, Sohan, Sanjay, Neha, and Rakesh) for their sincere support and providing me a great work environment during my stay at IIT Roorkee.

Finally, I thank my parents, sister and all the relatives and friends for encouraging me at all the times which helped me a lot in tough times. Last but not the least I express love and gratitude to my husband for his unending love, patience, understanding and constant personal support.

Last but not the least, I express my gratitude to the Almighty God for always keeping me in high spirit during all tenure of this work and providing me strength to perform this task successfully.

(Parul)

LIST OF PUBLICATIONS

1. **Parul Bhardwaj**, Joshi A., Bhardwaj S. **(**2017), Multi-channel Analysis of Surface Waves for shallow subsurface studies in Garhwal Himalayas, India - A case study, 12th Biennial International Conference and Exposition 2017: Energy through Synergy, Society of Petroleum Geophysicists, India.

2. Joshi A., **Parul Bhardwaj** (2018), Site characterisation using Multi-channel Analysis of Surface Waves at various locations in Kumaon Himalayas, India. The Journal of Indian Geophysical Union, v.22, no.3, pp: 265-278.

TABLE OF CONTENTS

LIST OF SYMBOLS AND ABBREVIATIONS

μ	Shear modulus
A	Amplitude
A_h	Amplification of horizontal component of vertically incident body wave
A_v	Amplification of vertical component of vertically incident body wave
d_i^M	phase velocity of measured dispersion curve
d_i^T	phase velocity of theoretical dispersion curve
F_{p}	Predominant frequency
H	Thickness
h	Layer thickness
H/V	Horizontal to Vertical Ratio
H_b	Horizontal spectra at the basement
H_f	Horizontal spectra at surface
H_s	Horizontal spectra of Rayleigh wave
M	Richter magnitude of an earthquake
MASW	Multi-channel analysis of surface waves
M_{s}	Surface-wave magnitude
M_{w}	Moment magnitude of an earthquake
N	Standard Penetration Test Blow count
PI	Plastic index
QTS	Quasi Transfer Spectra
RMSE	Root Mean Square Error
S_u	Undrained shear strength
v	Velocity
υ_0	Displacement amplitude at the free surface.
V_b	Vertical spectra at the basement
V_f	Vertical spectra at surface
$\upsilon_n{}'$	Displacement of the downward travelling SH waves in n^{th} layer
$\upsilon_n{}''$	Displacement amplitude of the upward travelling SH waves in n^{th} layer
V_P	P-wave velocity
V_r	Rayleigh wave velocity
V_s	Vertical spectra of Rayleigh wave

V_{s30}	Shear wave velocity up to 30m
V_{sb}	Shear wave velocity at basement
V_{ss}	Shear wave velocity at surface
w	Water content
β	Transverse wave velocity $(\mu/\rho)^{1/2}$
λ	Wavelength
ρ	Density of earth medium
ϕ, ψ	Displacement potentials
Δx	Correction matrix
y	Residual velocity matrix
a	Jacobian matrix
ε	Damping parameter
I	Identity matrix
f^{obs}	Observed Values
f^{cal}	Theoretical Values

LIST OF FIGURES

LIST OF TABLES

Chapter – 1

INTRODUCTION

The study of the effects of local site conditions is crucial for geo-technical studies. Local geology of the station appears to be the prominent factor for the variation of responses in ground motion and determination of the site-specific seismic hazard. It has been identified since long that, a different category of sediment reacts differently when it is exposed to strong ground motion. These observations are made by comparing earthquake records taken from sites with different underlying soil types. It has been well established that local geology leads to huge amount of amplitude variation. Various studies analyzed the site characteristics using data of the Mexico earthquake (M_w 8.0), 1985, the Loma Prieta earthquake 1989 (M_w 6.9) and Bhuj earthquake (M_w 7.6), 2001 (Singh et al., 1988; Hough et al., 1990, Chopra et al., 2013). These studies established that the strong ground motions cause substantial effect on site conditions including the amplitudes and response spectral characteristics. Some sites amplify the strong ground motion and some don't (Boore, 2004). The behavior of site characteristics for the strong ground motion varies from one location to another. These effects of site conditions are termed as site amplification functions.

Generally ground motions are amplified more at sites containing soft sediments than at those pertaining to older and compacted sediments. Different location has its own natural frequency, which depends upon the thickness of sediments and geological structures present near the site. Local site characteristics are directly related to the destruction caused by earthquakes at that site. Thus, the site specific studies related to seismic hazard and micro-zonation always consider local site conditions as one of the crucial parameter. These studies are mandatory for the simulation of strong ground motion. Therefore, the responses of such local site studies are very crucial for the regional seismic hazard analysis. The amplification of seismic waves may be caused mainly due to impedance changes due to velocity gradient and resonance effect due to a soft layer. As we know (Lay and Wallace, 1995).

$$A_1/A_2 = [\rho_2 v_2/\rho_1 v_1]^{0.5}$$

Where A: Amplitude, ρ: density and v : Velocity

When $\rho_2 v_2 > \rho_1 v_1$ then $A_1 > A_2$ i.e. amplitude of the wave in layer 1 (sediments) is amplified relative to its incoming amplitude from layer 2 (bed rock). The site amplification phenomenon

can be seen directly from the recorded ground motion. Figure 1.1 shows the recorded ground motions at soil site and rock site due to an earthquake (after Boore, 2004). These sites are approximately at the same distance from the earthquake source. It has been noted that, the ground motions at the soft site have been amplified as compared to those of at rock site.

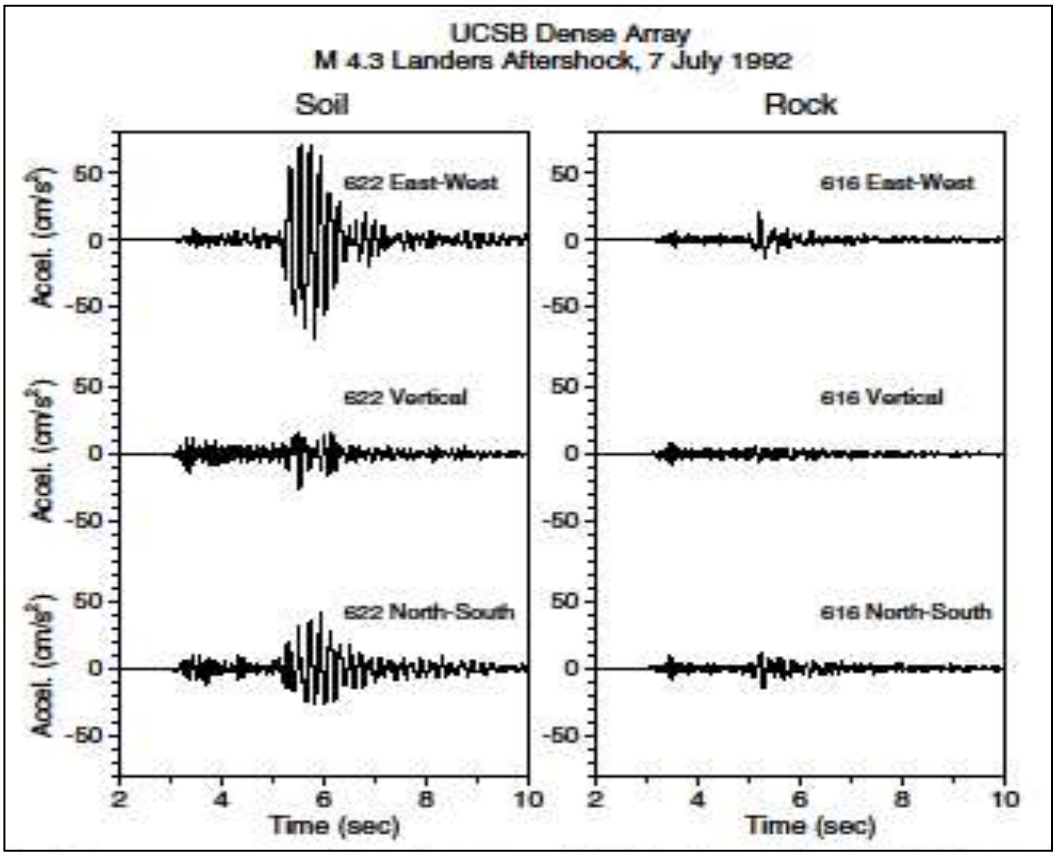

Figure 1.1: Recorded earthquake ground motions at soft and hard rock sites (after Boore, 2004)

The site amplification functions are essential elements for earthquake assessment, regional seismic zonation studies and seismic hazard analysis. Microzonation studies aim to estimate amplification difference of the ground motion at close sites. Such studies can be done with the help of microtremor as well as strong ground motion data. The microtremor data are very useful as one of basic sources of information for seismic microzoning (Irikura et al., 1980). The site characteristics are also important because most of the human population is concentrated on sediments (soft sites). Therefore, the responses of such local site studies are very crucial for the regional seismic hazard analysis. The site classification map can be used for indirect evaluation of the site amplification.

1.1 Literature Survey

The Himalaya is one of the youngest and most emblematic mountains in the world. It is made up of sedimentary and metamorphic rocks formed due to collision of Indian and Eurasian plate which is continuously in the stage of movement and uplift. It is an arcuate shaped having length of approximately 2400 km from North-Northwest to East-Southeast. A highly destructive earthquake in 1803, with a magnitude ≥ 7.5, has been reported in the region (Smith, 1843). Since last 121 years, Himalayas has produced four large earthquakes of magnitude ≥ 7.8 and nine earthquakes of magnitude >7.0.

Indian subcontinent has experienced four great earthquakes of magnitude greater than 8 in the time span of 53 years (1897-1950). These are the Assam earthquake of 1897, the Kangra earthquake of 1905, the Bihar–Nepal earthquake of 1934 and the Assam earthquake of 1950. There were about 30,000 causalities and heavy economic loss due to these earthquakes (Middlemiss, 1910; Auden and Ghosh, 1934 and Richter, 1958).

1. **Assam earthquake of 1897** (M_w 8.0)**:** The earthquake has been caused by slippage on subsurface thrust at a depth of about 15 km (Gahalaut and Chander, 1992; Khattri, 1993). Gahalaut and Chander (1992) estimated the dimensions of the rupture zone as 170 km x 100 km on the basis of numerical simulation of ground level changes due to a rectangular rupture on a buried fault.
2. **Kangra earthquake of 1905** (M_s 7.8)**:** Chander (1988) found that the observed co-seismic elevation changes are consistent with a 80 km wide sub-horizontal sub-surface fault extending 280 km between Dehradun and Shahpur in the northwest. The southern edge of the fault plane is at 10 km and northern edge is at a depth of 17 km.
3. **Bihar–Nepal earthquake of 1934** (M_w 8.0)**:** The northern edge of the fault plane is close to the MCT while southern edge is near the MBT in this section of Himalaya (Chander, 1989). On the basis of damage caused by the earthquake, the estimated length of the fault zone is 200 ± 100 km (Molnar and Pandey, 1989). An average dislocation obtained on this fault plane is about 6 km (Molnar, 1990).
4. **Assam earthquake of 1950** (M_w 8.5)**:** The rupture occurred primarily on a gentle north-northeast dipping thrust fault (Molnar and Pandey, 1989). The rupture length of this earthquake is about 350 km (Khattri and Tyagi, 1983). The fault dimension of the rupture is estimated to be 250 km x 100 km (Molnar and Pandey, 1989).

As shown in Figure 1.2, the great earthquakes occur at sections of the plate boundaries which have not ruptured during the past several decades or more (Mogi, 1985). These unruptured sections of the plate boundaries are called seismic gaps. Three seismic gaps in the Himalayan region have been established on the basis of study of the space-time patterns of seismicity of the region (Khattri and Tyagi, 1983; Khattri, 1987).

These seismic gaps are (i) the Kashmir gap, west of Kangra (1905) earthquake, (ii) the central seismic gap, between Kangra (1905) and Bihar–Nepal (1934) earthquakes and (iii) the Assam gap, between Assam (1897) and Assam –Tibet (1950) earthquakes.

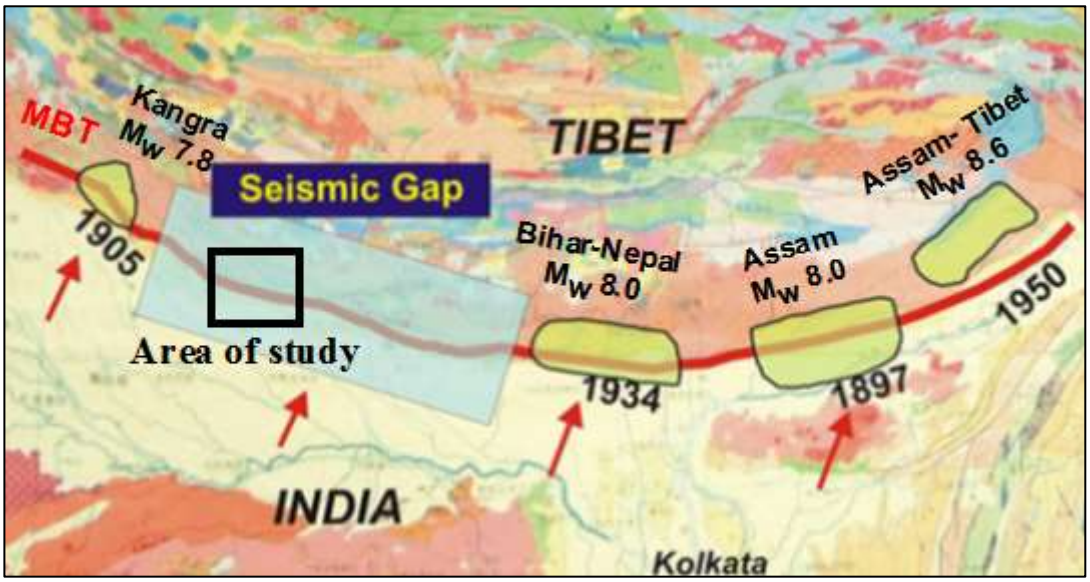

Figure 1.2: History of large earthquakes in Himalaya and location of central seismic gap (modified after Yeats and Thakur 1998; Richter 1958, Chopra et al. 2012).

The area of study, Kumaon and Garhwal Himalayas, for the present research work falls in central seismic gap. The central seismic gap has been recognized as seismic gap, and it has been interpreted to have accumulated potential slip for generating future great earthquake (Yeats and Thakur 1998; Richter 1958, Chopra et al. 2012). Gahalaut and Chander, 1997 analyzed the repeat leveling data related to 1905 Kangra earthquake and have shown the occurrence of great earthquakes in the Himalaya follow a cyclic nature. The return period is estimated to be 350 year using a slip rate of 18 mm/year and a slip of 6.2 m in the last great earthquake (corresponding to the 1934-Bihar earthquake) (Khattri, 1999). As a result, using the time-predictable model of the earthquakes, Khattri (1999) estimated the 100 year (beginning the year 1999) probability of occurrence of a great earthquake is 0.52 in the central seismic gap. The 100 year probability of occurrence of one or more great earthquake in the Himalaya is 0.89 (Khattri, 1999).

Post seismic deformations studies has also been done by the researchers for large earthquakes like Bhuj earthquake, 2001 and Kangra earthquake, 1905 (Wallace et al., 2005; Choudhury et al., 2013). Several scientists proved from Global Positioning System (GPS) observations that the uninterrupted seismic activity is constantly occurring in Himalayas (Banerjee and Burgmann, 2002; Bettinelli et al., 2006; Feldl and Bilham, 2006) and derived average slip deficit from these observations (Bilham and Ambraseys, 2005; Bilham and Wallace, 2005). The gravity along with geomorphological studies in the region has also established the strain accumulations in the Himalayan region. (Berthet et al., 2014; Hetényi et al., 2006, 2007, 2014, 2016). Thus, it is important to estimate the shallow velocity profiles of the region.

Considering the historical earthquakes across these two plates, Kumaon and Garhwal Himalayas are in the central seismic gap. It is seismically a very active region. This region has experienced 294 earthquakes in last few years. Figure 1.3 shows of various activities in the Kumaon and Garhwal Himalayas during 1973 to 2012, as reported by United States Geological Survey (USGS).

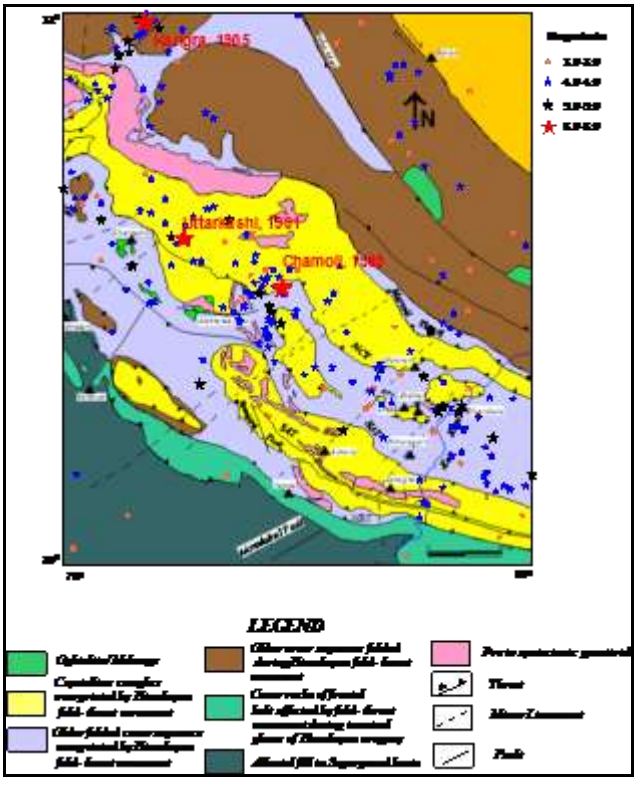

Figure 1.3: Locations of various events in the Garhwal and Kumaon Himalayas during 1973 to 2012 as reported by United States Geological Survey (USGS). The geology and tectonics of the region is after GSI (2000).

The Himalayas including Kumaon and Garhwal region and its nearby areas has been mapped, modeled and analyzed actively by using various state-of-the-art geophysical techniques. Unfortunately, the Kumaon and Garhwal Himalayas find itself within central seismic gap. Since the energy is stacking up due to the collision of Indian plate with the Eurasian plate but there has been no giant outflow of this accumulated energy from past many years except two moderate earthquakes in the past i.e. Uttarkashi earthquake and 1991, (Mw 6.8) and Chamoli earthquake (Mw 6.5), 1999 in Garhwal Himalayas. As a result, the central part of Himalaya can expect a great earthquake in the immediate future (Bilham et al., 2001). Since 1950, the state of temporary inactivity in the Himalayas has been a matter of uneasiness among various geoscientists (Satyabala and Gupta, 1996). Absence of surface rupture associated with the great earthquakes motivates seismologists and geoscientists for variety of research work in this region. Caldwell et al. in 2012 used conversion point (CCP) stacking of Ps receiver functions to image the crust and upper mantle beneath the western (Garhwal) Himalaya and suggested horizontal Moho at 35-40 km depth beneath the Lower Himalaya deepens to 45-50 km beneath the Higher Himalaya.

The Garhwal Himalayas have witnessed two moderate earthquakes in the past i.e. Uttarkashi earthquake 20 October 1991 (M_w 6.8) and Chamoli earthquake 28 March 1999 (M_w 6.5), as a result more research has been performed out in the Garhwal Himalaya as compared to the Kumaon Himalaya.

The data produced by these earthquakes are vital for evaluation of seismic hazard. Site amplification functions play an important role for determining the site specific seismic hazard (Chopra et al., 2012). The site amplification functions are also required for the simulation of earthquake strong ground motions at the surface (Sandhu et al., 2017). The areas which lie in the vicinity of Himalaya are equally under threat. Site amplification function (Sandhu et al., 2017) and simulation of great earthquake (Singh et al., 2002, 2010) within National Capital Region (NCR) has also been analyzed.

Various studies have been made to understand the site characteristics of Himalaya using data of the Dharmsala earthquake (M_w 5.5), 1986 the Uttarkashi earthquake, 1991 (M_w 6.8) and Chamoli earthquake (M_w 6.5), 1999 (Sriram and Khattri, 1997; Sriram et al., 2005; Kumar et al., 2005, Sriram and Khattri, 1999).

A number of techniques are available to extract the information about the site effects from the seismic recordings. Such techniques are based on various empirical and theoretical

approaches. The theoretical approach needs site specific detailed geophysical and geological constraints and refined computational procedures. The empirical approaches need the observed seismic values recoded at various sites. These techniques include (1) Standard Spectral Ratio Technique (SSR), (2) Horizontal to Vertical Spectral Ratio Technique (HVSR), (3) Generalized Inverse Scheme (GIS), (4) Coda Wave Technique (CWT).

Borcherdt (1970) proposed SSR in which the soil spectrum of a site is divided by the rock spectrum of the site using strong ground motion data recordings. The division of these two spectra will remove the source and path effects since these two effects are same for two nearby sites. This procedure has been used for various geological settings (e.g. Borcherdt and Gibbs, 1976; King and Tucker, 1984; Jarpe et al., 1988; Singh et al., 1988; Mittal et al. 2011, 2013). To carry out the standard spectral ratio technique the following conditions are to be fulfilled:

(i) Recording of earthquake on soil and reference site should be simultaneous,
(ii) The reference site should be free from site effects
(iii) Smaller distance between soil and reference site

The rock site can have the site response that may lead to under estimation of site effect. It was also proposed to use ambient seismic noise instead of earthquake recordings in order to apply the technique of Borcherdt (1970) in the regions of low seismicity. The ambient seismic noise includes short period as well as long period called microtremors and microseisms, respectively. Various methods have been proposed for the evaluation of site effects that do not require any reference station.

HVSR, also known as non -reference site method was initially studied by Nogoshi and Igarashi (1971) using ambient noise. They compared horizontal to vertical ratio (H/V) of Rayleigh wave of recorded microtremors and concluded that the microtremors are mostly composed of Rayleigh wave. Nakamura studied later in 1989, the peak frequency of H/V of Rayleigh wave is approximately equal to zero and trough frequency of H/V which contains the maximum energy (Nakamura, 1989). He explained peak frequency of microtremor is from incident shear wave.

In this technique, the site response is generated by the division of horizontal component with that of vertical component of noise spectrum. He claimed that the vertical component of ambient noise is not affected by a soft sediment layer overlying a half space. In this approach,

the microtremors are inferred as Rayleigh waves spreading in a single layer over a half space. It has been validated that the method proposed by Nakamura envisages only the fundamental resonant frequency and generates inconsistencies with the estimated amplitude (e.g. Field and Jacob, 1993; Seekins et al., 1996).

Nakamura (1989) approach has been further used for strong ground motion recorded during 1985 Michoacán earthquake at single station instead of miceotremors by Lermo and Chávez-García (1994). It has been found that if the site effects are caused by simple geology, dominant period and local amplification level and can be obtained using earthquake records of single station. They observed that the site effects are not much influenced by the vertical component, as compared to the horizontal component. Thus, the HVSR of an earthquake can be utilized for the site characterization studies. They established that dominant period and local amplification level can be obtained using an earthquake record of single station if the site effects are originated under normal and simple geological conditions. This method has been broadly applied on feeble as well as strong ground motion records (Chavez-Garcia el al., 1996; Castro et al., 1997; Riepl et al., 1998; Zare et al., 1999; Nath et al., 2000, 2002, 2005, 2008; Mandal et al., 2008).

In past, many studies have frequently shown the capabilities of the HVSR technique to deliver good and reliable site responses (Nakamura, 1989; Lachet and Bard, 1994; Kudo, 1995; Bard, 1998). However, two contradictory arguments regarding its theoretical basis exist. Nakamura (1989, 2000) claims that in HVSR technique, S-wave resonance in soft surface layer (removing effects of surface waves) are broadly reflected. Thus, HVSR curves deliver a reliable site amplification function. This "body wave" explanation has been challenged by many authors explaining the relationship between the HVSR and the ellipticity of fundamental mode Rayleigh waves (Lachet and Bard, 1994; Kudo, 1995; Bard, 1998). Thus, the existence of any simple and straight forward relation between HVSR peak value and the real site amplification factor (the HVSR peak would then be associated with the vanishing of the Rayleigh wave vertical component, instead of amplification of S-wave on horizontal components) can be questioned. This summarizes the two hypothetical origins of the HVSR peak. Recent studies done by Bonnefoy – Caudet et al. in 2008 shows H/V spectral ratios curves of ambient noise records gives a peak near fundamental resonance of the soil.

Andrews (1986) estimated site effects by solving the large inverse problem based on multiple recorded events for all source/path effects and site effects simultaneously. This method

is known as GIS which gives reliable information of the source and site effect at all sites of the network even when there is no simultaneous recording of all earthquakes (Field and Jacob, 1995). This approach has been used for local site effect estimations for various regions of the world (Boatwright et al., 1991; Hartzell, 1992; Seekins and Boatwright, 1994; Harmsen, 1997; Zhao et al., 2004; Mandal et al., 2008). This technique requires a high quality data.

Coda Wave Technique (CWT) method is applied when there is common coda decay curve. Estimation of the coda decay curve is done by using back scattering model. It is assumed that the coda waves of local earthquakes are composed of single backscattered body waves. Sharma et al., 2008 used CWT for site amplification studies in Koyna, Gujarat and used 37 local earthquakes for the site amplification estimations using coda decay curve.

The different techniques have been used in few studies done for the estimation of site amplification functions in the Kumaon and Garhwal Himalayas. This region is a densely populated area due to rapid industrialization and hence site amplification study in these regions plays an important role. Several workers have performed attenuation studies related to body and coda waves using different techniques from available data in the Garhwal and the Kumaon Himalaya, India (Gupta et al. 1995; Mandal et al. 2001, 2013; Gupta and Kumar 2002; Paul et al. 2003; Joshi 2006b; Mukhopadhyay et al. 2008; Padhy 2009; Singh et al. 2012; Kumar, 2015).

Scientists have determined the three-dimensional attenuation structure in the Pithoragarh region of Kumaon Himalaya using spectral acceleration data (Joshi et al., 2006a, 2007, 2010). Kumar and Joshi, 2015 used strong motion data for attenuation tomography of Kumaon Himalaya in Pithoragarh region.

A significant contribution has been made by various researchers of India and other parts of the world. Srinagesh et al., 2011 used SSR for studying the site amplification functions at sites in the central Indo-gangetic basin in Himalaya. Chopra et al., 2012 used stochastic finite fault modeling technique (SFFMT) to simulate the constrained ground motion parameters using Uttarkashi (1991) and Chamoli (1999) earthquakes at average shear velocity at 30m depth V_{s30} of 520 ms^{-1} and 620 ms^{-1} respectively (Boore and Joyner, 1997). Several seismologists used ground motions to develop attenuation relations for Garhwal and Kumaon Himalaya (Joshi et al., 2006a, 2007, 2010, Kumar and Joshi, 2015).

Mundepi in 2013 used HVSR technique on ambient noise records at various locations of Dehradun, Uttarakhand, for site amplification studies. The attenuation relation developed for

Garhwal and Kumaon Himalaya revealed that these two regions have distinct attenuation rates (Joshi et al., 2012) and hence due to these reasons it is important to estimate velocity model of Kumaon and Garhwal region.

Sharma et al., 2014 compared the results obtained from HVSR and GIS techniques for the site response characteristics and the estimated results from both the techniques show one to one correspondence. The site amplification factor varies between 2.3 and 9.4 using HVSR and between 2.6 and 10.9 using GIS among different stations. The predominant frequency ranges from 1.3 to 8.3 Hz with HVSR and from 1.3 to and 9.0 Hz with GIS.

In the present study, the records are analyzed using three different methods: (a) Reference site dependent method : Standard Spectral ratio, (b) Non- Reference site method : the horizontal to vertical (H/V) spectral ratio on ambient noise records, and (c) Non- Reference site method : the horizontal to vertical (H/V) spectral ratio on strong ground motion records. The evaluation has been done for both SSR and HVSR results to authenticate the attained parameters. The outputs are linked in terms of site amplification functions i.e. amplification level and predominant frequency.

These parameters are highly affected by the local geology or soil types of the area. It has been established that various soil types responds uniquely when exposed to ground motion generated by either passive (E.g. earthquakes and microtremors etc.) or active source (E.g. dynamite and vibroseis etc.) of energies. The literature survey suggests that the local site effects can cause considerable modification in seismic amplitudes. In the recent past, engineering geophysics community has started focusing on the dispersive property of surface waves by analyzing the fundamental mode of Rayleigh waves. Shear wave velocity can also be extracted after inverting the phase velocity of the surface wave which mainly contains Rayleigh and/or Love waves (Dorman and Ewing, 1962; Aki and Richards, 1980). Various kind of surface wave techniques have been proposed for shallow subsurface imaging involving huge variety of configurations, processing methods and inversion algorithms.

The microtremor measurements are used to find shear-wave velocity profiles in high-density urban areas and providing maps for spectral acceleration in Iran (Shafiee et al., 2011). Although it is a current practice in Iran to use seismic surveys, borehole investigations and microtremor measurements for ground motion microzonation, in many projects ground motion studies are limited to microtremor measurements, an efficient and low cost method of seismic

hazard microzonation. These measurements, where ever possible, are combined with seismic weak motion and strong motion records to produce microzonation maps that include site period and amplification of ground vibration.

Nazarian et al., 1984, presented a wave propagation method to produce the shallow subsurface velocity profiles called as Spectral Analysis of Surface Waves (SASW). This method involves the spectral analysis of ground roll caused by an impulsive source recorded by two geophones. The single pair of receivers is configured repeatedly based on wavelength calculations made during data acquisition. The records are examined to generate dispersive curves in the frequency domain which in turn results the shear wave velocity (V_s) profiles with only a pair of receivers. Besides being expensive, the interpreter faces difficulties while separating signal from noise in this method (Park, Miller & Xia, 1999; Xia et al., 2002). Considering the limitations of SASW geoscientists have started using Multi-channel Surface Waves Analysis (MASW). MASW is the most popular method utilized to investigate the shear wave velocity profiles up to 30m i.e. V_{s30}. It is a non-invasive, non-destructive, continuous profiling method that is being applied to earthquake geotechnical engineering problems for the microzonation and site response studies using several receivers (generally 24 geophones). This seismic method can be broadly utilized for the geotechnical characterization of shallow subsurface (Park et al, 1999; Xia et al, 1999; Miller et. al 1999).

The earthquake ground motions are affected by the source processes, propagation of seismic waves in the medium, and the site characteristics. The study of effects of local site conditions is one of the most vital areas of earthquake engineering. For site classification, V_{s30}, shear wave velocity up to 30 m, is a key parameter. The top 30 m has an important role in defining the characteristics of earthquake strong ground motion during an earthquake. The strong ground motion plays an important role for the evaluation of seismic hazard in the region. Since 30 m is a typical depth of borings and detailed site characterization in engineering site investigation, hence, most of the site-effect studies in earthquake ground motions are based on the properties in the upper 30 m (Anderson et. al, 1996).

To estimate V_{s30}, the engineering geophysics community is focusing on the analysis of the fundamental mode of Rayleigh waves, using their highly dispersive property. Spectrum of surface waves can enormously benefit the geophysics domain (Bullen, 1963; Mitchell, 1973; Mooney et al., 1966; Tsai et al., 1969). Also, V_{s30} estimate can be used to suggest the possible amplification and de-amplification of sites (Dobry et. al, 2000). The site classification as per

National Earthquake Hazards Reduction Program (NEHRP) is used to group sites into different classes (Borcherdt, 1994; Shafiee et. al, 2007; Wen et. al, 2008). The current NEHRP approach categorizes soils into A, B, C, D, E and F based on their vertical shear wave velocity profile, thickness and liquefaction potential (Thitimakorn et. al, 2012).

MASW has been used to for V_{s30} models and thickness of soil column in Dehradun (Ranjan, 2005). Mahajan et al., 2007 has done seismic micro-zonation of Dehradun using geophysical and geotechnical characteristics.

The shear wave velocity models generated by MASW are up to 30m depth and are generated using least square inversion. These models are good for a near surface quick V_{s30} estimates and for site specific geo-technical studies. However site amplification studies of micro tremors and strong ground motion data constrains shear wave velocity for deeper depths (500m in the present work) within the subsurface. The present study utilizes a global optimization method i.e. Genetic Algorithm (GA) for generating the shear velocity models using initial guess for shallow layer obtained from MASW technique.

GA is a global optimization method. It is based on mechanism of natural selection. This algorithm has been used widely in many optimization problems and has the potential to make valuable contribution in the field of geosciences. Genetics is the source for the term GA where many individuals are grouped together to form a population. It consists of selection, crossover and mutation of individuals in a population. Iteratively it evaluates one set of population and generates a new one. Each successive population is known as generation.

In the process of evaluation of population, a fitness function is required. The individuals are selected on the basis of their fitness for the next generation. This process is analogous to the "survival of the fittest" principle. To facilitate convergence to an optimal solution so that the "best" model with good fitness value are carried forward to the succeeding generation. As compared to local optimization methods Genetic algorithm, a global optimization method, is robust, accurate and provides consistent results with minimum error. GA has been applied to many applications of earthquake studies including determination of source parameter of 1988 Nepal-India border earthquake (Zhou et al., 1995) and simulation of earthquake strong ground motions modeling of the 1991 Uttarkashi, Himalaya earthquake (M_w 6.8) (Kumar et al., 2011).

Using dispersion curves, obtained from strong ground motion data and ambient noise data, GA search gives shear wave velocity for the layers present in the subsurface (Yamanaka and Ishida, 1996). This method is utilized to obtain subsurface structural model. Many such

regional studies have been successfully carried out for near surface profiles (Horike, 1985; Cara, 1983; Kafka and Reiter, 1987).

In order to apply GA, we have solved the forward problem using Haskell matrix (Haskell, 1953) method. Dispersion curves obtained from the observed surface wave propagation in a horizontally layered structure can be calculated. Generally, a dispersion curve is a nonlinear function of shear and/or compressional-wave velocities, densities and thickness for each layer.

Generally dispersion curves are inverted considering it as linear inverse problem. In this process, the higher-order terms in the Taylor series expansion are neglected and the model is perturbed iteratively to obtain optimum solution (Aki and Richards, 1980). Since linear inversion have computational difficulties in the presence of noise and the assumption of an initial model, which should be close to the real model, is difficult to set. Thus, solving geophysical problems using non –linear inverse algorithm gives better results.

To reduce the error a non-linear optimization method which uses a GA, has been useful in numerous domains (Goldberg, 1989). Genetic Algorithms have already been used in many geophysical applications .Inversion of 1D reflection seismogram using GA was carried out by Stoffa and Sen in 1991.Static corrections using GA were determined by Wilson and Vasudevan, 1991 in Seismic reflection data processing. Later, GA was applied to waveform inversion of reflection seismograms Sambridge and Drijkoningen, 1992. Moreover this algorithm was successfully utilized by Sambridge and & Gallagher in 1993 to determine hypocenter locations by using travel-time data. Furthermore, Kobayashi and Nakanishi determined fault-plane solutions of earthquakes using GA in 1994.Yamanaka and Ishida, 1996 has applied later the GA to invert group velocities of surface waves (Love waves) dispersion data.

Some authors have been trying to find observational proof of the nonlinearity from seismological data and estimate how much it influences strong ground motions (Ordaz and Faccioli, 1994; Aguirre et al., 1994; Satoh et al., 1995). Satoh et al., 2001 has estimated shear wave velocity model of Taiching basin using microtremor records. Earthquake data has been utilized by various scientists for estimating the soil behavior and discussing the nonlinearity of the soil (Aguirre and Irikura, 1997; Pavlenko, 2003). Fah et al., 2001, 2003 obtained shear velocity structures using micro-tremors data and theoretical estimation of average H/V ratios. Kuo et al. 2009, 2011 has made a detailed shear velocity models in Ilan, Taiwan using GA

inversion as one of the three different techniques. Various authors correlated Vs_{30} with N- value (Standard Penetration Test Blow count) for generating the empirical equations (Chen et al. 2003; Kuo et al. 2011).

1.2 Study Area

The Kumaon and Garhwal Himalayas lie in the state of Uttarakhand, India which shares its border with Nepal. It falls in the seismic zone IV and V, as per the Seismic Zoning map of India (BIS, 2002). The main driving force that causes high seismic activity in this region is under thrusting of the Indian plate beneath the Himalaya. Robust wraps and recurrence of many former faults and thrusts during Quaternary are evident in this region. It falls between the Eurasian plate and Indo-Australian plate, where the stress is constantly getting accumulated giving indications of a potential major earthquake (M>8.0). Himalaya is considered one of the key study areas for all seismologists and in view of the shortening rate of 20 mm/yr. across the Himalaya (Lyon- Caen and Molnar, 1985; Avouac and Tapponier, 1993; Gahalaut and Chander, 1997; Bilham et al., 1998). The geologic section in Himalaya has been raised by the stacking of the slices of the Indian crust by repeated thrusting at Himalaya plate boundary and is dominated by old metamorphic and igneous complexes. They are also subjected to very high compressive stresses (e.g., Singh, 1981; Cloeting and Wortel, 1986; Chander and Gahalaut, 1995). The plate tectonic implications of Himalayan region have been thoroughly studied by various scientists (Prasad et al. 2011; Khan, 2005).

A great earthquake, resulting in massive damage of the natural and human habitat along the Himalayan foothills, in this region has been predicted by many researchers and scientists (Kumar et al., 1999; Nath S., 2008). The present study on the estimation of shallow shear wave velocity models is important for this region. However, due to limited database available in the rough and difficult terrain of Kumaon region, less research work has been done to estimate site amplification functions in this part of Himalaya. The site amplification functions have been estimated for Kumaon and Garhwal Himalayas using earthquakes and ambient noise data recorded locally at 27 sites from Kumaon and Garhwal region. The study area is shown in Fig.1.4.

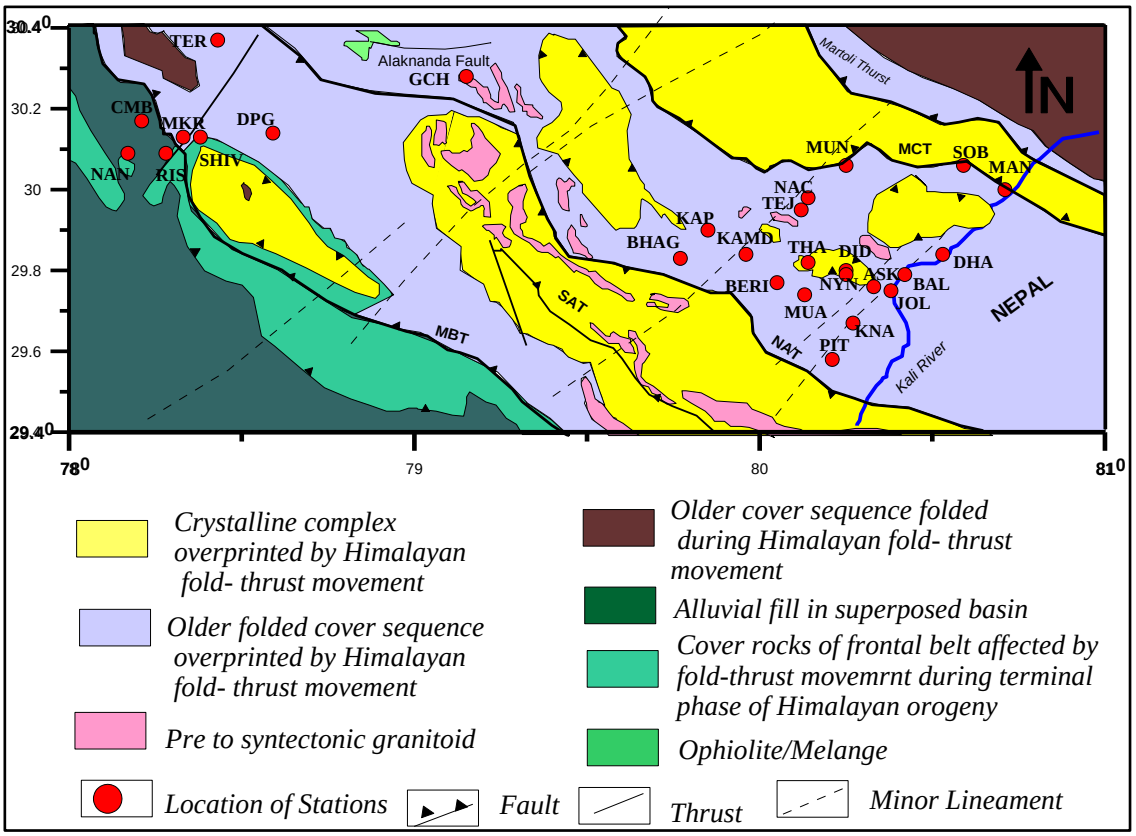

Figure 1.4: Location map of Kumaon and Garhwal Himalayas, India. MBT = Main Boundary Thrust, MCT = Main Central Thrust, SAT = South Almora Thrust and NAT = North Almora Thrust. Source of the tectonics and geology of the region is Geological Survey of India (2000).

The HVSR and SSR techniques have been applied on the records and the results are compared for this purpose because these techniques are conventional techniques. The present study is based on new locations in Kumaon and Garhwal Himalayas as compared to previous studies. Such studies in this part of Himalaya are required for better assessment of seismic hazard potential of the region.

1.3 Research Gap

The literature review of various techniques for estimation of site effects gives an extensive idea about the advantages and disadvantages of various techniques used for characterization of sites. Despite of high seismicity in the Himalayas, the quantitative study of the amplification of seismic waves is still lacking (Srinagesh et al., 2011). The present study generates shallow shear wave velocity models in Kumaon and Garhwal Himalayas after inversion of H/V curves using genetic algorithm.

No such in-depth study has been done in India yet, primarily because data acquisition in the terrains of Kumaon and Garhwal Himalayas is very tough. As a result, very few research

institutes record and analyze the strong ground motion and ambient noise data in Uttarakhand Himalayas.

Another part of the current research work involves MASW of the region. This method requires sufficiently flat areas in this hilly region which is again a difficult condition to fulfill. Following research gaps have been identified in the techniques to determine the site amplification studies:

1. Despite of high seismicity in the Himalayas, the quantitative study of the amplification of seismic waves is still lacking. Most of the site amplification studies are made through micro earthquake data. Very few site amplification are there which uses both strong motion data and ambient noise data as tabulated in Chapter 5.
2. The Genetic algorithm inversion, one of the global optimization techniques, is used for generating the shear velocity models using initial guess for shallow layers obtained from MASW technique. Till date none of the researchers have used global optimization technique to study the site effects in this region.
3. Peak ground acceleration is mainly controlled by shear waves in the strong motion record. The estimations and velocity models derived are useful in estimation of seismic hazard studies. The site amplification functions obtained from ambient noise data are compared with the earthquake data which are almost equal for both the cases. This comparative study was also not done earlier in this region.

The present thesis is an attempt to fill the above mentioned gaps in this region.

1.4 Research Objectives

Local site condition play an important role in damage distribution during earthquakes due to local site condition site amplification has been observed in the accelerogram. To apprehend the site effects of Uttarakhand Himalayas a very few studies have been done (Joshi et al., 2006a, 2006b).

Present work in this thesis is aimed to study the site effects using the accelerogram recorded by strong motion recorders. These results will be the confirmed by the Multi-channel Analysis of Surface Waves (MASW) are also useful for determination of geological structure of the region which is essential for the seismic hazard zonation study of the region. Necessary seismic factors should be taken into consideration for urban planning, industrialization, designing and construction of civil engineering structures (Mohanty et al. 2009a). Due to rapid industrialization in Uttarakhand, seismic microzonation of the region from V_{s30} using MASW

technique helps in the geotechnical studies. The area of study falls in central seismic gap hence these studies can help in preparing mankind in terms of constructing buildings, dams and schools.

Second part of the work involves estimation of site amplification functions, including amplification levels and predominant frequency, in this region which can further help in mitigating the risks. These site amplification functions are used for generating shear wave velocity models using a a global optimization method i.e. Genetic Algorithm. On the basis of work done and literature survey, the research work in the Ph.D. degree, is targeted with the following objectives:

1. To estimate 2D shear wave velocity model up to 30 m for Kumaon and Garhwal Himalayas using MASW.
2. To evaluate site characterization (H/V curves) of Kumaon and Garhwal Himalayas using strong ground motion as well as ambient noise records.
3. To invert the H/V curves using GA for evaluation of S-wave velocity models for different sites in Kumaon and Garhwal Himalayas.

1.5 Thesis Layout

This thesis comprises of seven chapters. The first chapter is an introduction to the thesis. It carries a detailed literature review and on the basis of literature review research gaps are identified. Based on these identified research gaps the objective of this thesis has been defined.

Second chapter discusses the theory and applications of MASW technique.

Third chapter details the data resources and various processing steps applied to condition the raw data used in the research. The chapter explains the Nakamura's Technique, Haskell Method and global optimization method i.e. Genetic Algorithm (GA) for generating the shear velocity models for constraining shear wave velocity model from strong ground motion and ambient noise data.

Chapter fourth presents the case study using MASW technique in various locations in the Kumaon and Garhwal Himalayas. The analysis of shear wave velocity structure is demonstrated using Seisimager software. The findings are then correlated with the local geology (Valdiya, 1980) of the station.

Chapter fifth discusses the site characterization of Kumaon and Garhwal Himalayas using the ambient noise and strong motion data recorded at various stations located in Kumaon and Garhwal Himalayas.

The records collected from the accelerograph have been processed using the procedure suggested by Boore and Bommer (2005).The results of inversion of H/V curves of S-wave Velocity models in the Kumaon and Garhwal Himalayas are presented in sixth chapter.

Seventh chapter summarizes the work and lists some of the future directions of research.

Chapter – 2

MULTI-CHANNEL ANALYSIS OF SURFACE WAVES (MASW): METHODOLOGY

In this chapter, the detailed theoretical features and methodology of Multi-Channel Analysis of Surface Waves (MASW) are explained. The acquired dataset are processed for noise elimination and signal enhancement and for the estimation of shear wave velocity by using "Seisimager" software (http://www.geometrics.com). The generation of dispersion curves and steps involves in inversion of dispersion curves are described in detail. The application of MASW is further briefed in the last section.

The engineering geophysics community is focusing on the analysis of the fundamental mode of Rayleigh waves, wherein utilizing the dispersive property of surface waves. In the layered media, the propagation velocity of surface waves depends on the frequency (or wavelength) of the wave on account of geometric dispersion. Shear wave velocity can be estimated from inverting the phase velocity of the surface waves which mainly consists of Rayleigh and /or Love waves (Dorman and Ewing, 1962, Aki and Richards, 1980).

Shear wave velocity of shallow sediments is a vital parameter in seismic wave amplification studies and thus V_{s30} is a widely used parameter for site classification. The inversion of surface wave seismic data is carried out to estimate the shear wave velocity models. This method (Anderson, 1996; Simons et al., 2002; Li and Detrick, 2003) is commonly used for seismological and the geotechnical applications. The low frequency waveforms in seismic trace are used for the study of deeper zones within the earth. However, relatively high-frequency waveform information can be used for the geotechnical purposes such as identification of geological patterns like cavities and tunnels, shallow surface crustal parameters and liquefaction studies etc. (Lin et al., 2004). Shear wave velocity is usually estimated for the depth less than 100 m below surface for number of geotechnical usages.

Various methods have been designed for near surface characterization with subject to the variety of testing configurations, processing methods and inversion algorithms. However, the following two methods are frequently used in the engineering geophysics:

1. SASW: Spectral Analysis of Surface Waves
2. MASW: Multi-channel Analysis of Surface Waves

In SASW method, the time taken for the data acquisition is less as compared to MASW (Nazarian et al., 1983). In MASW method, data is acquired using the multiple channels for recording of seismic waves. As a result, the quality of the raw data is better due to improved signal to noise ratio. Hence, MASW is gaining popularity for the usage in geotechnical applications such as shallow subsurface characterization. It is mostly used to estimate V_{s30} at different engineering sites.

2.1 Multi-channel Analysis of Surface Waves (MASW)

The vertical (and radial) components of raw seismic shot gathers contain Rayleigh waves (i.e. surface-wave or ground-roll). If the large velocity contrasts are present in the subsurface then the surface waves become more dispersive in nature (Liner, 2012).Therefore, the dispersion curves that are studied here are supposed to be layer induced apparent dispersion as opposed to intrinsic dispersion which is related to actual rock materials. The MASW method uses this dispersive property to estimate shear wave velocities. The MASW method has been developed with the assumption that the subsurface is vertically heterogeneous and laterally homogeneous (i.e. a layer-cake model). The MASW method is basically a two-fold procedure which is summarized as follows:

Step 1: Generation of the dispersion curves (phase velocity vs. frequency plots)

Step 2: Inversion of dispersion curves to generate shear wave velocity profiles.

With the technological advancement in the recent times, the development of the geophysical technique of Multichannel Analysis of Surface Waves (MASW) is proving powerful complimentary aid in subsurface exploration and site characterization. The frequency used in this method is high which provides us with a very good resolution, although the depth of investigation is limited to 100 m. Main advantages of MASW are:

- The recording of the waves through multiple channels allows effective spotting and isolation of noise as per distinctive coherency in trace and arrival of time.
- It is possible to continuously analyse and display each of frequency component since the recording technique in the method is similar to that of the vibroseis recording that is time variable frequency format.

- To get more accurate dispersion curves in faster manner, shot gather from multi-channel records are decomposed into a filtered frequency record.

2.2 Dispersion Curve and Rayleigh Wave

The MASW method is a wavefield transorm method (Park et al., 1998) which can directly convert raw shot gathers into the dispersion curves. In this method, Fourier Transformation technique is used to transform raw shot gather data i.e. offset-time domain into offset-frequency domain providing combination of amplitude and phase spectrum. The phase spectrum contains information about the dispersion whereas amplitude spectrum gives information about the attenuation, spherical divergence etc. (Park et al., 1998).

In the homogeneous medium, phase velocity remains nearly constant while the wavelength varies with depth i.e. on keeping the seismic properties constant (homogeneous medium), all the frequency components (harmonics) will travel with the same velocity as shown in Fig 2.1a. However, in case of the heterogeneous medium phase velocity also varies along with the wavelength with the change in depth i.e. in case of a layered medium with different seismic properties of different layers (vertically heterogeneous), different frequency components travel with different velocities depending on the seismic properties of that layer as shown in Fig 2.1b.

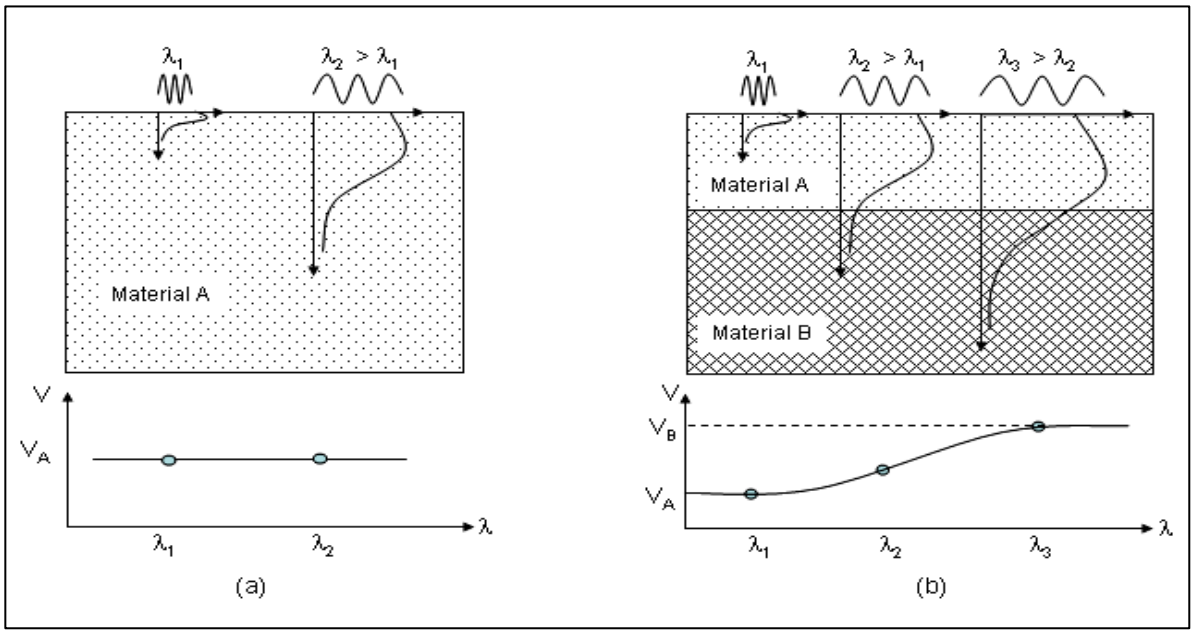

Figure 2.1.a) In a homogeneous medium all the wavelengths sample the same homogeneous layer, and the phase velocity is constant, b) when the properties are changed with depth the phase velocities depend on the wavelength. (Strobbia, 2003)

Therefore it is possible at a given frequency, phase velocities to be different for different modes of propagation, which can be exhibited simultaneously as shown in Fig 2.2b. Except the fundamental mode all the other modes exist only above their respective cutoff frequency. The number of modes is limited in a finite frequency band for a finite number of layers. Below the cutoff frequency of the first mode of oscillation only the fundamental mode can exist as shown in Fig 2.2b.

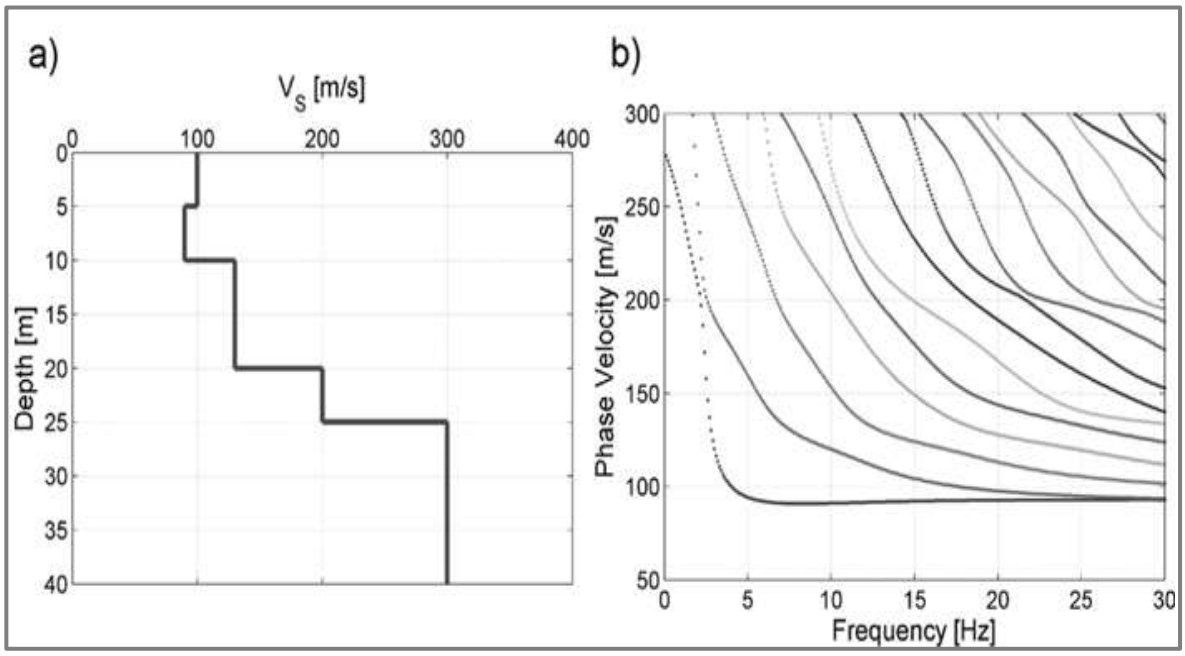

Figure 2.2.The dispersion curve shows the geometric dispersion of Rayleigh-waves: a) the S-wave velocity profile and b) the related dispersion curve. (Strobbia, 2003)

2.3 Inversion of Dispersion Curve

After the generation of good quality dispersion curves, the inversion technique can be applied to estimate the shear wave velocity from Rayleigh wave phase velocity data. In a homogeneous media, shear wave velocity (β) can be approximated from the Rayleigh wave velocity ($\mathbf{V_R}$) with the help of a linear relation given as follows:

$$\mathbf{V_R = 0.9194 * \beta}$$

Above relation can be derived by assuming the Poisson's ratio to be 0.25 (Sheriff and Geldart, 1985). In the first step of inversion process, initial shear wave velocity models are generated from the observed dispersion curves from forward modeling technique. Model response can be generated from the initial shear wave velocity model with each iteration step, root mean squared error is reduced between observed and the estimated value. After each iteration shear wave velocity model is updated. This technique of inversion is used on

individual shot gathers, thereby all the dispersion curves can be inverted to estimate one dimensional shear wave velocity structure. Inversion process is carried over all the shot gathers. We have used Haskell method for generating the layer model.

According to the Haskell equation, surface wave produces following plane wave solution to the elastic coupled wave equation (Haskell, 1953):

$$\partial^2\phi/\partial t^2 = V_p{}^2 \nabla^2\phi \quad \text{and} \quad \partial^2\Psi/\partial t^2 = V_s{}^2 \nabla^2\Psi$$

Where ϕ and Ψ represents displacement potentials and V_p and V_s represent P- and S-wave velocities, respectively. In most of the active source shallow surface surveys, when the compressional source is used, nearly two-third of the total seismic wave's energy generated is made up by the Rayleigh waves (Richart et al., 1970; Heisey et al., 1982). In most of the surface seismic surveys, Rayleigh wave constitutes to be the primary component of the Surface waves. As discussed earlier, the surface waves follow the property of dispersion i.e. different components of the frequency band has a different velocity of propagation (phase velocity), thereby different wavelengths for each component (Stokoe et al., 1994; Nazarian et al., 1983; Park et al., 1998).

One of the most common ways of using the dispersive properties of surface waves is constructing shear-wave velocity profiles after analyzing plane-wave fundamental mode Rayleigh waves (Bullen, 1963). The solutions to the wave equation enable us to determine the phase velocities for different wavelengths and by treating the closer to surface or near surface materials as layered earth (Haskell, 1953). Hence, by analysis of the dispersion property of ground roll which are present in seismic data, the shear wave velocity profiles can be obtained.

2.4 Inversion of Surface Waves Using Seisimager Software

To estimate the shear wave velocity structure from dispersion curves, one and two dimensional non- linear least square method is used. After minimizing the difference or residual the theoretical dispersion curve are obtained for shear wave velocity structure. The twenty layered model with variable layer thickness gradient 0.5 and bottom layer multiplier as 3 has been considered. Shear wave velocity of each layer is obtained after applying horizontal interpolation. The initial model is based on phase velocity curves. P wave velocity and the density are determined along with shear wave velocity during the process. In dispersion curve,

the shear wave velocity is obtained in the case of M layer structure. The velocity structure V_S is expressed by following vector x:

$$x^T = (V_{s1}, V_{s2}, \ldots\ldots V_{sM})$$

Here $V_{s1}, V_{s2}, \ldots\ldots V_{sM}$ are the shear wave velocities for first, second and M_{th} layer. The phase velocity obtained from the observed waveform is estimated as f^{obs} and from the calculated waveform is f^{cal}. The objective function of the inverse analysis is given by the following equation:

$$\sum_{i}^{N}\left(f_i^{obs} - f_i^{cal}(V_{s1}, V_{s2}, \ldots\ldots V_{sN})\right)^2 = \sum_{i}^{N}\left(f_i^{obs} - f_i^{cal}(x)\right)^2$$

Here, $f_i = f_i^{cal}(x)$ where i = 1to N: N is the number of observed values.

The matrix of partial differential coefficients (Jacobian matrix: a) is represented as:

$$a = \begin{bmatrix} \frac{\partial f_1}{\partial Vs_1} & \frac{\partial f_1}{\partial Vs_2} & \cdots \frac{\partial f_1}{\partial Vs_N} \\ \frac{\partial f_2}{\partial Vs_1} & \frac{\partial f_2}{\partial Vs_2} & \cdots \frac{\partial f_2}{\partial Vs_N} \\ \vdots & & \\ \frac{\partial f_n}{\partial Vs_1} & \frac{\partial f_n}{\partial Vs_2} & \cdots \frac{\partial f_n}{\partial Vs_N} \end{bmatrix} \rightarrow \text{Non linear problem} \rightarrow \text{Iterative } calculation$$

The unknown number x is the partial differential coefficient. The vector y of the observed phase velocity residuals is represented as:

$$y = \begin{bmatrix} f_1^{obs} - f_1^{cal}(x) \\ f_2^{obs} - f_2^{cal}(x) \\ f_3^{obs} - f_3^{cal}(x) \\ \vdots \quad\quad \vdots \\ f_N^{obs} - f_N^{cal}(x) \end{bmatrix}$$

where f_N^{obs} *and* f_N^{cal} are the observed and the theoretical values. The equation for correction matrix Δx is given by:

$$(a^T a + \varepsilon I)\Delta x = a^T y$$

where ε is known as damping parameter, y is a residual velocity matrix and I is the identity matrix.

In the i^{th} iteration, the estimate x^{l+1} of the new model is given as:

$$x^{l+1} = x^l + \gamma\Delta x$$

Where γ~1and after smoothening in the vertical direction the equation will be given as:

$$(a^T a + \alpha r_v^T r_v + \varepsilon I)\Delta x = a^T y$$

In case of 2D analysis, Jacobian combines single matrices ($a_1 \sim a_k$) into an 'A' matrix.

$$A = (a_1 + a_2 + a_3 \ldots + a_k) = \begin{bmatrix} a_1 & 0 & 0 & 0 & 0 \\ 0 & a_2 & 0 & 0 & 0 \\ 0 & 0 & a_3 & 0 & 0 \\ 0 & 0 & 0 & . & 0 \\ 0 & 0 & 0 & 0 & a_k \end{bmatrix}$$

A correction matrix Δx, a residual matrix Y and vertical difference rows collectively r_v is represented as:

$$\Delta X = \Delta x_1 + \Delta x_2 + \Delta x_3 + \ldots + \Delta x_k$$

$$R_v = r_{v1} + r_{v2} + r_{v3} + \cdots r_{vk}$$

$$Y = y_1 + y_2 + y_3 + \cdots y_k$$

The simultaneous equation is solved using iterative calculation by following equation:

$$(a^T a + \alpha R_v^T R_v + \beta R_h^T R_{\mathrm{h}} + \varepsilon I)\Delta x = a^T y$$

The values for α=0.2, β= 1 and ε =1 has been used in this analysis. The flowchart showing the process of Inversion is given in Figure 2.3.

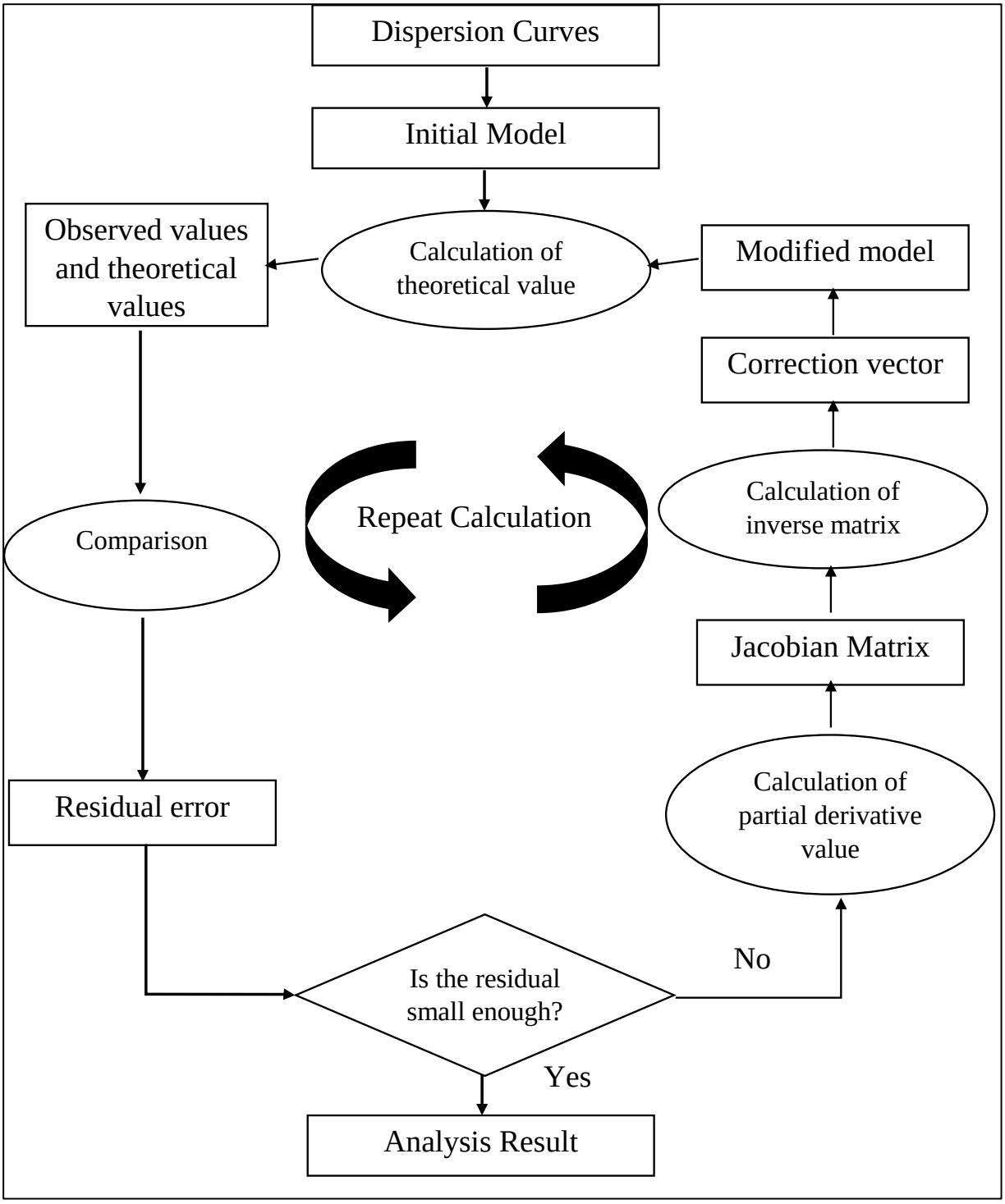

Figure 2.3.The flowchart showing the process of Inversion.

2.5 Application of MASW: Dynamic Properties of Rock

Identification and mapping of soil and rock profiles and evaluation of dynamic properties are very important part in seismic hazard, site response and microzonation studies (Anbazhagan et al., 2006). However these parameters are generally estimated using SPT (Standard Penetration Testing). Since it is difficult to carry out such tests in the hilly terrains

like Himalayas, MASW results can be useful. The results of MASW provide information about density and N- value (penetration resistance or number of blows) of the site along with shear wave velocity and P-wave velocity. Recently, this method has gained popularity because SPT is a very expensive and time consuming method as compared to MASW. Moreover, acquisition of SPT data is not readily available for tough terrains. N-values are not reported earlier in this region. Thus, the information is quite useful for soil characterization of the stations.

Table 2.1: National Earthquake Hazard Reduction Program (NEHRP) site classes (BSSC, 2003)

Site Classification	**Description**	**Average shear wave velocity up to 30 m(V_{s30}) ms^{-1}**
A	Very hard rocks	>1500
B	Rocks	$760 < V_{s30} < 1500$
C	Very hard soil and soft rock	$360 < V_{s30} < 760$ Or N > 50,Su >100 kPa
D	Hard soil (sands, clays and gravels)	$180 < V_{s30} < 360$ or 50 > N > 15,100 > Su > 50 kPa
E	Soft clay of thickness about H in site profiles	$V_{s30} < 180$ or H > 3m (PI > 20),w > 40%, Su < 25 kPa
F	Soils requiring site – specific evaluations	-
Where H: Thickness; Su: Undrained shear strength; N: Standard Penetration Test Blow count; PI: Plasticity Index; w: water content		

The MASW has been used widely for the estimation of 2D shear wave velocity structure for different regions (Bullen, 1963; Mitchell, 1973; Mooney et. al, 1966; Tsai et. al, 1969). Several Indian scientists have worked across various parts of India including Jabalpur, Delhi, Ahmedabad and Bangalore (Seshunarayana et. al, 2004; Satyam et. al, 2010; Anbazhagan et. al, 2006; Trivedi et. al, 2009). Studies have shown that a combination of active and passive MASW method gives an improved result (Ariffin et.al, 2015).

The definition of seismic bedrock or hard rock is however a matter of apprehension in ground motion microzonation studies as shown in Table 2.1. The depth of hard rock decides the overall budget of the assignment.

Commonly, the shear-wave velocity of hard rock falls within 700–800 m/s (Ishihara and Ansal 1982; ICBO 1997, 2003; BSSC 2001; BHRC 2005). However, it is recommended that

the upper crust, with a shear-wave velocity of about 3,000 m/s, be adopted as bedrock when large-scale structures with longer vibration period are being considered (Shima 1977).

Chapter – 3

DATA ACQUISITION, PROCESSING AND METHODOLOGY TO INVERT H/V CURVES

This chapter explains in detail the data used and various steps applied to process data acquired in the field. The Department of Earth Science, Indian Institute of Technology, Roorkee has deployed strong motion accelerographs at various stations under a major project sponsored by the Ministry of Earth Sciences, Government of India project. The data recorded in these accelerographs is regularly collected and processed for the research purpose.

3.1 Data Acquisition

A network of fourteen strong motion stations has been installed since 2006 by the Department of Earth Sciences, IIT Roorkee under a research project funded by the Ministry of Earth Sciences, Government of India. Many stations are moveable in nature in which recording has been carried out for continuous time. This array covers an area of 75×60 km. The minimum inter station distance between these stations is approximately 11km. This is one of the dense arrays installed in the Kumaon Himalayan region, India. Three-component force balance, accelerometer has been installed at each station.

The sites for installation of accelerographs have been selected on the basis of historical seismic activities. The historical events during 1973 to 2012 show a cluster of events between Main Central Thrust (MCT) and North Almora Thrust (NAT) in the Kumaon region as shown in Fig. 1.4 in Chapter 1. Most of the accelerographs are installed at various stations between MCT and NAT to record all earthquakes occurring in this region.

The elevation of these recording stations varies from 612 to 2239 m above MSL. Jouljibi and Munsyari have minimum and maximum elevation i.e. 612 m and 2239 m, respectively. Locations of all stations are shown in Fig 3.1. The coordinates of these recording stations along with corresponding elevations are tabulated in Table 3.1.

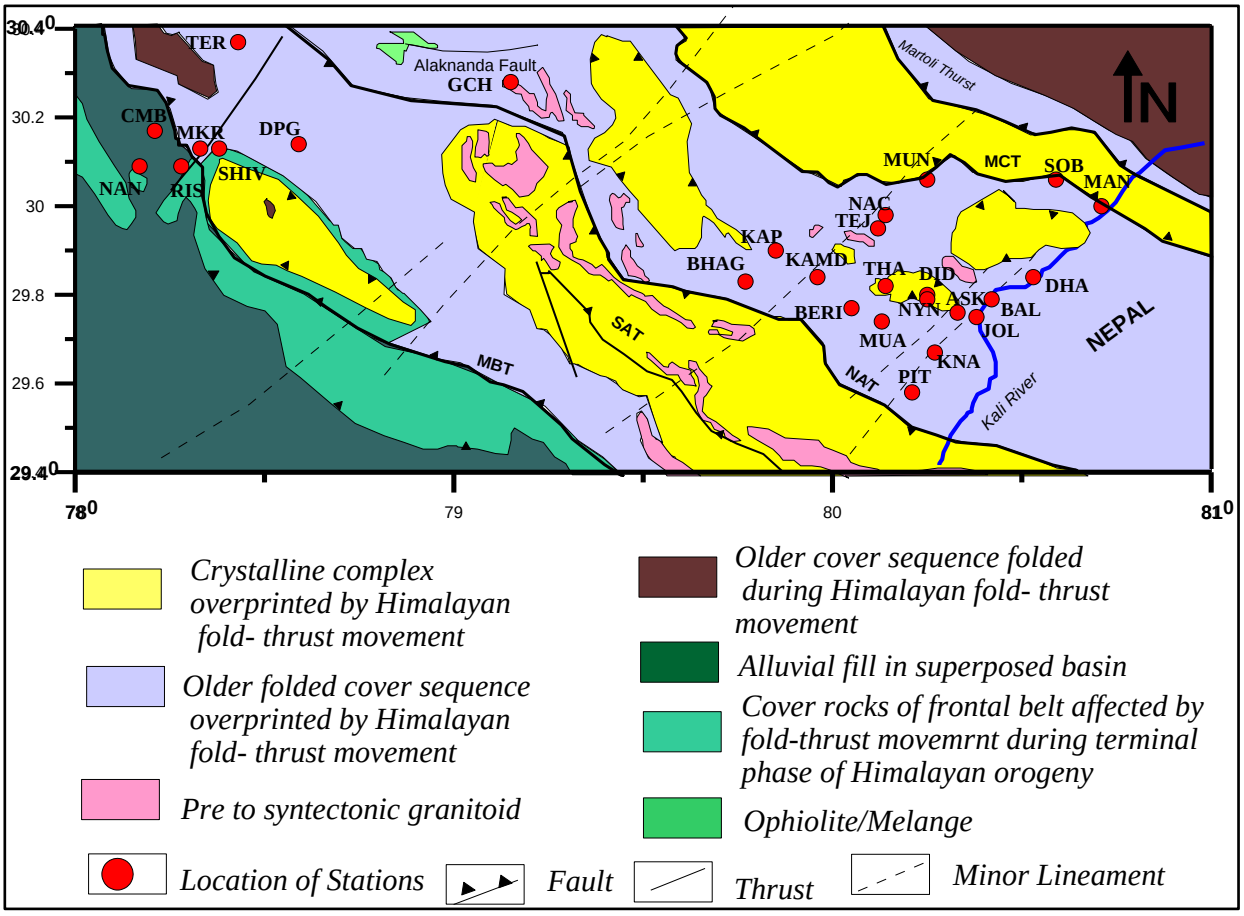

Figure 3.1: Location map of Kumaon and Garhwal Himalayas, India. MBT = Main Boundary Thrust, MCT = Main Central Thrust, SAT = South Almora Thrust, and NAT = North Almora Thrust. Red circles show the location of the stations with station codes as mentioned in Table 3.1. Source of the tectonics and geology of the region is Geological Survey of India (2000).

Ambient noise has been recorded at 27 sites and has been used in the present work. Strong motion accelerograph by Kinemetrics has been used to record these noises. The instrument used in the study has extensive range of earthquake monitoring. The data has been logged with in a resolution limit of 18 bits. The instrument has been set with a very low threshold level of 0.005% to record the small magnitude event. However, the full scale measurement is 2.5V and sensitivity is 1.25 V/g of this instrument.

Table 3.1: Locations of the stations in Kumaon and Garhwal Himalayas, India with station codes, co-ordinates and elevation from mean sea level MSL and number of noise data used in the present study.

Sr. No.	Station Name	Station Code	Latitude (Degree)	Longitude (Degree)	Elevation of the stations from MSL (meter)
1	Didihat	DID	29.80	80.25	1628
2	Pithoragarh	PIT	29.58	80.21	1574
3	Tejam	TEJ	29.95	80.12	968
4	Dharchula	DHA	29.84	80.53	935
5	Munsiari	MUN	30.06	80.25	2239
6	Askot	ASK	29.76	80.33	1258
7	Kamedidevi	KAMD	29.84	79.96	1811
8	Jouljibi	JOL	29.75	80.38	612
9	Baluakot	BAL	29.79	80.42	644
10	Knalichhina	KNA	29.67	80.27	1656
11	Muavani	MUA	29.74	80.13	822
12	Berinag	BERI	29.77	80.05	1684
13	Mangti	MAN	30.00	80.71	1609
14	Sobla	SOB	30.06	80.59	1628
15	Thal	THA	29.82	80.14	784
16	Bhageshwar	BHAG	29.83	79.77	873
17	Kapkot	KAP	29.9	79.85	1133
18	Nachni	NAC	29.98	80.14	2240
19	Narayannagar	NYN	29.79	80.25	1800
20	Rishkesh	RIS	30.09	78.28	372
21	Narendranagar	NAN	30.09	78.17	1326
22	Shivpuri	SHIV	30.13	78.38	449
23	Chamba	CMB	30.17	78.21	1524
24	Tehri	TER	30.37	78.43	1750
25	Muni ki reti	MKR	30.13	78.33	456
26	Gochar	GCH	30.28	79.15	800
27	Devprayag	DPG	30.14	78.59	830

The instrument was kept on the surface of the earth and screwed to the ground. The sampling interval of the recorded data is considered as 0.01 sec. The major components of entire accelerograph recording unit are the Sensor, Global positioning system (GPS) antenna, Solar panel, Battery and PCIMCIA card as shown in Fig. 3.2. The GPS antenna is connected through a cable to the main unit and is used to provide exact geographical locations and time in GMT. Solar panel and battery is used to supply the power backup to the accelerograph.

PCIMCIA is the memory card which is used to store the data. The strong motion accelerograh as shown in Fig 3.3 has been installed at each site. Data can be retrieved from the PCIMCIA card through a cable connected with laptop as shown in Fig 3.4.

Due to low threshold level, recording instruments have recorded microtremors together with seismic events occurring in the surrounding region. There is a huge database of microtremors at each station which has been used in the present work which includes 248 strong ground motion records and 427 ambient noise records.

The recorded noises (electric signals) have to be corrected and homogenized to same signal length eliminating some pre-identified unwanted signals (e.g.: high frequency and low amplitude wind noise).These corrected and homogenized raw data has been processed to obtain Fourier spectra. These were then used to calculate H/V spectral plots using Nakamura's technique (Nakamura, 1989; Lachet and Bard, 1994; Kudo, 1995; Bard, 1998). These calculated H/V response has been used to obtain 1-D velocity structure at each station using Haskell shear wave transfer function and genetic algorithm (Kuo et al. 2009, 2011).

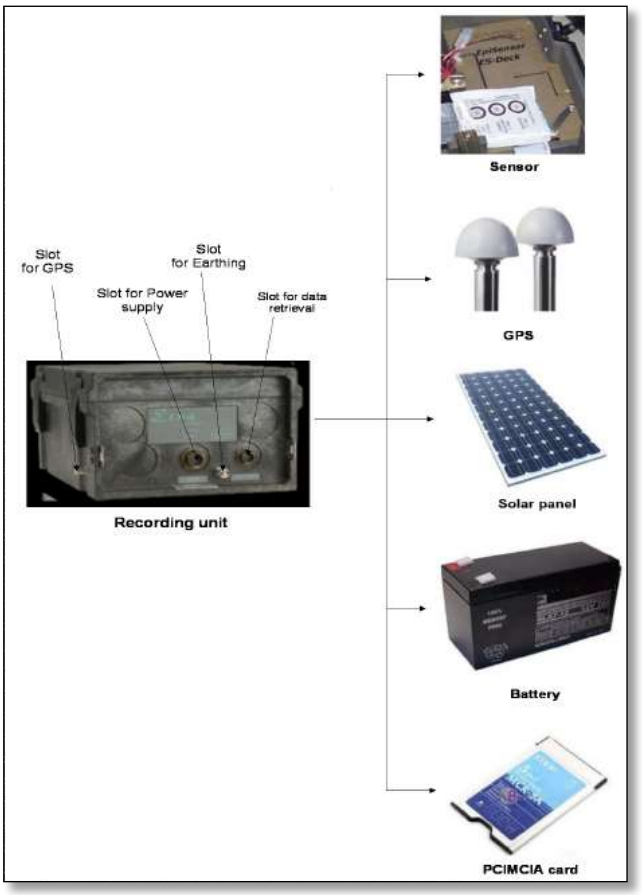

Figure 3.2: Various components of Strong motion accelerograph of Kinemetrics, U.S.A. installed at each site.

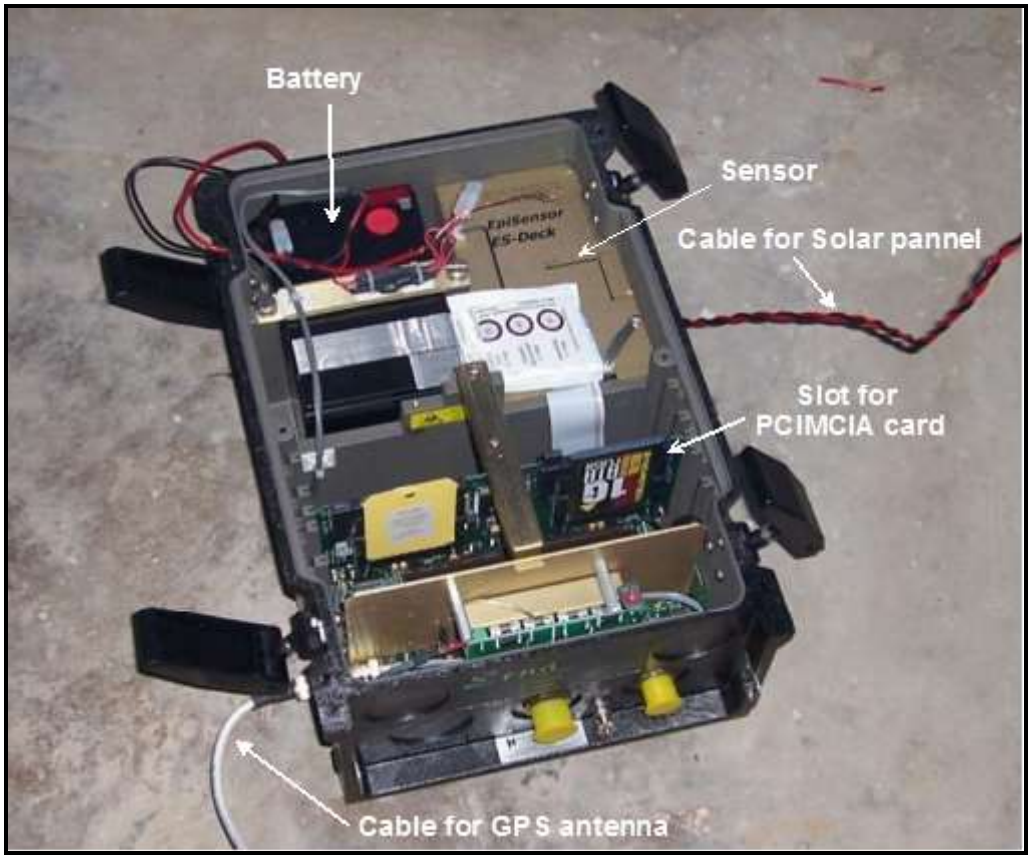

Figure 3.3: Strong motion accelerograph of Kinemetrics, U.S.A. installed at each site.

Figure 3.4: Obtaining the recorded data from accelerograph using laptop.

3.2 Data Processing

Data processing has been divided into three major steps. These steps have been summed up in the flowchart as shown in Fig. 3.5.

STEP 1: Computation of three components

For the computation of H/V ratio the noise data recorded at various sites of Kumaon and Garhwal Himalayas has been used. The raw data has been collected from various sites in .EVT file format. To convert the raw data into ASCII format KW2ASC.EXE application has been used. After extraction of ASCII files, the files with extension .001, .002 and .003 file are generated which represent the North-South (NS), East-West (EW) and vertical components, respectively. This data is in time domain. These three components are used for further processing and calculation of HVSR (Horizontal – Vertical Spectral ratio). A sample three component of an accelerogram recorded at Askot station is shown in Fig. 3.6.

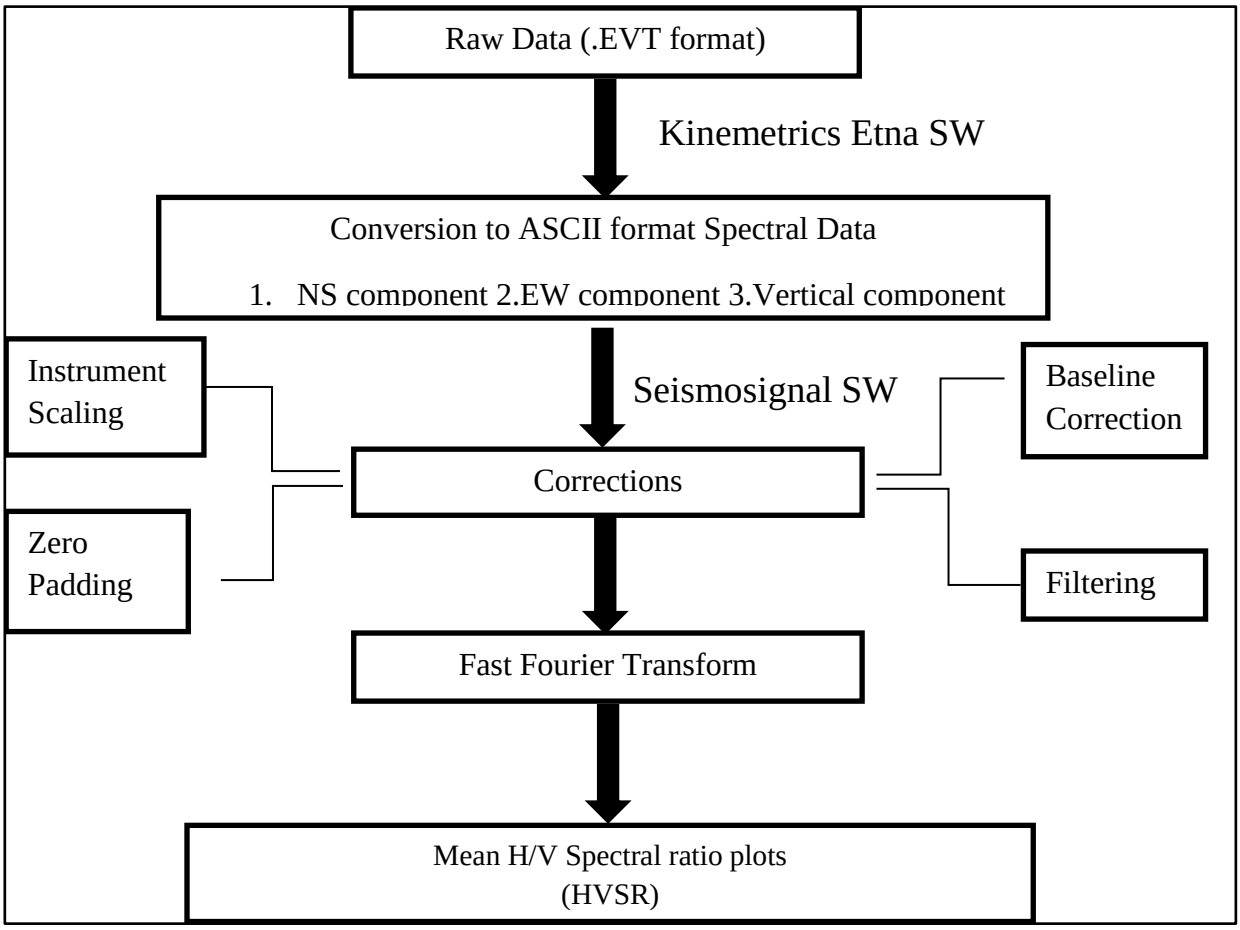

Figure 3.5: Schematic Flowchart explaining processing steps.

STEP 2: Corrections

Before converting the recoded data from time domain to frequency domain, it has to be corrected. The data processing involves various corrections as follows:

3.2.1 Instrument Scaling

Kinemetrics Etna records data in millivolts which has to be converted into acceleration records as the first correction. Instrument scaling is 1.25 V/g or 784 cms^{-2} which is the scaling

factor for the given instrument. Maximum acceleration that the instrument can record was 2.5Vand the range of sensitivity is +/-2g. The threshold value is 0.5% of this value i.e. 0.0125V.

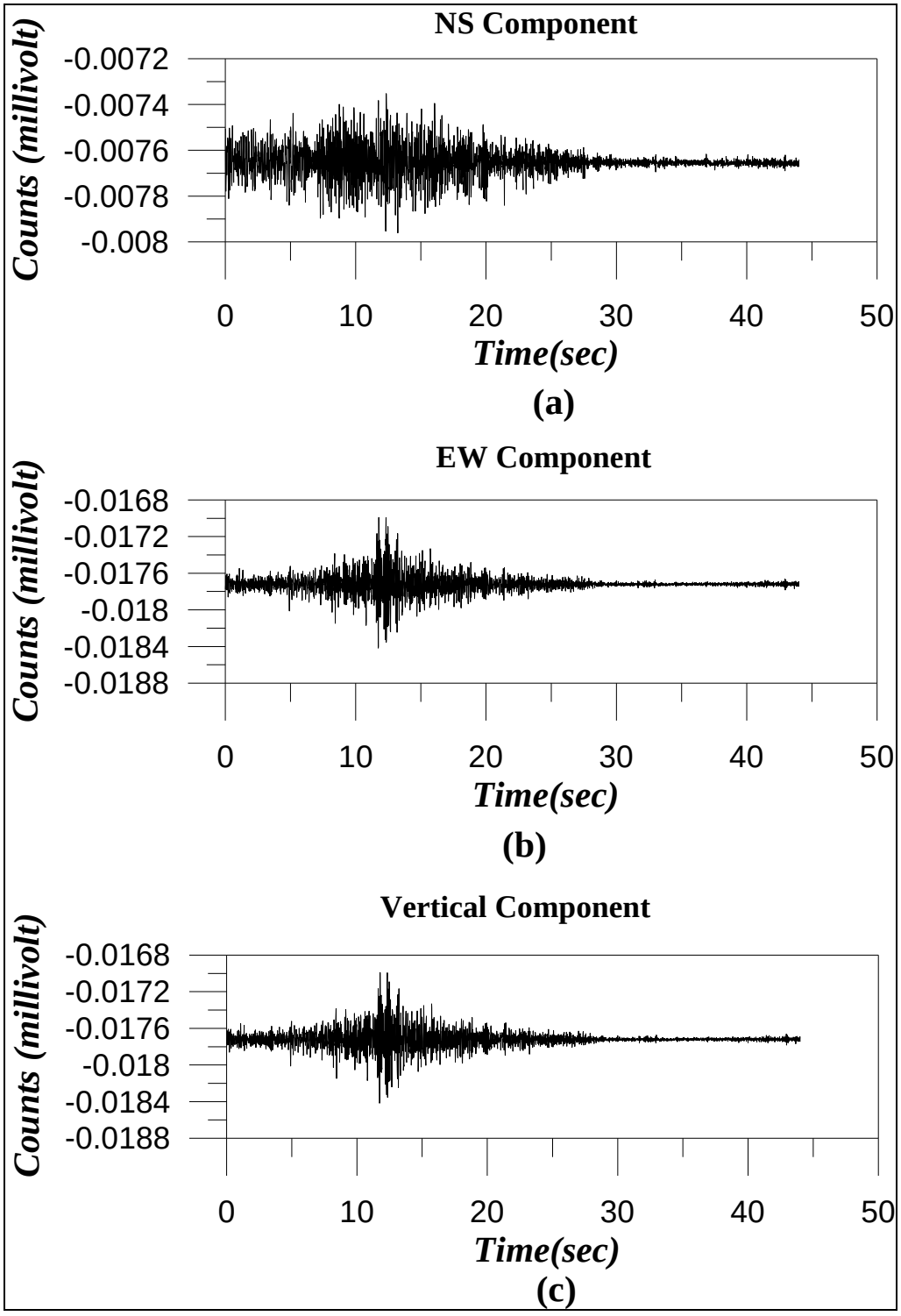

Figure 3.6: Raw record showing three components at Askot station. The event data 04/07/10

3.2.2 Baseline Correction

Determination of zero baseline of accelerogram is most crucial corrections. It requires subtracting of straight line from the input of time series. The line can be linear least square fit to the mean value of time series. Mean is calculated by considering the portion of record prior to P wave and in case of absence of pre event entire record can be used. It is further illustrated with an example in Fig 3.7.

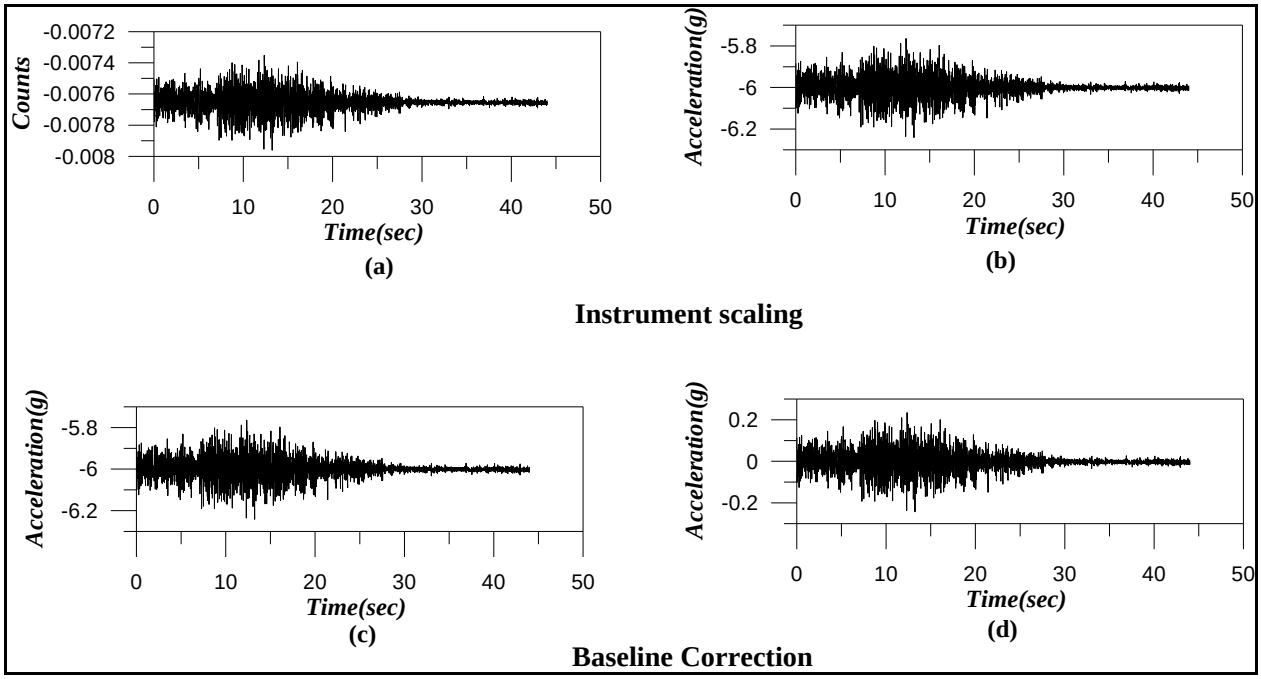

Figure 3.7: Example of instrument Scaling and Baseline correction for N-S component recorded at Askot station (a) Without instrument correction (b) With instrument correction (c) With instrument correction and without baseline correction (d) With instrument correction and baseline correction.

3.2.3 Zero Padding

Zero padding is applied before low cut frequency filtering. It extends both the leading and trailing ends of the time series in order to accommodate the filter transient. Impact of insufficient padding can be seen from long period departure of acceleration records from zero.

3.2.4 Filtering

Data contained vibrations with wide range of frequencies. High frequency wind noise which is large enough to cross the threshold of instrument is removed along with low frequency undulations using appropriate filter. Corner frequency of 80% of sampling rate has been

employed as suggested by Shakal et al (2004) for selecting band pass frequency Butterworth filter of 4th order.

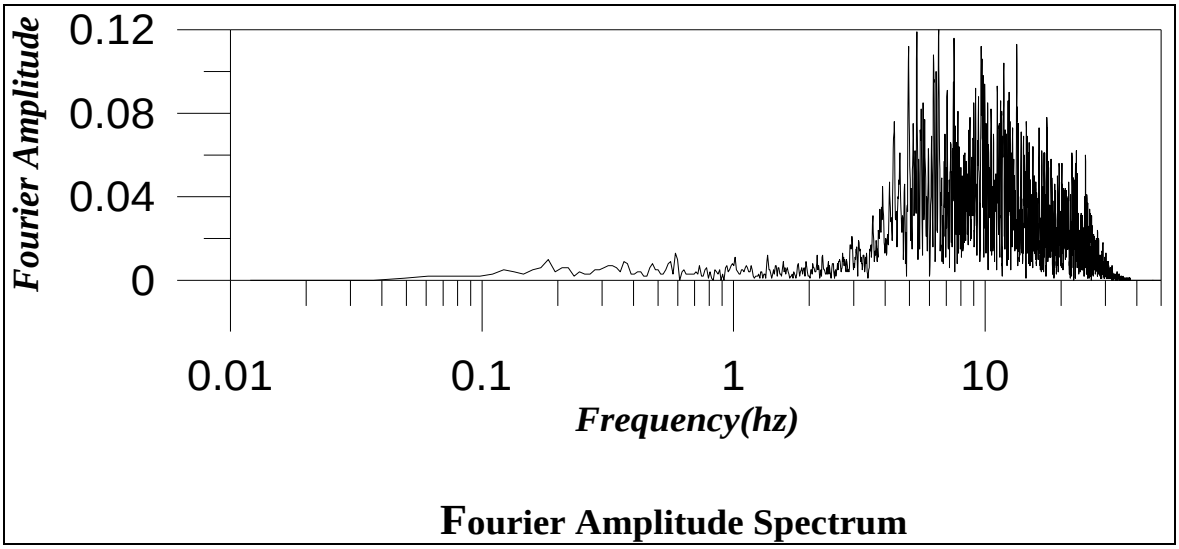

Figure 3.8: Fourier Amplitude Spectrum computed by means of Fast Fourier Transformation (FFT) for N-S component after processing at Askot station.

After obtaining corrected time series, records for all three components of noises at each stations, are transformed into frequency domain. Fig 3.8 shows Fourier Amplitude Spectrum which has been processed using band pass frequency Butterworth filter of 4^{th} order within frequency range of Freq1=0.10 Hz and Freq2=25 Hz. The spectra for a record at Askot station is shown in the Fig 3.8.

STEP 3: HVSR computation or Nakamura's Technique

The HVSR technique or more commonly known as Nakamura's technique was first proposed by the Nogoshi and Igarashi (1971). They compared the Horizontal to Vertical ratio (H/V) of the Rayleigh waves and the Love waves with that of microtremors (ambient noises) and concluded that ambient noises are mostly composed of the Rayleigh and Love waves. Later, this technique was popularized by the Nakamura (Nakamura, 1989). This technique uses the argument that the vertical component of ambient noise is relatively uninfluenced by a soft sediment layer overlaying a half space.

The average of HVSR spectra is computed by following equation:

$$\frac{\mathrm{H}}{\mathrm{V}} = \frac{(\mathrm{H}_1/\mathrm{V} + \mathrm{H}_2/\mathrm{V})}{2}$$

Where $\mathrm{H}_1$and H_2 are NS and EW spectra respectively.

In this technique Horizontal to Vertical spectral ratios in which NS spectra and EW spectra are divided with the vertical spectra are obtained as explained in Fig. 3.9.

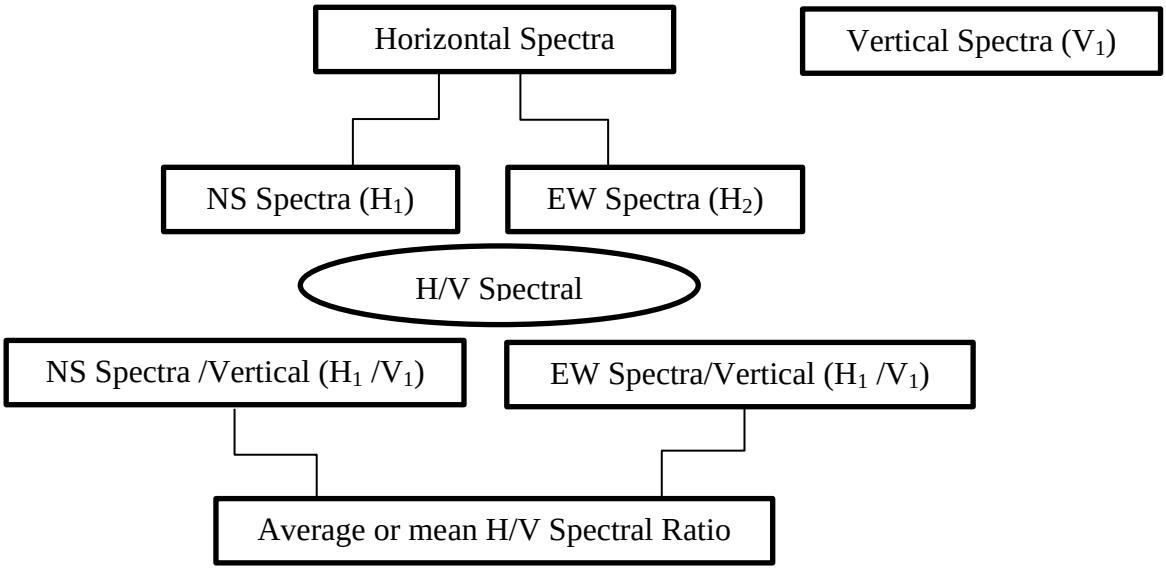

Figure 3.9: Flowchart explaining HVSR computation

This computation is done for all the ambient noises as well as strong ground motion records at every station. All these records are recorded at each station are then plotted on a single plot to observe correlation in predominant frequencies and spectra in general. All the plots are later shown in Chapter 5. As an example, mean H/V along with the individual H/V selected for computation of Askot station is shown in Fig 3.10.

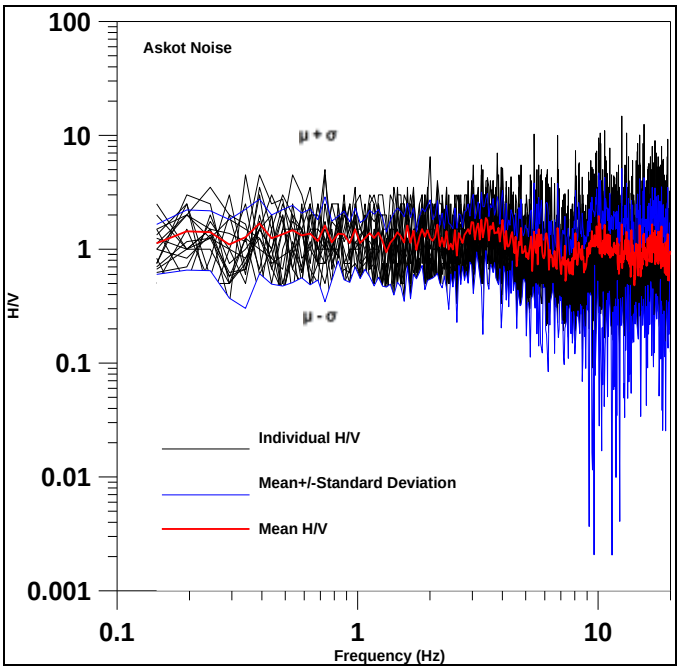

Figure 3.10: Mean H/V ratios and corresponding selected representative H/V curves for Askot station.

Nakamura disproved earlier theories of Nogoshi and Igarashi (1971), Lachet and Bard (1994), Konno and Ohmachi (1998), and Bard (1998) described that the peaks of H/V spectra curves can be explained by fundamental modes of Rayleigh waves. In this approach, the ambient noises are interpreted as Rayleigh and Love waves propagating in a single layer. Hence, the theory removes the effects of Rayleigh waves as noise by H/V process.The ambient noises can be modeled using the Haskell method (Haskell, 1960). The assumption is that the values of H/V would be unity in spite of wide range of frequencies. This technique is also known as Quasi Transfer Spectra which can be defined by following equation (Nakamura, 2000):

$$QTS = \frac{H_f}{V_f} = \frac{A_h * H_b + H_s}{A_v * V_b + V_s} = \frac{H_b}{V_b} \cdot \frac{\left[A_h + \frac{H_s}{H_b}\right]}{\left[A_v + \frac{V_s}{V_b}\right]} \qquad (3.1)$$

Where, QTS is Quasi Transfer Spectra, H_f and V_f are horizontal and vertical spectra at surface, A_h and A_v are amplification of horizontal and vertical component of vertically incident body wave, H_b and V_b are horizontal and vertical spectra at the basement and H_s and V_s are horizontal and vertical spectra of Rayleigh waves. The assumed geological structure is shown in the following Fig. 3.11.

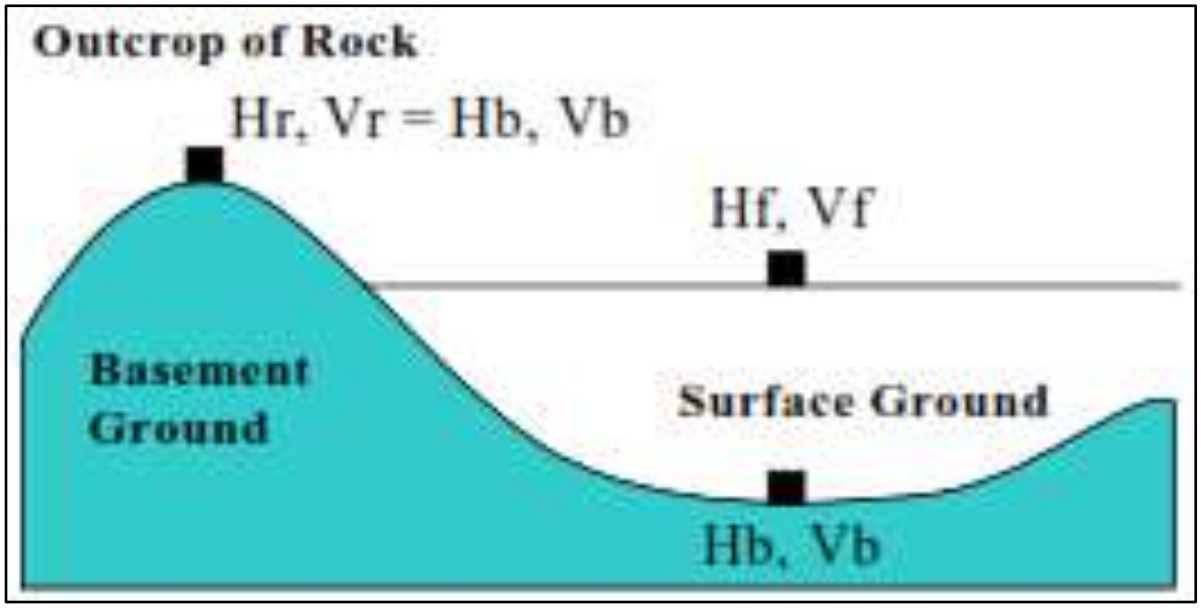

Figure 3.11: Theoretical geological structure (Nakamura, 2000)

Assuming $\frac{H_b}{V_b} = 1$ i.e. no effect of Rayleigh wave, $QTS = \frac{A_h}{A_v}$ which is site amplification.

If the influence of Rayleigh waves is taken into account, small value of V_s amounting to peak in H/V plot will which is due to multiple reflections of horizontal motions and Quasi Transfer Spectra that can be defined as:

$$QTS = A_h$$

Since, $A_v = 1$ in the vicinity of lowest proper frequency. Hence, it can be concluded that if microtemors are composed of both body and Rayleigh waves, amplification factor represented by H/V ratio (QTS) of recorded ambient noise data can be correctly estimate by considering first order proper frequency by multiple refractions of SH waves. Lermo and Chavez-Garcia (1993), Lachet and Bard (1994), Ibs-von Seht and Wohlenberg, (1999), Fäh et al (2001) later building upon this theory illustrated that the analysis of the H/V spectra curves of the microtremor allows us to measure the principal shear wave resonance frequency f of the sedimentary cover overlying infinite bedrock with a reasonable accuracy.

This relation can be modified for multi layered model of the earth; predominant frequency is governed by the shear wave structure of the foundation. The average shear wave velocity is obtained by following formula (Swada, 2004):

$$\frac{h}{\beta_s} = \frac{h_1}{\beta_{s1}} + \frac{h_2}{\beta_{s2}} + \frac{h_3}{\beta_{s3}} + \cdots + \frac{h_n}{\beta_{sn}} \qquad (3.2)$$

Where h_n is the thickness of n_{th} layer and β_{sn} is the shear velocity of n_{th} layer. Assuming predominant frequency is linked to the thickness h and the average shear wave velocity (β) of the sedimentary layer by the following ¼ wavelength relation (Nakamura, 2000; Swada, 2004; Castellaro S., 2016):

$$F_p = \frac{\beta}{4h} \qquad (3.3)$$

Where, F_p = Predominant frequency of the sedimentary layer

β = Shear wave velocity

h = Thickness of layer

Amplitude factor (A) related to this predominant frequency is related with the impedance ratio of the two layers. Considering equal densities for both basement and surface, A can be written as (Nakamura, 2000):

$$A = \frac{\beta_{sb}}{\beta_{ss}} \qquad (3.4)$$

Where, β_{sb} and β_{ss} are shear wave velocity at basement and surface layer, respectively. Thus, the layer thickness or the depth of basement can be estimated using following relation (Nakamura, 2000):

$$h = \frac{V_b}{4AF_p} \qquad (3.5)$$

It can be concluded from the above, that though this procedure sounds good but for modelling of amplification and realistic analysis, topography, lithology, local geology, seismo-tectonic models geo- technical and paleo- seismology are needed to provide a better and much more exact analysis. Some exploration techniques exist to obtain the shear wave velocity structure but in environmental sensitive areas it is not feasible to implement conventional seismic methods. Microtremor Array Measurement (MAM) is a recent technique to overcome this difficulty. This method makes use of microtremors, which is found in abundance in the surface of earth (Setiawan, 2016). It is very important to obtain the shear velocity structure of surface geology for H/V ratio technique.

Nakamura theory was primarily criticized because the assumption and results obtained were not validated especially in case of deep and complicated soft layered column by using a much simple layer. It can only determine the natural frequency of soft layer but it fails to provide the amplification case of surface waves.

3.3. Haskell Method

The Haskell Method is based on the SH-wave transfer function of the Haskell-Thompson matrix (Haskell, 1960). The H/V ratios obtained using these transfer function matches with the HV ratios calculated from the recorded ambient noises. Thus, these transfer function are highly suitable to model the H/V spectral ratios of the ambient noises recorded from both the passive and active seismic sources.

The relationship between the amplitude of the reflected and incident plane body waves of transverse and longitudinal type and the displacement of the free surface is available in the literature. As applied to the reflection of the seismic surface waves at the surface of the earth these relations only holds valid for wavelengths that are very long compared with the total thickness of the crustal layers. Explicit expressions for these quantities may be readily derived

in terms of the Thompson matrices for a crust composed of any number of horizontal, homogeneous layers.

However, in the case of incident P and S waves, numerical computations, covering all angles of incidence and a sufficiently wide range of periods to be of interest, would be too lengthy to be practicable except by high-speed machine methods, even for the simplest case of a single-layered crust. For a single layered crust, the computations involved are trivial because it becomes a simple case of incident wave as there is no coupling between different wave types. This simple case serves as the guide for the more complex cases and computations. SH wave propagation in n layered media is shown in Fig 3.12. The numbering of the sequence is from the free surface to the downwards and the use of the subscripts is made to denote the quantity for the particular layer in the subsurface.

Let,

ϑ'_n = displacement of the downward travelling SH waves in n^{th} layer

ϑ''_n = displacement amplitude of the upward travelling SH waves in n^{th} layer

ϑ_0= displacement amplitude at the free surface.

μ = shear modulus

ρ = density

$\beta = (\mu/\rho)^{1/2}$ = transverse wave velocity

h = layer thickness

$\mathcal{P}$= 2Πf =radian frequency

c = horizontal phase velocity

$k = \frac{\mathcal{P}}{c} = \frac{2\Pi}{\text{Wavelength}}$ (Horizontal)

$$R_\beta = \left[\left(\frac{c}{\beta}\right)^2 - 1\right]^{\frac{1}{2}}$$

$$Q = khR_\beta$$

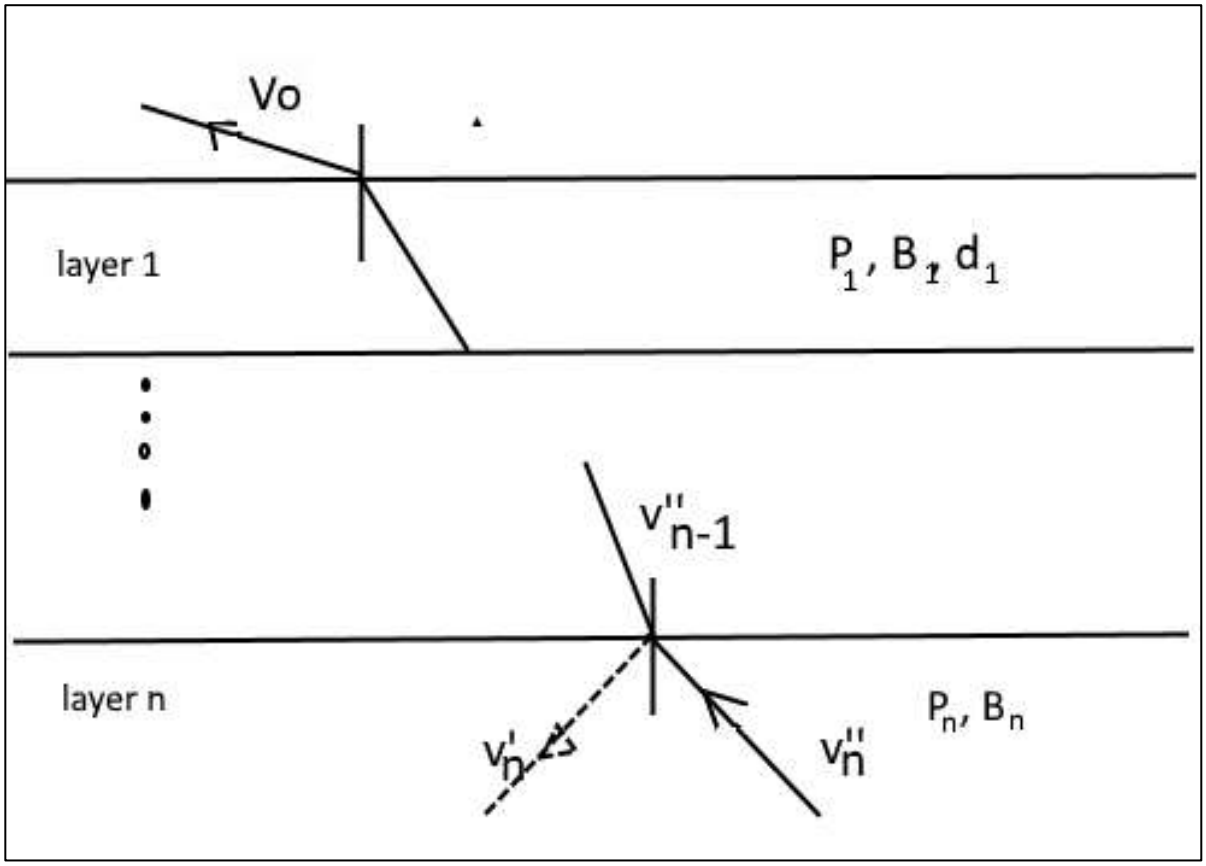

Figure 3.12: SH wave propagation in n layered media

According to the Snell's law the phase velocity, c, is related to the incident angles, $i_{m,}$ in various layers.

$$c = \beta_1 \csc i_1 = \beta_2 \csc i_2 = \cdots \ldots = \beta_n \csc i_n \quad (3.6)$$

Equating the transverse shear stress at free surface to zero (Haskell et. al. 1953):

$$\vartheta'_n + \vartheta''_n = A_{11}\vartheta_0 \quad (3.7)$$

$$\vartheta''_n - \vartheta'_n = \frac{A_{21}\vartheta_0}{\mu_n R_{\beta n}} \quad (3.8)$$

Where, A's are the elements of 2x2 matrix formed by taking product i.e. $A = a_{n-1} * a_{n-2} \ldots\ldots a_2 * a_1$, of the matrices a_m is given by:

$$a_m = \begin{bmatrix} \cos Q_m & i\mu_m^{-1} R_{\beta m}^{-1} \sin Q_m \\ i\mu_m R_{\beta m} \sin Q_m & \cos Q_m \end{bmatrix} \quad (3.9)$$

Now evaluating the ratio of amplitude of the reflected wave (ϑ_n') with that of incident wave (ϑ_n'') and of amplitude surface wave (ϑ_0') with the amplitude of incident wave following expression is obtained:

$$\frac{\vartheta_n'}{\vartheta_n''} = \frac{\mu R_{\beta n} A_{11} - A_{21}}{\mu R_{\beta n} A_{11} + A_{21}} \qquad (3.10)$$

$$\frac{\vartheta_0'}{\vartheta_n''} = \frac{2\mu_n R_{\beta n}}{\mu_n R_{\beta n} A_{11} + A_{21}} \qquad (3.11)$$

Amplitude of reflected and incident wave will be same as numerator and denominator of RHS of the equation and complex conjugate, as law of reflection says. For the two layer case, elements of the matrix will be:

$$A_{11} = \cos Q_1$$
$$A_{21} = i\mu_1 R_{\beta 1} \sin Q_1$$
$$n = 2$$

Then, equations 3.10 and 3.11 will be:

$$\frac{\vartheta_2'}{\vartheta_2''} = \frac{\cos Q_1 - ib\ \sin Q_1}{\cos Q_1 + ib\ \sin Q_1}$$
$$\frac{\vartheta_0'}{\vartheta_2''} = \frac{2}{\cos Q_1 + ib\ \sin Q_1}$$

Where $b(c) = \frac{\mu_1 R_{\beta 1}}{\mu_2 R_{\beta 2}}$

If we assume, c_1 as the phase velocity when b = 1 and use $R_\beta = ((c/\beta)^2 - 1)^{1/2}$, then

$$c_1^2 = \frac{\rho_2{}^2 \beta_2{}^4 - \rho_1{}^2 \beta_1{}^4}{\rho_2{}^2 \beta_2{}^2 - \rho_1{}^2 \beta_1{}^2} \qquad (3.12)$$

It can be seen that for two layer model, absolute value of V_0 as a function of frequency depends on whether b is less than (i.e. $c > c_1$) or greater than (i.e. $c < c_1$) unity. When $c > c_1$, $b<1$ comes out that in this case maximum value of $|\frac{\vartheta_0'}{\vartheta_2''}|$i.e. at the peaks is 2/b.

Hence, the ratio of amplitude of surface ground motion to the amplitude of incident SH wave is dependent on frequency, model parameters (thickness, SH wave velocity, density) of each layer. The transfer function of normally incident SH waves can be given as:

$$\frac{H}{V} = f(freq, \rho, \beta, \sigma, h, \theta)$$

This presents the solution for the SH waves. Since, SH wave will always be at normal incidence (i.e. $\theta = 0^o$) and σ is assumed to be constant. The parameters ρ, β and h are the model parameters.

This present study connects the theory propagated by Nakamura in 1989 and mathematical relation established by Haskell shear wave transfer function to evaluate model parameters of layered earth by using Genetic Algorithm.

3.4 Genetic Algorithm

3.4.1 Genetic Search

Optimization Algorithms finds the best solution out of the available solutions, based on some criteria. Rather than finding the exact solution they search for the best feasible solution. Most of the geophysical problems are non –linear in nature. Various methods including Monte Carlo, Gaussian- Newton, Simulation Annealing and Genetic Algorithm (GA) etc. are used for solving non - linear inverse problems. Unlike a pure random search, such as in a "Monte Carlo" method, the search used in GA is not directionless (Stoffa et. al, 1991). The GA search gives a controlled environment to the randomness. Hence, GA is a powerful tool as compared to other normal exhaustive and random search. GA search makes itself distinctive from other algorithms as it is applicable to those problems also which lack the linearity, continuity and derivative features.

GA is originated from Darwin's theory of evolution. The biological evolution of an individual always follows the survival of the fittest. This involves the evolution of the species from low to high optimization and then search for the best solution to any mathematical problem. The "fittest" (best) model out of the numerous available models that reproduces some measured properties of the empirical observations with least deviation is desired and searched.

Initially a model group having population of N member (equivalent to a biological population) is randomly generated as the initial model set. The model parameters of these model groups are coded into binary codes as the chromosomes of these members. A new generation of models is produced by applying the GA operators namely - selection, crossover and mutation on the current generation. The above process is repeated until the model population eventually evolves to the global optimal solution. Two key features of the GA are fitness score estimation and genetic reproduction method.

3.4.2 Initial model generation

. An initial model i.e. an input file is required for defining the parameters of populations to start with. To ensure gene diversity, a random selection of initial model group is generated.

3.4.3 Model Selection

In order to generate a new generation of models, a better individual is chosen to match. This election of a better individual is known as the model selection. GA starts with the randomly selected initial generation of models (velocity models in our case), each of which represents a possible solution. The synthetic data corresponding to each model is compared with the observed data.

In addition, a fitness function was used for each individual in the GA search selection. A fitness function should be able to determine how a model interprets the observed data. An individual with a larger fitness value has a higher probability of being included in the subsequent generation, thus ensuring good genes are easily transmitted. A root mean square error (E(m)) type of fitness function (Lin et al., 2009) given by the following equation is used:

$$E(m_i) = \sqrt{\frac{1}{N}\left(\sum_{i=1}^{N}\left(V_i^{obs} - V_i^{syn}\right)\right)^2} \qquad (3.13)$$

where N is the number of observed phase velocities; V^{obs} and V^{syn} are the i^{th} observed and synthetic phase velocities, respectively. The fitness function $F(m_i)$ is therefore defined as (Lin et al., 2009):

$$F(m_i) = 1 - E(m_i) \qquad (3.14)$$

and takes a value between 0 and 1, where 1 corresponds to a perfect model.

The objective or fitness function to optimize the problem used here is given as following (Stoffa, 1991):

$$P_s(m_i) = \frac{F(m_i)}{\sum_i F(m_i)} \qquad (3.15)$$

Where $P_s(m_i)$ is the probability of selection the i^{th} model, and

$F(m_i)$ is the fitness model of the i^{th} model m_i.

The GA operator is applied in such a manner that the new generation of models will at least have either same or greater average fitness score as compared to the older generations. This process of reproduction continues generation after generation, until either a required fitness score is achieved or the whole generation becomes homogeneous. At the end, each model of the final generation gives almost the same fitness score.

3.4.4 Tournament Selection

This method [e.g., Goldberg and Deb, 1991] simulates the competition that exists in nature among individuals for the right to mate. In the simplest inversion of the method, random pairs are selected from a population of, say n, individuals and their fitness values are computed. This fitness is compared and one of the two models is accepted on the basis of the tournament selection. Better models are favored. This procedure is repeated until there are n models in the offspring population. This number is an adjustable parameter. The selection can also be called regeneration, and its main role is to select the excellent individual model (higher fitness) of the parent from the model population. These individuals will be manipulated by crossover, mutation and other genetic operations as explained in upcoming steps.

3.4.5 Model breeding

The pairing of parent model at the chromosome level to produce the new set of chromosomes is called model breeding. This process consists of three genetic operations, namely, exchange, mutation and renewal.

3.4.6 Exchange operation (Crossover)

The exchange operation plays an important global search function in the genetic algorithm, which is one of the core operations of the genetic algorithm. Effective exchange strategy can guarantee the efficiency and quality of GA search. A schematic diagram of the exchange operation in case of binary coding scheme of single point crossover and uniform crossover is shown in Fig 3.13 and 3.14 respectively.

Single point Crossover

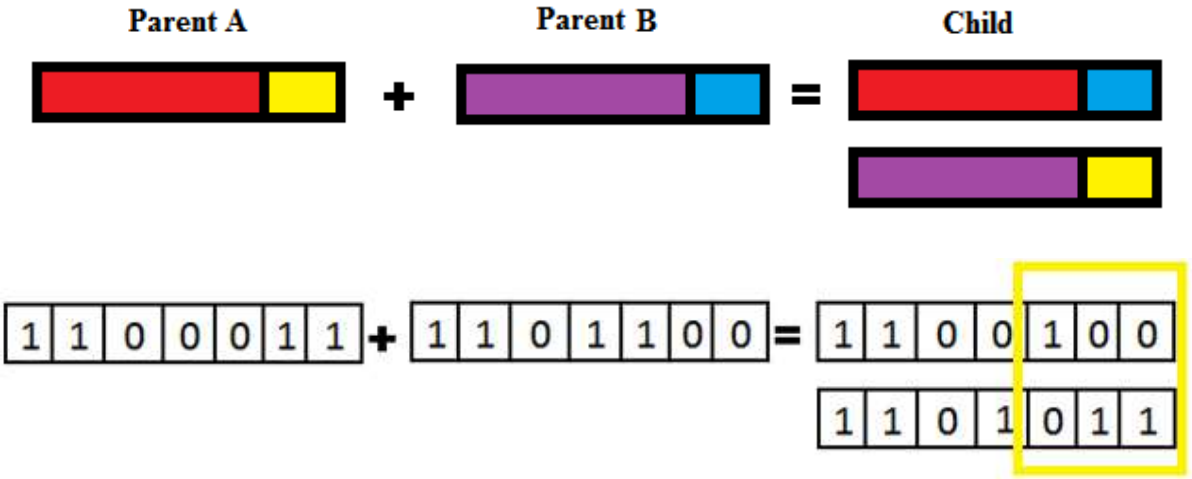

Figure 3.13: Schematic diagram of Single point crossover

Uniform Crossover

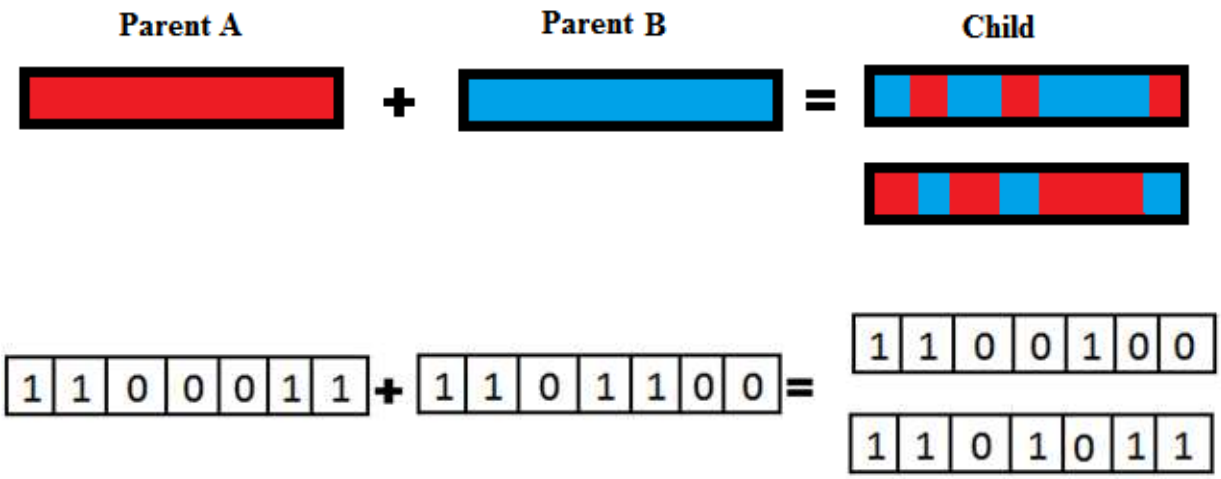

Figure 3.14: Schematic diagram of Uniform crossover

3.4.7. Mutation

Mutation is carried out to maintain diversity in population. This protects the algorithm against getting stuck at a local optimum instead of searching global optimum. The process is explained in Fig 3.15.

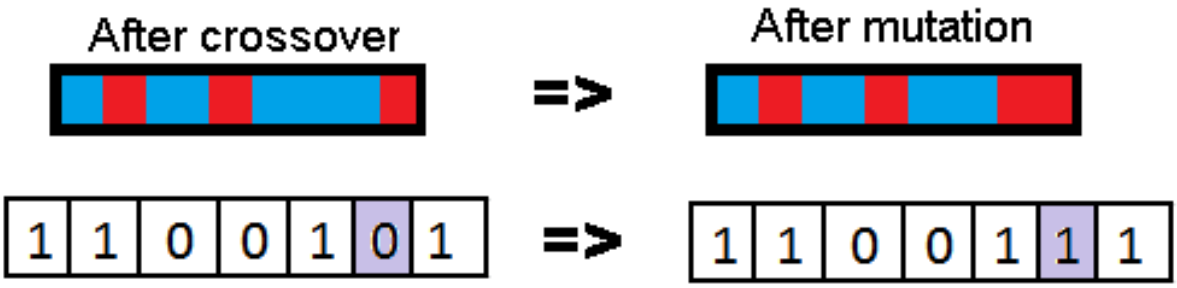

Figure 3.15: Schematic diagram of Mutation

In this study, a model with nine layers covering a half space is assumed for the GA search for two unknown parameters, S-wave velocity and layer thickness. P-wave velocities and the layer densities were determined on the basis of a simple relation with the S-wave velocities. In order to implement GA in the present study, the size of the population for the Generation 1 is considered as 100. The maximum 1000 generations have been produced to estimate the velocity structure of Kumaon and Garhwal Himalayas.

To increase the variety of optimal solutions, a complete GA process at a site included 6 single GA searches. Consequently, the total number of repetitions was 600,000 for one complete forward modeling. The probability of crossover was kept as 0.6. A probability of 0.01 has been found to be adequate for mutation purpose. In this case, GA searches also involved elite selection and tournament selection for improving competence and escaping early local convergence. The fitness of the most of the results of all sites are greater than 0.80. Sixth chapter gives a detailed illustration of the generated velocity models.

Application of GA for the estimation of two unknown parameters, i.e. Shear wave velocity and layer thickness, is as follows:

1. Generate the first generation (population): The size of the population for the Generation 1 is considered as 100.
2. Assign the fitness score to each model.
3. Calculate the probability of selection for each model using equation 3.15.
4. Assemble the models in relation to fitness score and accept the best model.
5. Select the two parent models and reproduce two child models by applying crossover (with probability 0.6) and mutation (with probability 0.01) operators.

6. Go to step 2, and repeat the procedure until entire population turn into homogeneous, i.e. as soon as each model of the population provides nearly similar fitness score. At this step, the average fitness score of the population will be almost equal to that of the highest model.
7. The highest model of the last generation will be the best model to continue.

Chapter – 4

2D SHEAR WAVE VELOCITY IN THE KUMAON AND GARHWAL HIMALAYAS USING MASW

The Kumaon and Garhwal Himalayas lie in the state of Uttarakhand, India. It falls in the seismic zone IV and V, as per the Seismic Zoning map of India (BIS, 2002). The main driving force that causes high seismic activity in this region is under thrusting of the Indian plate beneath the Himalaya. Robust wraps and recurrence of many former faults and thrusts during Quaternary are evident in this region. It falls between the Eurasian plate and Indo-Australian plate, where the stress is constantly getting accumulated. The Zonation map of India and Uttarakhand as shown in Figure 4.1 (National Disaster Management Authority) gives the distribution of Uttarakhand's major cites falling in Zone V and IV.

This chapter explains a brief about the geology and tectonics of the study area followed by the detailed discussion on data acquisition, processing and interpretation of the recorded data in the Kumaon and Garhwal Himalayas using MASW. The final outcomes of the method are 2D shear wave velocity profiles (V_{S30}) and the approximate bedrock thickness near surface 30 m. Geology of the stations considered in the present work has been correlated with the results obtained.

In MASW, the dispersive characteristics of Rayleigh waves are used for imaging the layers in the shallow-subsurface. The reliability of this method depends on the accuracy with which phase velocities were determined for Rayleigh waves traveling in horizontal direction. Due to multiple channel recordings, this method becomes very efficient. In multiple channel recordings, Signal by noise (S/N) ratio is enhanced as noise is reduced.

4.1. Geology and Tectonics of the Study area

Himalaya is the youngest chain of mountains in the world made up of sedimentary and metamorphic rocks formed due to collision of Indian and Eurasian plate which is continuously in the stage of movement and uplift. It is an arcuate shaped, synclinal range having length of approximately 2400 km from North-Northwest to East-Southeast. The movement in these plates resulting into earthquakes makes this region as geologically and as well as seismically active. The area of study lies in Northwest Himalayas. In Uttrakhand, Northwest Himalayan belt is known as Kumaon and Garhwal Himalaya. Lithotectonically, the Himalayan can be

divided into six major zones Trans-Himalayan batholith, Indus –Tsangpo suture zone, Tehthyan Himalayan, Greater Himalayan, Lower Himalayan and Sub-Himalayan (Sorkhabi,1999). Geological sketch map of the Himalaya modified after Sorkhabi, 1999 is shown in Figure 4.2.

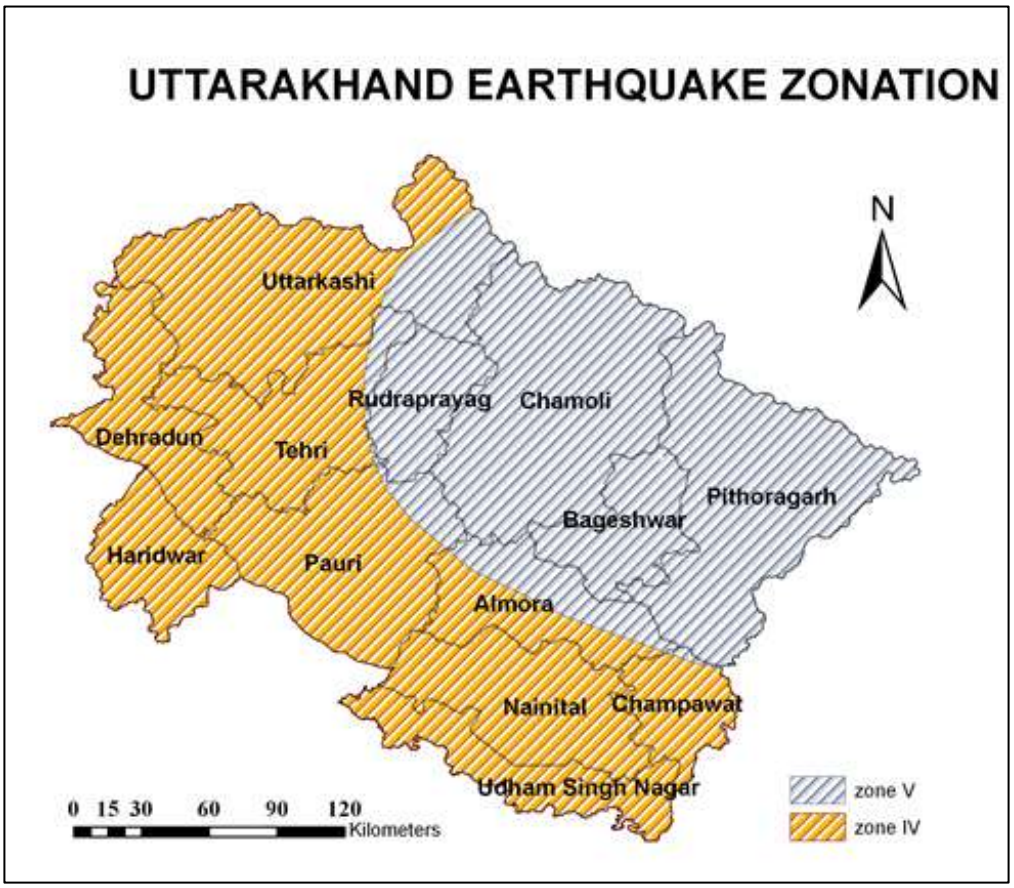

Figure 4.1: The Zonation map of Uttarakhand given by National Disaster Management Authority (Source www.ndma.gov.in)

1. **Trans –Himalayan batholith-** It is a linear complex covered by continental sedimentary rocks and fore arc rocks. The assemblage of these rocks has divided Trans-Himalayan batholith into Western Trans-Himalayan and Eastern Trans-Himalayan.
2. **Indus-Tsangpo suture zone (ITSZ)-**It mainly demarcates the zone along which the process of subduction of Tethys Himalayan takes place. A regime of high pressure was created all along this zone so mostly ophiolitic rocks are found in this suture zone.
3. **Tethyan Himalayan-**Tethyan or Tibetan Himalayan is situated in the south of ITSZ consist of marine sediments mostly formed on the surface of continental shelf and continental slope.

4. **Greater Himalayan**-The Greater Himalayan or Higher Himalayan units forms the topographical highest relief in the Himalayan region. It is somewhere also known as Central crystalline zone which has undergone multiphase deformation.

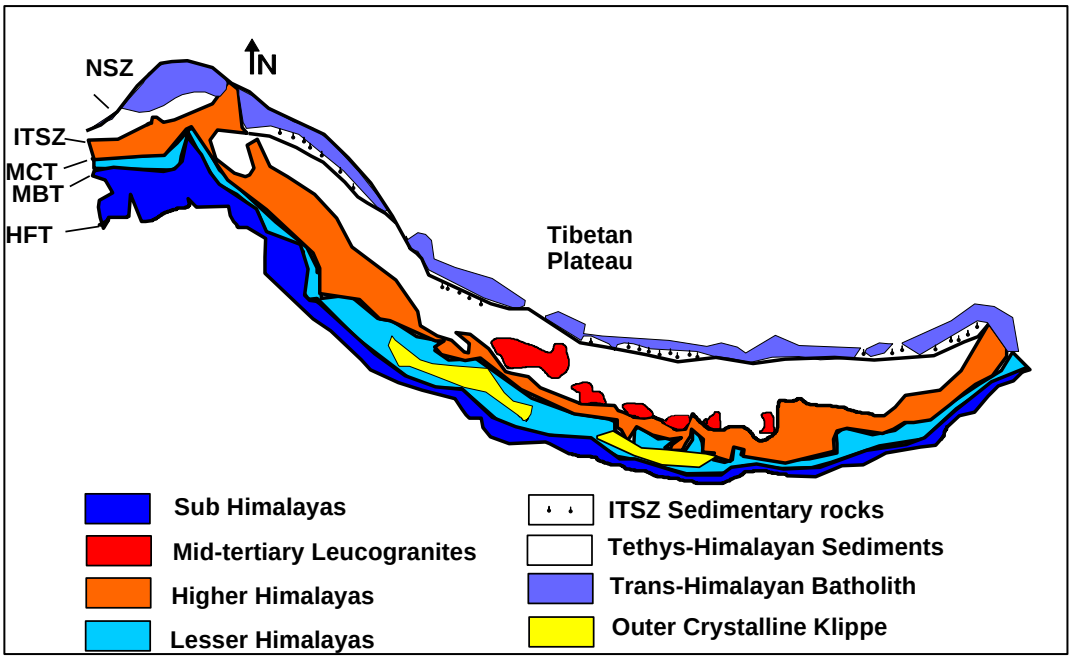

Figure 4.2: Geological sketch map of the Himalaya where NSZ - Northern Suture Zone, ITSZ - Indus-Tsangpo suture zone, MCT- Main Central Thrust, MBT - Main Boundary Thrust and HFT-Himalayan Frontal thrust. (Figure modified after Sorkhabi, 1999)

5. **Lower Himalayan**-This is also called as Lesser Himalayan and the sediments of Lower Himalyan are thrusted over Sub-Himalayan along the Thrust known as Main Boundary Thrust in the south and Greater Himalayan in the north..
6. **Sub-Himalayan**-It is also called as Siwaliks. The Siwalik is thrusted along Main Frontal Thrust over the Indo-gangetic plane or Quaternary deposits. These are sometimes known as Foot hill Himalayan. As the rocks are folded and faulted to form the Siwalik Hills in the foot of Himalaya. This zone of Himalayan is enriched by the vertebrates' fossils.

Generalized stratigraphy of Lesser Himalayas in northwest India i.e. Kumaon (Mandal et al., 2016) has been shown in Figure 4.3. Geology of the stations considered in the present work has been given in Table 4.1.

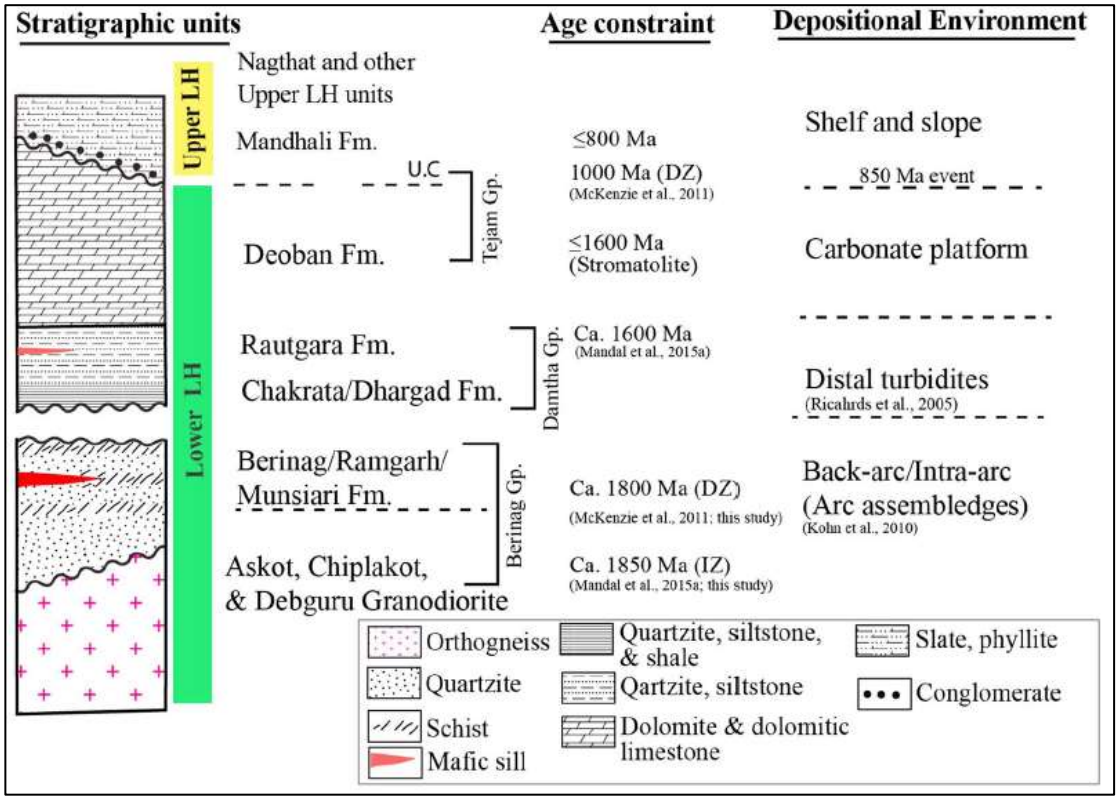

Figure 4.3: Generalized Lesser Himalayan stratigraphy of Kumaon in northwest India. The Lesser Himalaya is separated chronologically into lower and upper subdivisions. LH: Lesser Himalaya, DZ: Detrital zircon, IZ: Igneous zircon, and U.C: Unconformity (Mandal et al., 2016).

Table 4.1: Geology of various stations in Kumaon and Garhwal Himalayas (after Valdiya et al., 1980).

Station Name	**Formation**	**Lithology**	**Stratigraphy Units**	**Age**
Chaukori	Askot Crystalline	Granite, Gneiss	Askot Crystalline	Precambrian
Kamedidevi	Berinag	Quartzite	Jaunsar Group	Neo-Proterozoic
Tejam	Deoban	Quartzite, Dolomite	Tejam Group	Middle Riphean-Upper Riphean
Thal	Mandhali	Slate, Phyllite and Limestone, Dolomite	Tejam Group	Upper Riphean-Early Vendian
Didihat	Askot Crystalline	Granite Gneiss, Quartzite, mica-schist and amphibolite	Askot Crystalline	Meso-Proterozoic
Berinag	Berinag	Quarzite	Jaunsar Group	Precambrian
Bhageshwar	Berinag	Quartzite	Jaunsar Group	Neo-Proterozoic
Shivpuri	Blaini	Diamictites, siltstone and greywacke and slates.	Mussoorie Group	Neo-Proterozoic
Byasi	Nathuakhan	Quartzite interbedded with schists, phyllites and slates.	Ramgarh Group	Neo-Proterozoic

4.2. Data Acquisition and Data Processing

Data is acquired using McSeis-SX 24-channel digital engineering seismograph with 4.5 Hz geophone array. Two most important parameters of the survey are source and receiver-interval. The receiver-interval decides the resolution while the source-interval decides the depth of probing. The accuracy in the depth of investigation depends on the half of the total spread length. During the acquisition, geophone and source spacing has been kept same. The 4.5 Hz geophones are coupled to the seismograph through fixing cables. The seismic waves are generated using mechanical source (11 kg sledge hammer) and data is recorded in a multi-channel seismograph recorder. In the two-dimensional surface-wave method, fixed receiver source receiver configuration is used. Sources are placed in-between receivers and both ends (outside) of survey line. The conventional CMP rolling method with 0.01 msec sampling interval has been used. The number of hammering stacks is three which is hammered from the height of 5 ft. The recording length is 800 msec.

Software used for the data acquisition and analysis is SeisImager/SW with McSEIS-SXW instrument and computer. The information of the fundamental mode of the Rayleigh waves, is used for the generation of dispersion curves by picking highest energy portion in spectrum to draw curve which represents relationship between Rayleigh wave phase velocity and frequency.

The raw data for every position is recorded and stored in the instrument. The raw waveform data obtained is later analyzed and processed by the software. The 2D shear wave velocity models are generated for all the stations and the average V_{S30} is also calculated. The 2D shear wave velocity models can be used for the geotechnical purposes and for the investigation of earth's crust as well for model based predictions for strong ground motion in the area of interest. A schematic layout for data acquisition is shown in Figure 4.5.

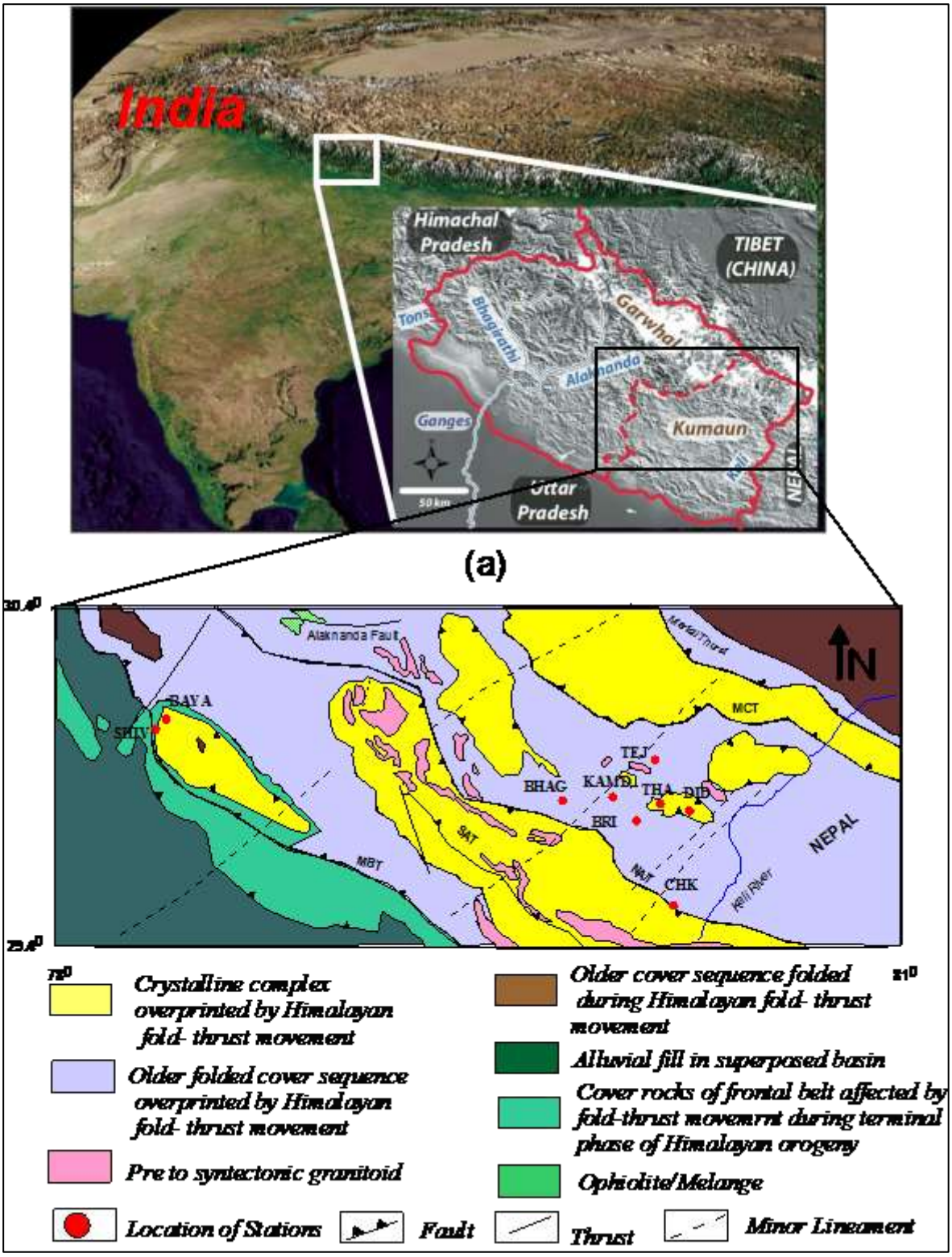

Figure 4.4: The present area of study belongs to the Kumaon and Garhwal Himalayas, India. MBT = Main Boundary Thrust, MCT = Main Central Thrust and NAT = North Almora Thrust. Red Circles show the location of the stations with station codes as mentioned in Table 4.1. Source of the tectonics and geology of the region is Geological Survey of India (2000).

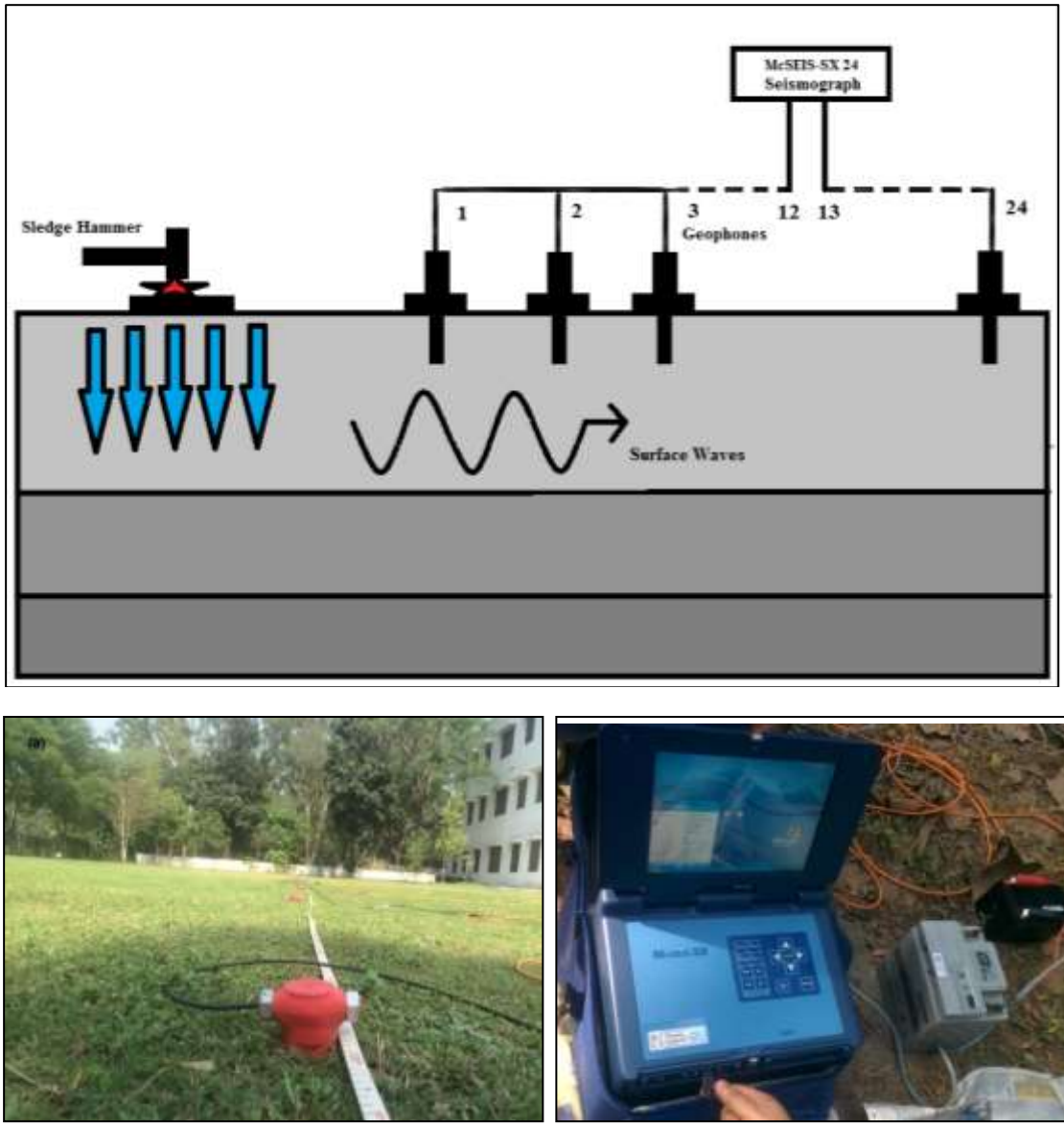

Figure 4.5: Schematic layout used for data acquisition with McSeis-SX seismograph.

MASW method has been applied at various sites of the tough and hilly terrains of Kumaon Himalaya, India for the estimation of shallow subsurface velocity structure. Data acquisition parameters of nine stations are given in Table 4.2. Geophone spacing varies from 1m to 3m depending on the availability of flat terrain at various stations. Since the study area is highly mountainous, therefore it is very tough to find a large flat area for the survey. Therefore, the survey is conducted on the relatively flat playgrounds of schools in various localities. This gives an idea about the velocity profile below schools which is an important part to prepare for better disaster management.

Table 4.2: Name, Code and acquisition parameters of the stations

Station name	**Latitude (in degree)**	**Longitude (in degree)**	**Station code**	**Geophone Spacing (m)**	**Source Spacing (m)**	**Spread length (m)**
Chaukori	29.52N	80.19E	CHK	2.5	2.5	60
Kamedidevi	29.84N	79.96E	KAMD	2.5	2.5	60
Tejam	29.95N	80.12E	TEJ	1	1	24
Thal	29.82N	80.14E	THA	2	2	48
Didihat	29.80N	80.25E	DID	3	3	72
Berinag	29.77 N	80.05 E	BERI	2.5	2.5	60
Bhageshwar	29.83 N	79.77 E	BHAG	2.5	2.5	60
Shivpuri	30.07 N	78.23 E	SHIV	3	3	72
Byasi	30.04 N	78.27 E	BAYA	2	2	48

As mentioned, data processing of the seismic data has been carried out using SeisImager software. The creation of dispersion curve is one of the most critical steps for attaining a correct shear wave velocity model. One dimensional (1D) shear wave velocity models are calculated using the dispersion curves by using non-linear least square method. As a result, two dimensional (2D) Vs profile is constructed. 2D shear wave velocity profile is generated using kriging algorithm of interpolation. The flowchart showing the steps of data processing is given in Figure 4.6.

The comparison of the unprocessed or raw and the processed seismic waveform at Didihat station in the Kumaon Himalayas have been shown in Figure 4.7.

Common Mid-Point (CMP) gathers and corresponding dispersion curves with initial and final shear wave models at various source spacing 0 m, 6 m, 12 m, 18 m, 24 m, 30 m, 36 m, 42 m, 48 m, 54m, 60 m, 66 m have been generated for all the stations. This detailed procedure is followed for each station during the processing. An example is shown in Figure 4.8 to 4.17 for source spacing 0 m, 6 m, 12 m, 18 m, 24 m, 30 m, 36 m, 42 m, 48 m, 54 m, 60 m and 66 m respectively for Didihat station in Kumaon region.

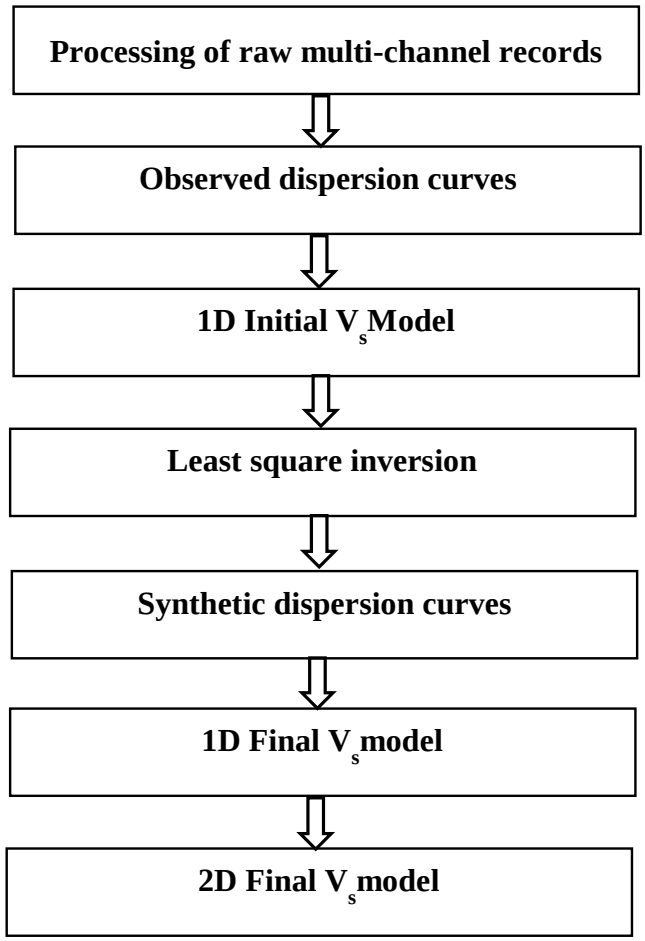

Figure 4.6: Flowchart depicting the processing steps

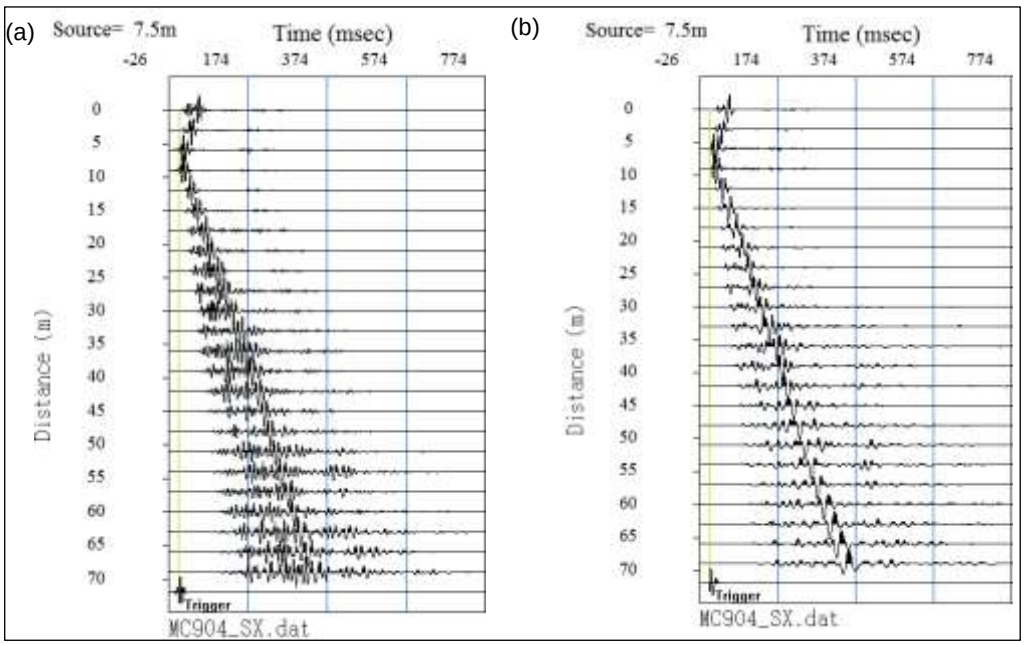

Figure 4.7: Multichannel Records (a) raw shot gather (b) processed shot gather at Kumaon Himalaya region.

Black curve shows the theoretical dispersion curve and red curve shows the observed dispersion curve to the corresponding source spacing. The theoretical and observed dispersive curve shows good match at various source spacing as shown in these snapshots.

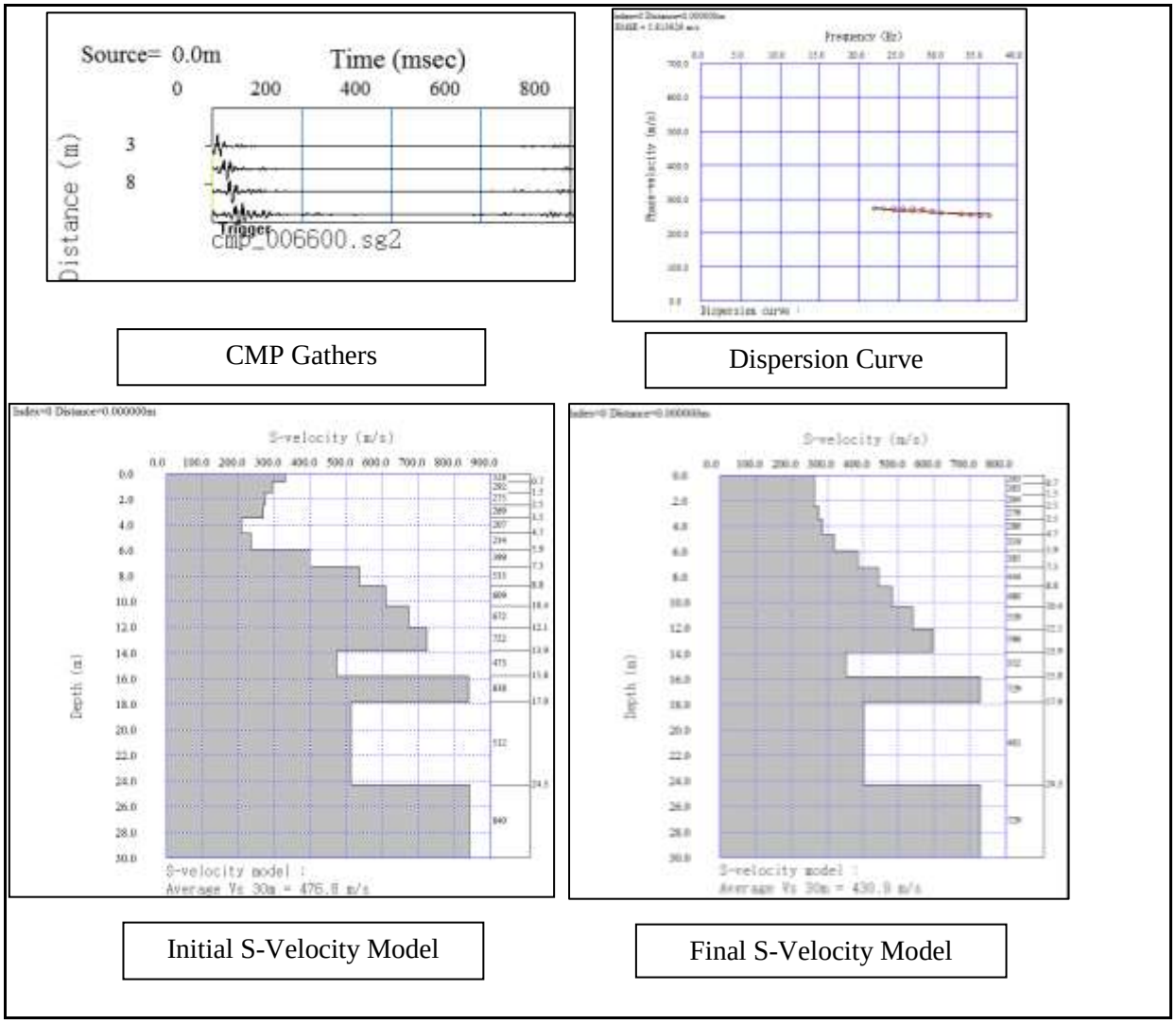

Figure 4.8: CMP gathers and corresponding Dispersion curve with initial and Final S- velocity model at Source =0 m at Didihat station.

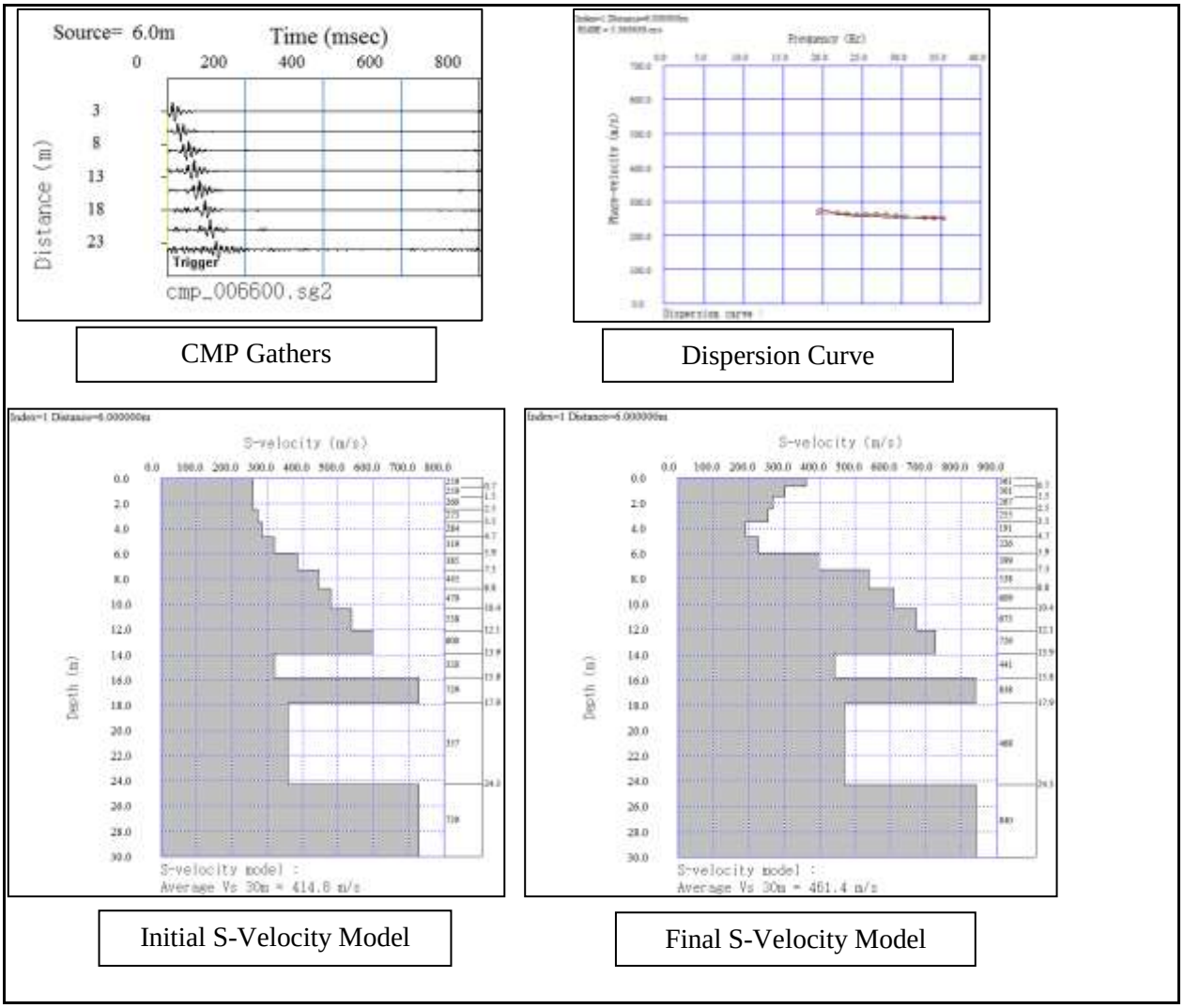

Figure 4.9: CMP gathers and corresponding Dispersion curve with initial and Final S- velocity model at Source =6 m at Didihat station.

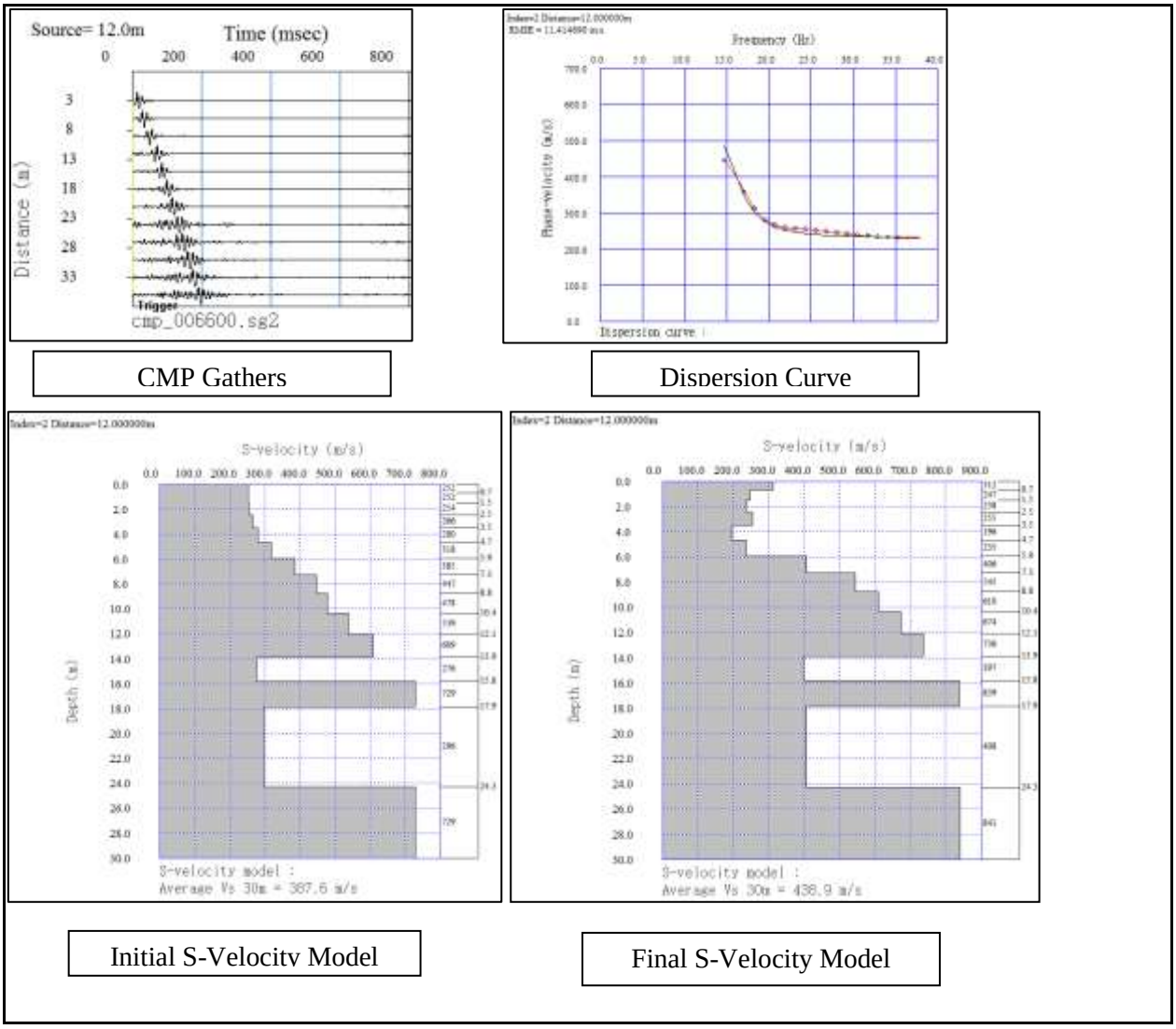

Figure 4.10: CMP gathers and corresponding Dispersion curve with initial and Final S- velocity model at Source =12 m at Didihat station.

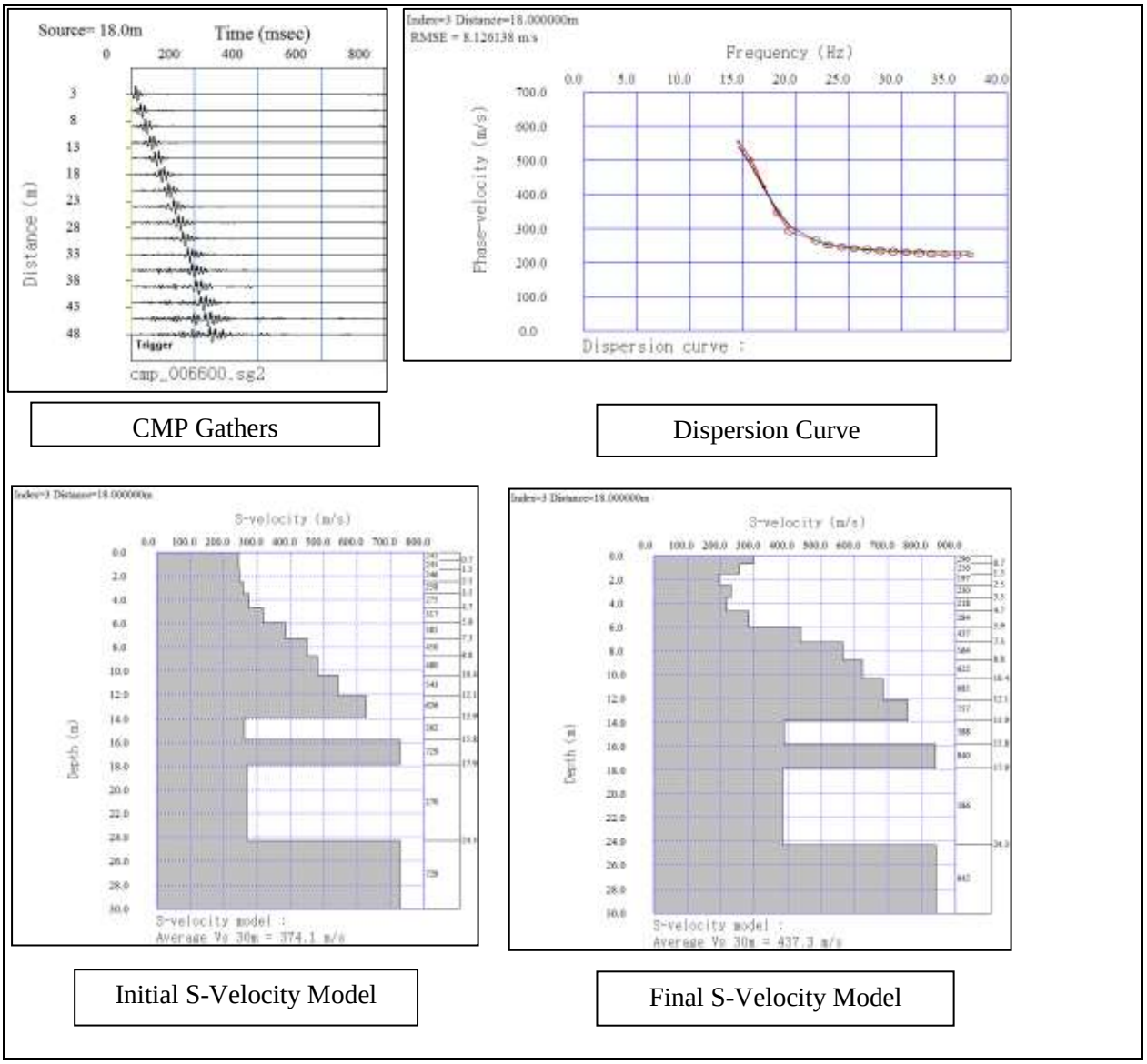

Figure 4.11: CMP gathers and corresponding Dispersion curve with initial and Final S- velocity model at Source =18 m at Didihat station.

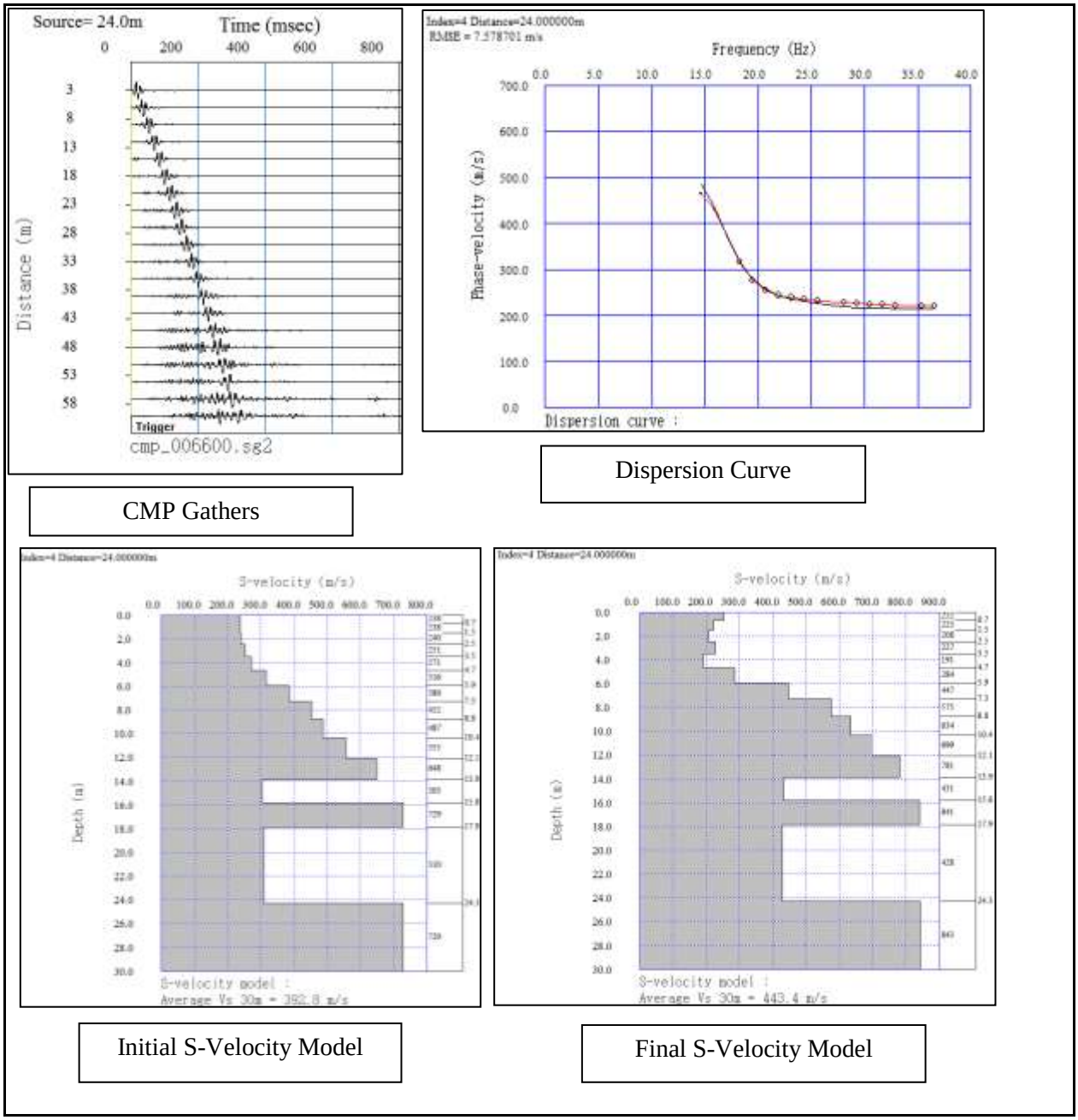

Figure 4.12: CMP gathers and corresponding Dispersion curve with initial and Final S- velocity model at Source =24 m at Didihat station.

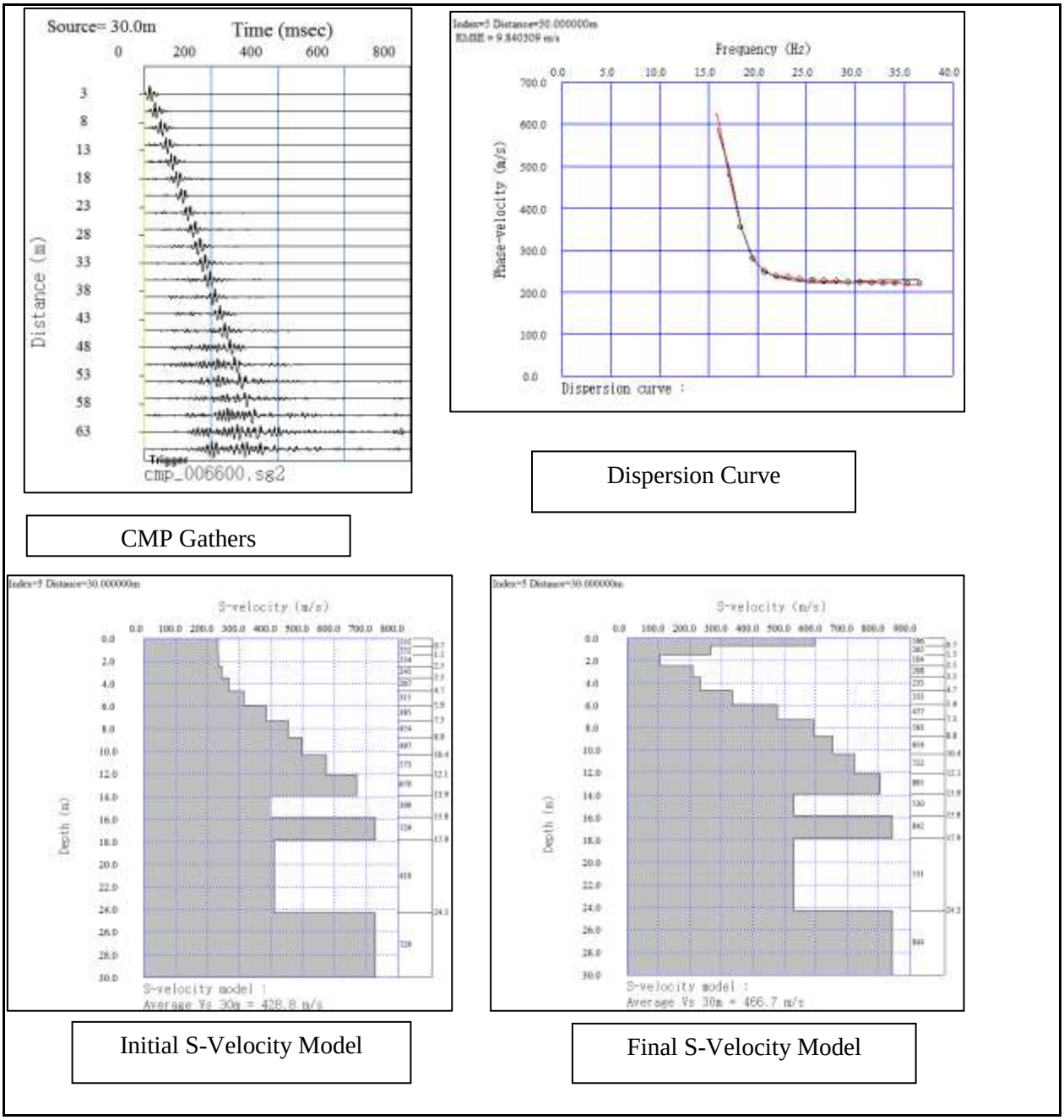

Figure 4.13: CMP gathers and corresponding Dispersion curve with initial and Final S- velocity model at Source =30 m at Didihat station.

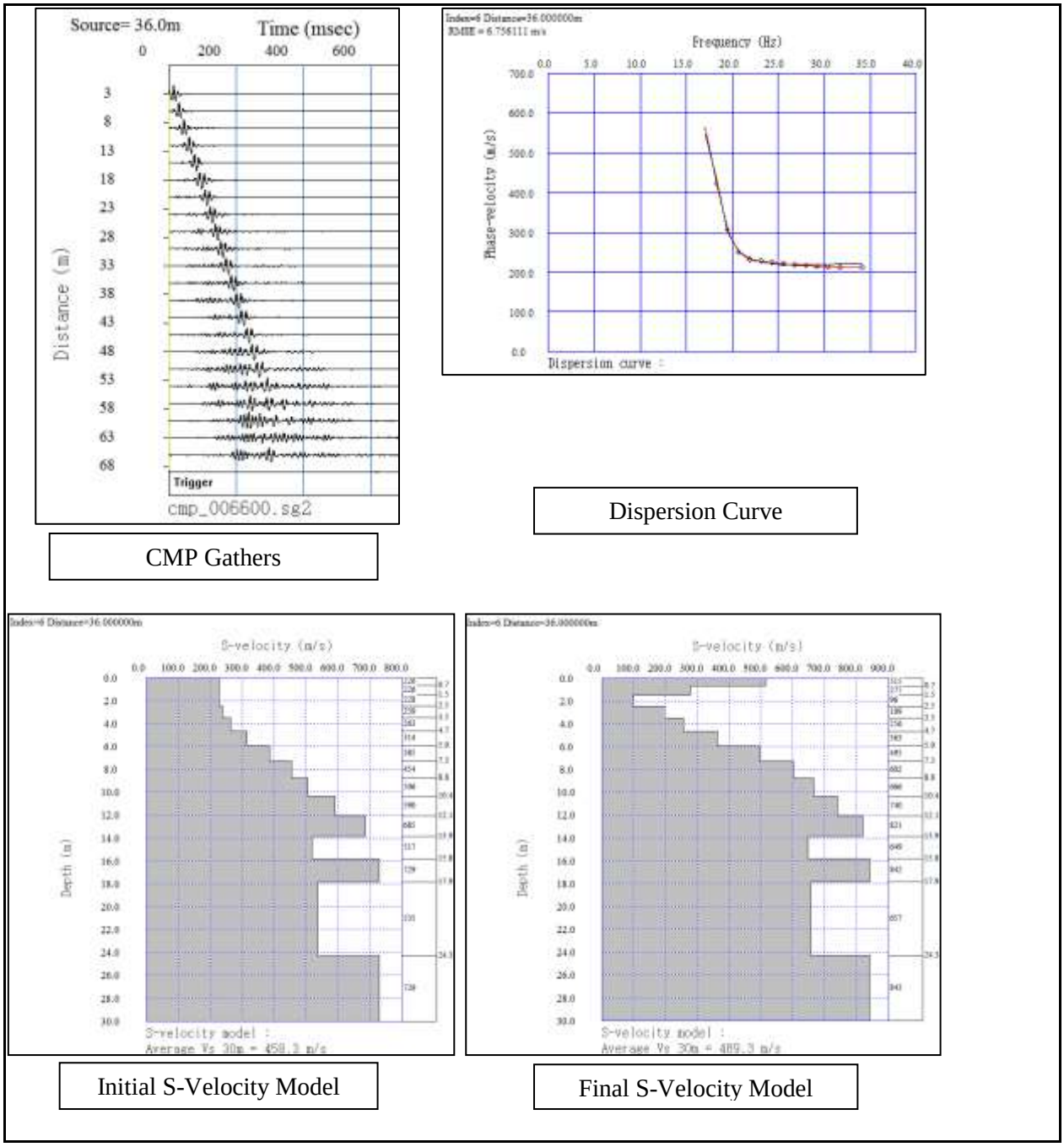

Figure 4.14: CMP gathers and corresponding Dispersion curve with initial and Final S- velocity model at Source =36 m at Didihat station.

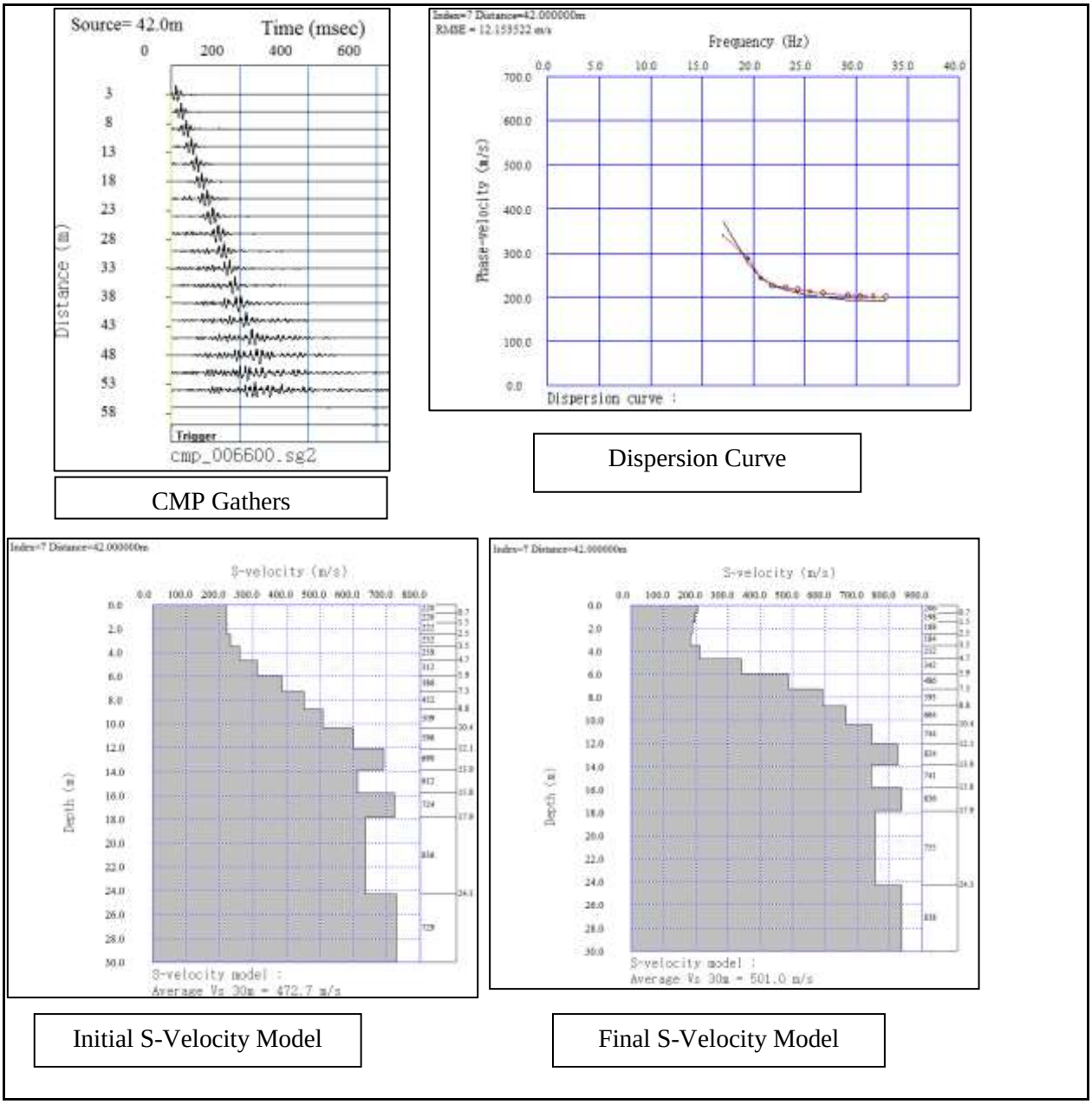

Figure 4.15: CMP gathers and corresponding Dispersion curve with initial and Final S- velocity model at Source =42 m at Didihat station.

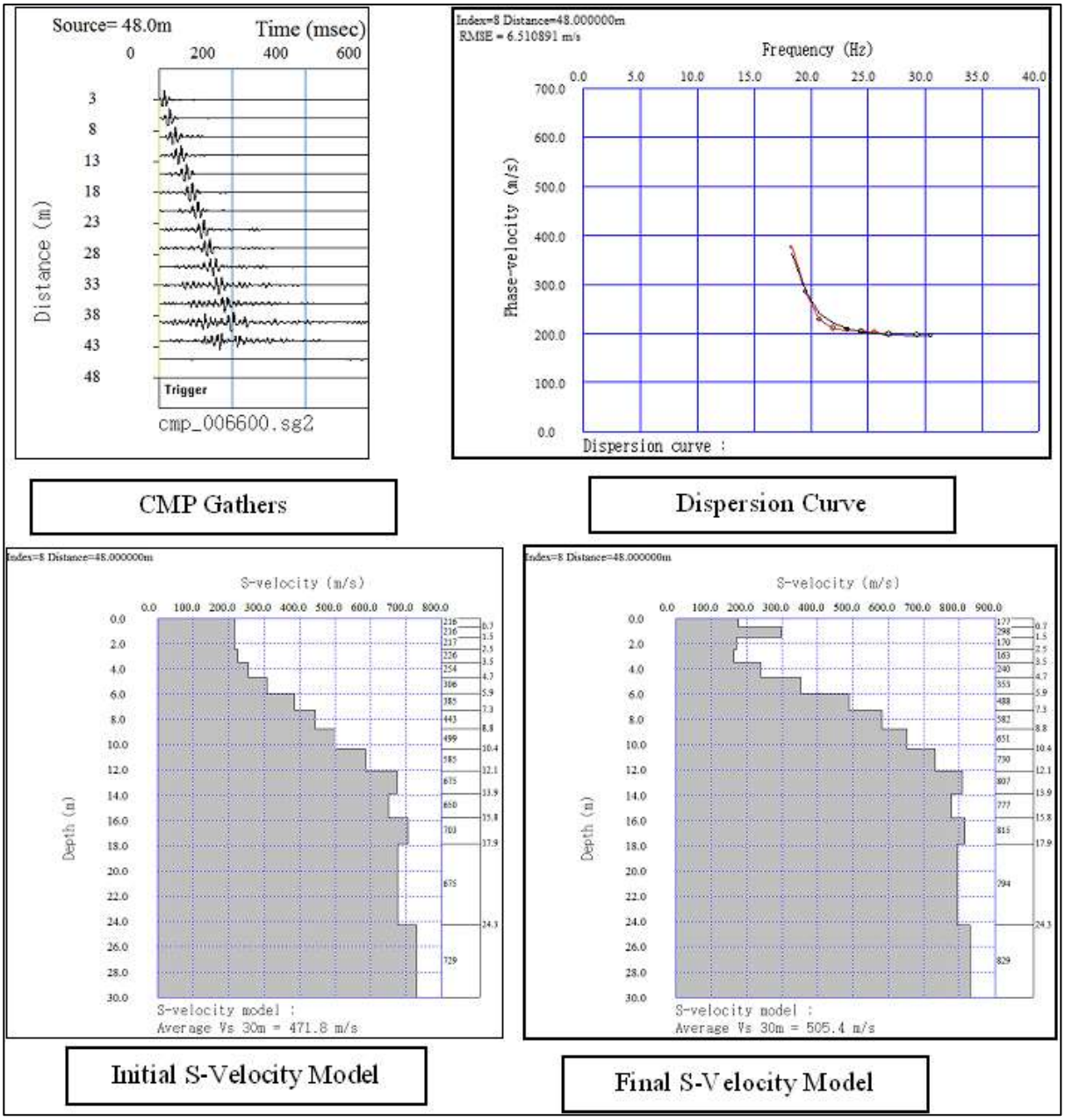

Figure 4.16: CMP gathers and corresponding Dispersion curve with initial and Final S- velocity model at Source =48 m at Didihat station.

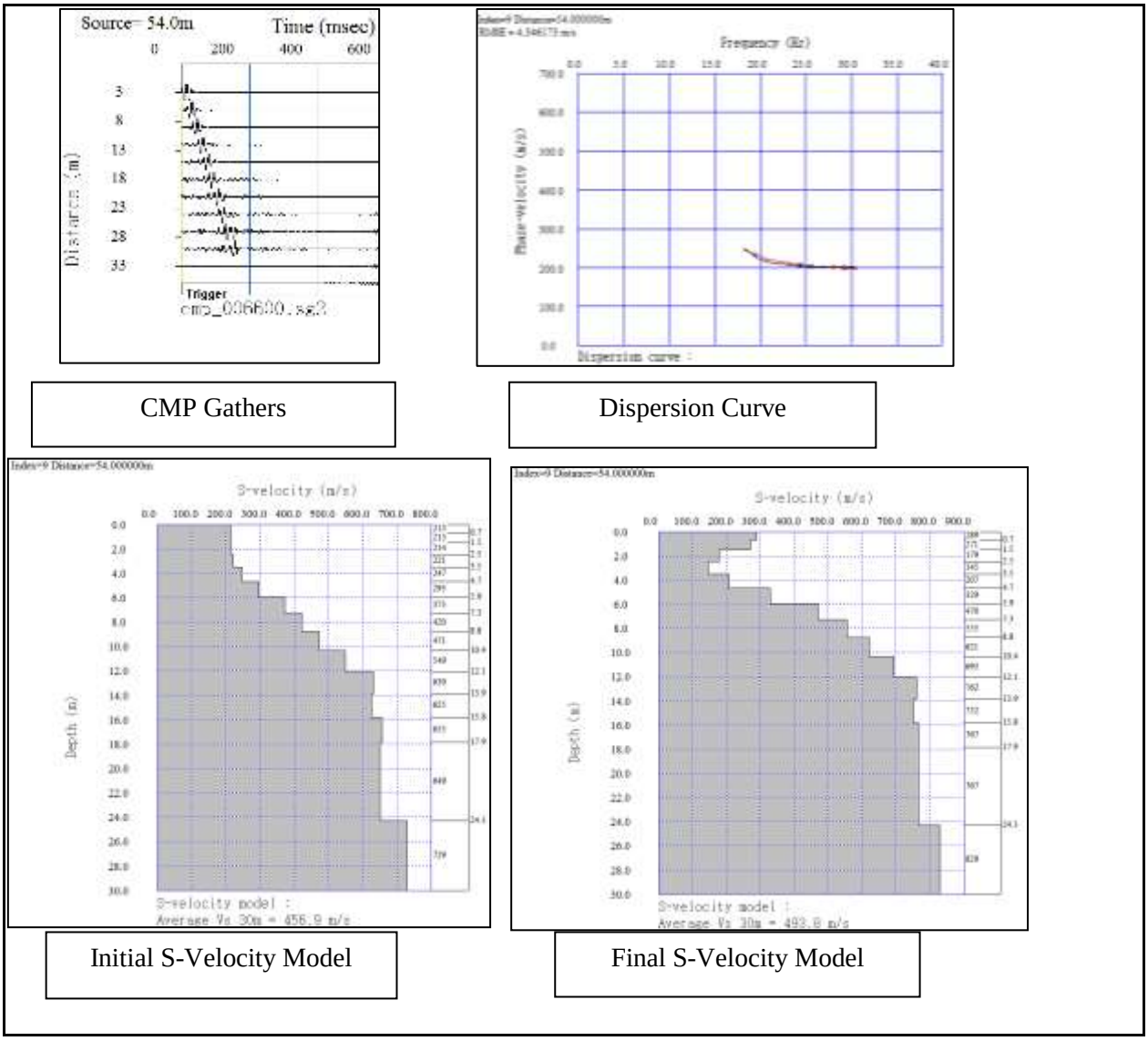

Figure 4.17: CMP gathers and corresponding Dispersion curve with initial and Final S- velocity model at Source =54 m at Didihat station.

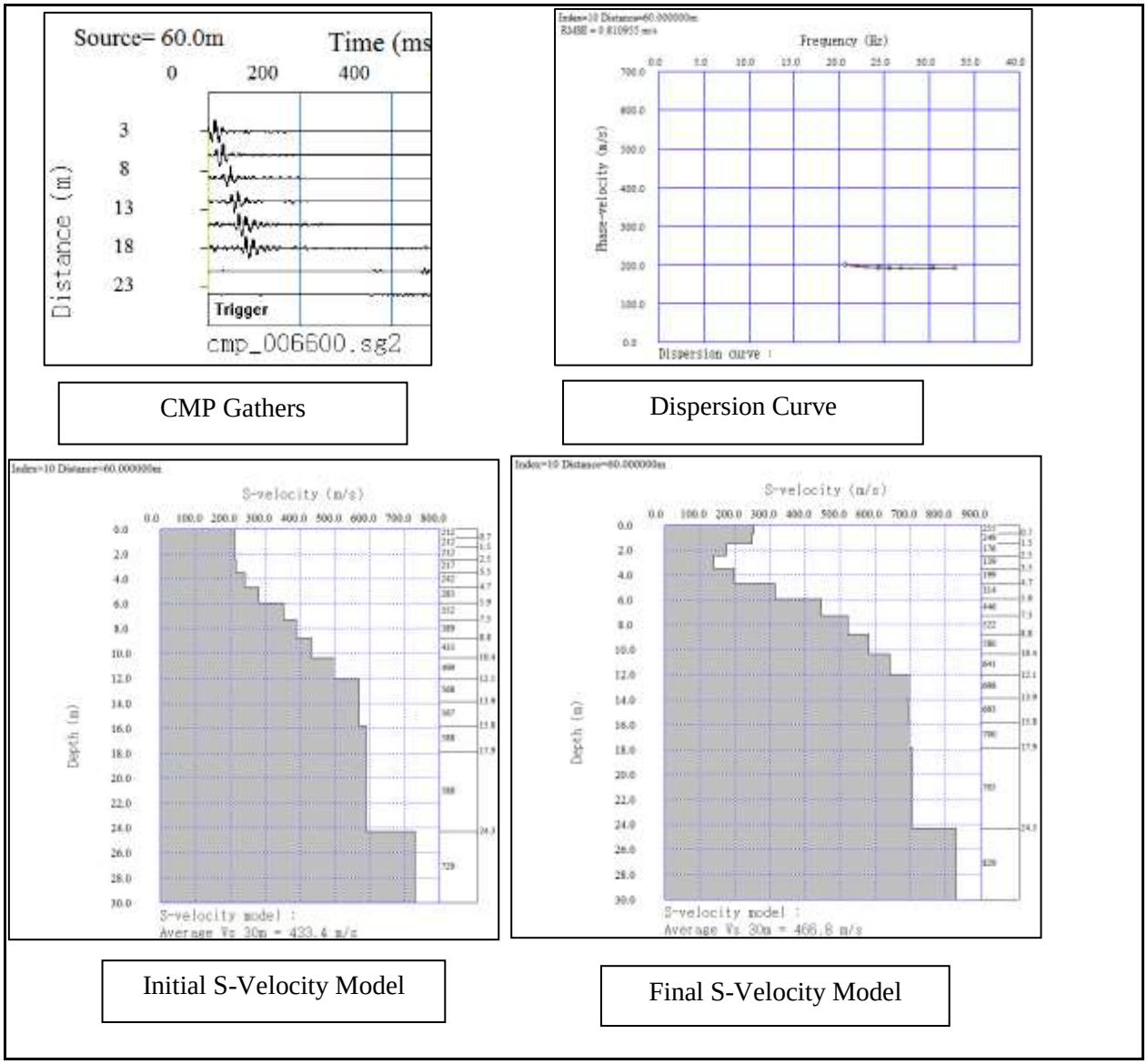

Figure 4.18: CMP gathers and corresponding Dispersion curve with initial and Final S- velocity model at Source =60m at Didihat station.

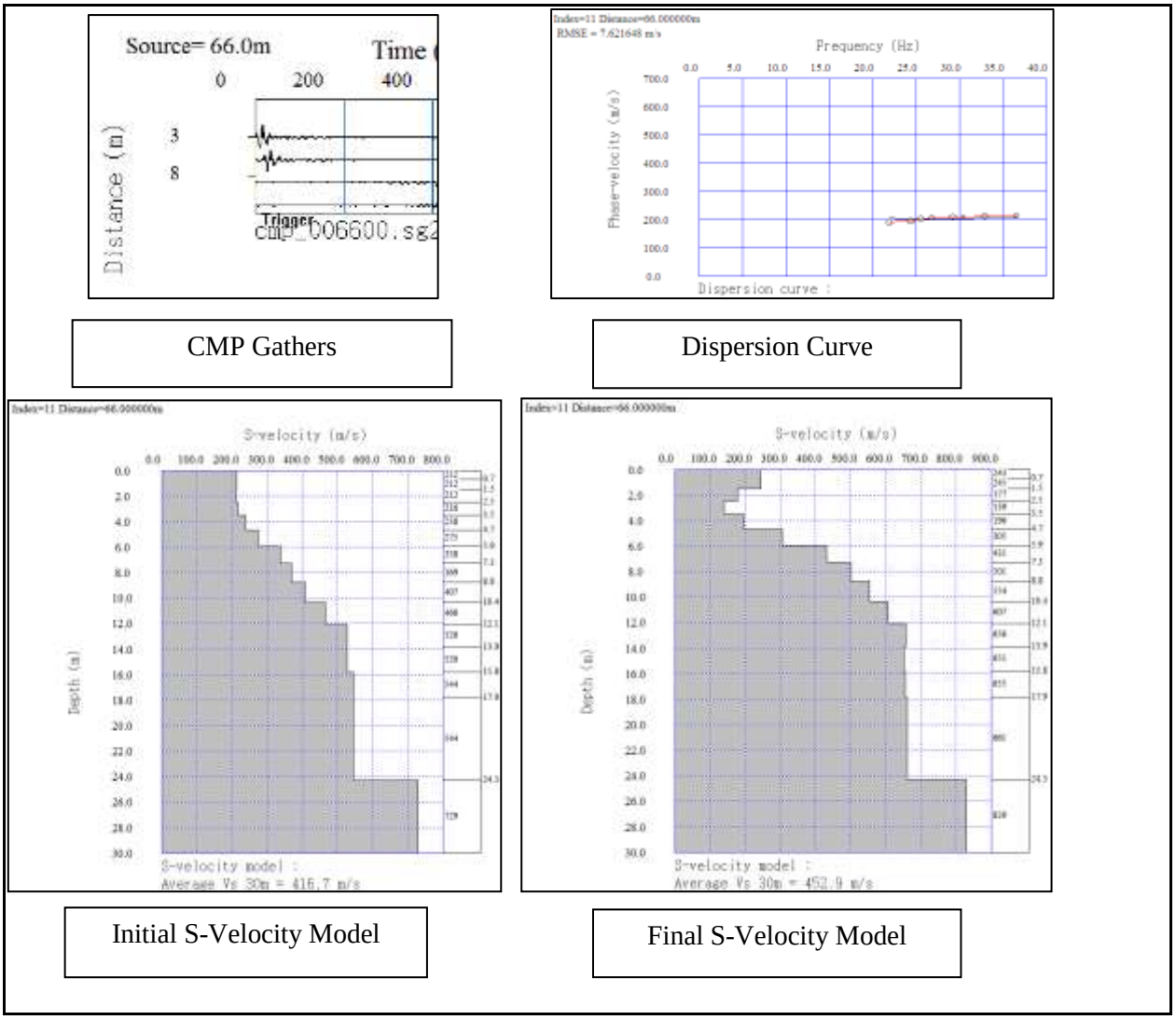

Figure 4.19: CMP gathers and corresponding Dispersion curve with initial and Final S- velocity model at Source = 66m at Didihat station.

Using obtained velocity model following equation has been used to estimate average value of V_{s30}:

$$V_{s30} = \frac{30}{\sum_{i=1}^{n}\left[\frac{h_i}{\beta_i}\right]} \qquad (4.1)$$

Where, h_i is the thickness at the i^{tch} soil layer in meters; β_i is the shear wave velocity for the i^{th} layer in ms^{-1}, and n is the number of layers above 30 m.

The predominant frequency is defined as frequency corresponding to the highest value in amplitude spectrum of soil column. It can also be estimated by the following equation:

$$F_p = \frac{V_{s30}}{4h} \qquad (4.2)$$

Where, F_p is the predominant frequency of the soil column in Hz, V_{s30} is shear wave velocity of the soil column in ms^{-1} and h is the thickness of the soil column i.e. 30 m. The Root Mean Square Error (RMSE) at various stations of the Kumaon Himalaya is tabulated in Table 4.3.

The RMSE is calculated using following equation:

$$\mathrm{RMSE} = \sqrt{\frac{1}{N}\left(\sum_{i=1}^{N}\left(d_i^M - d_i^T\right)\right)} \qquad (4.3)$$

Where N is the total number of data points and d_i^T and d_i^M are phase velocity of theoretical and measured dispersion curve respectively. With the successive iterations, the RMSE for shear wave velocity model decreases as shown in Table 4.3. The iterations were stopped when the RMS error is minimum. The RMSE is plotted against the number of iterations for all the stations - depicting the accuracy of the shear wave velocity profiles generated as shown in Figure 4.17.

Table 4.3: Root Mean Square Error obtained after inversion at various locations of the Kumaon and Garhwal Himalaya

S.No.	Station Name	RMSE			
		Initial Model Error		Final Model Error	
		Velocity(ms^{-1})	RMSE %	Velocity(ms^{-1})	RMSE %
1	**Chaukori**	99.4	29.0	20.7	2.3
2	**Kameridevi**	42.9	18.4	4.3	1.0
3	**Tejam**	27.8	35.8	5.0	7.2
4	**Thal**	40.3	6.8	5.4	0.9
5	**Didihat**	58.4	18.3	3.6	0.7
6	**Berinag**	23.1	17.4	1.3	2.1
7	**Bageshwar**	33.0	7.2	4.6	1.2
8	**Shivpuri**	120.9	16.7	9.5	1.6
9	**Byasi**	22.2	6.3	2.2	0.3

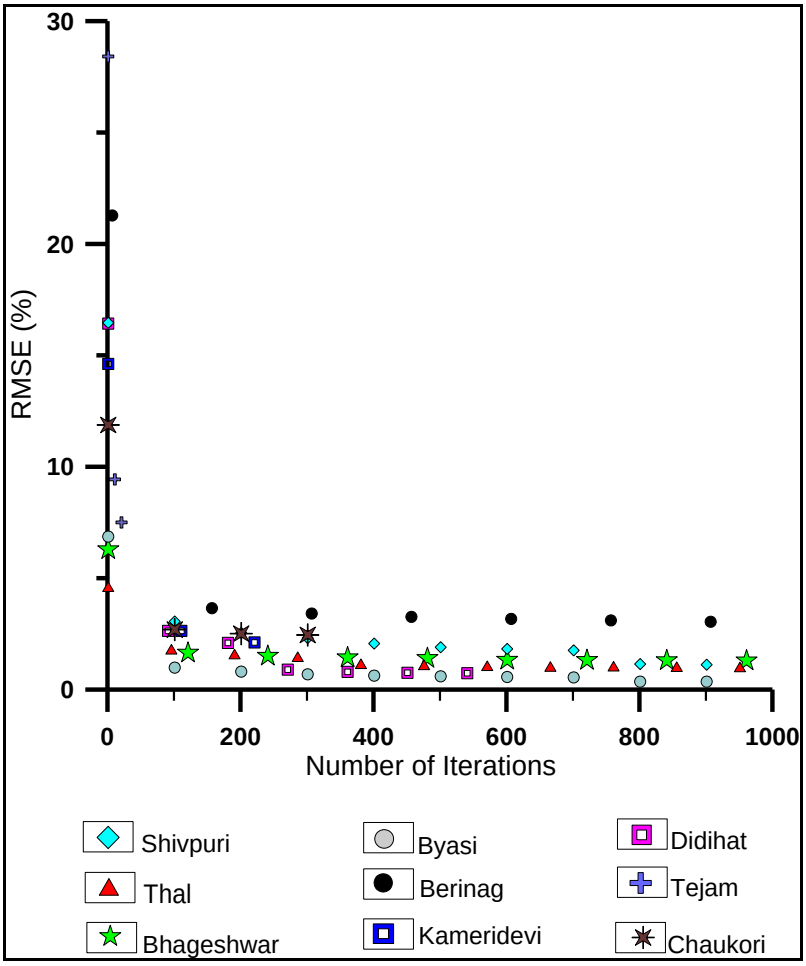

Figure 4.20: RMSE plot against the number of iterations for all the stations.

4.3. Results and Discussion

ninDispersion curves are extracted by keeping 4.50 Hz as minimum frequency. After processing the dispersion curves, the variation of phase velocity with respect to frequency is calculated. For Didihat, based on phase velocity data obtained in frequency domain, the frequency range is within 14.6 - 37.8 Hz with phase velocity in 200-700 ms^{-1} range. Similarly, the frequency range for Berinag, Tejam, Bhageshwar, Kameridevi, Thal and Chaukori varies from 25.62 - 39.04 Hz, 15.20 - 29.60 Hz, 7.32 - 39.04 Hz, 10.98 - 35.38 Hz, 8.54 - 39.04 Hz and 15.80 - 39.04 Hz, respectively and phase velocity varies from 307 - 772 ms^{-1}, 45 - 155 ms^{-1}, 278 - 441 ms^{-1}, 157 - 476 ms^{-1}, 446 - 576 ms^{-1} and 121 - 631 ms^{-1}, respectively.

MASW results, including dispersion curves, 1D velocity models and 2D velocity model, have been shown for the nine stations from Figure 4.21 to Figure 4.29.

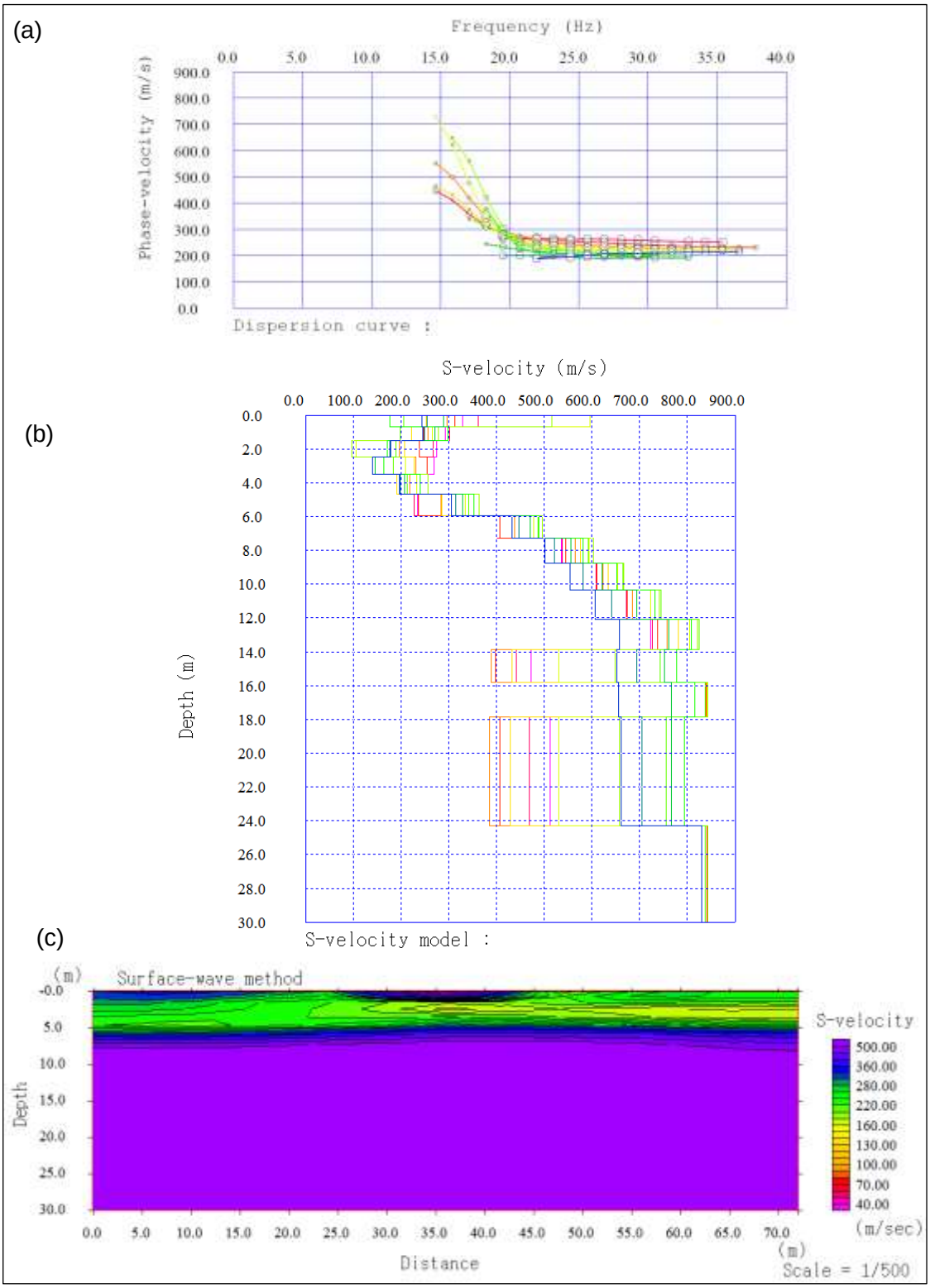

Figure 4.21: The results obtained at Didihat station (a) dispersion curve obtained from processed record , (b) 1D shear Wave Velocity Model inverted from trends in (a), (c) 2D shear Wave Velocity Model

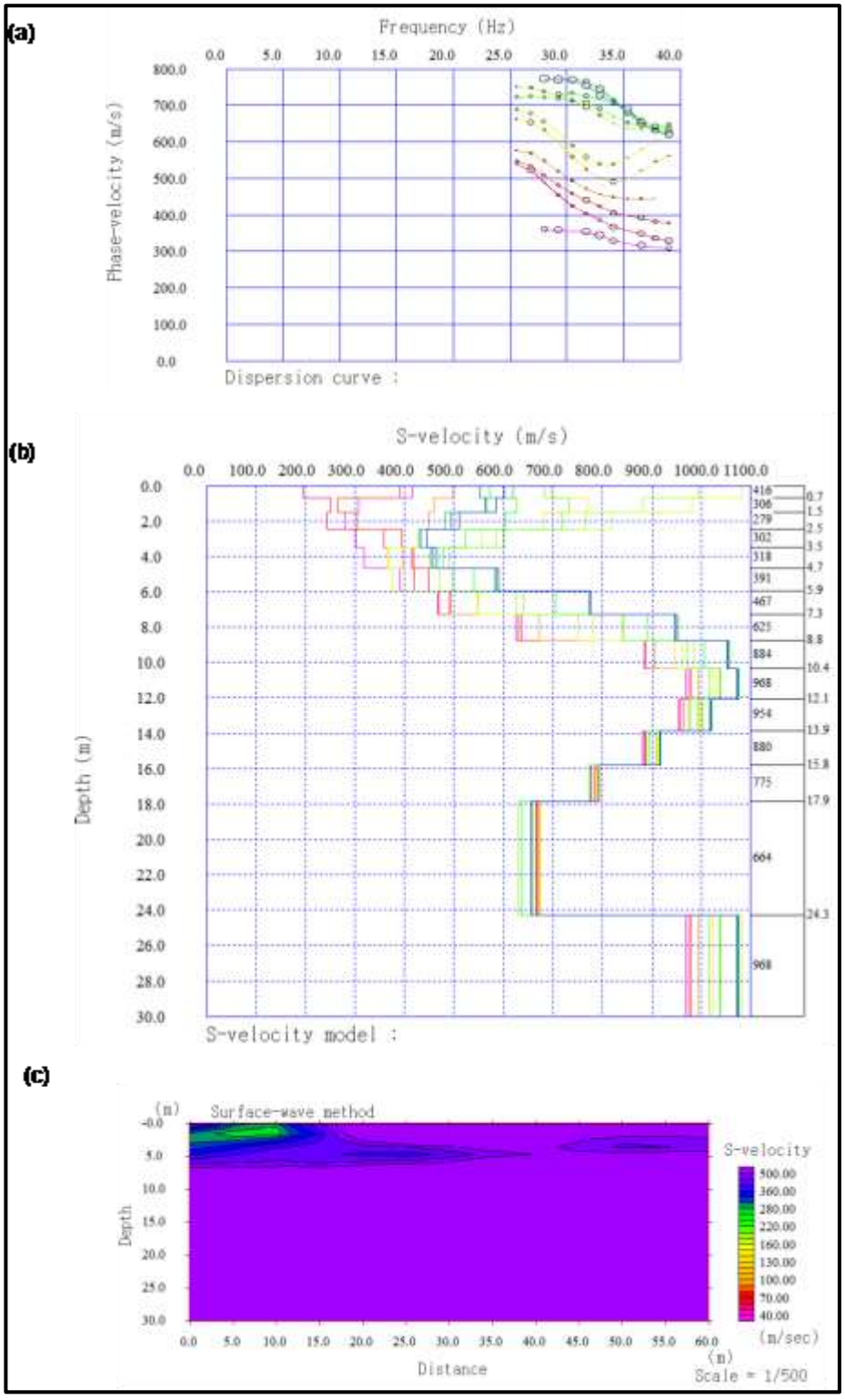

Figure 4.22: The results obtained at Berinag station (a) dispersion curve obtained from processed record , (b) 1D shear Wave Velocity Model inverted from trends in (a), (c) 2D shear Wave Velocity Model

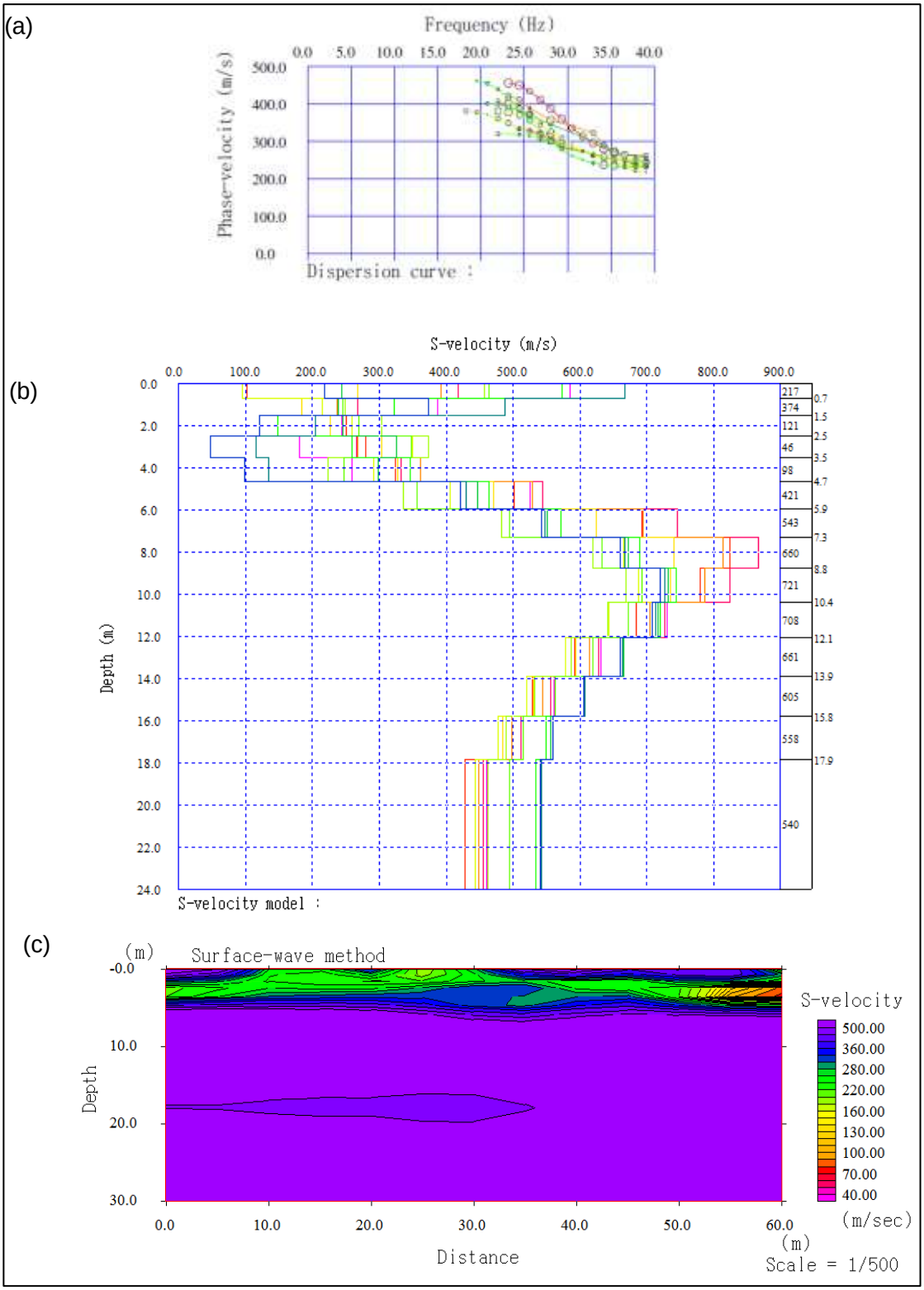

Figure 4.23: The results obtained at Chaukori station (a) dispersion curve obtained from processed record , (b) 1D shear Wave Velocity Model inverted from trends in (a), (c) 2D shear Wave Velocity Model

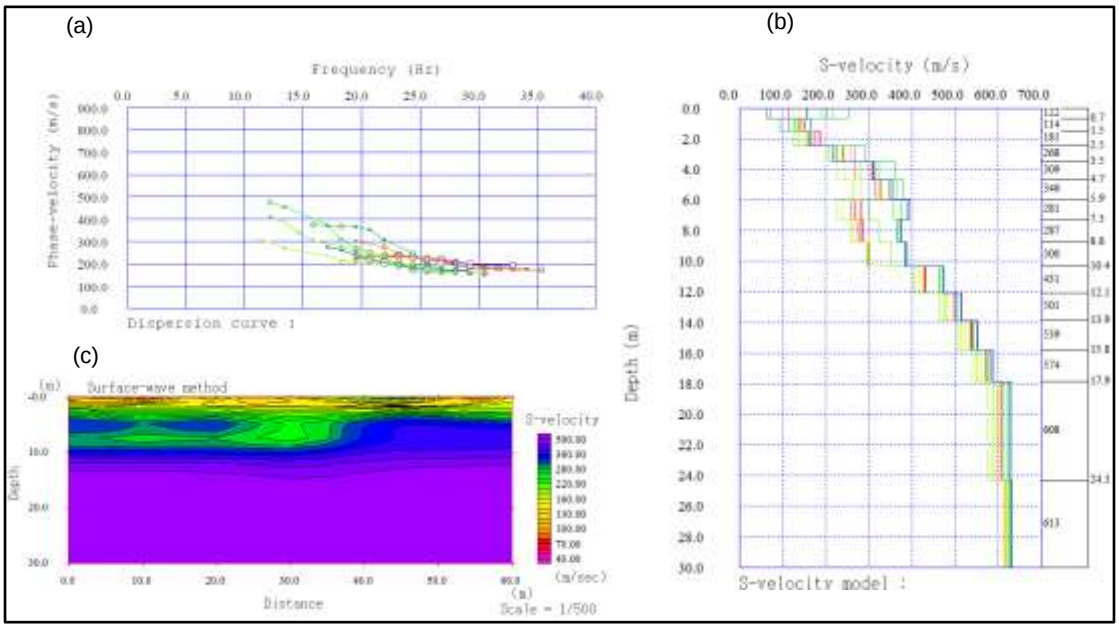

Figure 4.24: The results obtained at Kameridevi station (a) dispersion curve obtained from processed record , (b) 1D shear Wave Velocity Model inverted from trends in (a), (c) 2D shear Wave Velocity Model

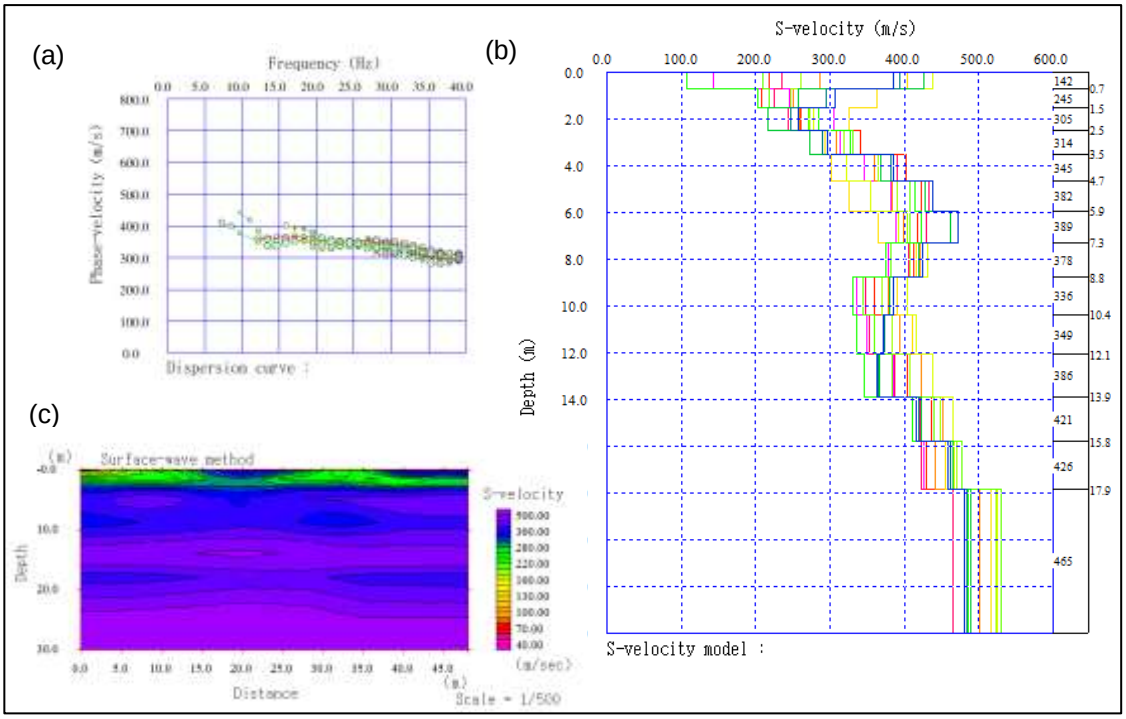

Figure 4.25: The results obtained at Bhageshwar station (a) dispersion curve obtained from processed record , (b) 1D shear Wave Velocity Model inverted from trends in (a), (c) 2D shear Wave Velocity Model

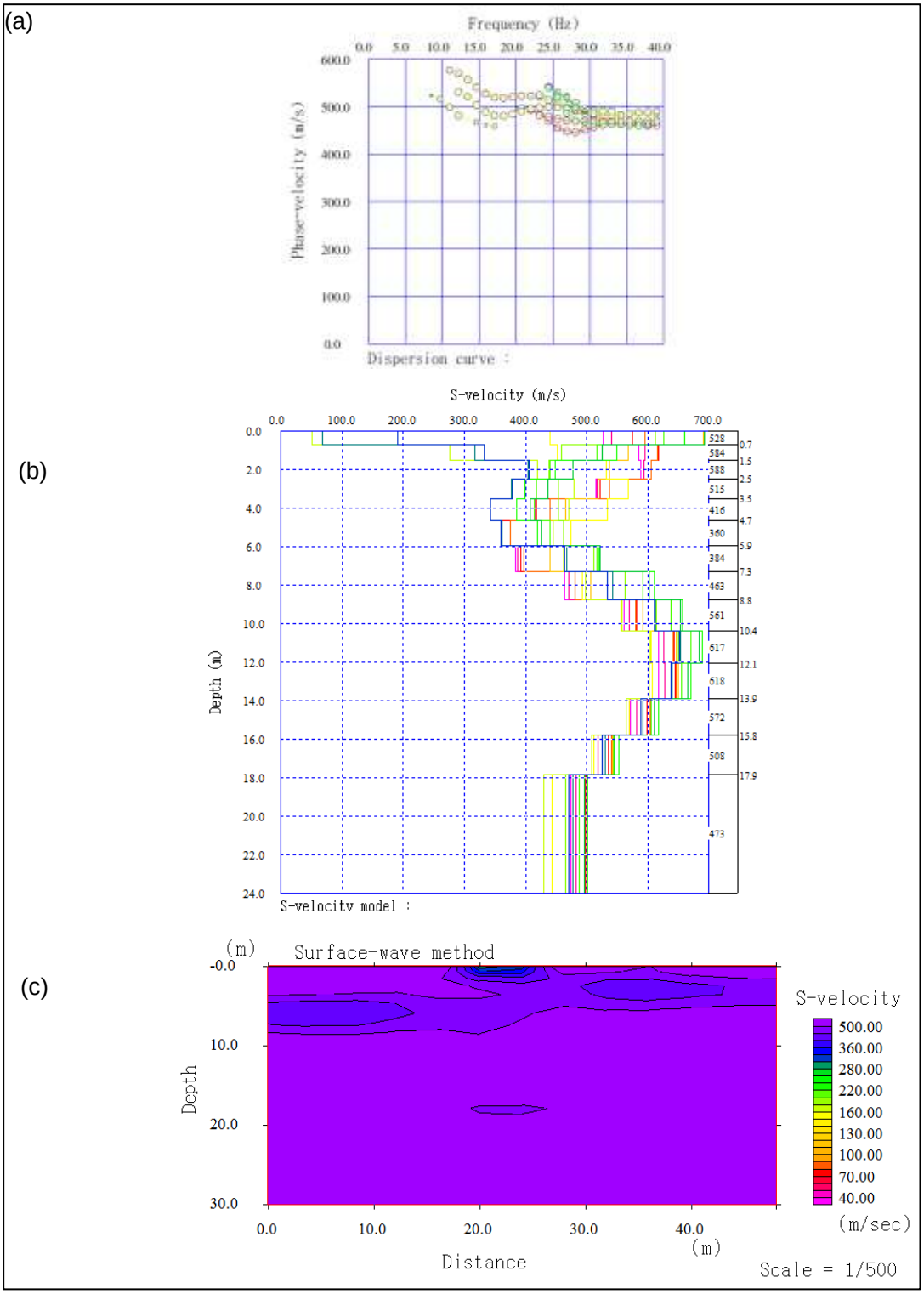

Figure 4.26:The results obtained at Thal station (a) dispersion curve obtained from processed record , (b) 1D shear Wave Velocity Model inverted from trends in (a), (c) 2D shear Wave Velocity Model

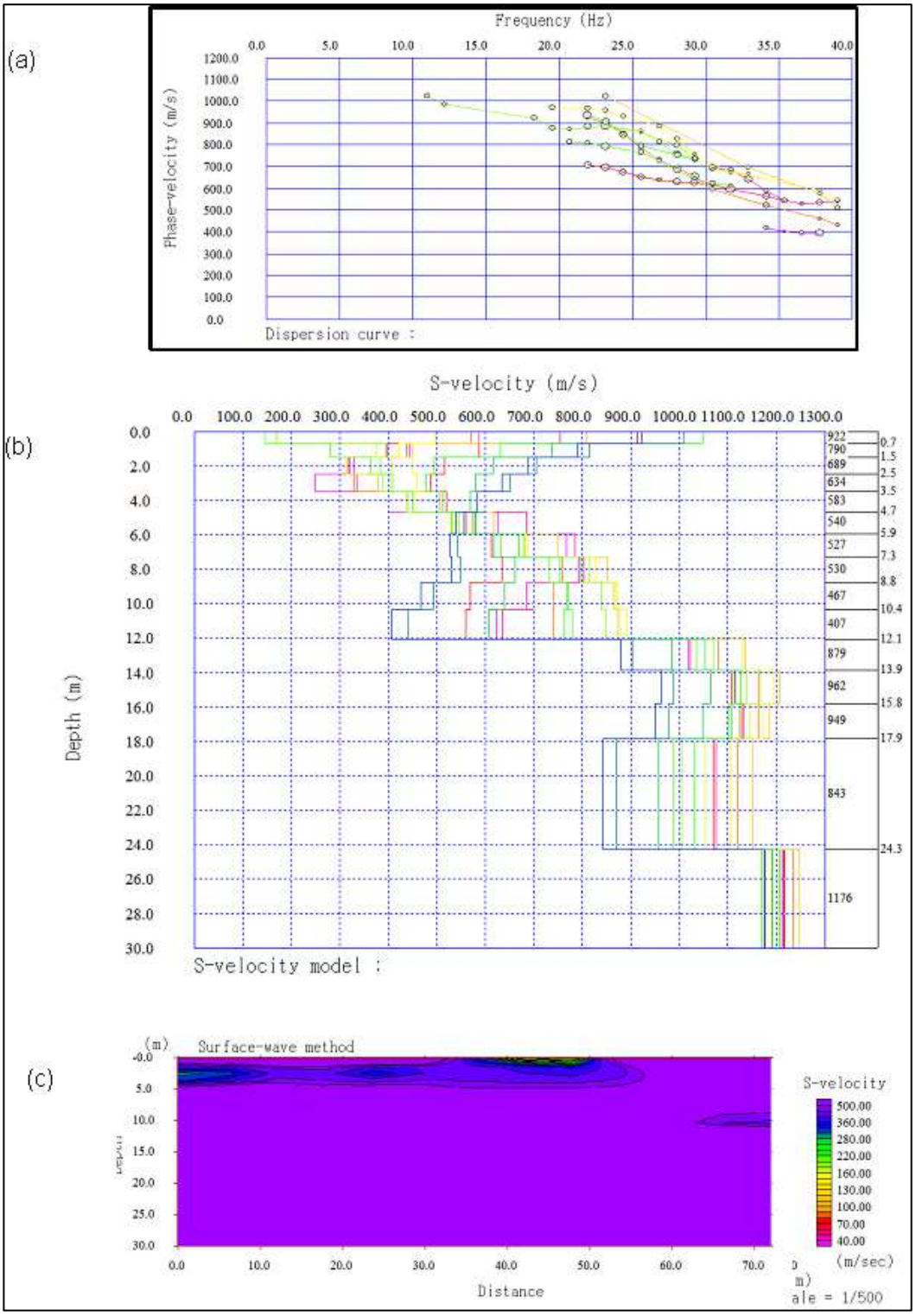

Figure 4.27: The results obtained at Shivpuri station (a) dispersion curve obtained from processed record , (b) 1D shear Wave Velocity Model inverted from trends in (a), (c) 2D shear Wave Velocity Model

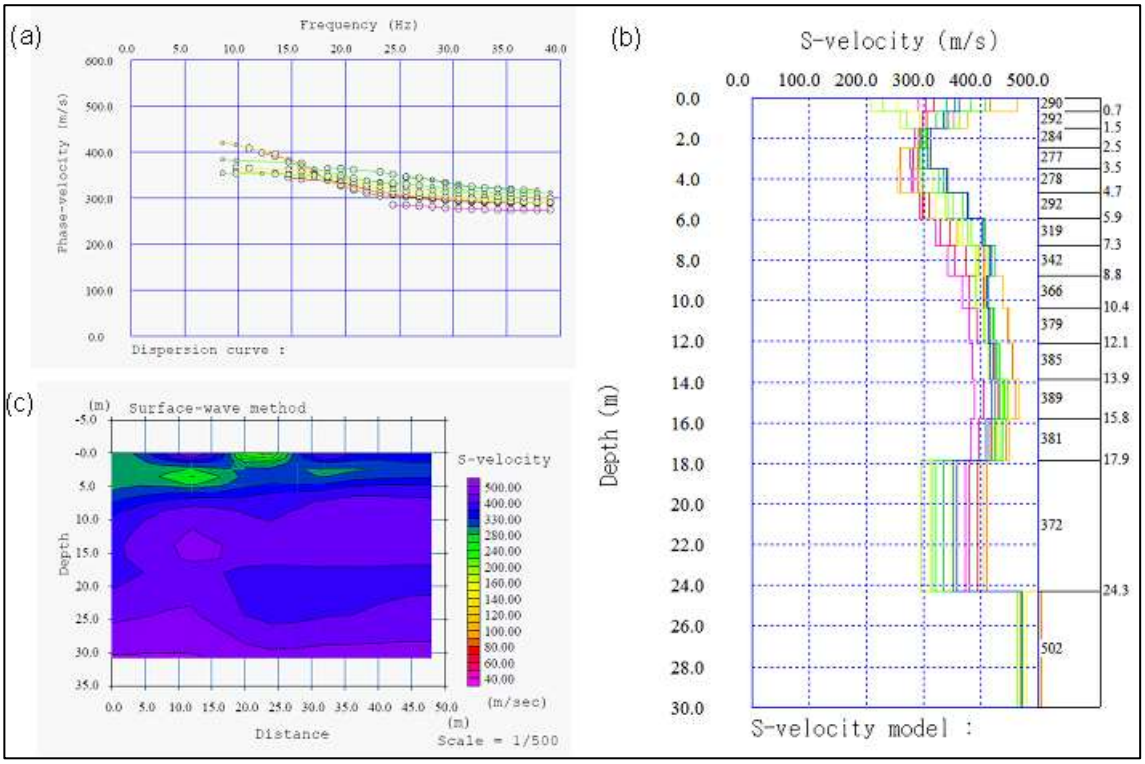

Figure 4.28: The results obtained at Byasi station (a) dispersion curve obtained from processed record , (b) 1D shear Wave Velocity Model inverted from trends in (a), (c) 2D shear Wave Velocity Model

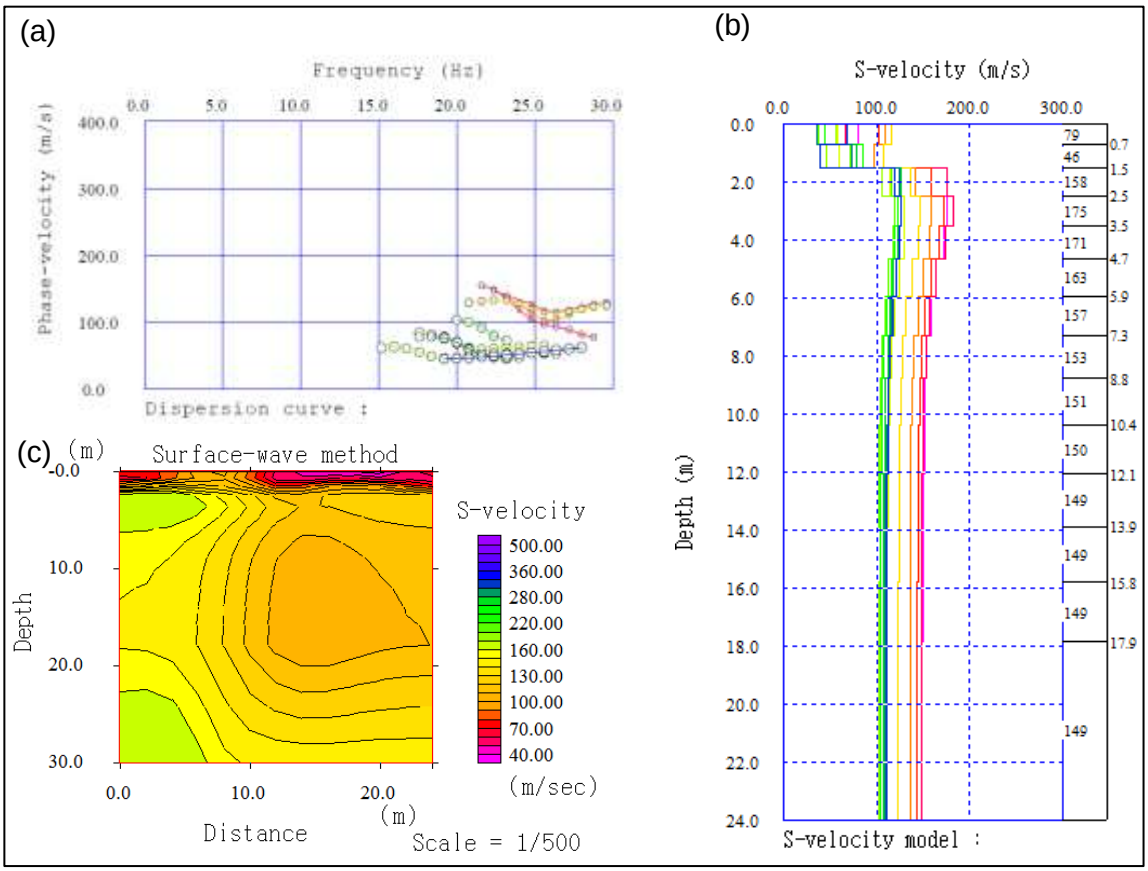

Figure 4.29:The results obtained at Tejam station (a) dispersion curve obtained from processed record , (b) 1D shear Wave Velocity Model inverted from trends in (a), (c) 2D shear Wave Velocity Model

Such 2D shear Wave Velocity models play an important role in earthquake engineering. According to Building Seismic Safety Council (BSSC, 2003) various sites has been classified with respect to N- value, thickness, undrained shear strength, water content and V_{s30} as given in Table 2.1.

It has been observed that geological setting and lithology of the area has a major influence on predominant frequency of the ground. The estimated predominant frequencies resulting from the present research work, derived using equation 4.2, vary from 3.92 - 4.05 Hz for the granitic and gneiss rocks, 3.17 - 5.94 Hz for the quartzite rocks, 3.17 - 5.94 Hz for the quartzite rocks, 1.01 Hz for quartzite along with dolomite rocks and 4.37 Hz for the slates, phyllites along with limestones and dolomite.

High-rise buildings typically have low natural frequency as compared to small buildings. While the region of Kumaon Himalaya has been populated with small to medium buildings, high predominant frequency obtained at various locations can be hazardous to small buildings. It is observed that predominant frequency in this region varies from 1.01 to 5.94 Hz indicating a wide range of damaging pattern to various structures in the region. Estimated predominant frequency is 1.01 Hz at Tejam which corresponds to Proterozoic crystalline formations containing quartzite and dolomitic limestones with bands and intercalations of limestones. The estimated predominant frequency is 5.94 Hz at Berinag which corresponds to quartzite rocks.

According to the site classification provided by NEHRP, the stations lie in C and E classes as shown in Table 4.4. Bhageshwar, Chaukori, Thal, Berinag, Kamedidevi and Didihat lie in class C with very hard soil and soft rock category. However, Tejam with shear wave velocity 120 ms^{-1} could be categorized under class E of soft clay category.

This seismic experiment has given an important idea about the velocity model of the various localities of Kumaon Himalayas. Attained 1D and 2D velocity model for every site gives an idea about the soil classification in terms of predominant frequencies, average shear wave velocities and depth of various layered units, respectively. Shear wave velocity increases with depth due to greater degree of compaction and central crystallization. Soil classification is done on the basis of the results obtained in terms of average shear wave velocity - showing the importance of study in geotechnical engineering studies.

Table 4.4: Predominant frequency of soil column obtained after inversion at various locations of the Kumaon and Garhwal Himalaya

S.No.	Station Name	Average V_{S30}	Average Predominant Frequency	Site classifications
1	**Chaukori**	470	3.92	C
2	**Kameridevi**	380	3.17	C
3	**Tejam**	121	1.01	E
4	**Thal**	524	4.37	C
5	**Didihat**	486	4.05	C
6	**Berinag**	712	5.94	C
7	**Bhageshwar**	409	3.41	C
8	**Shivpuri**	785	6.54	C
9	**Byasi**	383	3.19	C

Chaukori village is located in Berinag tehsil of Pithoragarh district of Uttarakhand. It is 86 Km away from district Pithoragarh at an elevation of 2010 m. Stratigraphically it falls in Askot Crystalline. The Askot Crystalline consists of granite and gneisses. Based on the phase velocity data obtained in frequency domain; the estimated frequency range is within 15.80 - 39.04 Hz and the range of phase velocity is 121 - 631 ms $^{-1}$. The average shear wave velocity of Chaukori is 470 ms $^{-1}$hence it can be classified in class C i.e. very hard soil and soft rock category. Its estimated average predominant frequency is 3.92 Hz.

Granite and gneisses are moderately suited for high rise structures such as dams and multi-story buildings and the site is more appropriate for low height buildings e.g. schools, primary health centers etc.

Kamedidevi is famous for the temple of goddess Shakti, situated in Bhageshwar district of Uttarakhand. Stratigraphically, it forms the part of Berinag Formation of Jaunsar Group having quartzite as lithological unit. Based on the phase velocity data obtained in frequency domain; the estimated frequency range is within 11.0- 35.0 Hz and the range of phase velocity is 157 - 476 ms $^{-1}$.

The average shear wave velocity of Kamedidevi is 380 ms $^{-1}$ hence it can be classified in class C i.e. very hard soil and soft rock category. Its estimated average predominant frequency is 3.17 Hz.

Quartzite type of rocks was profiled in this study and significant differences were found in near-surface velocity that appears to explain part of the measured differences in site

amplification. The rock sites are located in average shear wave velocity of 380 ms $^{-1}$which are quite significant for low rise buildings rather than high rise buildings.

Tejam village is located in Munsiari tehsil, 74 km away from district Pithoragarh. Stratigraphically it forms the part of Deoban Formation of Tejam Group having quartzite and dolomite as lithological unit. Based on the phase velocity data obtained in frequency domain; the estimated frequency range is within 15.0 – 29.5 Hz and the range of phase velocity is 45 - 155 ms $^{-1}$.

The average shear wave velocity of Tejam is 121 ms $^{-1}$hence it can be classified in class E i.e. soft clay category. Its estimated average predominant frequency is 1. 01 Hz. The results reveal that the quartzite interbedded with dolomite is not good for high rise structures and multi-storey buildings however the site is more suited for low rise buildings e.g. weirs, barrages etc.

Thal village lies in Pithoragarh district of Uttarakhand at an elevation of 784 m above mean sea level. It is located 245 km from the state capital Dehradun. It belongs to Mandhali Formation of Tejam Group. The rocks exposed are slate, phyllite, limestone and dolomite. Based on the phase velocity data obtained in frequency domain; the estimated frequency range is within 8.5 - 39.0 Hz and the range of phase velocity is 446 – 576 ms $^{-1}$.

The average shear wave velocity of Thal is 524 ms $^{-1}$hence it can be classified in class C i.e. very hard soil and soft rock category. Its estimated average predominant frequency is 4.37 Hz.

Didihat is a busy township in Pithoragarh and is situated at the hill top plains of Digtarh-Bhadigad with Charamgad River flowing below the town. Stratigraphically it falls in Askot Crystalline. The Askot Crystalline is mainly composed of granite and gneisses with some traces of mica-schist and amphibolite. It is located at an elevation of 1725 m. Based on the phase velocity data obtained in frequency domain; the estimated frequency range is within 14.5 - 38.0 Hz and the range of phase velocity is 200-700 ms $^{-1}$. The average shear wave velocity of Didihat is 486 ms $^{-1}$ hence it can be classified in class C i.e. very hard soil and soft rock category. Its estimated average predominant frequency is 4.05 Hz.

The results reveal that the lithology like granite and gneisses with some traces of mica-schist and amphibolite is not good for high rise structures and multi-storey buildings without

proper strengthening of material however the site is more suited for low rise buildings e.g. weirs, barrages etc.

Berinag is situated 160 km from Nainital in Pithoragarh district, Uttarakhand. It gets its name from temple situated at the top of Berinag hill. It is located at an elevation of 1860 m from mean sea level. Stratigraphically it falls in Berinag Formation of Jaunsar Group. The rock exposed is mostly quartzite of Neo-Proterozoic age. Based on the phase velocity data obtained in frequency domain; the estimated frequency range is within 26- 39 Hz and the range of phase velocity is 307 – 772 ms $^{-1}$.

The average shear wave velocity of Berinag is 712 ms $^{-1}$hence it can be classified in class C i.e. very hard soil and soft rock category. Its estimated average predominant frequency is 5.94 Hz.

This type of lithology mostly having quartzite is averagely suitable for the construction of high rise structures such as dams and buildings however the site is suitable for moderately to low height buildings e.g. schools, primary health centers etc.

Bhageshwar is well known for its scenic beauty, glaciers, rivers and temples. It is located on the confluence of Sarju and Gomati rivers. It is having rocks of Berinag Formation of Jaunsar Group. Quartzite of Neo Proterozoic age is exposed in this area. Based on the phase velocity data obtained in frequency domain; the estimated frequency range is within 7.0 - 39.0 Hz and phase velocity is within the range of 278 -441 ms $^{-1}$.

The average shear wave velocity of Bhageshwar is 409 ms $^{-1}$ hence it can be classified in class C i.e. very hard soil and soft rock category. Its estimated average predominant frequency is 3.41 Hz.

This type of lithology mostly having quartzite is averagely suited for construction of high rise structures such as dams and buildings however the site is perfectly suited for moderately to low rise buildings e.g. schools, primary health centers etc.

Shivpuri Village, located 16 km from Rishikesh, is famous for white water rafting in Ganges. It is located in the foot hills of Himalayas. Stratigraphically it falls in Blaini Formation of Mussoorie Group. The Blaini Formation contains diamictite and siltstone interbedded with greywacke and slates. Based on the phase velocity data obtained in frequency domain; the

estimated frequency range is within 10.0 – 39.0 Hz and the range of phase velocity is 400-1000 ms $^{-1}$.

The average shear wave velocity of Shivpuri is 785 ms $^{-1}$hence it can be classified in class C i.e. very hard soil and soft rock category. Its estimated average predominant frequency is 6.54 Hz.

The results show that the diamictite and siltstone are fragile to moderately consolidated in strength and the estimated frequency range is within 10.2 – 39.0 Hz is not suited for high rise structures but is more suited for low height buildings e.g. schools, houses, hotels etc.

Byasi Village located 35 km from Rishikesh, Uttarakhand besides the holy river Ganges. The village is well known for various rafting camps. Byasi is positioned between MBT and NAT over Lansdown klippe. Stratigraphically it falls in Nathuakhan Formation of Ramgarh Group. The Nathuakhan Formation contains quartzite interbedded with schists.

It has been observed that geological setting and lithology of the area has a major influence on predominant frequency of the ground. Shear wave velocity ranges of Byasi vary from 200 - 502 ms $^{-1}$and average V_{s30} is 382 ms $^{-1}$, hence it can be classified in class C i.e. very hard soil and soft rock category. Its estimated average predominant frequency is 3.19 Hz. The results reveal that the quartzite interbedded with schists, phyllite and slate is not suited for high rise structures such as dams and multi-story buildings however the site is more suited for low height buildings e.g. schools, primary health centers etc. Such analysis should be done for other sites of the Himalayas to obtain the better image of the subsurface. The velocity information is also important for the simulation of earthquake strong ground motions.

4.4. Conclusion

MASW technique is a non-destructive method to measure shear wave velocity and is useful to measure shear wave velocity in an urban region. This technique gives a 2D shear wave velocity model with depth, which can easily be interpreted. This seismic experiment has given important information about the velocity model of the various localities in Kumaon and Garhwal Himalayas. Attained 1D and 2D velocity models help in the soil classification in terms of predominant frequencies, average shear wave velocities and depth of various layered units. Shear wave velocity increases with depth due to greater degree of compaction and central crystalline formation present in the region. Soil classification is carried out on the basis of the results obtained in terms of average shear wave velocity; showing the importance of study in

geotechnical engineering studies. Such analysis should be done for other sites of the Himalayas as well to obtain the better image of the subsurface structure. The underground rock conditions very rapidly, therefore it is critically important to carry out new local measurements for every site. Since most sites analyzed here fall in category C, one in category E, therefore, in general for the Himalaya, resistant building construction seems to be an obligation. The derived velocity information is also important for simulation of earthquake strong ground motions.

Chapter – 5

SITE CHARACTERIZATION OF KUMAON AND GARHWAL HIMALAYAS

Uttarakhand is among seismically active regions of India. The state has encountered several local earthquakes in the recent past. The Kumaon and Garhwal Himalayas lie in the central seismic gap therefore this region is seismologically important (Khattri and Tyagi, 1983; Bilham et al., 2001). The present chapter comprises of the seismo-tectonic of the study area and generalized stratigraphy of the stations. It comprises of the site amplification functions of the region has been estimated using ambient and strong ground motion records. The widely used HVSR technique has been used for the same. The comparison between SSR and HVSR has also been done in this chapter.

Strong motion accelerographs of Kinametrics, USA, have been installed in each stations of this network. Because of high seismic activity and seismic gap of major earthquakes present in this region this strong motion network has great importance in recording recent seismic activities of the region.

Traditionally, the seismic risk study focuses on the seismic hazard estimation. But, over the years another factor of site amplification has been found to be as important as the seismic risk estimation. The site amplification effects in the area predominantly depend on the soil compaction. The soil compaction study requires the knowledge of the subsurface shear wave velocity structure. This velocity structure can then be used to classify the soil in the region in number of classes, depending upon the compaction levels.

The HVSR technique introduced by Nogoshi and Igarashi (1971) and made popular by Nakamura (1989) by considering H/V ratio of microtremors to estimate site amplification factors. It has been assumed in this approach that the vertical component of ground motion contains more information on the source of ground motion than that of horizontal component and the vertical component are free of any kind of site effect. It has been found in some studies that the H/V ratios for short-period microtremors agree with the theoretical site amplification factors (e.g. Wakamatsu and Yasui 1995; Konno and Ohmachi 1998). The approach of Nakamura (1989) has been extended by Lermo and Chavez-Garcia (1993) by using earthquake records, instead of microtremors, recorded at single station and concluded that a first estimate

of dominant period and local spectral amplification level can be obtained using H/V ratio of earthquake if site effects are caused by simple geology. They have shown that the period of the first resonant mode and the overall amplification level can be reasonably estimated from H/V ratio. It has been shown in some studies that Nakamura (1989) approach gives reliable estimates of fundamental resonant frequency and underestimates the amplification levels (Field and Jacob 1995; Seekins et al. 1996). The validity of the assumptions involved in using H/V ratio technique has been tested by Castro et al. (1997) and concluded that as long as vertical component of motion is not contaminated by surface waves, the source effect can be eliminated from S wave spectra by calculating H/V ratios. Huang and Teng (1999) compared the site effects estimated using H/V ratio with those of obtained using SSR approach and found that the resonant frequency and spectral amplification level of the site response can be estimated using H/V technique.

5.1. Seismo-tectonics of the region

The Kumaon and Garhwal Himalayas lie in the state of Uttarakhand, India and share its border with Nepal. It falls in the seismic zone IV and V, as per the Seismic Zoning map of India (BIS, 2002). Himalayan fold thrust movement causes high seismic activity in this region. Recurrence of many former faults and thrusts during Quaternary period is evident in this region. It falls between the Eurasian plate and Indo-Australian plate, where the stress is constantly getting accumulated giving indications of a potential major earthquake (M_w>8.0). Considering the historical earthquakes across these two plates, Kumaon Himalayas find itself in a central Himalayan seismic gap. Hence, the site amplification studies are important for this region.

The present area of study belongs to the Kumaon and Garhwal Himalayas, India as shown in Figure 3.1, along with the stations. Red Circles show the location of the stations with station codes as mentioned in Table 4.1. The stations as per the generalized stratigraphy and lithology are tabulated in Table 5.1 and 5.2 (Valdiya, 1980).

Table 5.1: Generalized stratigraphy and lithology at various stations in Kumaon Himalayas.

Sr. No.	Station Name	Formation	Lithology	Group / Stratigraphy units	Age
1	Didihat	Askot Crystalline	Granite Gneiss, Quartzite, mica-schist and amphibolite	Askot Crystalline	Mesoproterozoic
2	Pithoragarh	Mandhali	Limestone, Dolomite and Quartzite	Tejam Group	Upper Riphean-Early Vendian
3	Tejam	Deoban	Quartzite, Dolomite	Tejam Group	Middle Riphean-Upper Riphean
4	Dharchula	Mandhali	Slate, Phyllite and Limestone, Dolomite	Tejam Group	Upper Riphean-Early Vendian
5	Munsyari	Munsyari	Granite Gneiss, Quartzite, mica-schist and amphibolite	Almora Group	Mesoproterozoic
6	Askot	Askot Crystalline	Granite Gneiss, Quartzite, mica-schist and amphibolite	Askot Crystalline	Mesoproterozoic
7	Kamedidevi	Berinag	Quartzite	Jaunsar Group	Neo-Proterozoic
8	Jouljibi	Mandhali	Slate, Phyllite and Limestone, Dolomite	Tejam Group	Upper Riphean-Early Vendian
9	Baluakot	Rautgara	Quartzite, Slate and conglomerate bands	Damtha Group	Lower Riphean-Middle Riphean
10	Knalichhina	Deoban	Quartzite, Dolomite	Tejam Group	Middle Riphean-Upper Riphean
11	Muavani	Deoban	Quartzite, Dolomite	Tejam Group	Middle Riphean-Upper Riphean
12	Berinag	Berinag	Quartzite	Jaunsar Group	Neo-Proterozoic
13	Mangti	Munsyari	Granite Gneiss, Quartzite, mica-schist and amphibolite	Almora Group	Mesoproterozoic
14	Sobla	Munsyari	Granite Gneiss, Quartzite, mica-schist and amphibolite	Almora Group	Mesoproterozoic
15	Thal	Mandhali	Slate, Phyllite and Limestone, Dolomite	Tejam Group	Upper Riphean-Early Vendian
16	Bhageshwar	Berinag	Quartzite	Jaunsar Group	Neo-proterozoic
17	Kapkot	Deoban	Quartzite, Dolomite	Tejam Group	Middle Riphean-Upper Riphean
18	Nachni	Deoban	Quartzite, Dolomite	Tejam Group	Middle Riphean-Upper Riphean
19	Narayan Nagar	Askot Crystalline	Granite Gneiss, Quartzite, mica-schist and amphibolite	Askot Crystalline	Mesoproterozoic

Table 5.2: Generalized stratigraphy and lithology at various stations in Garhwal Himalayas.

Sr. No.	Station Name	Formation	Lithology	Group / Stratigraphy units	Age
1	Rishkesh	Blaini	Diamictites, siltstone and greywacke and slates.	Mussoorie Group	Neo-Proterozoic
2	Narendra Nagar	Blaini	Diamictites, siltstone and greywacke and slates.	Mussoorie Group	Neo-Proterozoic
3	Shivpuri	Blaini	Diamictites, siltstone and greywacke and slates.	Mussoorie Group	Neo-Proterozoic
4	Chamba	Nagthat	Quartzite	Jaunsar Group	Neoproterozoic
5	Tehri	Chandpur	Phyllite	Jaunsar Group	Neoproterozoic
6	Muni Ki reti	-	Alluvium/Doon Gravel	Quaternary	Quaternary
7	Gochar	Garhwal Group	Quartzite	Garhwal Group	Precambrian
8	Devprayag	Chandpur	Phyllite	Jaunsar Group	Neoproterozoic

5.2. Site Amplification Functions

The total 27 stations of Kumaon and Garhwal Himalayas, India has been used to carry out the site characterization. Total number of ambient noise and event data used in the study has been tabulated in Table 5.3.

Whenever the density of the data is more, best twenty records are selected considering good data quality at each station. The strong ground motion data could not be recorded at five stations out of eight Garhwal stations. The stations of the Kumaon and Garhwal Himalayas with station codes along with the total number of ambient noise and event data used in the present study are tabulated in Table 5.3.

Table 5.3: The stations of Kumaon and Garhwal Himalayas, India with station codes are tabulated along with the total number of ambient noise and event data used in the present study.

Sr. No.	Station Name	Station Code	Number of ambient noise data used in the analysis	Number of event data used in the analysis
1	Didihat	DID	20	14
2	Pithoragarh	PIT	19	9
3	Tejam	TEJ	20	13
4	Dharchula	DHA	20	20
5	Munsyari	MUN	20	12
6	Askot	ASK	16	20
7	Kamedidevi	KAMD	20	10
8	Jouljibi	JOL	20	17
9	Baluakot	BAL	20	20
10	Knalichhina	KNA	20	14
11	Muavani	MUA	20	20
12	Berinag	BERI	20	17
13	Mangti	MAN	20	4
14	Sobla	SOB	18	4
15	Thal	THA	20	7
16	Bhageshwar	BHAG	19	12
17	Kapkot	KAP	16	12
18	Nachni	NAC	14	2
19	Narayannagar	NYN	20	4
20	Rishkesh	RIS	18	1
21	Narendranagar	NAN	7	-
22	Shivpuri	SHIV	8	-
23	Chamba	CMB	3	11
24	Tehri	TER	4	5
25	Muni ki reti	MKR	14	-
26	Gochar	GUC	9	-
27	Devprayag	DPG	2	-

The hypocentral parameters of events used in the present study and the error obtained in its localization are tabulated in Table 5.4 along with ERH and ERZ which define the error of epicenter and focal depth, respectively from year 2006 to 2012 at the various sites in Kumaon Himalayas. The hypocentral parameters of events used in the present study in Garhwal Himalayas are tabulated in Table 5.5.

Table 5.4: Hypocentral parameters of events used in the present study and the error obtained in its localization. ERH and ERZ define the error of epicenter and focal depth, respectively from year 2006 to 2012 at the various sites in Kumaon Himalayas.

Sr. No.	Date D/M/Y	UTC Origin time Hr:min:Sec	Epicenter	Depth (km)	No. of Stations (Station code)	RMSE	ERH (km)	ERZ (km)
1	01/04/06	19:42:52.1	30º12.73', 80º 24.13'	11	03 (DHA,DID, SOB)	0.03	0.4	1.1
2	05/05/06	8:00:28.72	29º42.65', 80º 42.16'	30	05(DHA,DID,PIT,THA, SOB)	0.31	2.7	1.7
3	05/05/06	8:49:46.48	29º41.43', 80º 45.98'	25	05(DHA,DID,PIT,THA, SOB)	0.27	4.2	13
4	07/05/06	06:46:03.72	29º57.57', 80º 47.89'	35	03 (DHA,DID, THA)	0.45	14.1	4.5
5	30/05/06	18:25:18.03	29º54.14', 80º 26.95'	03	04 (DHA,DID,THA,SOB)	0.25	0.9	1.9
6	27/10/06	7:55:01.39	29º57.46', 80º 15.23'	13	02 (PIT, THA)	0.27	5.6	3.1
7	27/10/06	08:01:32.23	29º52.35', 80º 17.70'	16	01 (THAL)	0.21	3.1	1.3
8	05/02/07	07:57:35.08	29º51.96', 80º 16.55'	31	01 (PIT)	0.04	0.8	0.5
9	19/08/08	10:54:32.17	29º45.16', 79º 42.27'	34	01 (MAN)	4.88	71	84
10	04/09/08	12:53:10.14	30º8.38',80º 15.28'	15	02 (DHA,MAN)	0.13	1.7	1.0
11	04/09/08	17:38:14.20	29º80.17', 80º 19.03'	03	02 (DHA,MAN)	1.28	11.3	3.9
12	17/09/08	16:59:09.12	30º04.49', 80º 35.62'	25	03 (DHA,MAN)	3.03	50	41
13	06/12/09	04:35:51.56	29º54.19', 80º 15.21'	05	02 (DHA,PIT)	1.50	6.6	53
14	08/12/09	07:05:16.70	30º22.39', 80º 13.22'	13	02 (DHA,PIT)	0.53	8.4	5.6
15	11/01/10	05:15:14.61	29º48.68', 80º 25.06'	12	02 (DHA)	0.03	0.2	0.6
16	12/01/10	09:35:21.62	29º51.73', 80º 21.30'	05	02 (DHA,PIT)	0.29	0.4	7.2
17	26/01/10	06:51:13.30	29º51.82', 80º 19.89'	03	02 (DHA,PIT)	0.40	2.3	1.5
18	07/02/10	07:16:41.68	29º52.14', 80º 21.48'	03	02 (DHA,PIT)	0.15	0.92	0.8
19	26/02/10	04:43:44.63	28º43.94', 80º 45.50'	25	01 (DHA)	0.21	3.1	----
20	04/07/10	02:24:02.70	29º51.27', 80º 20.28'	11	01 (ASK)	0.06	0.7	0.7
21	04/07/10	02:35:57.50	29º51.28', 80º 21.16'	13	01 (ASK)	0.23	2.4	1.9
22	04/07/10	07:46:38.09	29º47.47', 80º 28.16'	08	01 (ASK)	0.11	1.6	1.8
23	06/07/10	19:08:21.96	29º50.05', 80º 21.59'	12	01 (ASK)	0.02	0.3	0.2

24	06/07/10	19:11:54.09	29º47.73', 80º 27.61'	07	01 (ASK)	0.09	1.2	1.6
25	10/07/10	03:16:22.67	29º45.16', 80º 35.62'	49	01 (ASK)	0.45	11	9
26	19/07/10	00:08:41.44	29º52.41', 80º 26.38'	11	01 (ASK)	0.31	2.9	2.0
27	23/07/10	23:22:36.53	29º35.04', 80º 34.07'	06	01 (ASK)	0.47	13	8.2
28	08/10/10	17:10:13.64	29º48.57', 80º 35.62'	18	01 (ASK)	0.27	5.7	3.2
29	15/12/10	05:33:02.45	29º45.16', 80º 27.00'	25	02 (DHA, ASK)	2.6	54	29
30	16/12/10	10:34:08.21	29º45.16', 80º 23.73'	19.7	02 (DHA, ASK)	0.93	18.3	11.1
31	17/12/10	12:14:50.84	29º48.45', 80º 16.91'	16.4	03 (DHA, DID, ASK)	0.37	3.1	2.5
32	09/01/11	11:48:46.06	29º32.95', 80º 35.62'	22.5	02 (DHA, ASK)	2.9	44	51
33	14/03/11	09:01:33.39	29º55.49', 81º 26.31'	17	02 (DID, ASK)	1.31	45	---
34	16/03/11	02:16:46.73	29º54.09', 80º 14.19'	3.5	01 (ASK)	0.26	3.2	2.3
35	21/03/11	09:52:44.75	29º31.94', 80º 55.59'	16.2	01 (ASK)	1.2	6.1	9.3
36	04/04/11	11:31:41.13	29º35.44', 80º 24.66'	25	01 (ASK)	1.7	8.8	8.3
37	05/05/11	07:15:22.18	30º01.56', 80º 37.94'	37	01 (ASK)	0.14	8	2.6
38	08/05/11	12:32:15.32	30º03.55', 80º 37.40'	34	03 (ASK)	0.04	2.5	1.1
39	11/06/11	02:59:03.70	30º13.08', 80º 22.11'	20.8	04 (DID)	0.16	6.0	4.5
40	23/06/11	06:27:19.53	30º37.72', 80º 49.80'	25	01 (MUN)	1.38	12	6
41	12/07/11	01:41:01.54	29º48.26', 80º 30.45'	12.3	02 (JOL, KNA)	0.24	3.6	1.6
42	12/07/11	01:44:26.07	29º48.32', 80º 30.43'	11.3	01 (JOL)	0.15	2.9	1.2
43	01/08/11	10:14:23.52	29º58.34', 79º 58.70'	25	02 (BHAG, MUA)	2.28	51	52
44	08/08/11	05:31:06.95	29º49.63', 80º 32.82'	6.7	01 (JOL)	0.7	15	6
45	19/08/11	01:52:42.91	29º40.89', 80º 24.37'	8.4	05 (JOL, BERI, BHAG, MUN, MUA)	2.89	39	97
46	06/09/11	08:54:28.61	29º45.16', 80º 22.91'	2	04(ASK, BAL, JOL, MUA)	1.37	6.5	5.7
47	17/09/11	00:21:39.64	29º52.43', 80º 25.69'	1.15	01 (JOL)	0.2	18	21
48	18/09/11	12:41:00.56	27º45.16', 88º 12.00'	30	04 (JOL, BERI, BHAG, MUA)	0.52	----	----
49	01/10/11	04:26:53.38	29º53.16', 80º 27.84'	25	01 (MUA)	2	2.5	5.1
50	09/10/11	07:34:55.69	29º56.93',	22	06 (DHA, JOL, TEJ,	----	3.2	4.7

			80º 30.53’		KANA BERI, MUA)			
51	06/11/11	18:34:46.05	29º56.09’, 80º 25.07’	17	05(KNA,BERI,BHAG, MUN, MUA)	----	2.1	3.2
52	11/11/12	18:39:21.29	29º56.54’, 81º 13.35’	29	01 (DID)	0.95	3.1	9.7
53	15/11/12	06:46:05.64	29º53.44’, 79º 59.86’	14	01 (DID)	0.56	5.0	3.9
54	18/11/11	09:50:37.56	29º51.00’, 79º 54.02’	31	05(BAL, BERI, BHAG, MUN, MUA))	1.54	14	9
55	23/11/11	00:27:09.20	29º35.74’, 80º 29.18’	3.4	02 (BAL, MUN)	0.94	3.4	3.6
56	05/12/12	00:18:50.26	29º54.37’, 79º 58.06’	20	01 (DID)	1.02	5.6	7.7
57	09/12/11	08:22:47.12	29º51.25’, 80º 29.84’	10	05(BAL, KNA BERI, MUN, MUA)	0.44	4.3	2.9
58	25/12/11	08:28:48.31	29º49.30’, 80º 31.34’	10.87	03 (BALW, JOL, MUA)	0.92	19	5.7
59	07/01/12	13:13:04.34	29º52.37’, 80º 25.51’	3.85	02 (BAL, JOL)	0.31	5.7	11.3
60	09/01/12	10:41:15.17	29º51.38’, 80º 35.62’	25	03 (BAL, JOL, MUA)	1.97	27	11
61	11/01/12	09:00:27.44	29º47.73’, 80º 29.76’	13	02 (BAL, MUN)	0.42	10	3.5
62	13/01/12	01:26:18.19	29º55.12’, 80º 35.62’	25	01 (BAL)	1.8	7.1	8.1
63	16/01/12	05:01:50.15	29º46.81’, 79º 59.46’	25	05(BAL, JOL, BERI, MUN, MUA,)	0.27	5	2.3
64	19/01/12	00:47:10.70	29º40.71’, 81º 14.06’	15.11	02 (BAL, MUN)	6.25	---	---
65	09/02/12	19:17:31:60	30º32.21’, 79º 35.62’	26	03 (JOL, BHAG, MUN)	0.51	4.2	5.0
66	12/02/12	06:40:02.17	29º45.16’, 79º 41.22’	17.24	03 (KNA, BERI, MUA)	1.02	9.8	---
67	26/02/12	22:57:01.35	29º45.16’, 80º 35.62’	25	06(KNA, KMD, BERI, BHAG,MUN, MUA)	1.2	7.9	4.5
68	26/02/12	23:06:05.92	29º40.42’, 80º 48.93’	16.11	05(KNA, KMD, BERI, BHAG, MUN)	2.4	3.4	1.5
69	16/03/12	15:22:42.07	29º54.67’, 80º 04.02’	11.47	01 (KMD)	0.23	3.5	5.2
70	16/03/12	19:35:50.36	29º50.84’, 79º 50.52’	20	03 (KMD, BERI, BHAG)	0.60	7.6	4.3
71	27/03/12	05:30:42.62	29º45.39’, 80º 27.79’	5.97	01 (KNA)	0.69	9.6	4.0
72	08/04/12	07:38:14.81	29º57.69’, 80º 15.93’	13.8	01 (KMD)	1.46	9.8	4.2
73	11/04/12	02:53:12.09	29º45.16’, 80º 35.62’	25	03 (TEJ, KNA, BHAG)	----	---	---
74	06/05/12	08:10:53.87	29º45.16’, 80º 35.62’	12.35	01 (KNA)	1.1	2.3	2.2
75	10/05/12	22:00:38.82	30º07.20’, 79º 35.14’	17	03 (KNA, KMD, BHAG)	0.3	5.4	3.4
76	17/05/12	03:31:38.54	29º34.58’, 80º 35.62’	25	04 (KNA, KMD, BERI, BHAG)	0.32	6.1	4.2

77	17/06/12	07:44:29.32	29º53.87’, 80º 20.34’	19	01 (BAL)	0.41	1.4	8.4
78	21/06/12	07:36:18.36	29º22.20’, 80º 35.62’	21	02 (BAL, KNA)	1.86	5.2	4.3
79	19/07/12	22:36:51.30	29º49.53’, 80º 08.04’	24	02 (BAL, BERI)	1.12	10.5	10.7
80	27/07/12	01:46:55.72	29º48.28’, 80º 21.62’	21	01 (BAL)	0.11	1.7	1.2
81	28/07/12	05:48:05.83	29º49.48’, 80º 32.47’	25	02 (BAL, BERI)	0.40	5.4	5.1
82	30/07/12	11:43:39.34	29º43.32’, 80º 35.14’	22	01 (BAL)	0.05	1.0	0.8
83	02/08/12	16:43:30.46	29º43.77’, 80º 35.92’	24	01 (BERI)	0.04	0.9	0.7
84	04/08/12	22:05:27.34	29º47.87’, 80º 21.20’	20	01 (BERI)	0.65	6.7	5.3
85	27 /08/12	16:19:20.38	29º45.51’, 80º 11.54’	18	02 (BAL, BERI)	0.98	1.2	4.6
86	09/09/12	17:02:33.05	29º49.97’, 80º 20.05’	27	01 (BAL)	1.2	2.2	4.5
87	11/11/12	18:39:21.29	29º26.54’, 81º 13.35’	29	01 (KNA)	0.95	3.1	9.7
88	15/11/12	06:46:05.64	29º53.44’, 79º 59.86’	14	02 (KMD, BERI)	0.56	5.0	3.9
89	27/11/12	12:15:17.34	30º11.18’, 79º 08.15’	29	01 (KMD)	1.44	11.0	9.8
90	22/04/15	01:30:02.67	29º45.16’, 80º 35.62’	12	01 (KAP)	5.36	10	3.5
91	25/04/15	06:46:20.54	29º26.41’, 80º 35.62’	16	01 (KAP)	0.57	----	----
92	01/01/16	06:54:30.76	29º07.16’, 80º 07.09’	07	02 (KAP, NYN)	1.63	1.7	1.2
93	15/02/16	16:35:29.00	30º20.00’, 79º 60.00’	10	01 (KAP)	1.11	3.4	1.5
94	10/04/16	10:28:57.01	36º40.00’, 71º 20.00’	190	01 (NYN)	1.33	----	----
95	11/04/16	10:36:13.05	29º59.20’, 80º10.00’	10	03 (KAP,NAC,NYN)	0.98	6.1	4.2
96	13/04/16	13:55:13.25	23º00.00’, 94º90.00’	134	01 (KAP)	0.05	10	3.5
97	05/05/16	18:00:30.33	30º40.00’, 80º10.00’	15	03 (KAP,NAC,NYN)	1.60	1.7	1.2
98	07/06/16	20:10:37.18	29º90.00’, 80º20.00’	13	01 (KAP)	0.66	----	----
100	29/06/16	09:27:02.08	29º20.00’, 81º10.00’	10	01 (KAP)	1.30	3.4	1.5
101	02/07/16	20:10:37.09	29º40.00’, 81º10.00’	11	01 (KAP)	0.53	----	----
102	09/07/16	20:42:08.55	29º90.00’, 80º20.00’	10	01 (KAP)	1.78	----	----
103	13/08/16	15:41:03.14	30º00.00’, 80º20.00’	9	01 (KAP)	1.05	6.1	4.2

Table 5.5: Hypo-central parameters of events used in the present study. The recorded data is from year 2005 to 2013 at the various sites in Garhwal Himalayas from PESMOS network.

Sr. no.	**Date D/M/Y**	**UTC Origin time Hr:min:Sec**	**Epicenter**	**Depth (km)**	**Magnitude**	**No. of stations (Station Code)**
1	14/12/2005	07:09:48	30.9 N79.3 E	25.7	5.2	1(TER)
2	04/10/2007	5:14:15	32.5 N 76.0 E	10.0	3.8	1(CMB)
3	29/05/2008	22:30:24	29.8 N 79.7 E	-	-	1(CMB)
4	31/01/2009	03:07:15	32.5 N 75.9 E	10.0	3.7	1(CMB)
5	04/06/2009	13:50:54	29.8 N 79.7E	-	-	1(CMB)
6	17/07/2009	11:07:47	32.3 N 76.1E	39.3	3.7	1(CMB)
7	03/05/2010	17:15:08	30.4 N 78.4 E	8.0	3.5	1(TER)
8	21/06/2010	08:40:16	32.5 N 76.1E	-		1(CMB)
9	04/04/2011	11:31:40	29.6 N 80.8 E	10.0	5.7	1(TER)
10	20/06/2011	06:27:18	30.5 N 79.4E	12.0	4.6	2(TER,RIS)
11	27/11/2012	12:15:15	30.9 N 78.4E	12.0	4.8	1(TER)
12	28/02/2013	08:13:14	29.8 N 79.7E	-	-	1(CMB)
13	04/06/2013	17:33:30	29.8 N 79.7E	-	-	1(CMB)
14	05/06/2013	22:04:00	32.8 N 76.3E	10.0	4.5	1(CMB)
15	20/10/2013	19:45:05	35.8 N 77.5E	80.0	5.5	1(CMB)
16	06/11/2013	14:53:08	31.4 N 76.1E	10.0	4.9	1(CMB)

In the present work many events and ambient noise records have been used at each station. Some of the processed event records used in the present work is shown in Fig. 5.1 to 5.22. The epicenter and origin time of the events are also shown along with the location of recording station in the tectonic map of the region taken from GSI (2000).

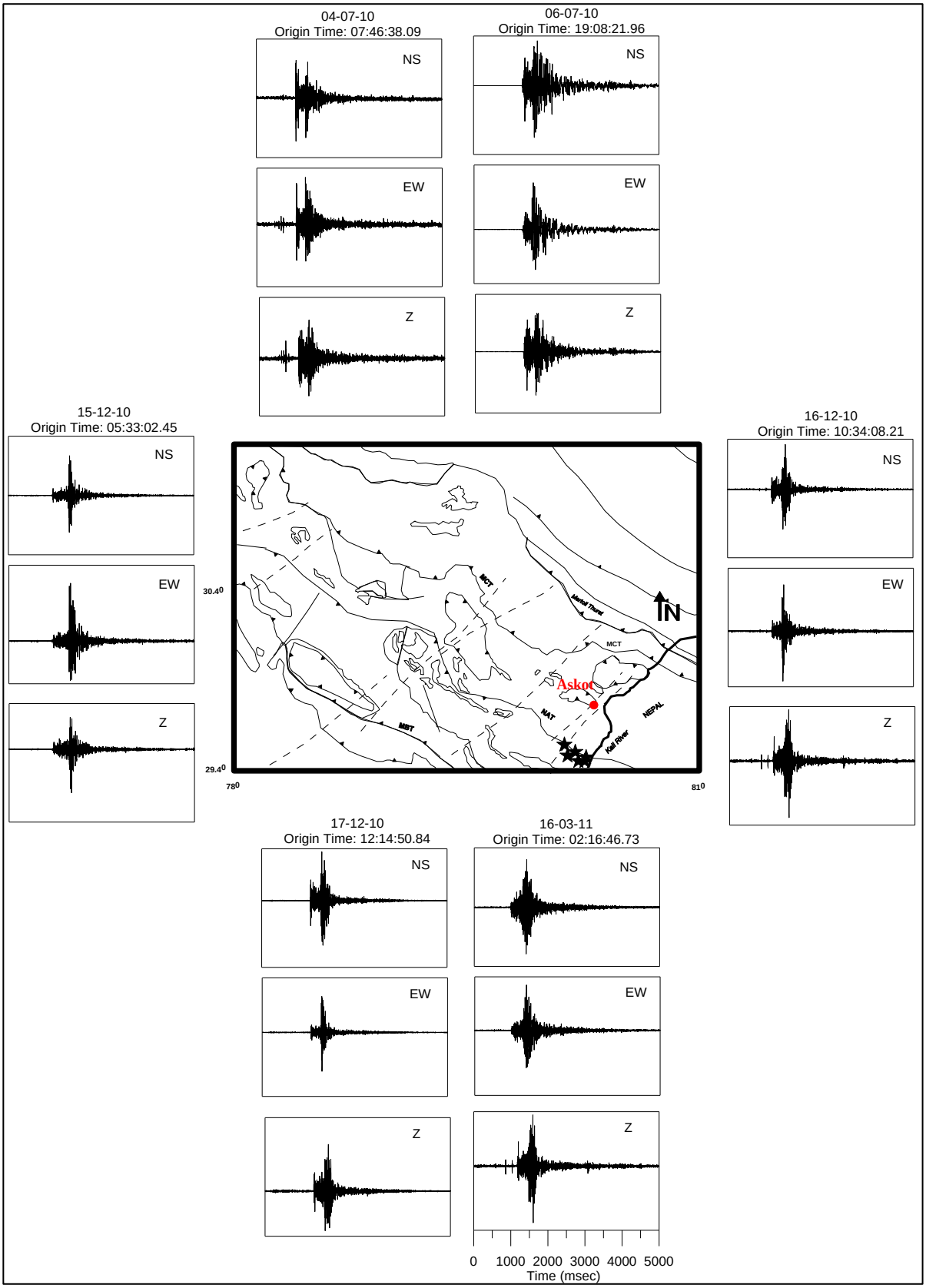

Figure 5.1: Normalized processed NS, EW and Z component of accelerograms of the shown events used at Askot station. Star denotes the epicenter of events. Solid red circle shows the location of recording station. The tectonics of the region is taken after GSI (2000).

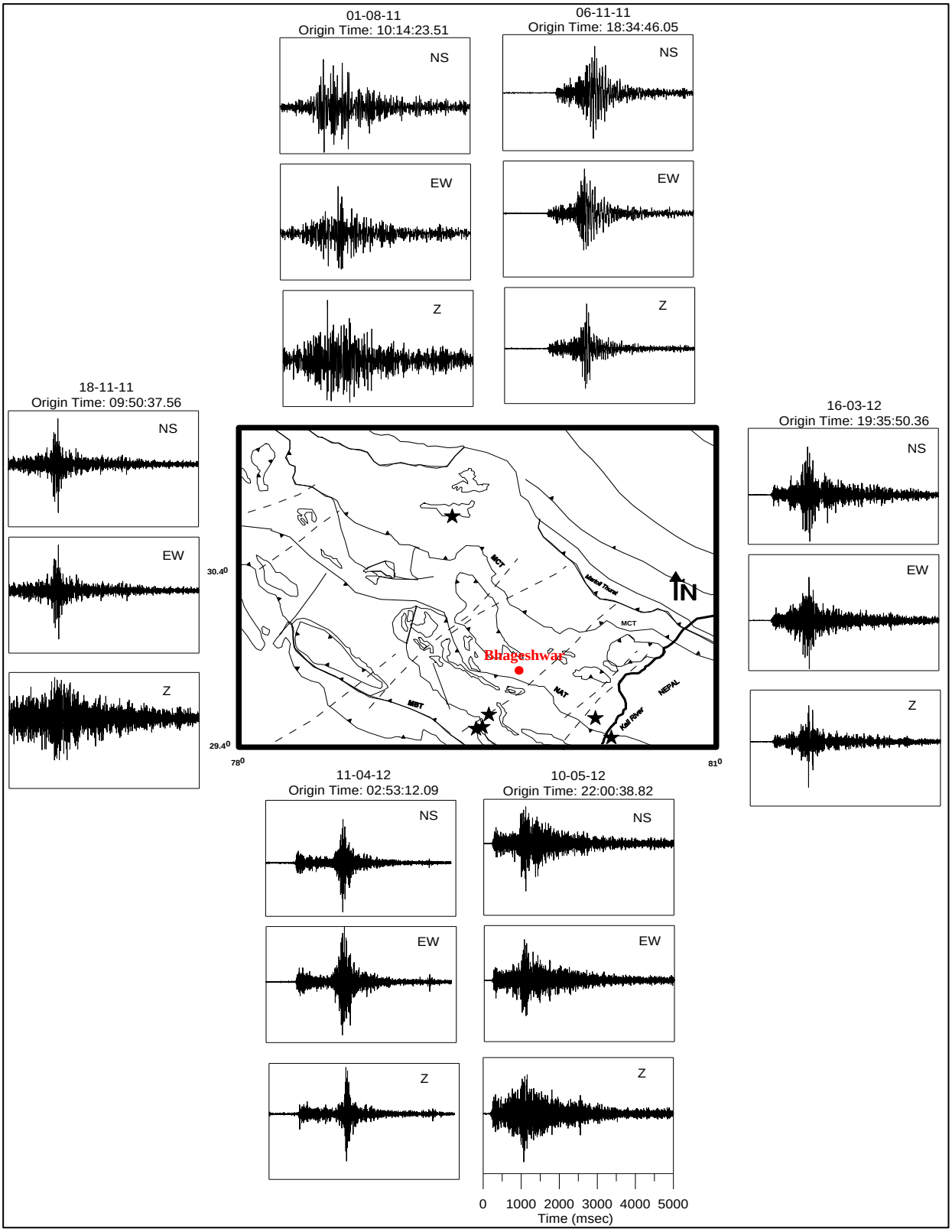

Figure 5.2: Normalized processed NS, EW and Z component of accelerograms of the shown events used at Bhageshwar station. Star denotes the epicenter of events. Solid red circle shows the location of recording station. The tectonics of the region is taken after GSI (2000).

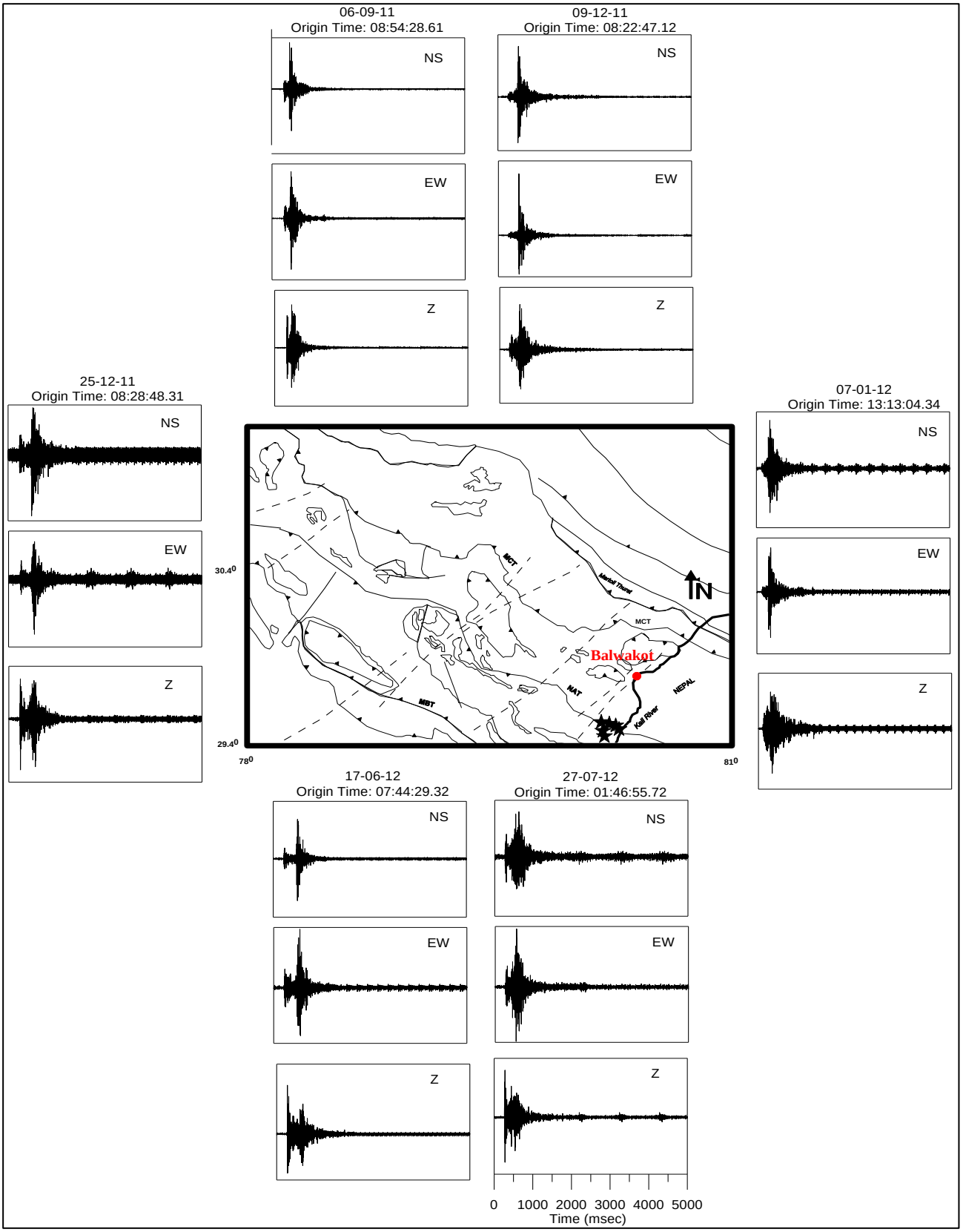

Figure 5.3: Normalized processed NS, EW and Z component of accelerograms of the shown events used at Baluakot station. Star denotes the epicenter of events. Solid red circle shows the location of recording station. The tectonics of the region is taken after GSI (2000).

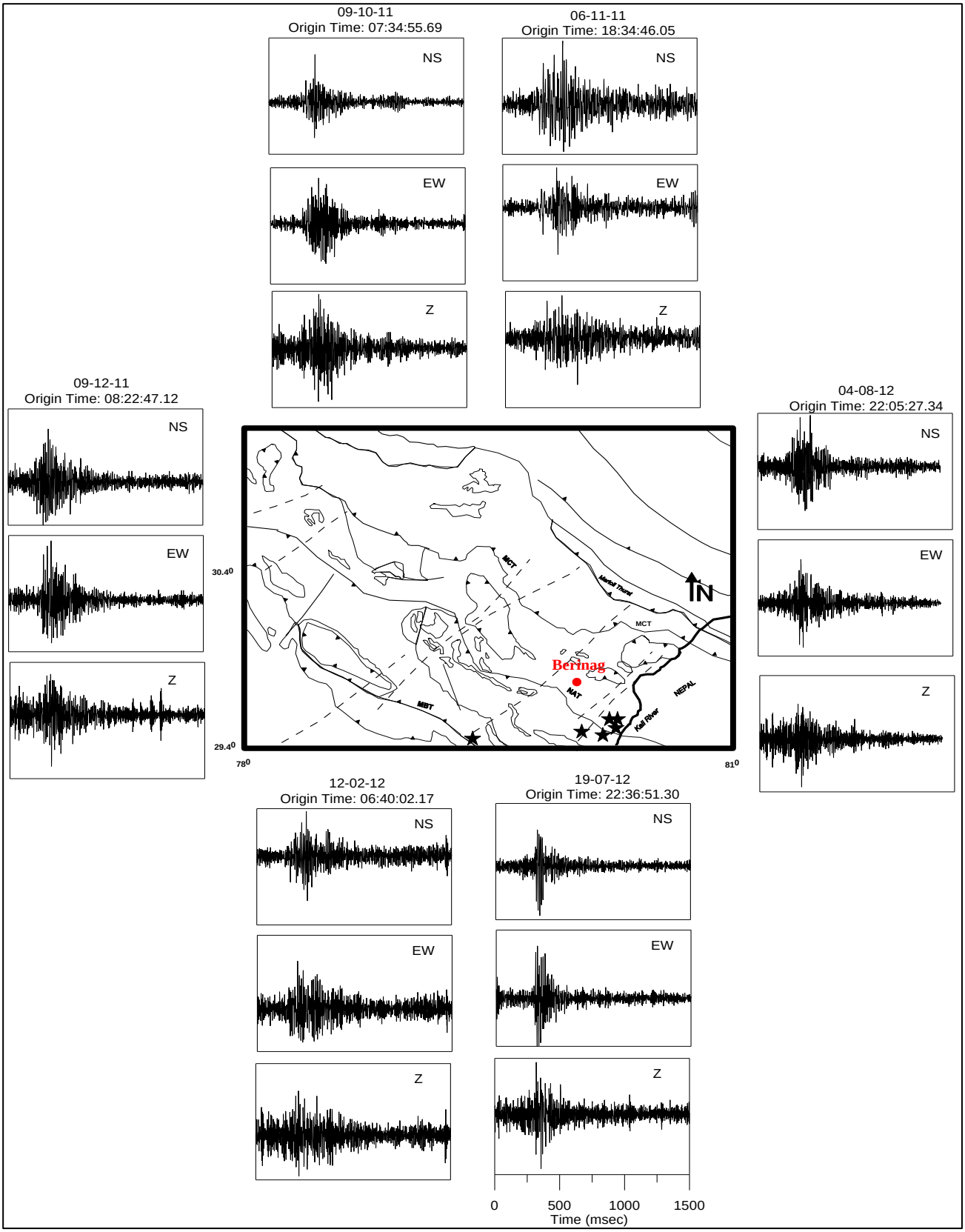

Figure 5.4: Normalized processed NS, EW and Z component of accelerograms of the shown events used at Berinag station. Star denotes the epicenter of events. Solid red circle shows the location of recording station. The tectonics of the region is taken after GSI (2000).

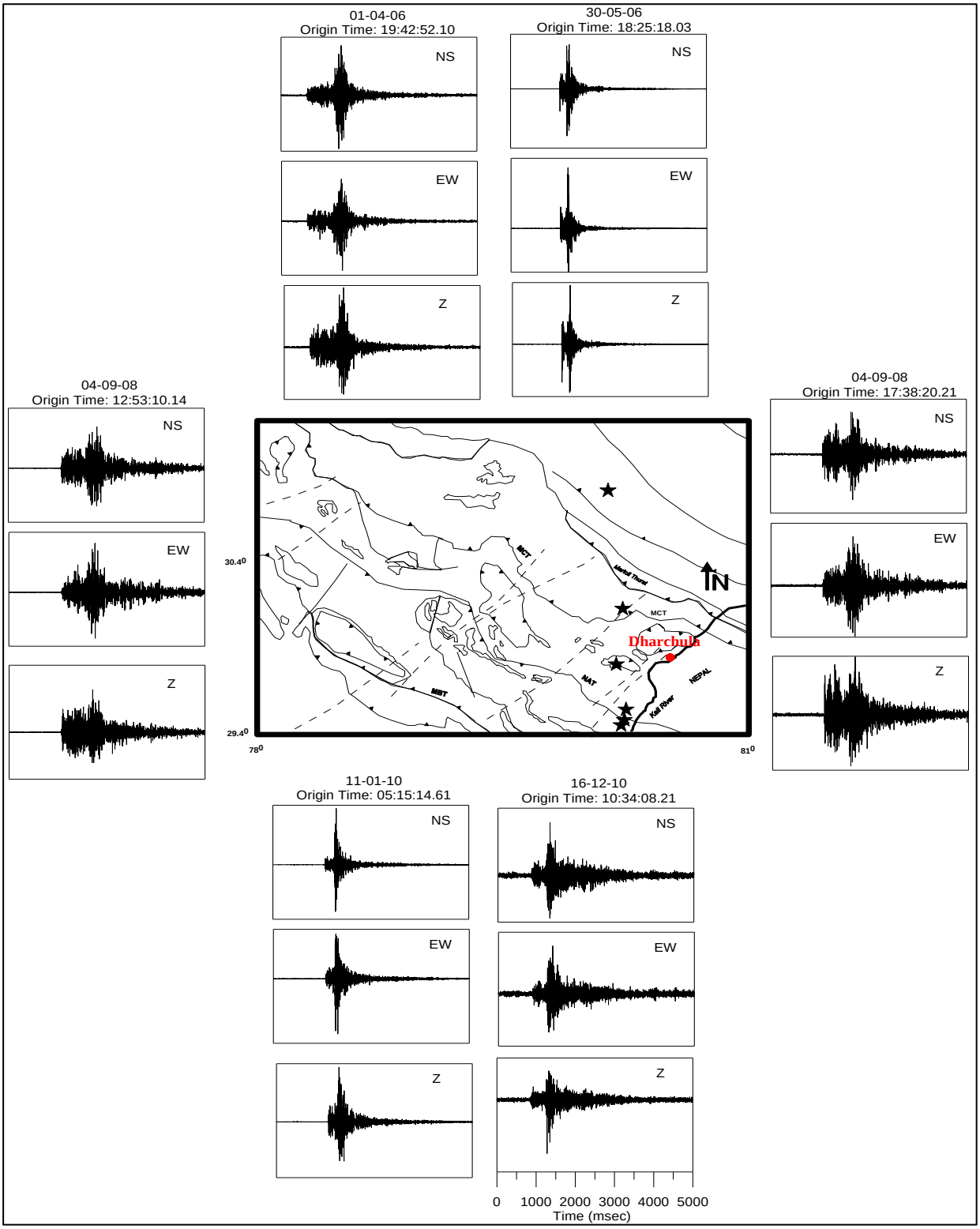

Figure 5.5: Normalized processed NS, EW and Z component of accelerograms of the shown events used at Dharchula station. Star denotes the epicenter of events. Solid red circle shows the location of recording station. The tectonics of the region is taken after GSI (2000).

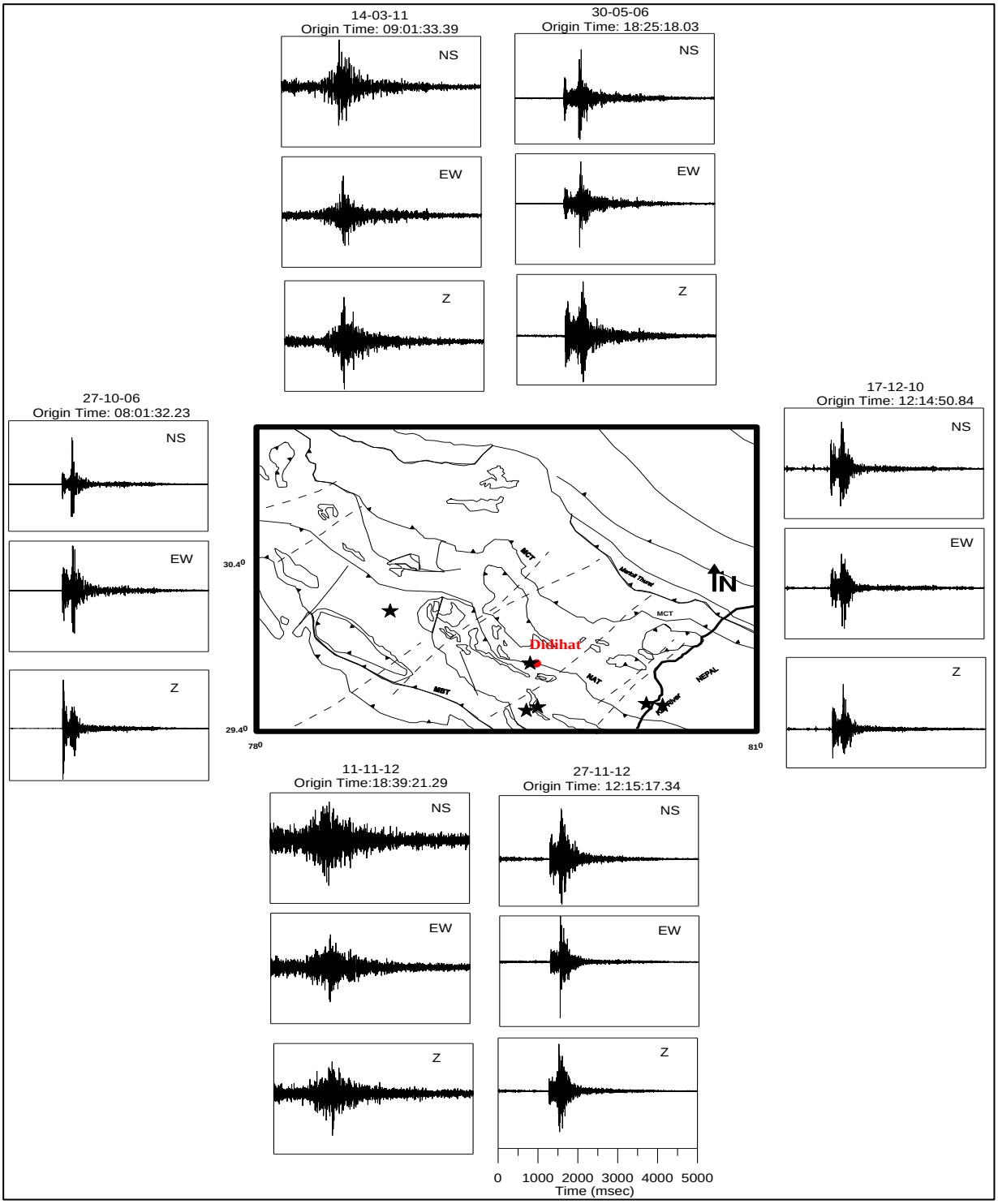

Figure 5.6: Normalized processed NS, EW and Z component of accelerograms of the shown events used at Didihat station. Star denotes the epicenter of events. Solid red circle shows the location of recording station. The tectonics of the region is taken after GSI (2000).

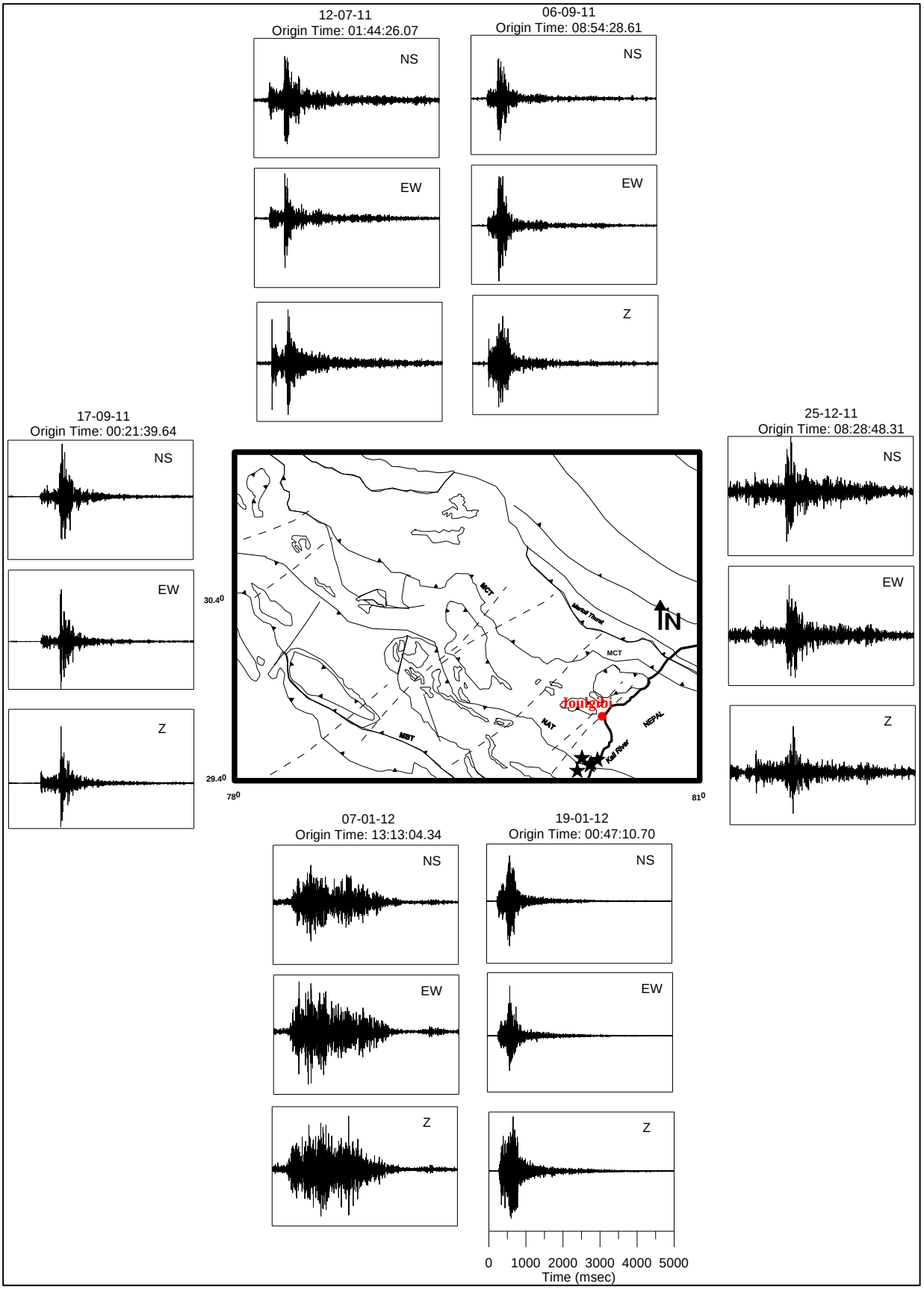

Figure 5.7: Normalized processed NS, EW and Z component of accelerograms of the shown events used at Jouljibi station. Star denotes the epicenter of events. Solid red circle shows the location of recording station. The tectonics of the region is taken after GSI (2000).

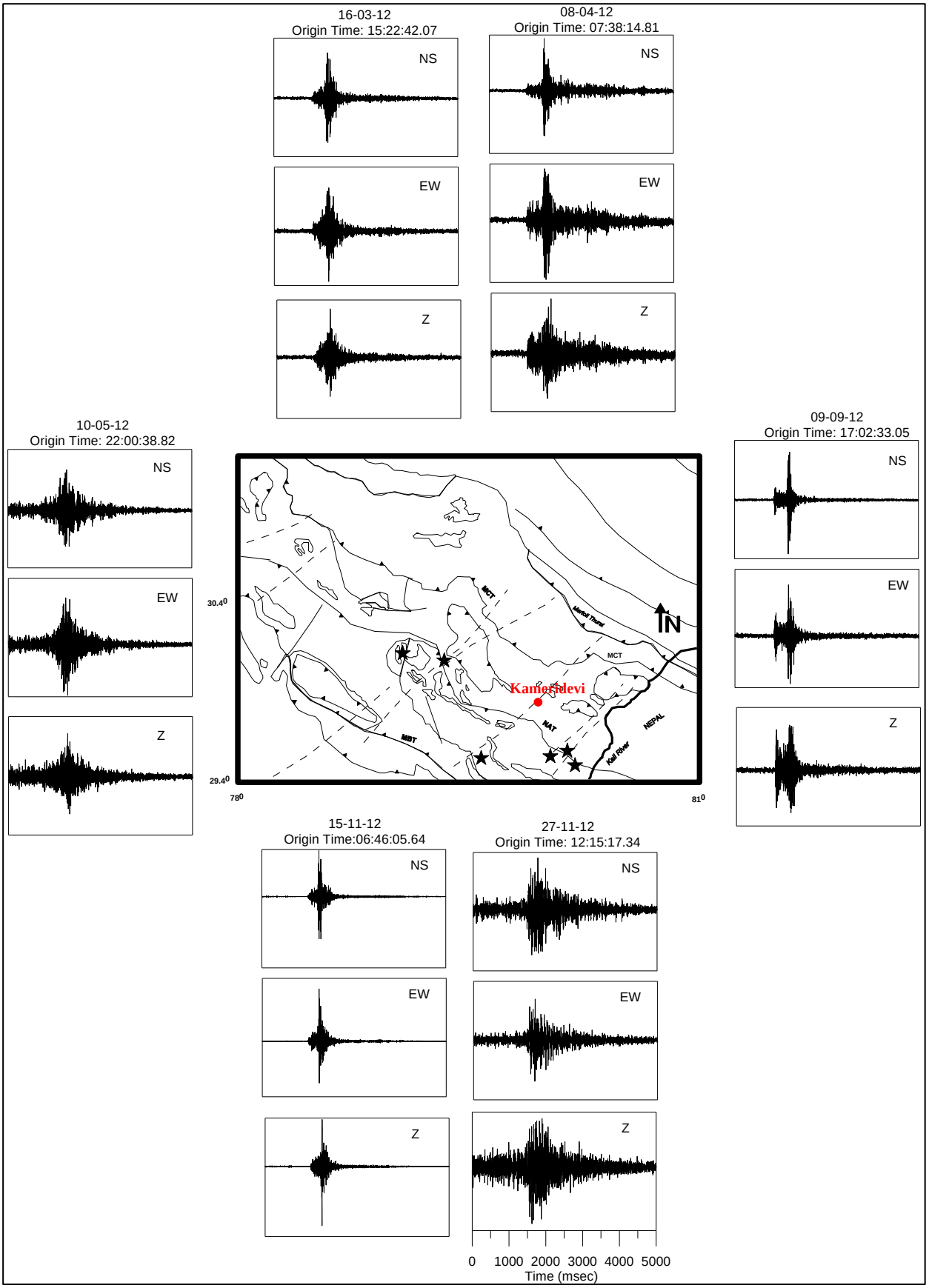

Figure 5.8: Normalized processed NS, EW and Z component of accelerograms of the shown events used at Kameridevi station. Star denotes the epicenter of events. Solid red circle shows the location of recording station. The tectonics of the region is taken after GSI (2000).

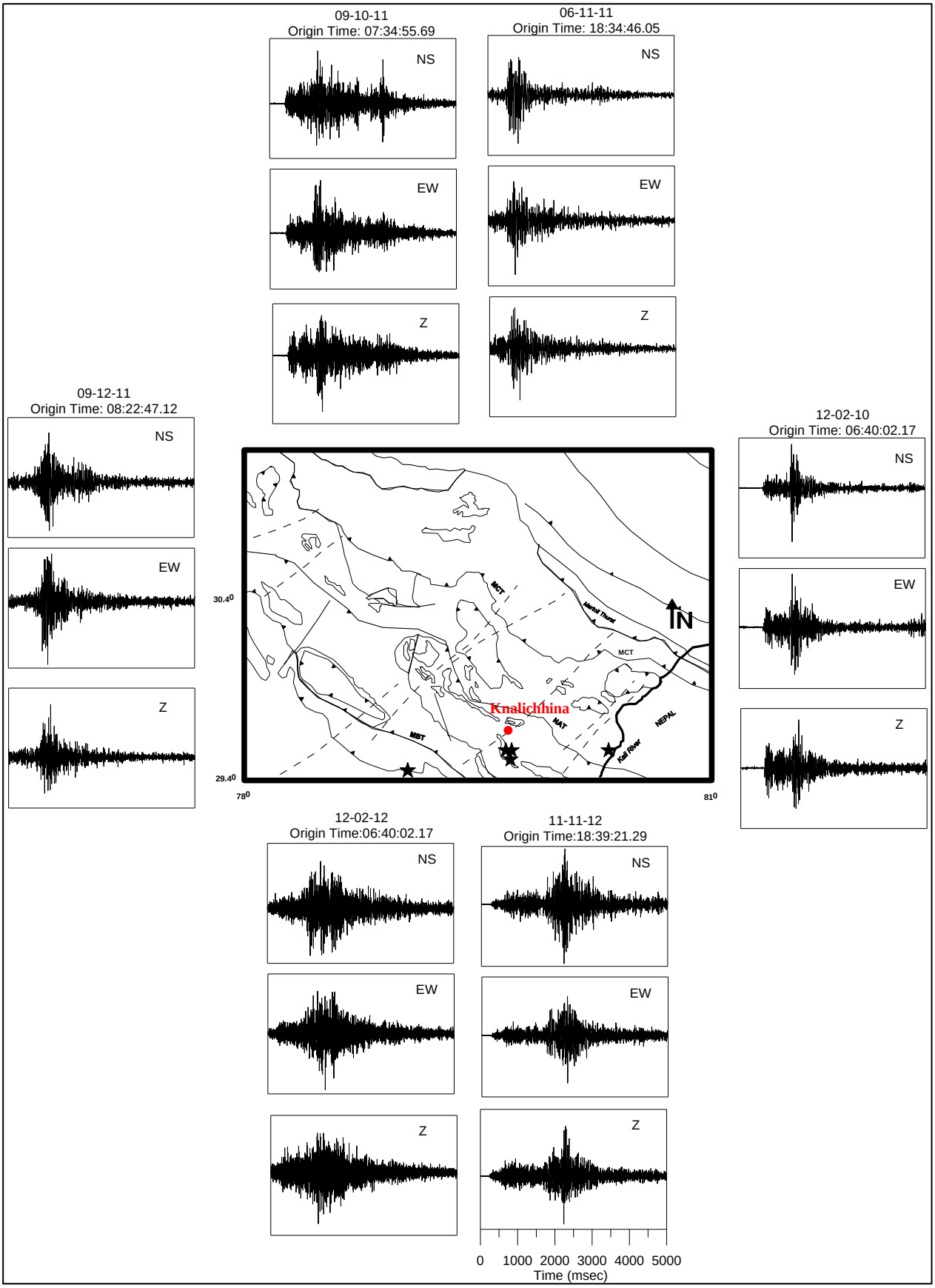

Figure 5.9: Normalized processed NS, EW and Z component of accelerograms of the shown events used at Knalichhina station. Star denotes the epicenter of events. Solid red circle shows the location of recording station. The tectonics of the region is taken after GSI (2000).

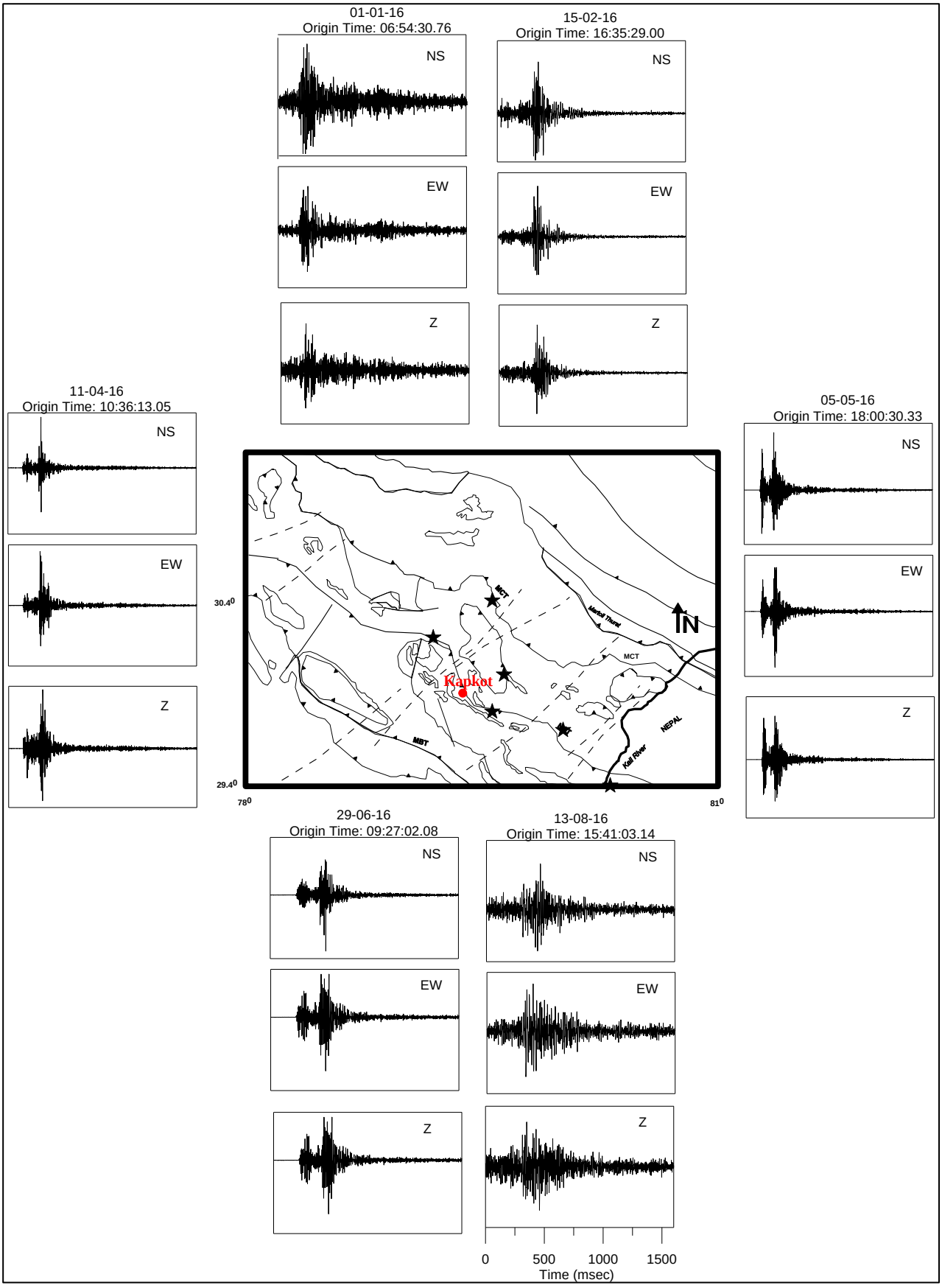

Figure 5.10: Normalized processed NS, EW and Z component of accelerograms of the shown events used at Kapkot station. Star denotes the epicenter of events. Solid red circle shows the location of recording station. The tectonics of the region is taken after GSI (2000).

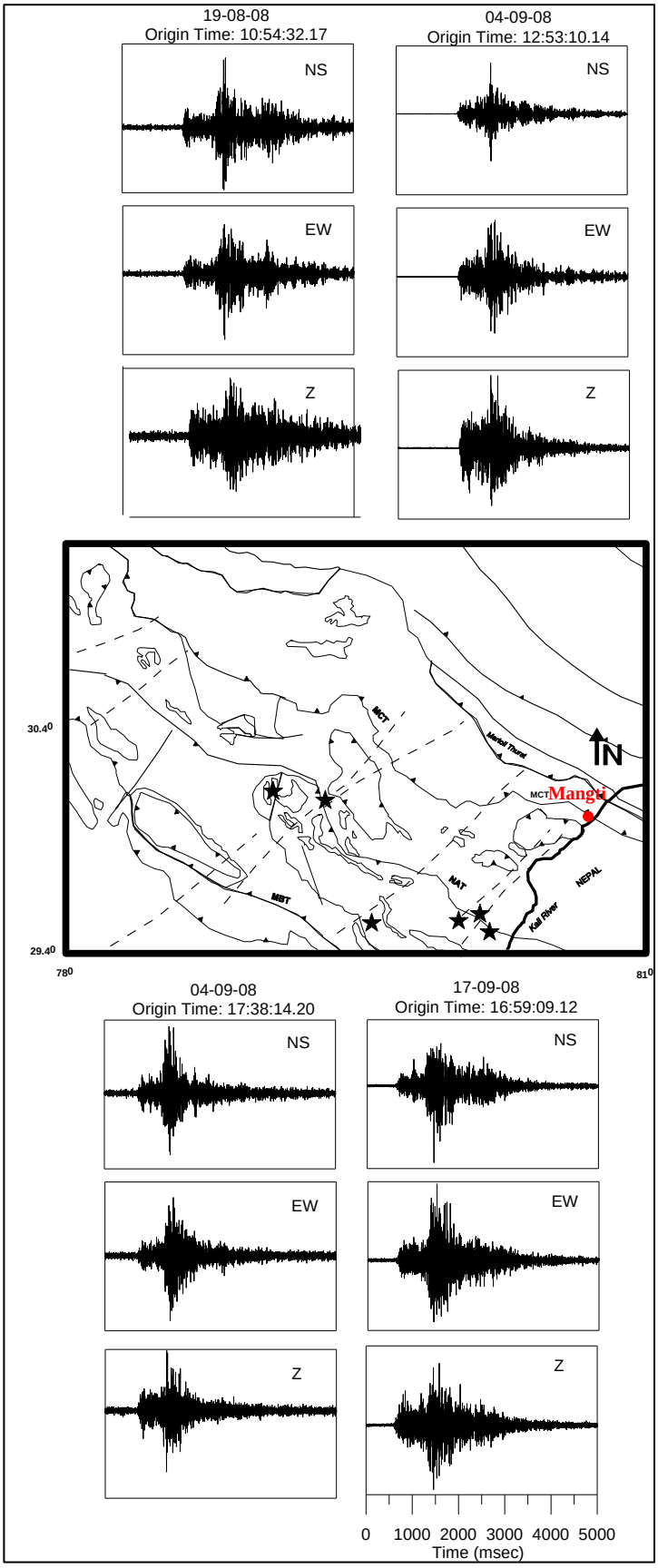

Figure 5.11: Normalized processed NS, EW and Z component of accelerograms of the shown events used at Mangti station. Star denotes the epicenter of events. Solid red circle shows the location of recording station. The tectonics of the region is taken after GSI (2000).

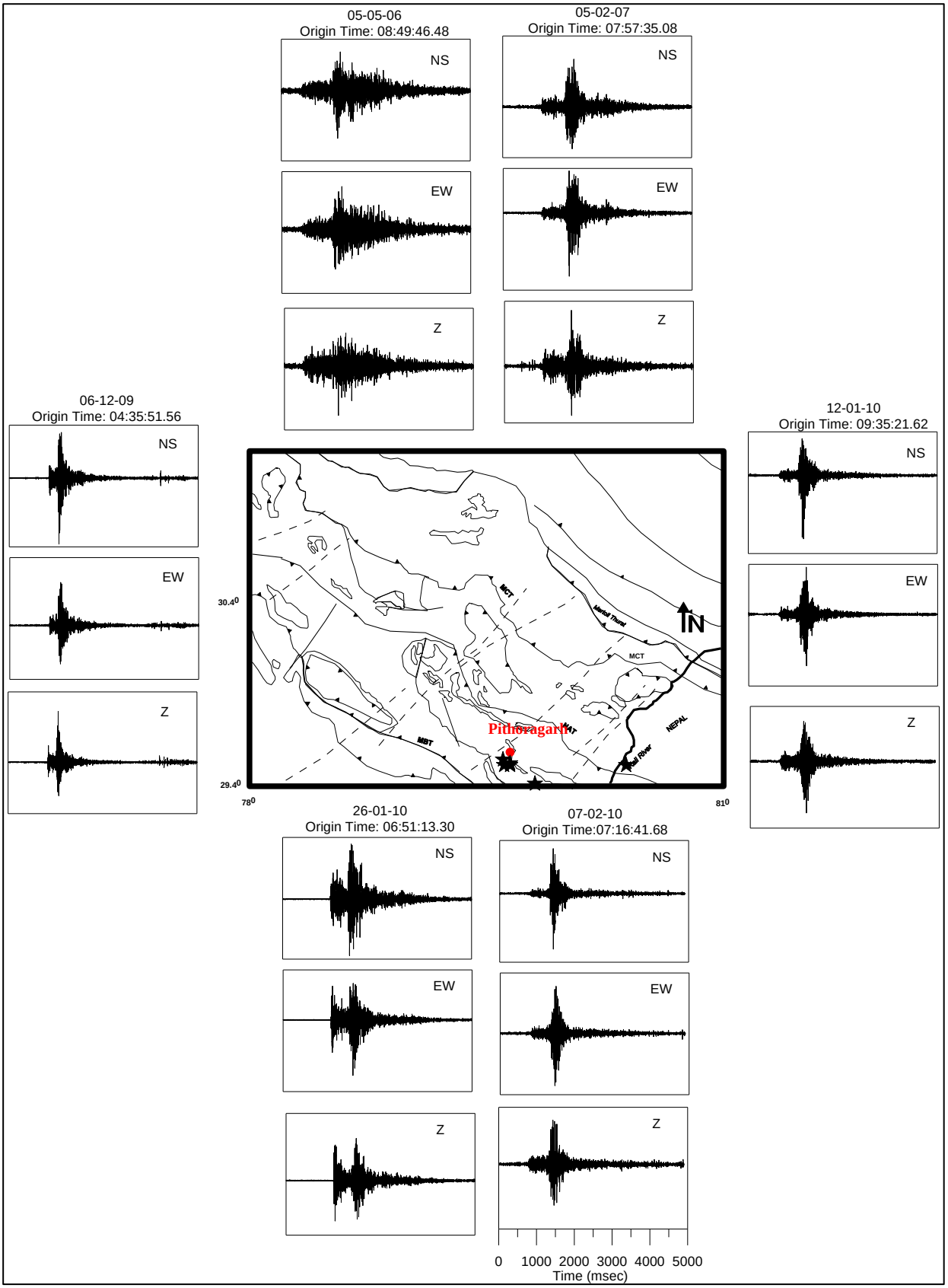

Figure 5.12: Normalized processed NS, EW and Z component of accelerograms of the shown events used at Pithoragarh station. Star denotes the epicenter of events. Solid red circle shows the location of recording station. The tectonics of the region is taken after GSI (2000).

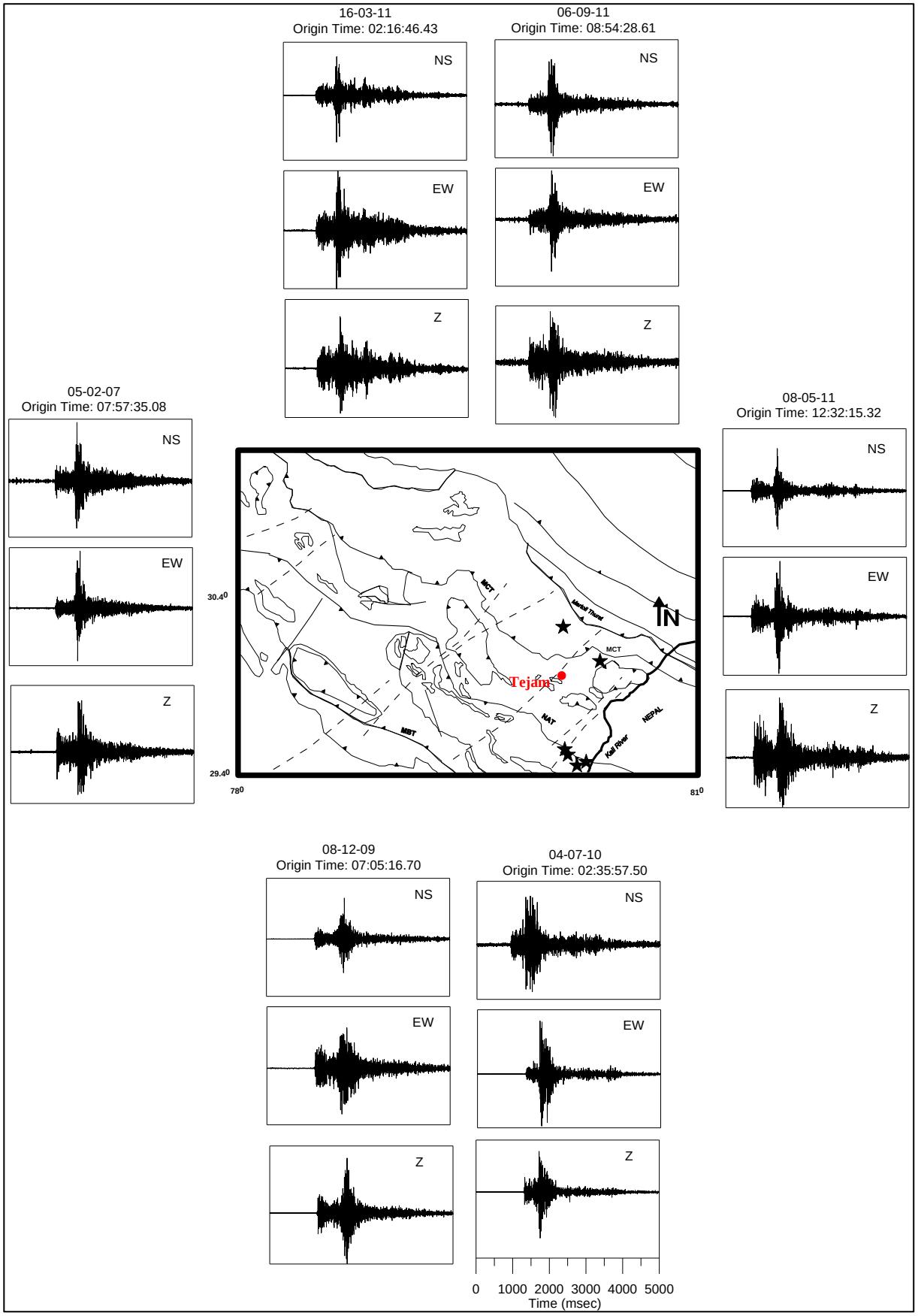

Figure 5.13: Normalized processed NS, EW and Z component of accelerograms of the shown events used at Tejam station. Star denotes the epicenter of events. Solid red circle shows the location of recording station. The tectonics of the region is taken after GSI (2000).

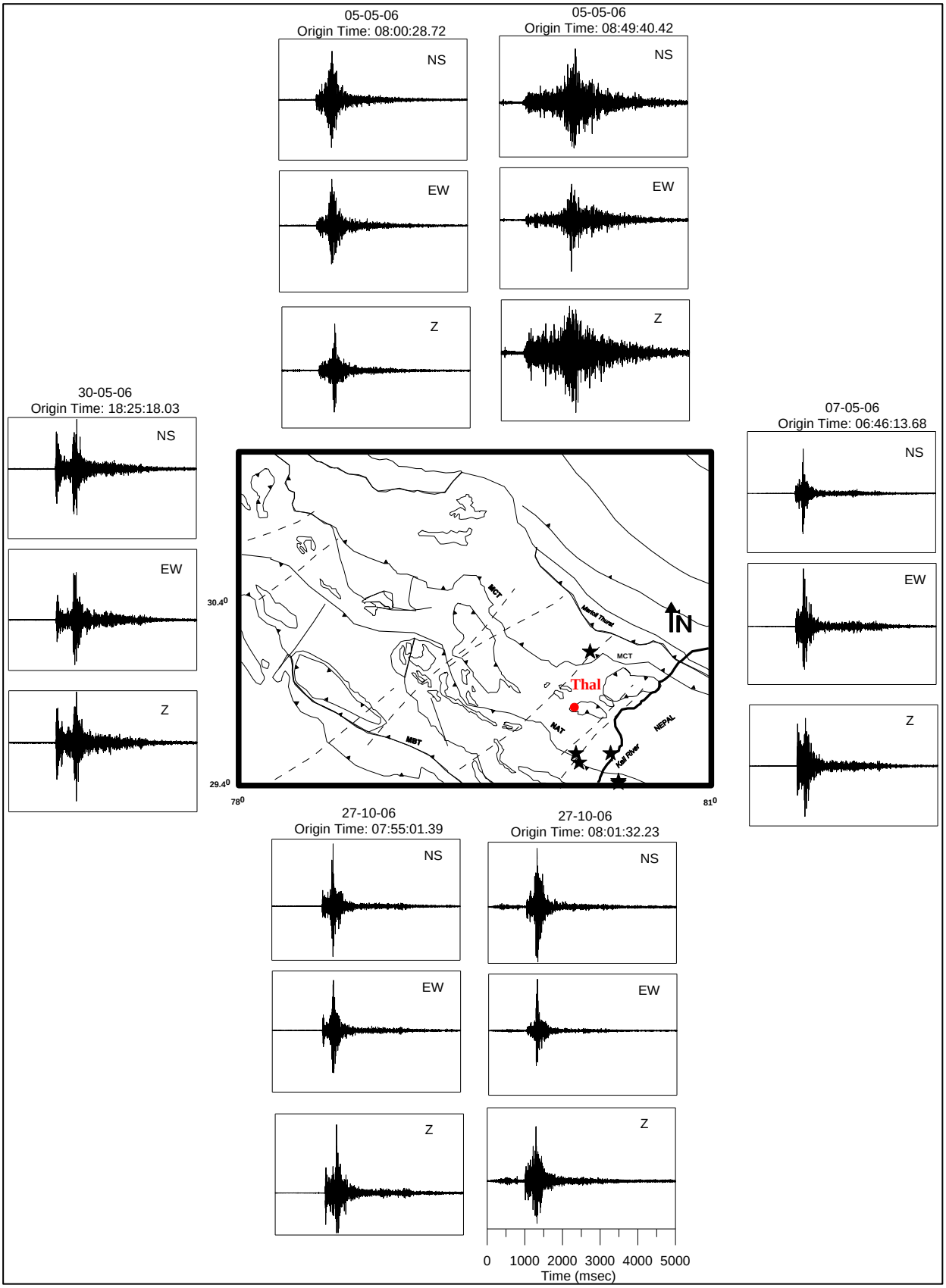

Figure 5.14: Normalized processed NS, EW and Z component of accelerograms of the shown events used at Thal station. Star denotes the epicenter of events. Solid red circle shows the location of recording station. The tectonics of the region is taken after GSI (2000).

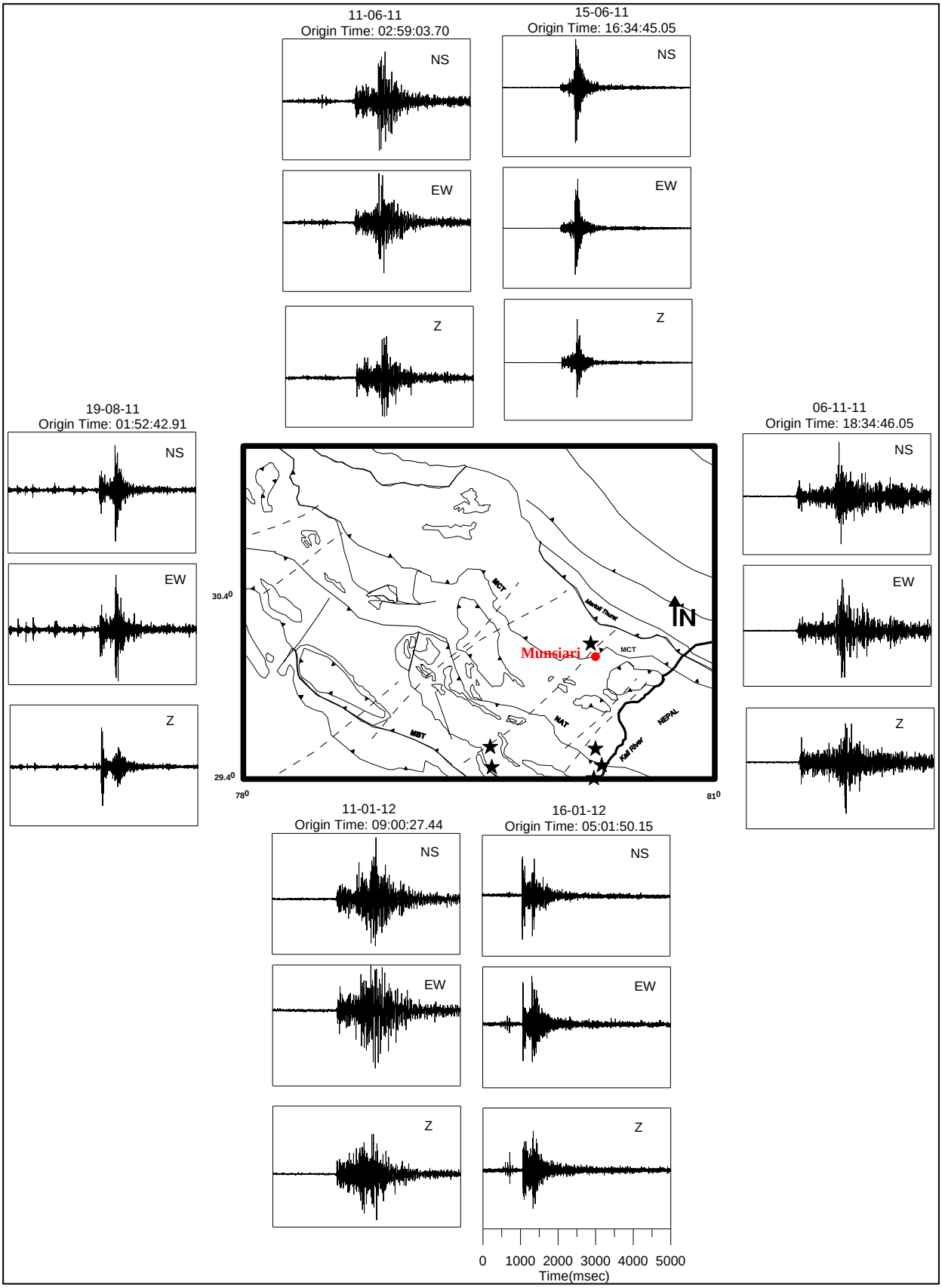

Figure 5.15: Normalized processed NS, EW and Z component of accelerograms of the shown events used at Munsiari station. Star denotes the epicenter of events. Solid red circle shows the location of recording station. The tectonics of the region is taken after GSI (2000).

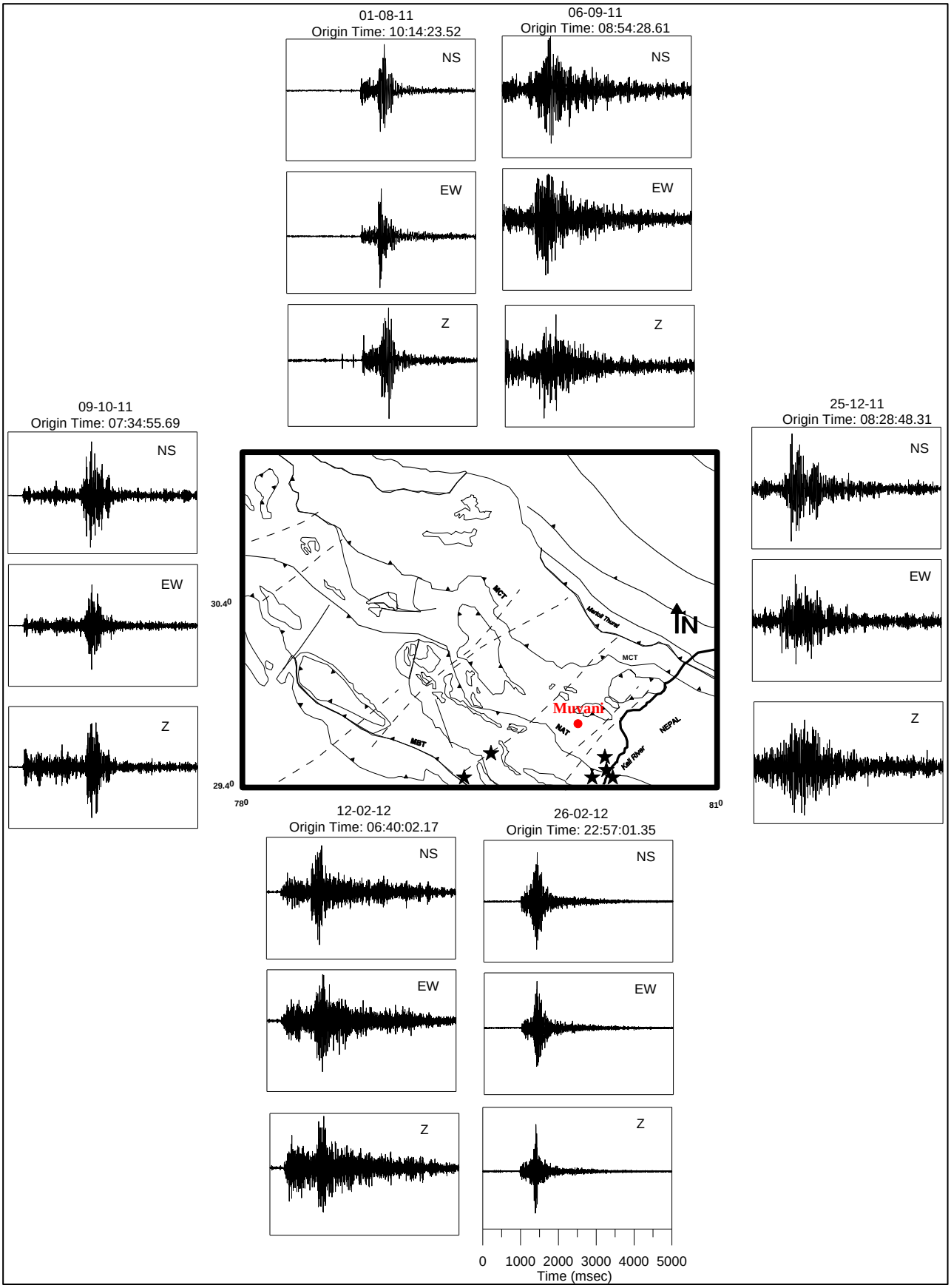

Figure 5.16: Normalized processed NS, EW and Z component of accelerograms of the shown events used at Muwani station. Star denotes the epicenter of events. Solid red circle shows the location of recording station. The tectonics of the region is taken after GSI (2000).

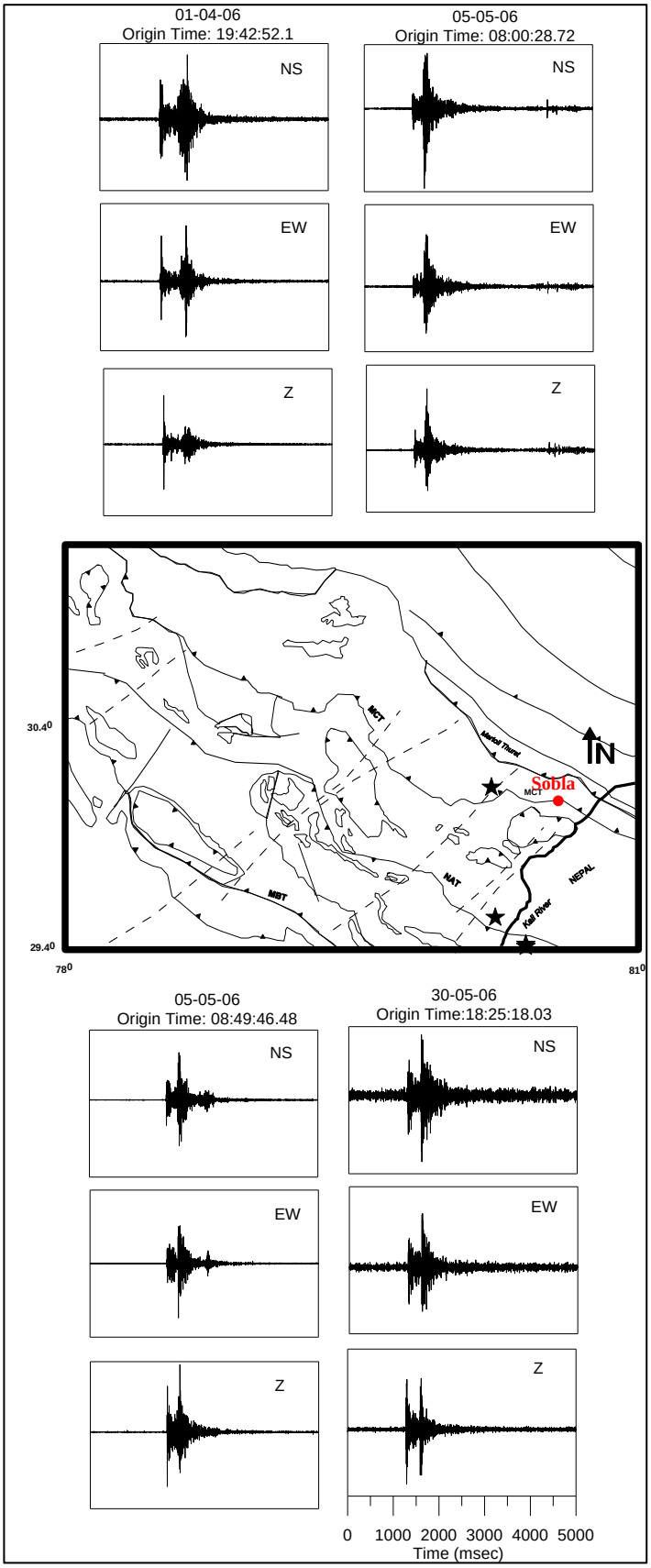

Figure 5.17: Normalized processed NS, EW and Z component of accelerograms of the shown events used at Sobla station. Star denotes the epicenter of events. Solid red circle shows the location of recording station. The tectonics of the region is taken after GSI (2000).

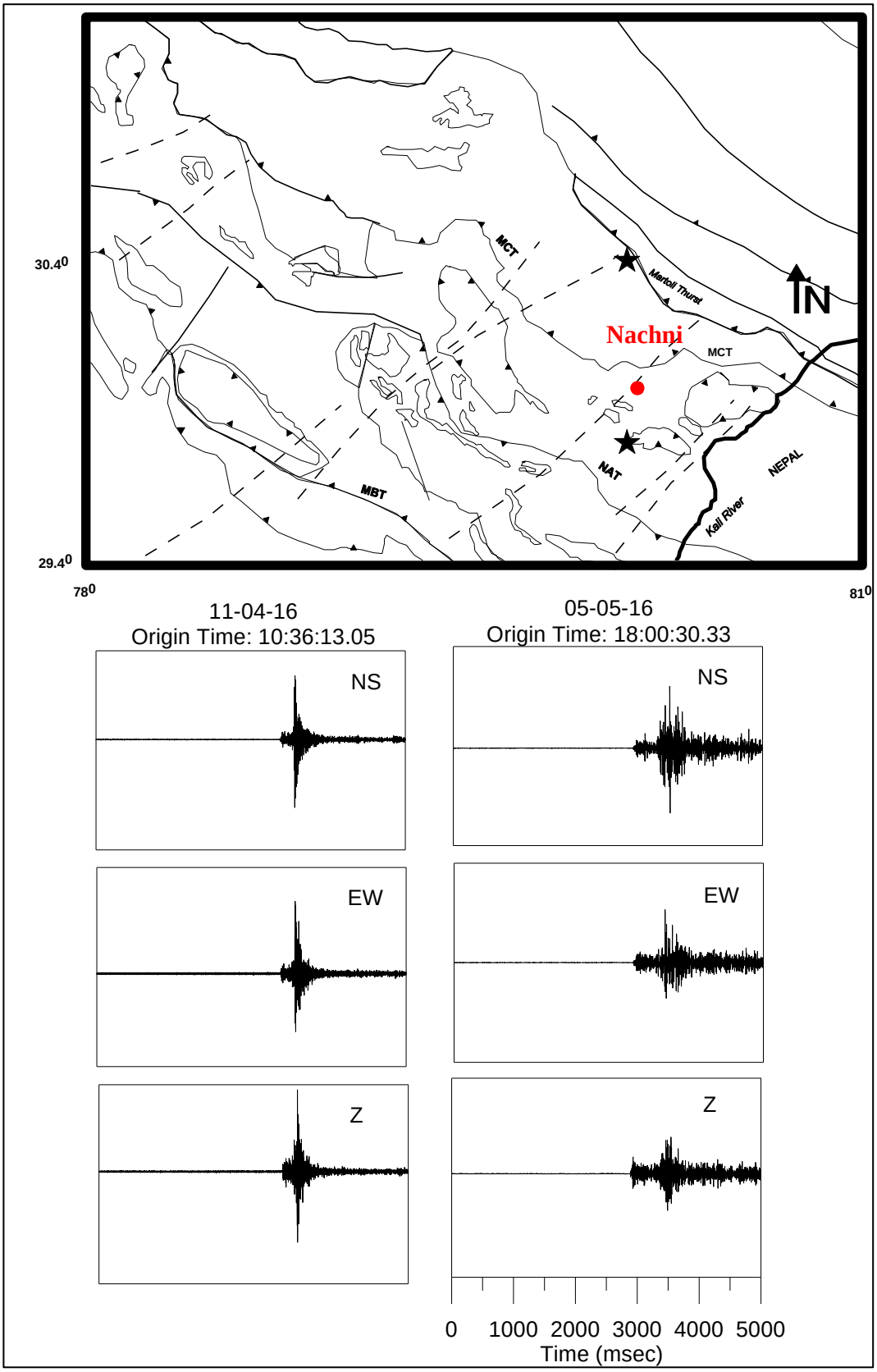

Figure 5.18: Normalized processed NS, EW and Z component of accelerograms of the shown events used at Nachni station. Solid red circle shows the location of recording station. The tectonics of the region is taken after GSI (2000).

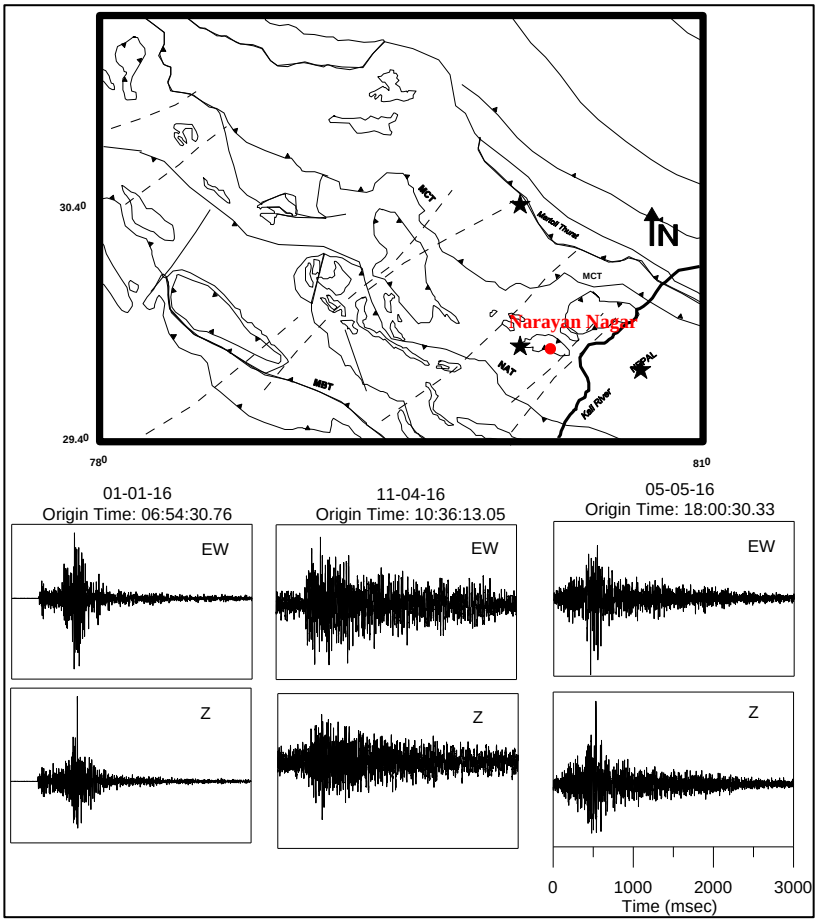

Figure 5.19: Normalized processed NS, EW and Z component of accelerograms of the shown events used at Narayan Nagar station. Solid red circle shows the location of recording station. The tectonics of the region is taken after GSI (2000).

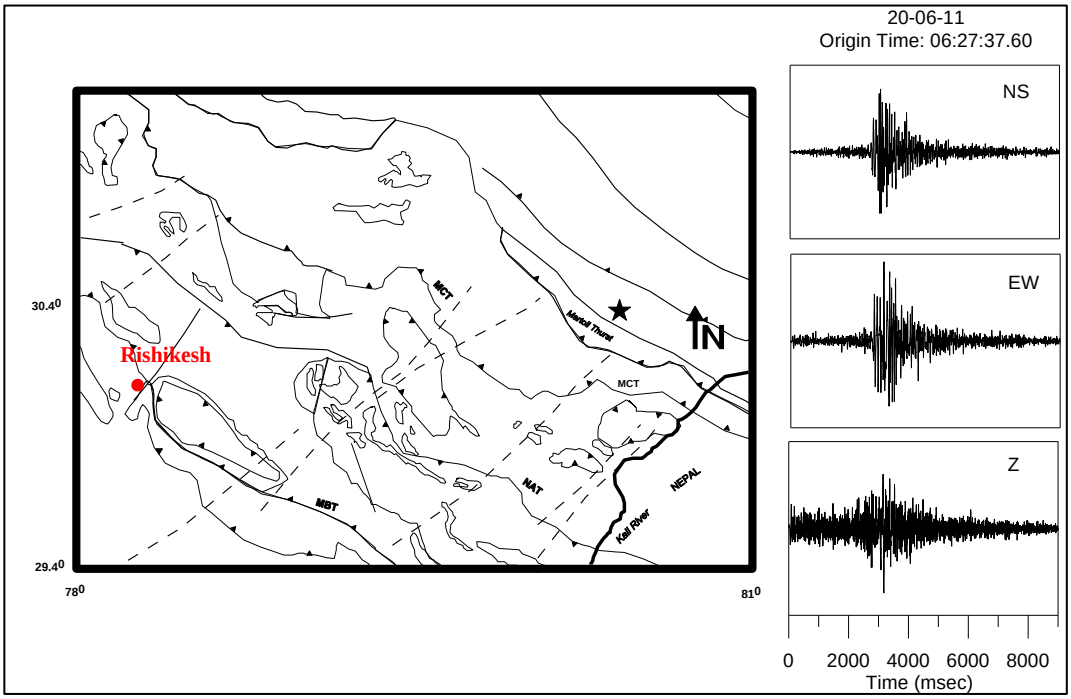

Figure 5.19: Normalized processed NS, EW and Z component of accelerograms of the shown events used at Rishikesh station. Star denotes the epicenter of events. Solid red circle shows the location of recording station. The tectonics of the region is taken after GSI (2000).

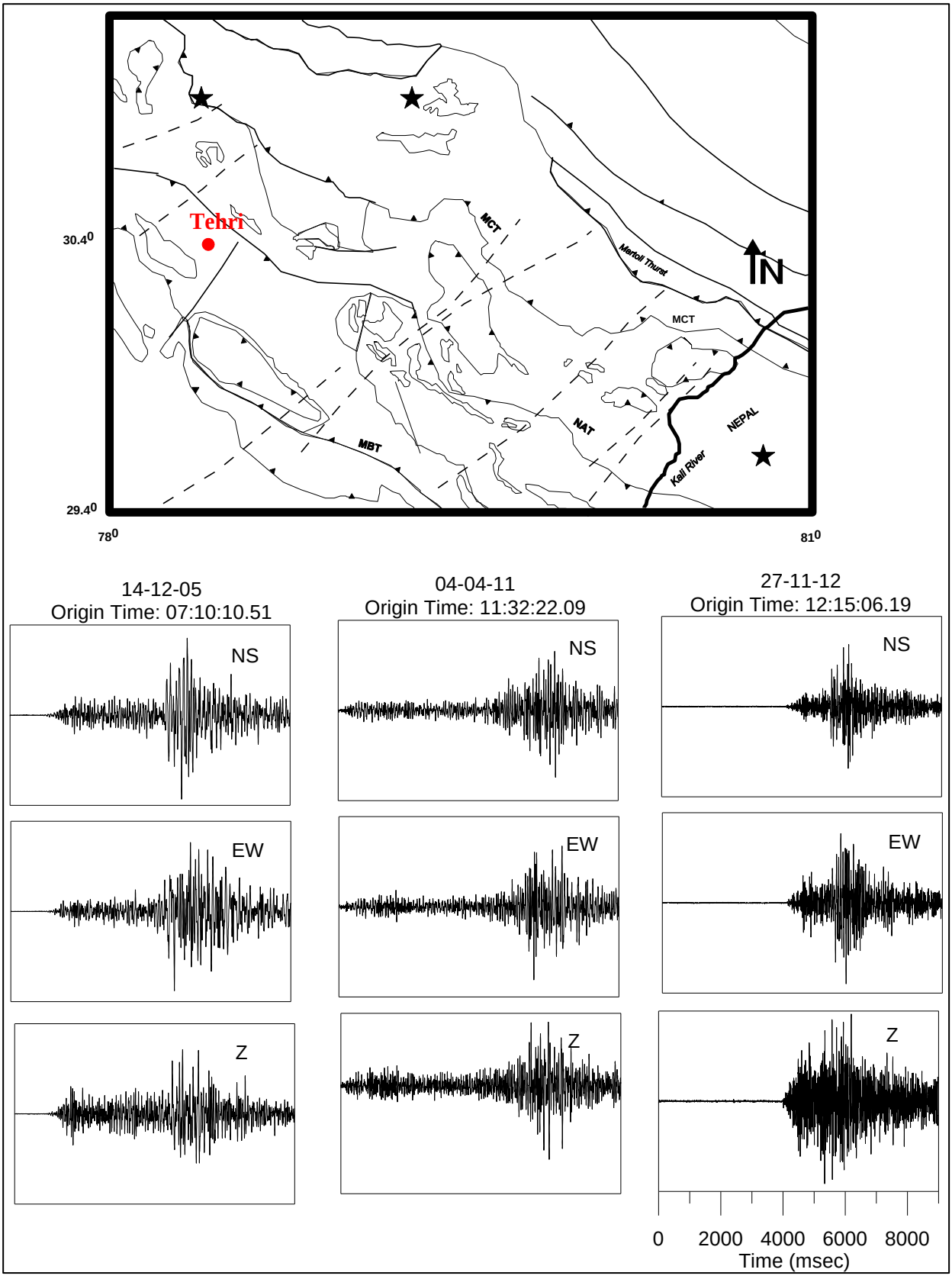

Figure 5.20: Normalized processed NS, EW and Z component of accelerograms of the shown events used at Tehri station. Star denotes the epicenter of events. Solid red circle shows the location of recording station. The tectonics of the region is taken after GSI (2000).

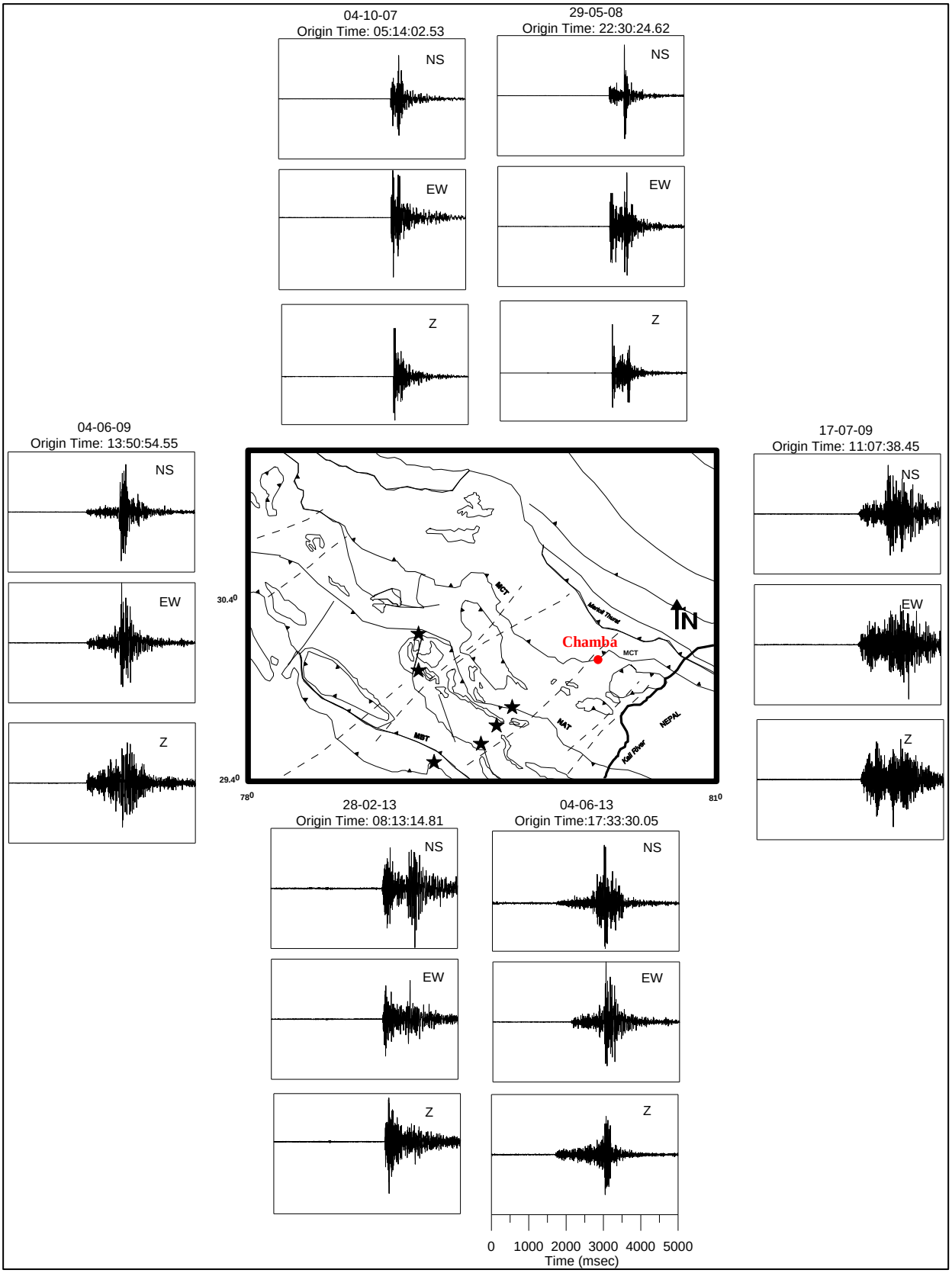

Figure 5.21: Normalized processed NS, EW and Z component of accelerograms of the shown events used at Chamba station. Star denotes the epicenter of events. Solid red circle shows the location of recording station. The tectonics of the region is taken after GSI (2000).

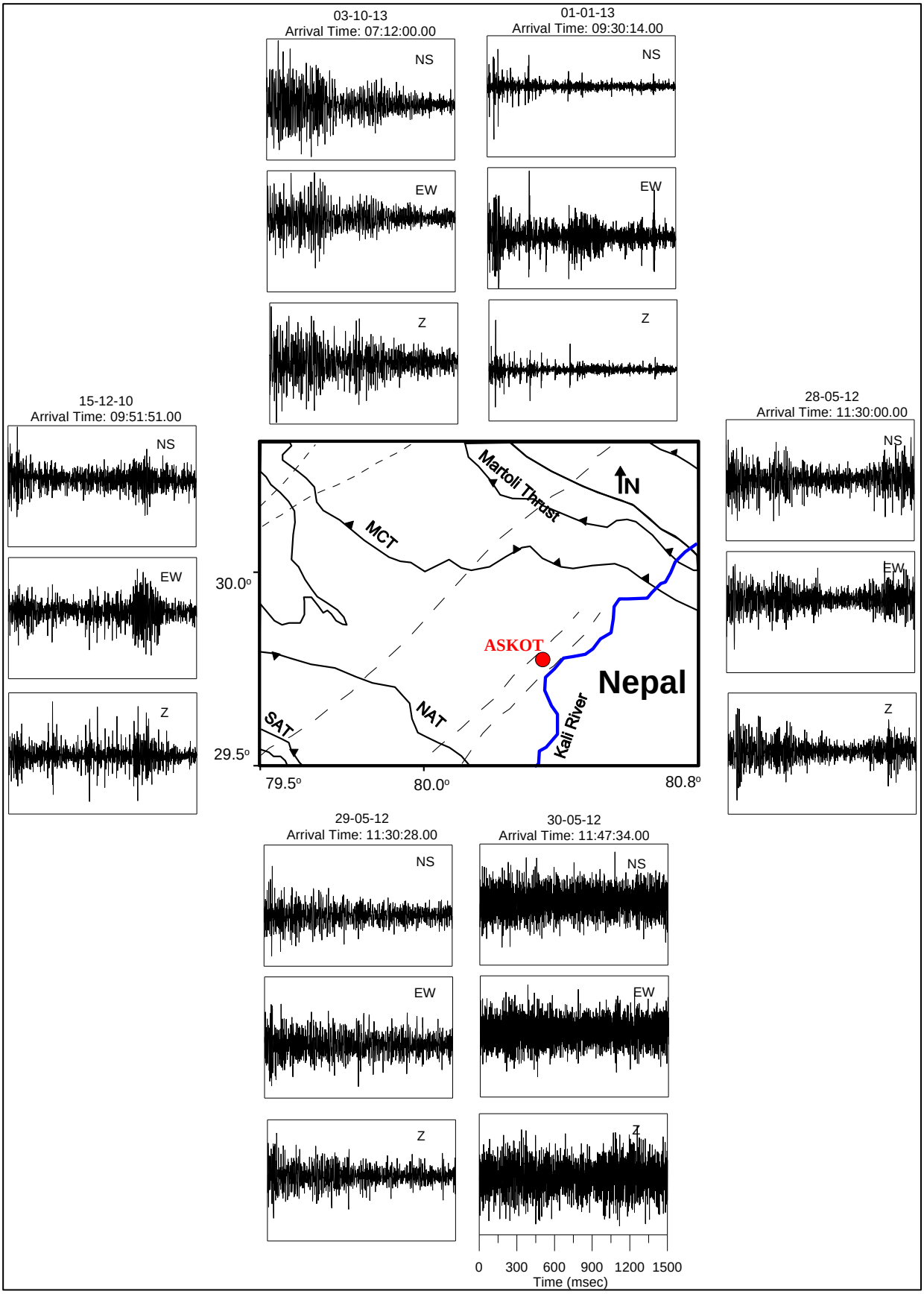

Figure 5.22: Normalized processed NS, EW and Z component of accelerograms of the shown ambient noise used at Askot station. Solid red circle shows the location of recording station. The tectonics of the region is taken after GSI (2000).

The results obtained after the estimation of Horizontal-Vertical (H/V) spectral ratio using Nakamura Technique at individual stations is shown in Figure 5.23 to Figure 5.30. Red curve in the results shows the mean H/V and blue curve shows the standard deviation from the mean i.e. average ± standard deviation ($\mu \pm \sigma$). Average site amplification term obtained by inversion is shown by the red line. The area between two blue curves denotes the region between $\mu + \sigma$ and $\mu - \sigma$ of the site amplification obtained using technique given by Lermo and Chavez-Garcia (1993). Parameters 'μ' and 'σ' describe the mean and standard deviation, respectively.

The Horizontal-Vertical (H/V) ratio calculated using strong motion records (shown in right panel) and ambient noise data (shown in left panel) using Nakamura Technique at individual stations has been shown in Figure 5.23 to Figure 5.30. The time window of 1500 ms has been used here. The window has been selected in such a way that the record containing ambiet noise is separated from the event window in case of ambient noise analysis. Similarly the event window length is selected for strong ground motion analysis. As a result, the analysis is confined only to the required portion of the record. Red curve shows the mean and blue curve shows the standard deviation from the mean.

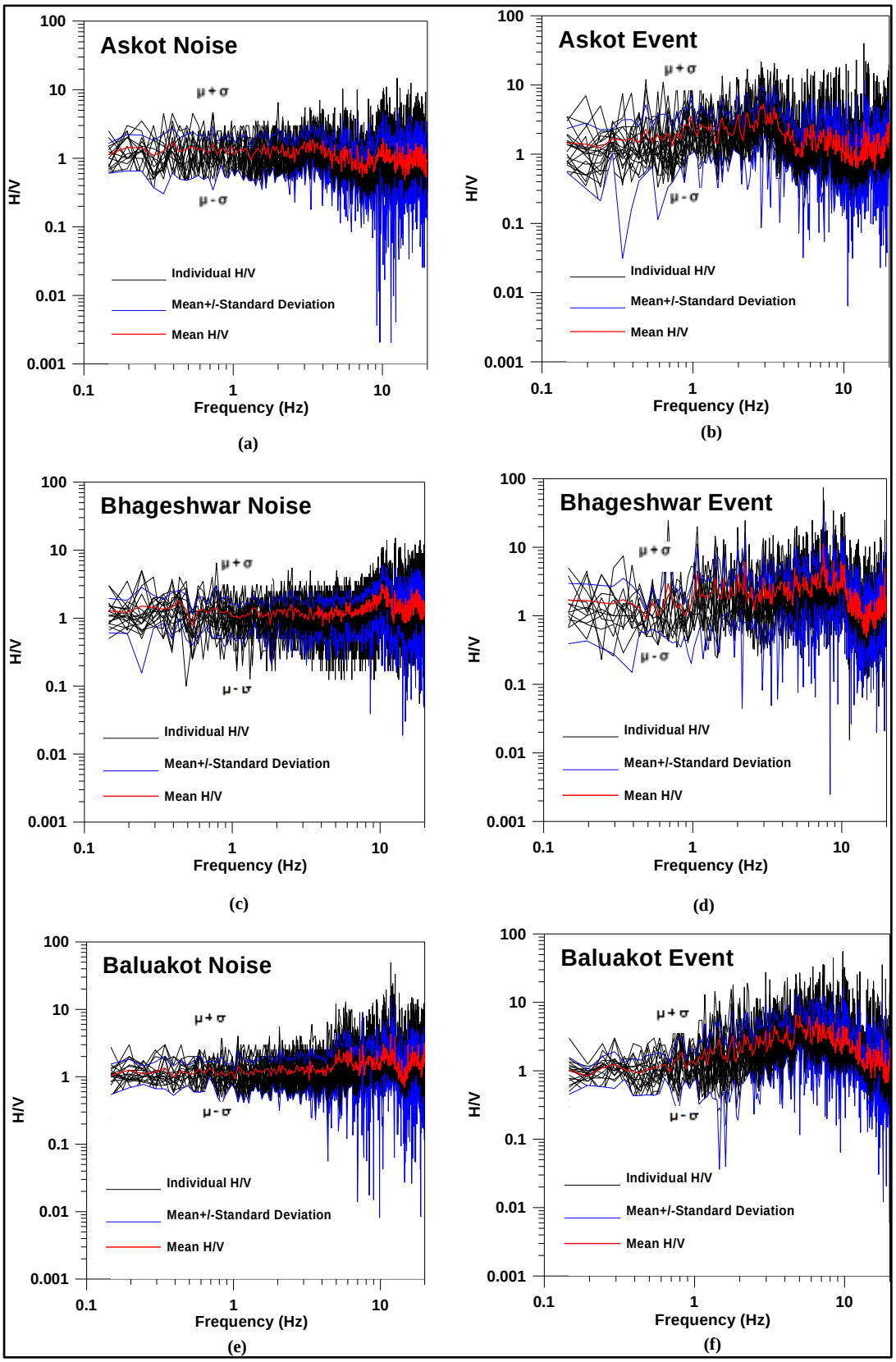

Figure 5.23: The Horizontal-Vertical (H/V) ratio calculated using Nakamura Technique at individual stations. Red curve shows the mean and blue curve shows the standard deviation from the mean. (a)Askot Noise (b) Askot Event (c) Bhageshwar Noise (d) Bhageshwar Event (e) Baluakot Noise (f) Baluakot Event.

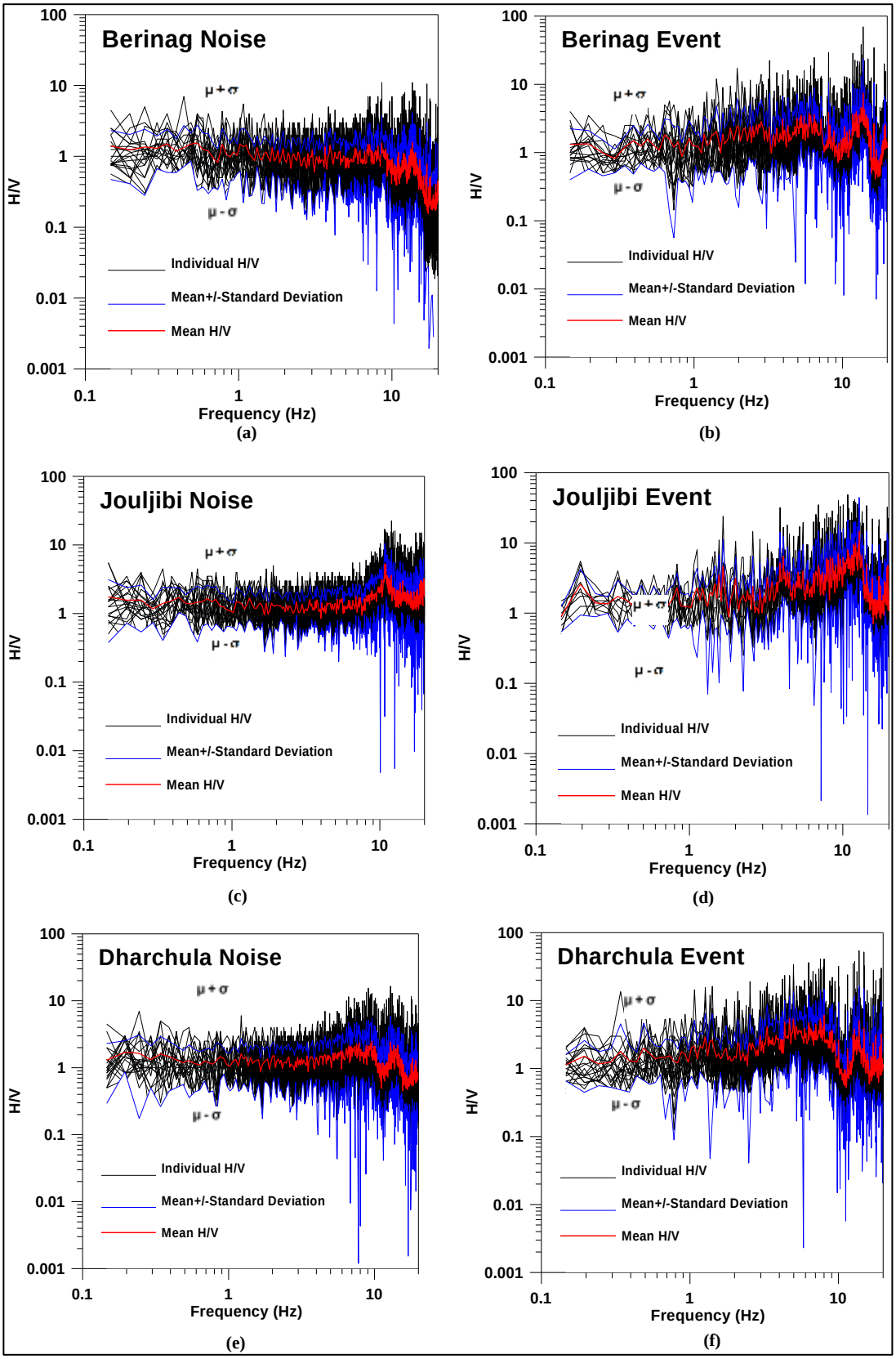

Figure 5.24: The Horizontal-Vertical (H/V) ratio calculated using Nakamura Technique at individual stations. Red curve shows the mean and blue curve shows the standard deviation from the mean. (a) Berinag Noise (b) Berinag Event (c) Jouljibi Noise (d) Jouljibi Event (e) Dharchula Noise (f) Dharchula Event.

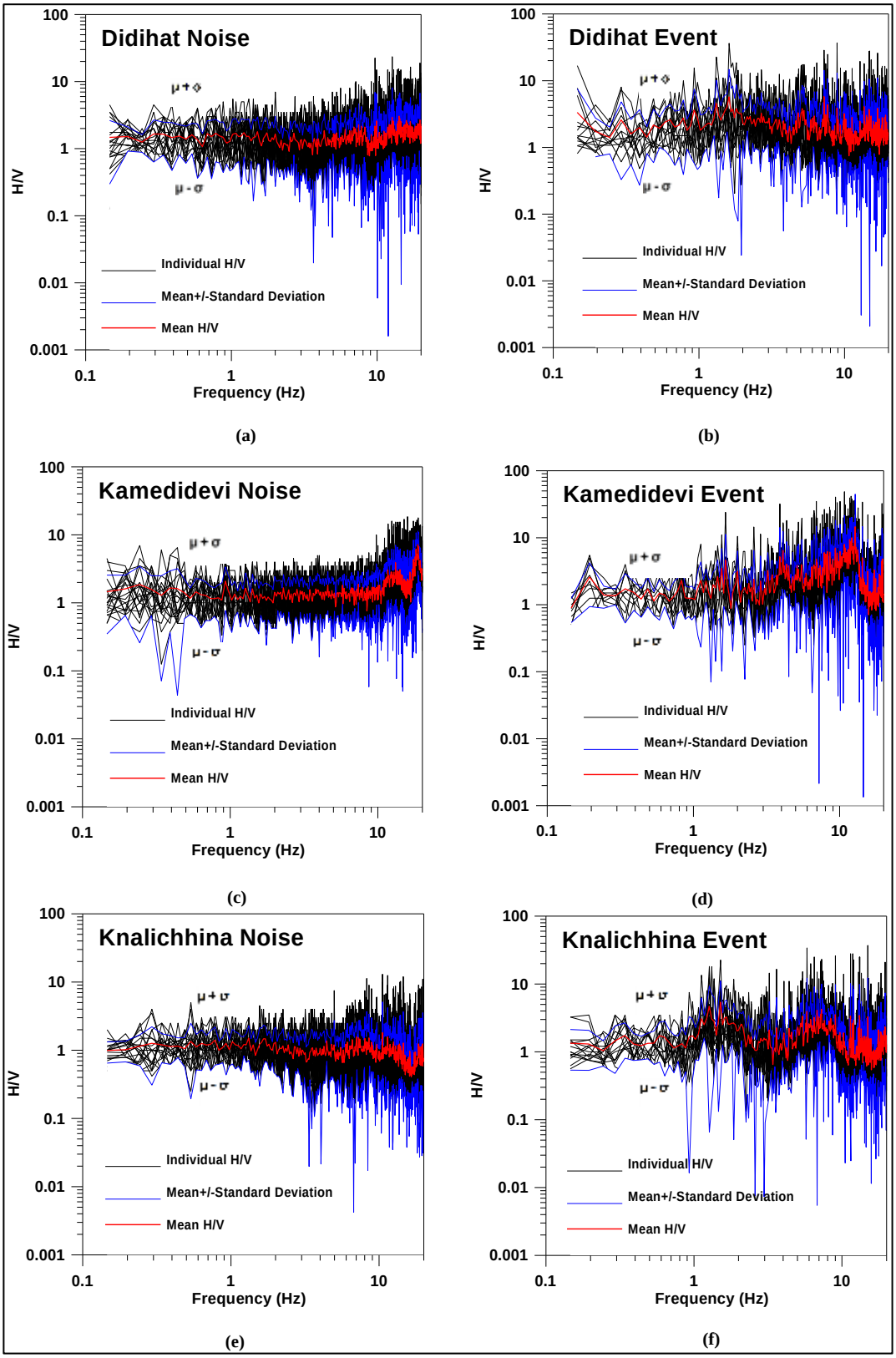

Figure 5.25: The Horizontal-Vertical (H/V) ratio calculated using Nakamura Technique at individual stations. Red curve shows the mean and blue curve shows the standard deviation from the mean. (a)Didihat Noise (b) Didihat Event (c) Kamedidevi Noise (d) Kamedidevi Event (e) Knalichhina Noise (f) Knalichhina Event.

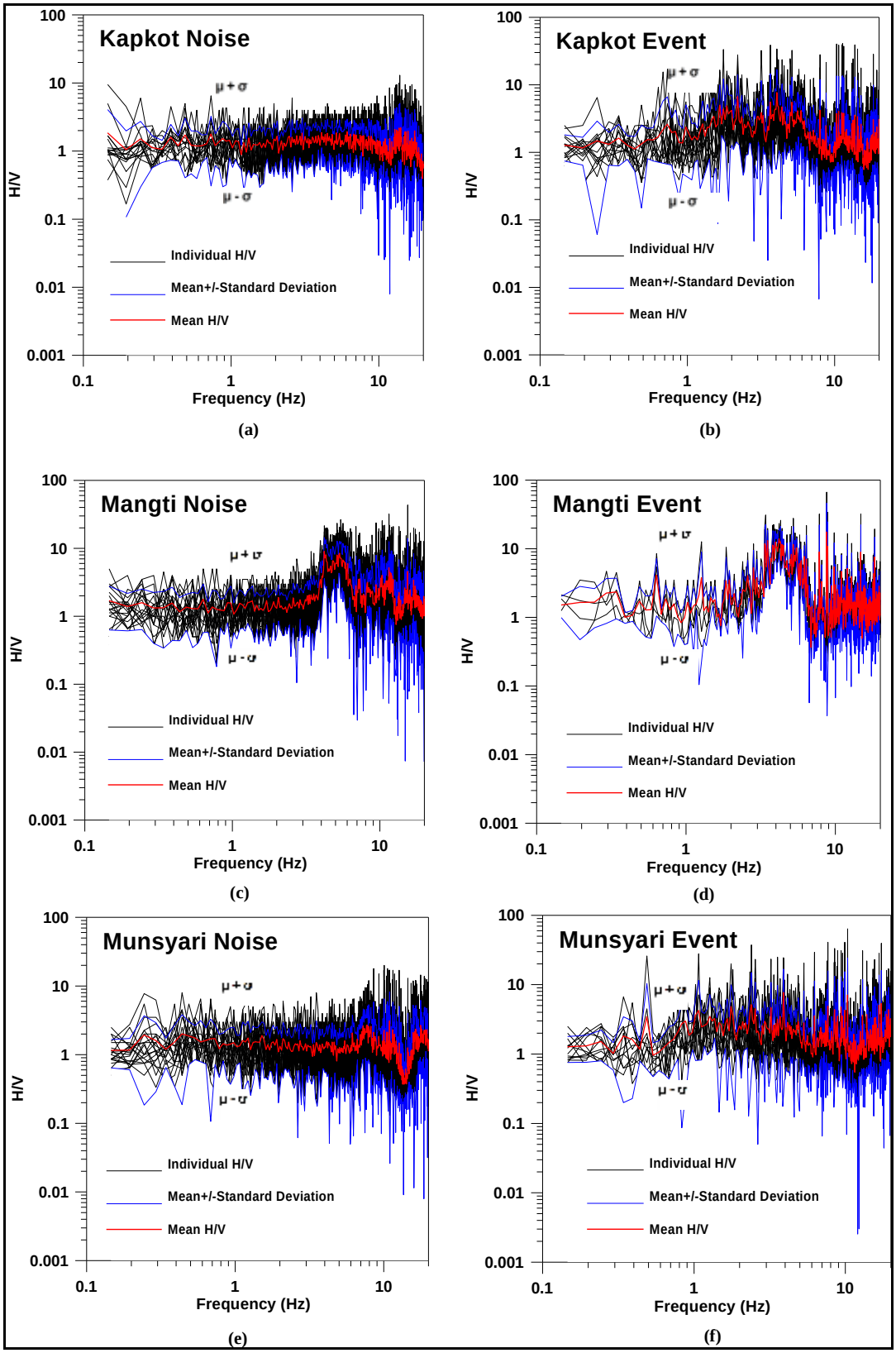

Figure 5.26: The Horizontal-Vertical (H/V) ratio calculated using Nakamura Technique at individual stations. Red curve shows the mean and blue curve shows the standard deviation from the mean. (a) Kapkot Noise (b) Kapkot Event (c) Mangti Noise (d) Mangti Event (e) Munsyari Noise (f) Munsyari Event.

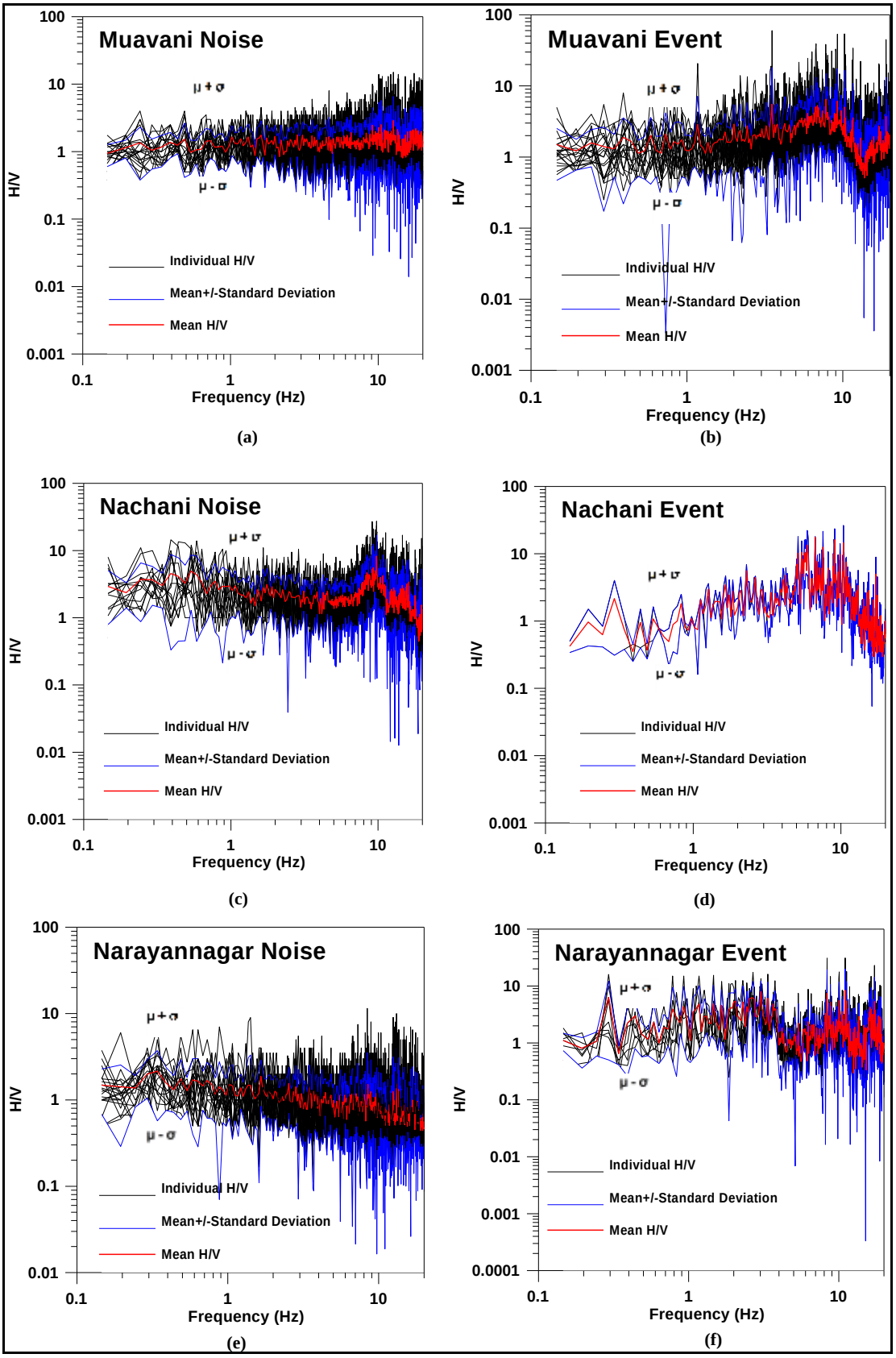

Figure 5.27: The Horizontal-Vertical (H/V) ratio calculated using Nakamura Technique at individual stations. Red curve shows the mean and blue curve shows the standard deviation from the mean. (a) Muavani Noise (b) Muavani Event (c) Nachni Noise (d) Nachni Event (e) Narayannagar Noise (f) Narayannagar Event.

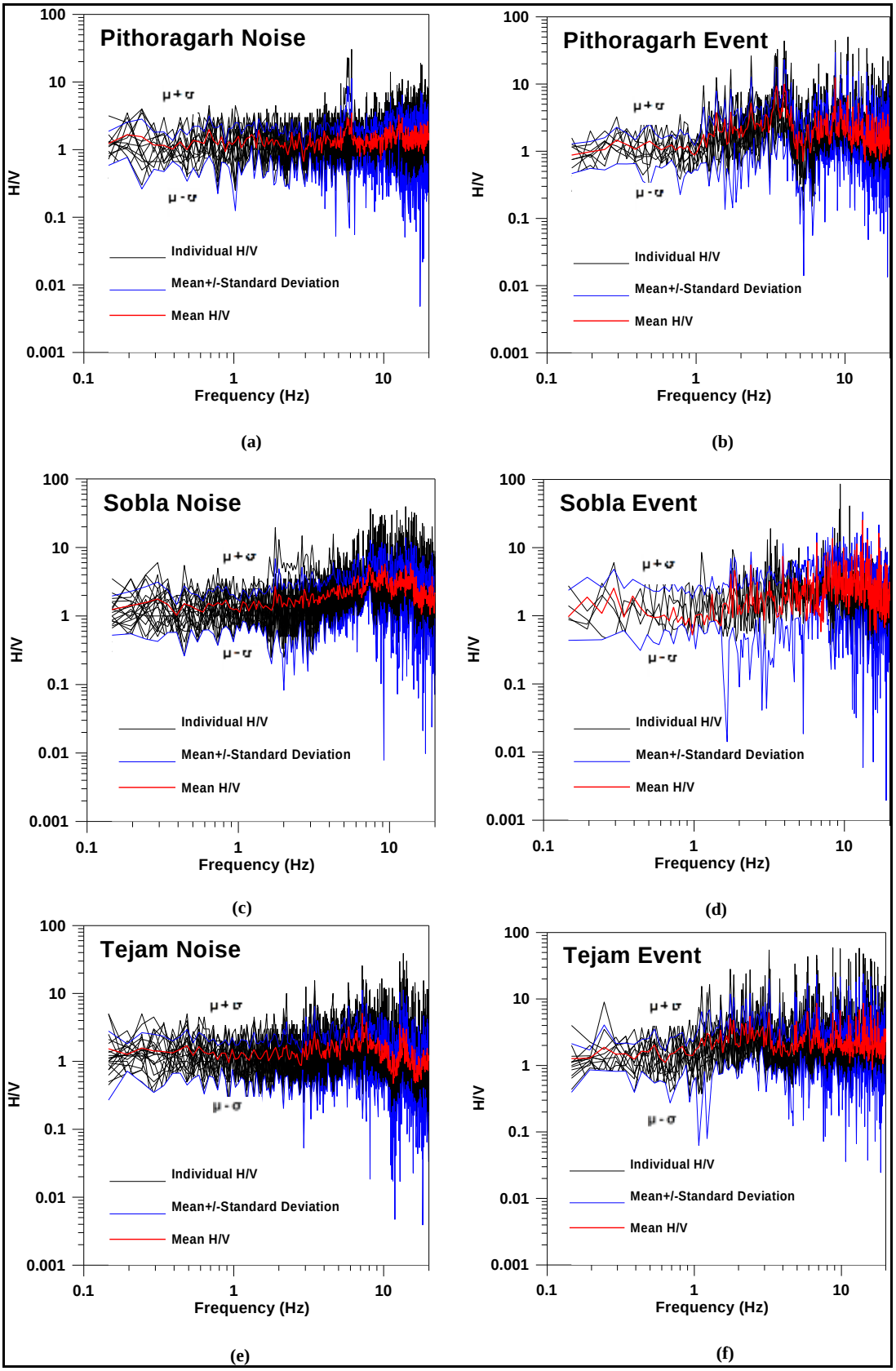

Figure 5.28: The Horizontal-Vertical (H/V) ratio calculated using Nakamura Technique at individual stations. Red curve shows the mean and blue curve shows the standard deviation from the mean. (a) Pithoragarh Noise (b) Pithoragarh Event (c) Sobla Noise (d) Sobla Event (e) Tejam Noise (f) Tejam Event.

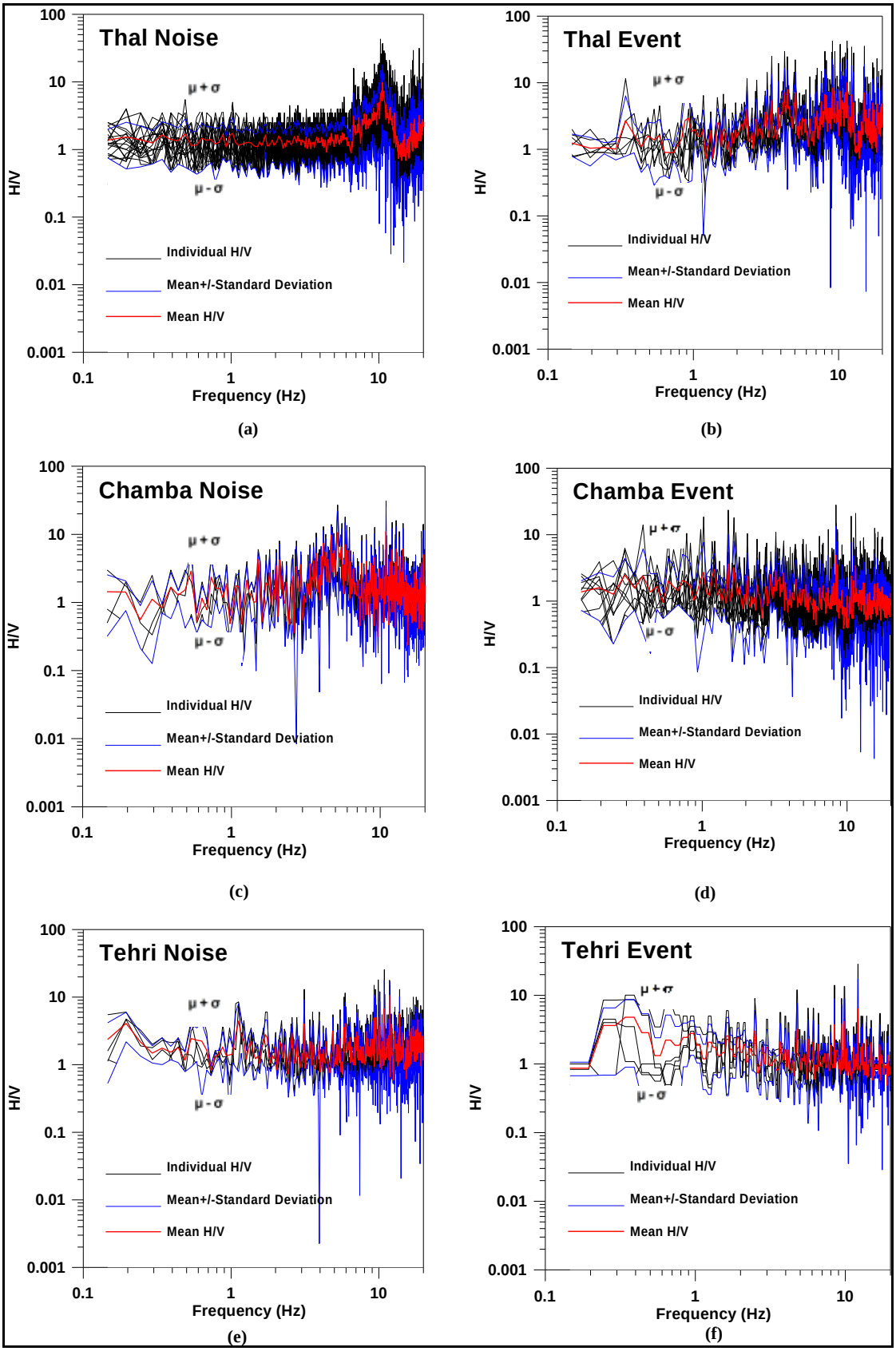

Figure 5.29: The Horizontal-Vertical (H/V) ratio calculated using Nakamura Technique at individual stations. Red curve shows the mean and blue curve shows the standard deviation from the mean. (a) Thal Noise (b) Thal Event (c) Chamba Noise (d) Chamba Event (e) Tehri Noise (f) Tehri Event.

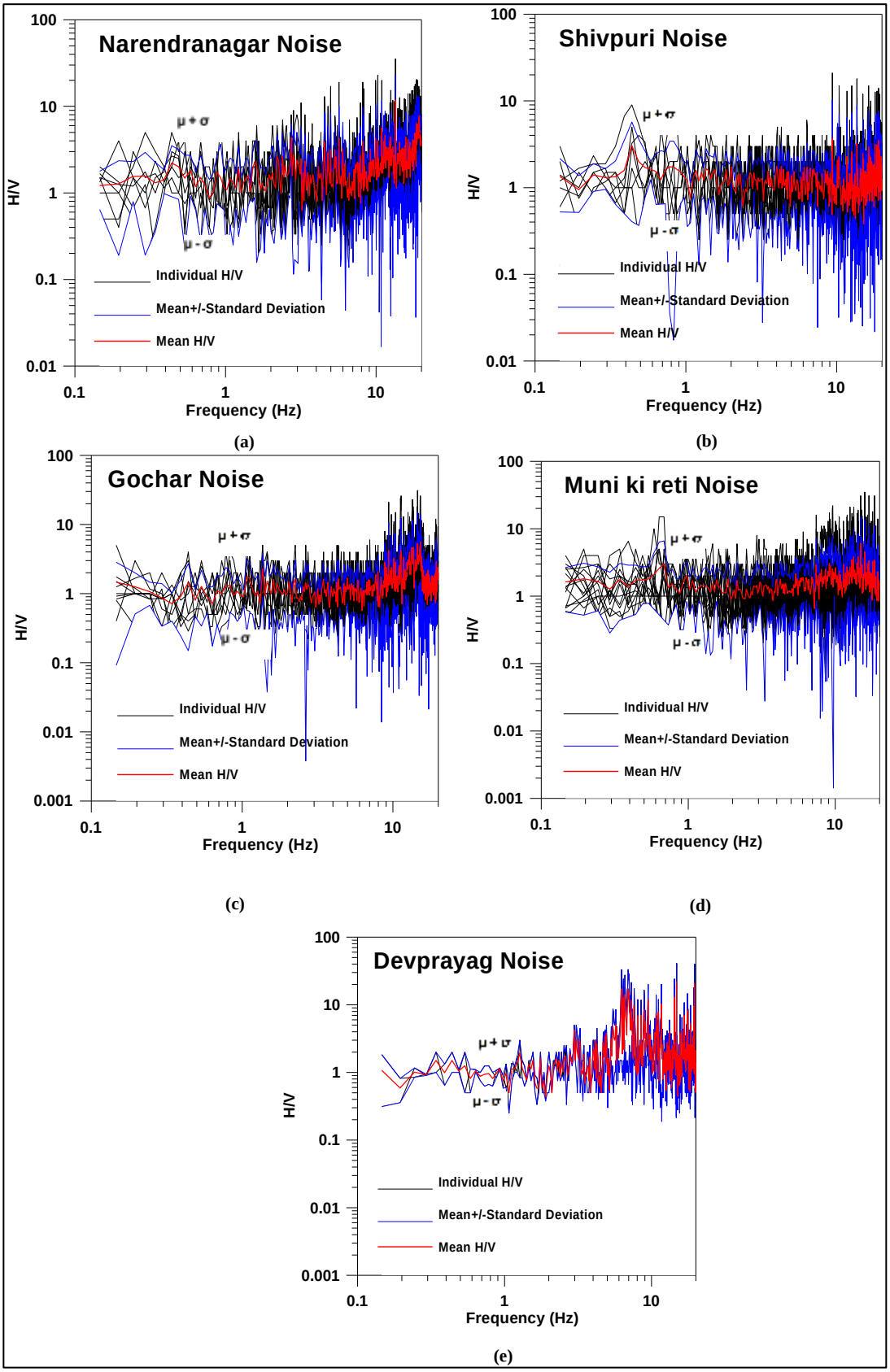

Figure 5.30: The Horizontal-Vertical (H/V) ratio calculated using Nakamura Technique at individual stations. Red curve shows the mean and blue curve shows the standard deviation from the mean. (a) Narendra Nagar Noise (b) Shivpuri Noise (c) Gochar Noise (d) Muni ki reti Noise (e) Devprayag Noise.

5.3. Results and Discussion

Pithoragarh is situated in the middle of the western part of the Soar Valley and is positioned at the focus of 4 hills which are Chandak, Dhwaj, Kumdar and Thal Kedar and expanding to the southern border to Jhulaghat delineated by the Kali River attached with the infertile summits of Nepal hills. It has an altitude of 1514 m. Rocks exposed are slate, phyllite and limestone and dolomite and belongs to Mandhali Formation of Tejam Group. Based on H/V curves, the predominant frequency estimated from strong ground motion is 10.7 ± 1.8 Hz and for ambient noise is 12.2 ± 1.3 Hz.

Dharchula is located about 83 km northerly of Pithoragarh at an elevation of 935 m along the banks of Kali River. It belongs to Mandhali Formation of Tejam Group. The rocks exposed are slate, phyllite and limestone and dolomite. The predominant frequency estimated from strong ground motion is 9.6 ± 2.6 Hz and for ambient noise is 10.3 ± 1.7 Hz.

Munsyari is located in Pithoragarh district of Uttarakhand. It is a beautiful hill station in Kumaon region. It is situated in the Greater Himalaya ranges, at an altitude of 2200 m from MSL. Stratigraphically it falls in Munsyari Formation of Almora Group. The Munsyari Formation contains granite, gneisses, quartzite, mica-schist and amphibolite.

The average shear wave velocity of Munsyari is 1043 ms^{-1} which quite significant for high rise buildings like dams and multistoried buildings etc. with proper design and suitable site selection. The Munsyari Formation contains granite, gneisses, quartzite, mica-schist and amphibolite. The predominant frequency estimated from strong ground motion is 9.1 ± 1.4 Hz and for ambient noise is 10.9 ± 1.3 Hz.

Askot located at Pithoragarh district in Uttarakhand, India forms a portion of Didihat Tehsil and Knalichhina expansion unit. It is located at an elevation of 1258 m. Askot is situated on the bank of Kali – Gori-Ganga river topographical division. Stratigraphically it falls in Askot Crystalline. The Askot Crystalline contains granite and gneisses. The predominant frequency estimated from strong ground motion is 11.2 ± 2.8 Hz and for ambient noise is 11.3 ± 1.7 Hz. The average shear wave velocity of Askot is 408 ms^{-1}.

Joljibi a petty township located at an elevation of 612 m, near Indo-Nepal border in Uttarakhand is placed at the convergence of Kali and Gori rivers. This is a significant trading center bordering Nepal and 68 km from Pithoragarh. The rocks belong to Mandhali Formation of Tejam Group. The rocks exposed are slate, phyllite and limestone and dolomite. The

predominant frequency estimated from strong ground motion is 9.7 ± 1.5 Hz and for ambient noise is 11.5 ± 0.6 Hz. The average shear wave velocity of Joljibi is 658 ms^{-1}.

Baluakot located around Dharchula tehsil in Pithoragarh district of Uttarakhand is near to Mahakali River. It falls in Damta Group and Rautgara Formation consisting of quartzite slates and conglomerates. It is located at an elevation of 644 m. The predominant frequency estimated from strong ground motion is 10 ± 2.5 Hz and for ambient noise is 11.1 ± 1.1 Hz. The average shear wave velocity of Baluakot is 619 ms^{-1}.

Knalichhina is situated within Pithoragarh constituency of the Uttarakhand. It is termed on "Chhin" in the Kumauni language meaning open deep section between the two mounds and is supported by windy topography and valley on further side. It lies in Tejam Group of Deoban Formation having Dolomite and Quartzite as main lithological units. It has an altitude of 968 m. The predominant frequency estimated from strong ground motion is 11.5 ± 2.8 Hz and for ambient noise is 12.6 ± 1.7 Hz. The average shear wave velocity of Knalichhina is 1073 ms^{-1}.

Muavani is a village in Knalichhina tehsil of Pithoragarh district of state Uttarakhand. It is situated 18 km towards North from District headquarters Pithoragarh. It lies in Tejam Group of Deoban Formation having Dolomite and Quartzite as main lithological units. It has an altitude of 822 m. The predominant frequency estimated from strong ground motion is 9.0 ± 1.6 Hz and for ambient noise is 11.9 ± 1.8 Hz. The average shear wave velocity of Muavani is 715 ms^{-1}.

Mangti is situated in Kali river valley in Pithoragarh district of Uttarakhand. Stratigraphically it falls in Munsiari Formation of Almora Group. The Munsiari Formation contains granite, gneisses, quartzite, mica-schist and amphibolite. It has an altitude of 2239 m. The predominant frequency estimated from strong ground motion is 10 ± 3.1 Hz and for ambient noise is 11.6 ± 1.6 Hz. The average shear wave velocity of Mangti is 620 ms^{-1}.

Sobla is located in Darma valley of Pithoragarh near Darchula. It has an altitude of 1628 m. Stratigraphically it falls in Munsiari Formation of Almora Group. The Munsiari Formation contains granite, gneisses, quartzite, mica-schist and amphibolite. The predominant frequency estimated from strong ground motion is 9.4 ± 0.9 Hz and for ambient noise is 10.3 ± 1.9 Hz. The average shear wave velocity of Sobla is 700 ms^{-1}.

Kapkot lies in Tejam Group of Deoban Formation having Dolomite and Quartzite as main lithological units. It has an altitude of 1133 m. The predominant frequency estimated

from strong ground motion is 10.7 ± 1.8 Hz and for ambient noise is 12.2 ± 1.3 Hz. The average shear wave velocity of Kapkot is 774 ms^{-1}.

Nachni lies in Munsiari tehsil of Pithoragarh district, Uttarakhand. Nachni is a small village just at road side, 13 Km northwards on Thal-Munsyari road. In Nachni there is a culmination of Ramganga and Bhujgarh rivers. Tejam Group of Deoban Formation is having Dolomite and Quartzite as main lithological units. It has an altitude of 2240 m. The predominant frequency estimated from strong ground motion is 11.4 ± 2.1 Hz and for ambient noise is 13.7 ± 0.9 Hz. The average shear wave velocity of Nachni is 638 ms^{-1}.

Narayannagar is located at Pithoragarh district in Uttarakhand. It is located at an elevation of 1800 m. Stratigraphically the area falls in Askot Crystalline. The Askot Crystalline contains granite, gneisses, quartzite, mica-schist and amphibolite. The predominant frequency estimated from strong ground motion is 10.1 ± 1.4 Hz and for ambient noise is 11.4 ± 2.2 Hz. The average shear wave velocity of Narayannagar is 599 ms^{-1}.

Rishikesh, city of Sadhu's lies 45 km from the state capital Dehradun. It is a pilgrimages town and refers as one of the famous holy destination for Hindus and also famous for Yoga Extensive geological studies illustrate the deposition of Blaini tillite, limestone (probably due to turbulent water supersaturated with calcium carbonate), sandstone and siltstone. It has an altitude of 1628 m. The predominant frequency estimated from strong ground motion is 9.2 Hz and for ambient noise is 12.7 ± 2.3 Hz. The average shear wave velocity of Rishikesh is 541 ms^{-1}.

Narendranagar is located at an elevation of 1326 m and falls in in Tehri Garhwal district in Uttarakhand situated at about 20 km from Rishikesh. The town is located on the left bank of Chandrabagha River on higher reaches. Most of the rocks exposed such as dimctites and tillites of Blaini Formation of Mussorie Group rocks are thinly foliated, folded, partially weathered and dissected by few prominent joint sets. The predominant frequency estimated from ambient noise is 11.4 ± 2.2 Hz. It is located at an elevation of 1725 m. The average shear wave velocity of Narendernagar is 668 ms^{-1}.

Muni Ki Reti lies between Rishikesh and Narayan Nagar along NH 108. River Ganga flows adjacent to it in deep valley. It lies in foothills of Himalayas at the confluence of River Ganga and Chandrabhaga River from North and South respectively. Most of the rocks exposed are doon gravel and alluviums of Quaternary age. It has an altitude of 456 m. The predominant

frequency estimated for ambient noise is 14.3 ± 1.6 Hz. The average shear wave velocity of Muni ki Reti is 682 ms^{-1}.

Chamba is a town in Tehri Garhwal district in the state of Uttarakhand, India. It is situated at a junction of roads connecting Mussoorie and Rishikesh with the Tehri Dam reservoir and New Tehri. Most of the rocks exposed are quartzite of Nagthat Formation of Jaunsar Group. It has an altitude of 1524 m. The predominant frequency estimated from strong ground motion is 9.9 ± 1.8 Hz and for ambient noise is 11.9 ± 0.9 Hz. The average shear wave velocity of Chamba is 1080 ms^{-1}.

Tehri is located in Tehri District in the state of Uttarakhand. It lies in Jaunsar Group of Chandpur Formation having Phyllite as main lithological units. It has an altitude of 1628 m. The predominant frequency estimated from strong ground motion is 9.8 ± 1.4 Hz and for ambient noise is 10.7 ± 1 Hz. The average shear wave velocity of Tehri is 691 ms^{-1}.

Devprayag is situated at the confluence of Bhagirathi and Alakananda River. It is one of the five sacred confluences in the hills and is an important place of pilgrimage for devout Hindus. It lies in Jaunsar Group of Chandpur Formation having Phyllite as main lithological units. It has an altitude of 1628 m. The predominant frequency estimated for ambient noise is 14.5 ± 0.3 Hz. It is located at an elevation of 830 m. The average shear wave velocity of Devprayag is 606 ms^{-1}.

Gochar is situated in Karnaprayag tehsil within Chamoli district of Uttarakhand . Gochar is situated on the left bank of river Alaknanda at an altitude of 800 m above the sea level. This quiet little town is unique in terms of its geographical location and topography. Gochar is located on one of the largest pieces of flatland in this mountainous region of Uttarakhand. The rocks exposed in Gochar are mainly quartzite of Garhwal Group of Precambrian age. The predominant frequency estimated for ambient noise is 12.6 ± 2.4 Hz. The average shear wave velocity of Gochar is 1244 ms^{-1}.

The predominant frequency of Kamedidevi estimated from strong ground motion is 11.8 ± 1.6 Hz and for ambient noise is 13.3 ± 1.4 Hz. Stratigraphically, it forms the part of Berinag Formation of Jaunsar Group having quartzite as lithological unit. The predominant frequency of estimated from strong ground motion is 12.6 ± 2.4 Hz and for ambient noise is 12.2 ± 1.7 Hz. Stratigraphically it forms the part of Deoban Formation of Tejam Group having quartzite and dolomite as lithological unit. It has an altitude of 1628 m.

The predominant frequency of Thal estimated from strong ground motion is 11.6 ± 1.9 Hz and for ambient noise is 11.0 ± 1.1 Hz. It belongs to Mandhali Formation of Tejam Group. The rocks exposed are slate, phyllite and limestone and dolomite.

The predominant frequency of Didihat estimated from strong ground motion is 10.7 ± 3.1 Hz and for ambient noise is 12.4 ± 1.7 Hz. Stratigraphically it falls in Askot Crystalline. The Askot Crystalline is mainly composed of granite and gneisses with some traces of mica-schist and amphibolite.

The predominant frequency of Berinag estimated from strong ground motion is 13.0 ± 1.5 Hz and for ambient noise is 11.7 ± 2.3 Hz. Stratigraphically it falls in Berinag Formation of Jaunsar Group. The rock exposed is mostly quartzite of Neo-Proterozoic age.

The predominant frequency of Bhageshwar estimated from strong ground motion is 8.7 ± 1.2 Hz and for ambient noise is 12.2 ± 1.6 Hz. It is having rocks of Berinag Formation of Jaunsar Group. Quartzite of Neo Proterozoic age is exposed in the area. It has an altitude of 1628 m.

The predominant frequency of Shivpuri estimated from ambient noise is 12.0 ± 1.9 Hz. Stratigraphically it falls in Blaini Formation of Mussoorie Group. The Blaini Formation contains diamictite and siltstone interbedded with greywacke and slates.

High-rise buildings typically have low natural frequency as compared to small buildings. Kumaon region is mostly populated with small to medium buildings. It is observed that Predominant Frequency in this region varies from 9.8 to 14.5 Hz indicating a wide range of damaging pattern to various structures in the region.

In case of ambient noise, Nachni station has minimum frequency peak i.e. at 9.8 Hz while Kapkot has maximum frequency peak i.e. at 13.7 Hz in Kumaon Himalayas where as Tehri station has minimum frequency peak i.e. at 10.7 Hz while Devprayag has maximum frequency peak i.e. at 14.5 Hz in Garhwal Himalayas

The comparison of average predominant frequency of ambient noise and events data used at various stations of Kumaon and Garhwal Himalayas are shown in Fig. 5.31.

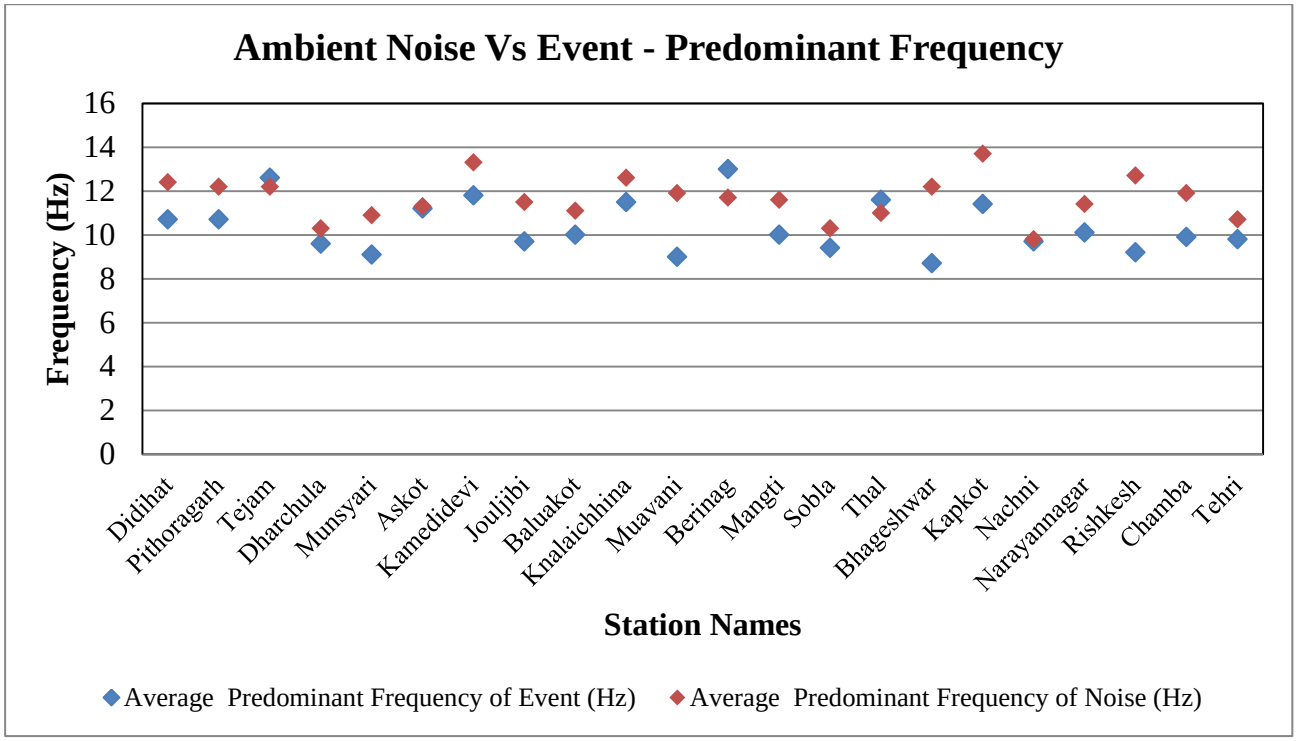

Figure 5.31: The comparison of average predominant frequency of ambient noise and events data used at various stations of Kumaon and Garhwal Himalayas.

The estimated predominant frequency and standard deviation of ambient noise and events data at various stations of Kumaon and Garhwal Himalayas, India are given in Table 5.6.

Table 5.6: Estimated predominant frequency and standard deviation of ambient noise and events data at various stations of Kumaon and Garhwal Himalayas, India.

S.No.	Station Name	Formation	Event		Ambient Noise	
			Average Predominant Frequency (Hz)	Standard Deviation	Average Predominant Frequency (Hz)	Standard Deviation
1	Didihat	Askot Crystalline	10.7	3.1	12.4	1.7
2	Pithoragarh	Mandhali	10.7	1.8	12.2	1.3
3	Tejam	Deoban	12.6	2.4	12.2	1.7
4	Dharchula	Mandhali	9.6	2.6	10.3	1.7
5	Munsyari	Munsiari	9.1	1.4	10.9	1.3
6	Askot	Askot Crystalline	11.2	2.8	11.3	1.7
7	Kamedidevi	Berinag	11.8	1.6	13.3	1.4
8	Jouljibi	Mandhali	9.7	1.5	11.5	0.6
9	Baluakot	Rautgara	10	2.5	11.1	1.1
10	Knalaichhina	Deoban	11.5	2.8	12.6	1.7
11	Muavani	Deoban	9	1.6	11.9	1.8
12	Berinag	Berinag	13	1.5	11.7	2.3
13	Mangti	Munsiari	10	3.1	11.6	1.6
14	Sobla	Munsiari	9.4	0.9	10.3	1.9
15	Thal	Mandhali	11.6	1.9	11	1.1
16	Bhageshwar	Berinag	8.7	1.2	12.2	1.6
17	Kapkot	Deoban	11.4	2.1	13.7	0.9
18	Nachni	Deoban	9.7	0.9	9.8	1.4
19	Narayan Nagar	Askot Crystalline	10.1	1.4	11.4	2.2
20	Rishkesh	Blaini	9.2	0	12.7	2.3
21	Chamba	Nagthat	9.9	1.8	11.9	0.9
22	Tehri	Chandpur	9.8	1.4	10.7	1
23	Shivpuri	Blaini	-	-	12	1.9
24	Narendra Nagar	Blaini	-	-	11.4	2.2
25	Muni ki reti	-	-	-	14.3	1.6
26	Goucher	Garhwal Group	-	-	12.6	2.4
27	Devprayag	Chandpur	-	-	14.5	0.3

The amplification levels for different frequencies for different stations of Kumaon and Garhwal Himalayas using recorded ambient noise and earthquake data have been estimated and

given in Table 5.7 and Table 5.8, respectively. These estimated amplification levels are useful for evaluation of seismic hazard to different story buildings in the region (Sandhu et. al, 2016).

Table 5.7: Estimated amplification levels for different frequencies for different stations of Kumaon and Garhwal Himalayas using recorded ambient noise.

S. No.	Station Code	Amplification at							
		0.5 Hz	1 Hz	3 Hz	5 Hz	7 Hz	10 Hz	15 Hz	20 Hz
1	ASK	1.02	1.13	1.72	0.85	0.60	1.04	0.58	0.81
2	BHA	0.87	1.04	1.07	1.28	1.16	2.21	0.86	1.31
3	BAL	0.77	0.92	1.08	1.55	1.43	1.43	0.91	1.26
4	BER	0.97	1.48	1.23	0.94	1.16	0.89	0.68	0.30
5	DHA	0.88	1.05	1.10	1.16	1.46	1.30	1.11	0.80
6	DID	1.13	1.63	1.36	1.66	1.69	1.06	1.22	1.70
7	JOL	1.05	1.02	1.19	1.39	1.04	1.98	1.66	1.87
8	KAM	0.77	1.09	1.35	1.18	1.12	1.80	2.24	2.80
9	KNA	0.73	1.33	1.00	0.84	1.34	0.97	0.44	1.20
10	KAP	1.28	1.11	1.83	1.41	1.72	1.37	1.23	0.63
11	MAN	1.02	1.08	1.28	6.01	2.37	2.43	2.37	1.03
12	PIT	1.15	1.32	1.06	1.37	1.48	1.43	1.78	1.53
13	TEJ	1.08	1.07	1.97	1.36	1.57	1.69	0.75	0.77
14	THL	0.95	1.73	1.39	1.30	1.84	3.90	0.78	1.63
15	MUN	1.34	1.30	1.12	1.27	1.52	2.13	0.85	1.64
16	MUA	0.75	1.65	1.45	1.25	1.30	1.54	0.87	0.94
17	SOB	1.17	1.13	1.94	2.31	3.34	2.96	3.74	1.49
18	NAC	2.59	2.53	1.86	1.37	2.39	3.03	1.60	0.78
19	NYN	1.16	1.51	0.81	0.98	0.85	1.74	0.72	0.68
20	RIS	0.95	2.20	1.32	1.56	0.90	1.31	0.75	1.18
21	NAN	1.23	1.09	2.18	1.24	1.07	1.90	1.91	2.89
22	SHI	1.06	1.20	1.29	1.37	1.51	0.91	2.14	1.37
23	CMB	1.17	0.87	0.54	3.82	2.17	2.25	0.65	1.95
24	TER	1.48	1.43	1.46	0.95	1.62	1.88	0.87	0.85

Table 5.8: Estimated amplification levels for different frequencies for different stations of Kumaon and Garhwal Himalayas using recorded earthquake.

No.	Station Code	Amplification at							
		0.5 Hz	**1 Hz**	**3 Hz**	**5 Hz**	**7 Hz**	**10 Hz**	**15 Hz**	**20 Hz**
1	ASK	1.42	2.13	3.43	1.25	1.41	1.08	1.42	1.16
2	BHA	1.08	2.12	1.77	3.52	3.40	2.68	0.86	1.50
3	BAL	1.03	1.20	1.88	6.41	2.68	3.07	0.78	1.05
4	BER	1.03	1.24	2.06	2.34	1.82	1.25	1.81	1.10
5	DHA	1.66	2.02	1.81	4.11	4.47	2.65	1.26	0.87
6	DID	1.78	1.80	2.73	3.27	2.10	1.45	1.80	1.18
7	JOL	1.28	1.86	1.85	5.66	2.05	1.43	1.41	1.41
8	KAM	1.20	1.19	1.37	2.33	4.23	2.65	1.10	1.21
9	KNA	1.03	1.52	1.50	2.31	2.19	1.10	1.04	1.26
10	KAP	1.07	1.89	3.39	3.50	1.43	1.42	1.40	1.39
11	MAN	1.48	1.65	2.32	6.03	0.83	2.98	0.98	0.93
12	PIT	1.28	1.01	3.11	1.44	1.86	1.59	2.84	6.91
13	TEJ	1.78	1.73	3.18	1.60	1.78	2.20	1.56	3.10
14	THL	1.53	1.99	2.26	7.13	3.02	2.16	7.04	2.40
15	MUN	1.14	3.57	2.39	1.67	2.06	1.25	1.31	3.56
16	MUA	1.30	1.21	2.49	2.59	3.89	2.05	1.60	1.40
17	SOB	1.13	1.13	1.81	1.57	2.41	2.32	1.55	0.81
18	NAC	1.06	0.79	1.32	6.88	4.79	3.98	1.13	0.63
19	NYN	4.76	1.10	7.91	1.25	0.96	4.14	1.86	1.65
20	RIS	0.35	0.93	0.48	0.23	0.57	0.68	1.00	0.40
21	CMB	1.70	2.70	1.38	1.50	1.00	1.19	0.76	1.01
22	TER	4.55	1.87	1.74	0.82	0.96	1.46	0.93	0.86

5.4. Comparison of Standard Spectral Ratio (SSR) and HVSR methods

In this section, a comparison has been made between SSR and HVSR outputs to validate the obtained parameters. The parameters i.e. amplification level and pre-dominant frequencies are obtained by using both SSR and HVSR techniques. SSR method involves comparing records of two nearby sites considering one site as a reference site. In general, the reference site involved should be installed on hard rock.

In Standard Spectral Ratio (SSR) technique, the Horizontal component (N-S and E-W) of the site under consideration is divided with the same component of reference site (N-S and E-W) respectively. A time window length 1500 ms is considered for both the reference site as well as the site under consideration. Such analysis has been carried out for total ten stations using strong ground motion data. The average of the two components has been considered for the final result or output.

$$A = \frac{N-S\ component\ of\ site\ under\ consideration}{N-S\ component\ of\ reference\ site}$$

$$B = \frac{E-W\ component\ of\ site\ under\ consideration}{E-W\ component\ of\ reference\ site}$$

$$Average\ SSR = \frac{A+B}{2}$$

We compared the two techniques i.e. SSR and HVSR to constrain the parameters (i.e. amplification level and pre-dominant frequencies) in the Kumaon region. These results are used to limit the range defined in this region. It has also been observed that the peak amplification obtained by these two methods for the site under consideration is matching which confirms the reliability of the obtained results. Thus, it may be stated that there is no large difference in the peak amplifications obtained using the two methods. The general shape of the ratios and the range of amplification frequency are matching and are in good agreement with each other.

As it appears from table 5.10, more number of events is used for HVSR as compared to SSR. In SSR technique, the events should be considered which are simultaneously recorded at various stations along with the reference station (Berinag). In HVSR, the number of events used is independently chosen for a particular station. Thus, less number of recorded stations and number of event data could be utilized.

Table 5.9: Recorded earthquake data from year 2011 to 2012 at the various sites in Kumaon Himalayas used in SSR technique. Δ denotes the reference site i.e. Berinag and * denotes the records used in the analysis.

Sr. No.	Date	BAL	JOL	KNA	KAMD	BERI	BHAG	MUN	MUA
1	19/08/11		*			Δ		*	*
2	18/09/11		*			Δ			*
3	09/10/11		*	*		Δ			*
4	06/11/11			*		Δ		*	*
5	18/11/11	*				Δ	*	*	*
6	09/12/11	*		*		Δ		*	*
7	16/01/12	*	*			Δ		*	*
8	12/02/12			*		Δ			*
9	26/02/12			*	*	Δ	*	*	*
10	26/02/12			*	*	Δ	*		*
11	16/03/12				*	Δ	*		
12	17/05/12			*	*	Δ	*		
13	19/07/12	*				Δ			
14	28/07/12	*				Δ			
15	27/08/12	*				Δ			
16	15/11/12				*	Δ			

Table 5.10: Number of event data used in the analysis at the various sites in Kumaon Himalayas used in HVSR and SSR technique.

Sr. No.	Station Name	Station Code	Number of event data used in the analysis (HVSR)	Number of event data used in the analysis (SSR)
1	Munsiari	MUN	12	6
2	Kamedidevi	KAMD	10	5
3	Jouljibi	JOL	17	4
4	Baluakot	BAL	20	6
5	Knalichhina	KNA	15	7
6	Muavani	MUA	20	10
7	Bhageshwar	BHAG	12	5

5.5. Results and Discussion

In this chapter, the records are analyzed using three different methods: (a) Reference site dependent method : Standard Spectral ratio, (b) Non- Reference site method : the horizontal to vertical (H/V) spectral ratio on ambient noise records, and (c) Non- Reference site method : the horizontal to vertical (H/V) spectral ratio on strong ground motion records. The comparison among the techniques is shown in the following Figure 5.32.

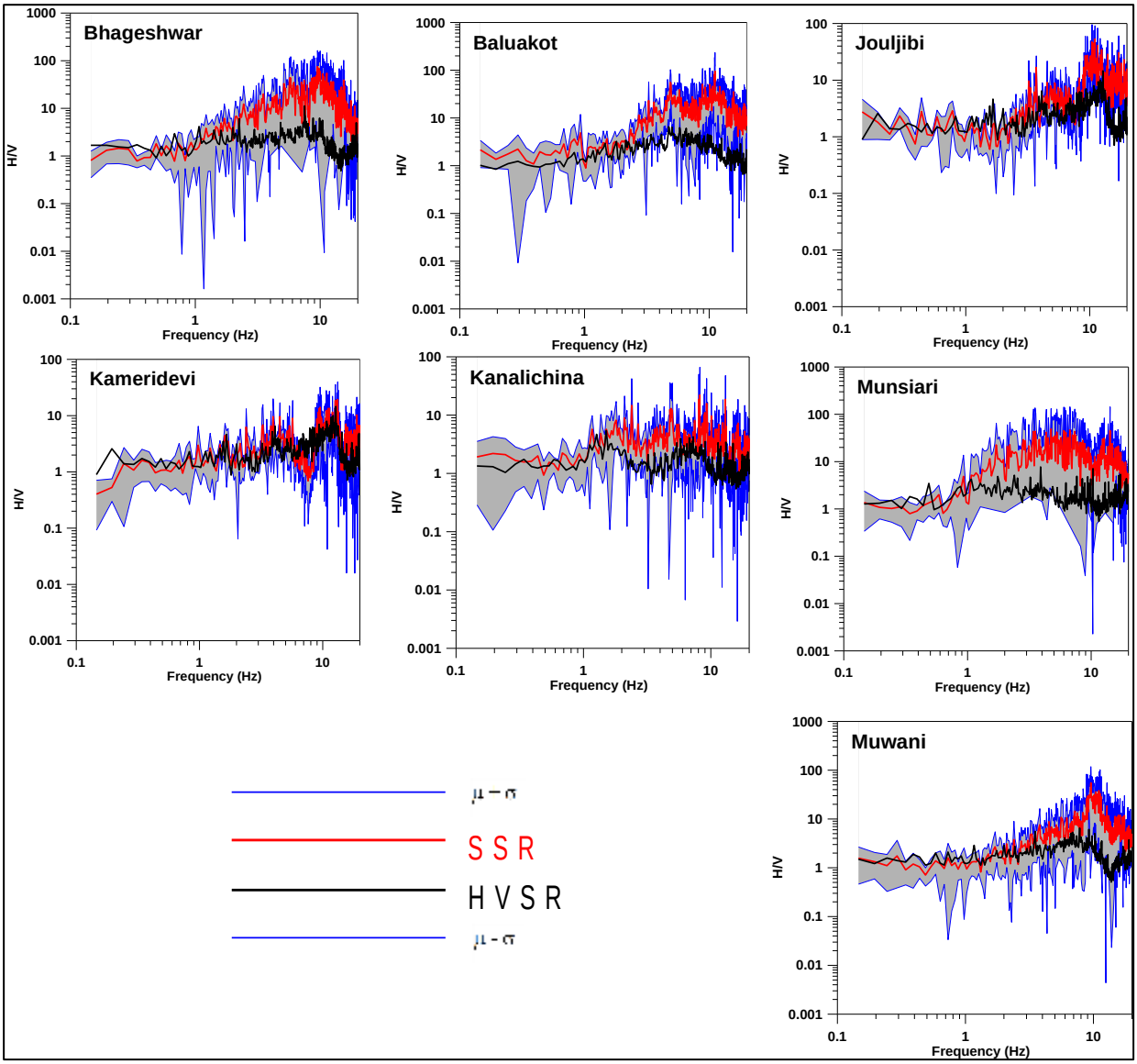

Figure 5.32: Comparitive study of HVSR and SSR technique at various stations of Kumaon Himalayas. The black and red lines show the site effects obtained by HVSR and SSR techniques, respectively. The grey shaded area between blue lines denotes the region between μ +σ and μ –σ of the site amplification obtained using technique given by Lermo and Chavez-Garcia (1993). Parameters 'μ' and 'σ' describe the mean and standard deviation, respectively.

The comparison has been made between SSR and HVSR outputs to validate the obtained parameters as tabulated in Table 5.11. Sediment to bedrock spectral ratio estimates between pairs of stations are compared with the ratio obtained using non- reference site estimate i.e. horizontal to vertical component spectral ratio of strong ground motion records and ambient noise. The outputs are compared in terms of site amplification functions i.e. amplification level and predominant frequency.

Table 5.11: Comparison of predominant frequency results derived from three methods namely, HVSR using strong ground motion records, HVSR using ambient noise records and SSR using strong ground motion records.

S. No.	Station Name	Formation	HVSR Event		HVSR Ambient Noise		SSR Event	
			Average P.F. (Hz)	S.D.	Average P.F. (Hz)	S.D.	Average P.F. (Hz)	S.D.
1	Munsiari	Munsiari	9.1	1.4	10.9	1.3	14.9	1.5
2	Kamedidevi	Berinag	11.8	1.6	13.3	1.4	12.1	1.0
3	Jouljibi	Mandhali	9.7	1.5	11.5	0.6	10.6	1.0
4	Baluakot	Rautgara	10	2.5	11.1	1.1	11.3	1.5
5	Knalaichhina	Deoban	11.5	2.8	12.6	1.7	10.4	2.2
6	Muwani	Deoban	9	1.6	11.9	1.8	10.1	0.7
7	Bhageshwar	Berinag	8.7	1.2	12.2	1.6	10.1	1.4

* P.F. - Predominant Frequency, S.D. – Standard Deviation

. It has been found that there is no significant change in the results obtained using two different techniques and three arrangements of datasets. The site amplification functions i.e. amplification level and predominant frequency are matching among these methods.

The frequency dependent character of the site response is well constrained using these methods. Thus results are used to constrain the range defined in the study area. It has also been observed that the peak amplification obtained by these two methods for the site under consideration is matching which confirms the reliability of the obtained results. Such comparison studies were earlier done by various scientists in different parts of the world including California, Greece, China (Field and Jacob 1995; Lachet et al. 1996, Zhang et al. 2001). They found that all the methods give almost same predominant peaks in the region of their study as shown in Figure 5.33.

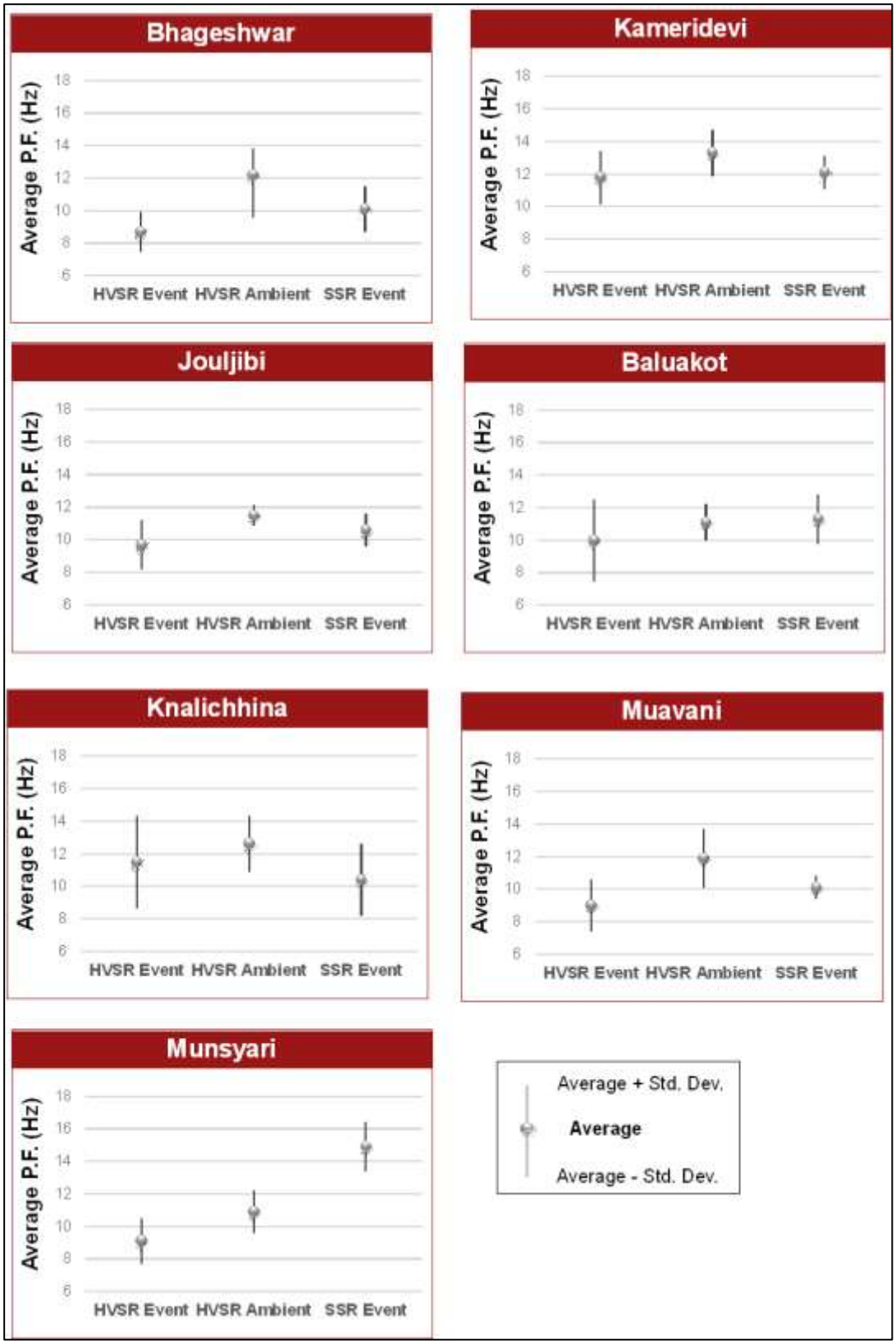

Figure 5.33: Comparison of predominant frequency results derived from three methods namely, HVSR using strong ground motion records, HVSR using ambient noise records and SSR using strong ground motion records.

5.6. Conclusion

There are number of techniques available for site characterization in literature. These techniques need various inputs which may not be available at all the sites of Kumaon and Garhwal Himalayas. In such scenario, HVSR technique can be used. This technique can be processed quickly to yield evocative outcomes. This method can be applied on both strong ground motion as well as ambient noise records. It is useful even if there is scarcity of recorded events in an area.

Site characterization studies for different sites of Kumaon and Garhwal Himalayas show the estimated predominant frequency using both ambient noise records as well as strong ground motion data which are found to be varying from 8.70 Hz to 11.60 Hz and from 9.80 Hz to 14.50 Hz, respectively. This can also be concluded that there is no substantial variation in predominant frequency values among various sites of Kumaon and Garhwal Himalayas. The site amplification factor varies between 0.23 and 7.91 using HVSR (strong ground motion records) and between 0.30 and 6.01 using HVSR (ambient noise records) among different stations.

It has been found that there is no significant change in the results obtained using two different techniques and three arrangements of datasets. The site amplification functions i.e. amplification level and predominant frequency are matching among these methods.

The frequency dependent character of the site response is well constrained using these methods. Thus results are used to constrain the range defined in the study area. It has also been observed that the peak amplification obtained by these two methods for the site under consideration is matching which confirms the reliability of the obtained results.

Chapter – 6

SHEAR WAVE VELOCITY MODELS OF KUMAON AND GARHWAL HIMALAYAS

This chapter includes the 1D shear wave velocity profiles obtained from the ambient noise and strong ground motion data of Kumaon and Garhwal region. The records collected from the accelerograph have been processed using the procedure suggested by Boore and Bommer (2005). The processing steps involve baseline correction, instrument scaling, padding and frequency filtering as discussed in detail in Chapter 4.

The hypocentral parameters of events used in the present study and the error obtained in its localization are tabulated in Table 5.4 along with ERH and ERZ which define the error of epicenter and focal depth, respectively from year 2006 to 2012 at the various sites in Kumaon Himalayas. The hypocentral parameters of events recorded in Garhwal Himalayas are tabulated in Table 5.5 in Chapter 5.

A large number of active and passive source methods are available to measure the shear wave velocity profile. But most of the methods require special instruments and are expensive to execute. Shear wave profile estimates are based on Horizontal to Vertical ratio (H/V) of ambient noise and strong ground motion records, recorded at different stations, is relatively fast and inexpensive technique. In this technique, the observed HVSR are fitted with the synthetic HVSR generated using trial and error forward modelling technique. The present study uses GA-Haskell method to achieve its purpose. The GA-Haskell method uses shear waves transfer function to model H/V spectral curves, which are then constrained by the GA to get the best fit.

6.1. Shear Wave Velocity Models

In order to implement GA in the present study, the size of the population for the Generation 1 is considered as 100. The maximum 1000 generations have been produced to estimate the velocity structure of Kumaon and Garhwal Himalayas. The probability of crossover was kept as 0.6. A probability of 0.01 has been found to be adequate for mutation purpose. The 1D shear wave velocity models are obtained using ambient noise and strong ground motion records at various stations of Kumaon and Garhwal Himalayas. The regional

shear wave velocity models are also derived from the 1D shear wave velocity profiles at various locations. Two 2D shear wave velocity line profiles in Kumaon and one in Garhwal Himalayas are generated on the basis of estimated 1D shear wave velocity profiles.

6.2. Results and Discussion

The 1D shear wave velocity models obtained from ambient noise and strong ground motion records at various stations of Kumaon and Garhwal Himalayas are compared. It has been observed that the observed H/V showing good match with synthetic H/V and 1D shear wave velocity models appear almost similar in both the datasets as shown in Figure 6.1 and 6.22.

The results obtained at various locations of Kumaon and Garhwal Himalayas along with H/V plot of recorded ambient noise and strong ground motion records are presented in this chapter. It has been found that the observed H/V shows good match with synthetic H/V. The 1D shear wave velocity model has been calculated from the best model obtained after enough GA runs. These results are shown from Figure 6.1 to 6.27.

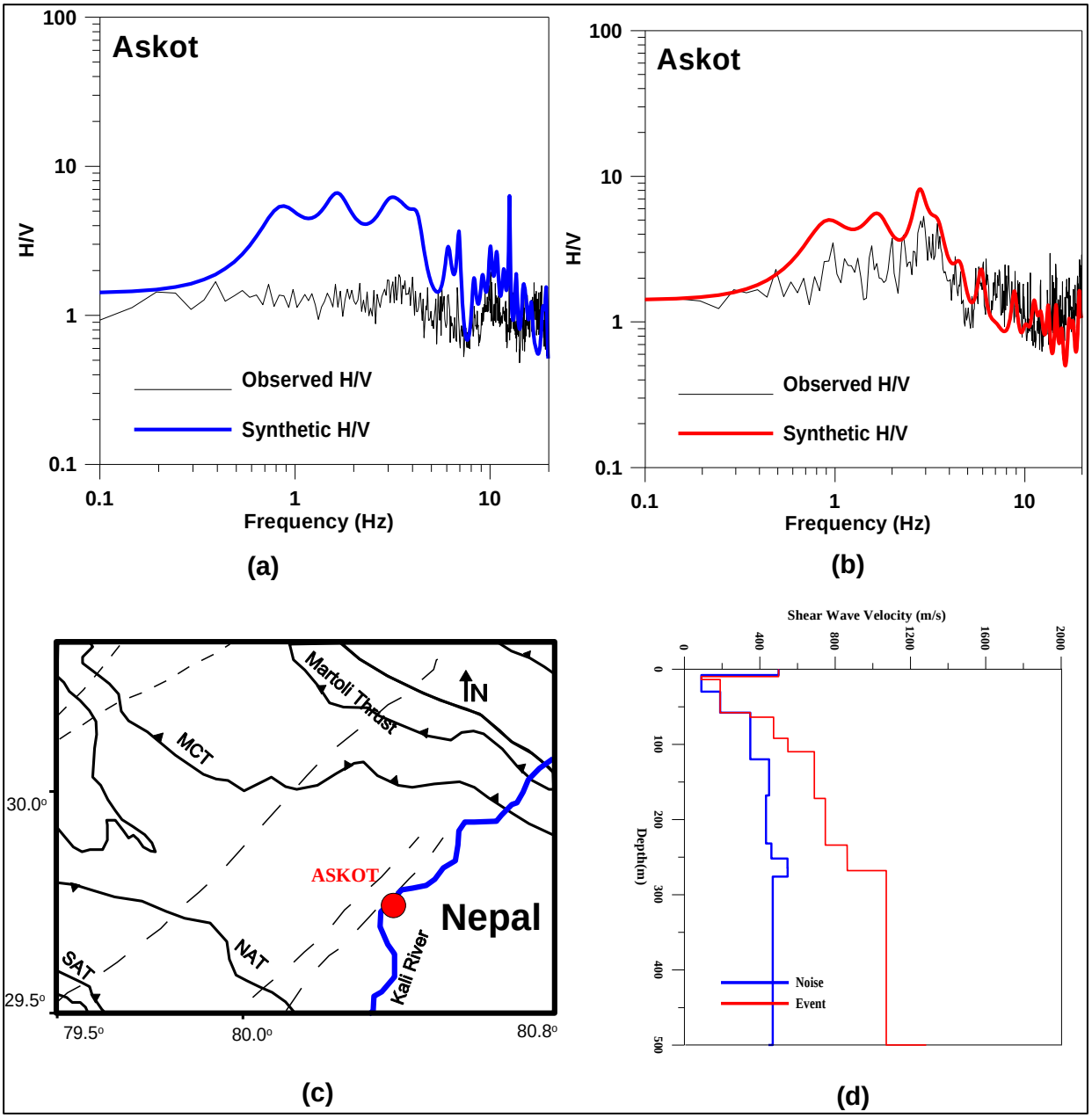

Figure 6.1: The results obtained at Askot station. Observed H/V showing good match with synthetic H/V using (a) Ambient noise records (b) Strong ground motion records (c) Solid red circle shows the location of recording station. Source of the tectonics of the region is GSI (2000) (d) 1D Shear wave velocity model generated using ambient noise (blue) and strong ground motion (red).

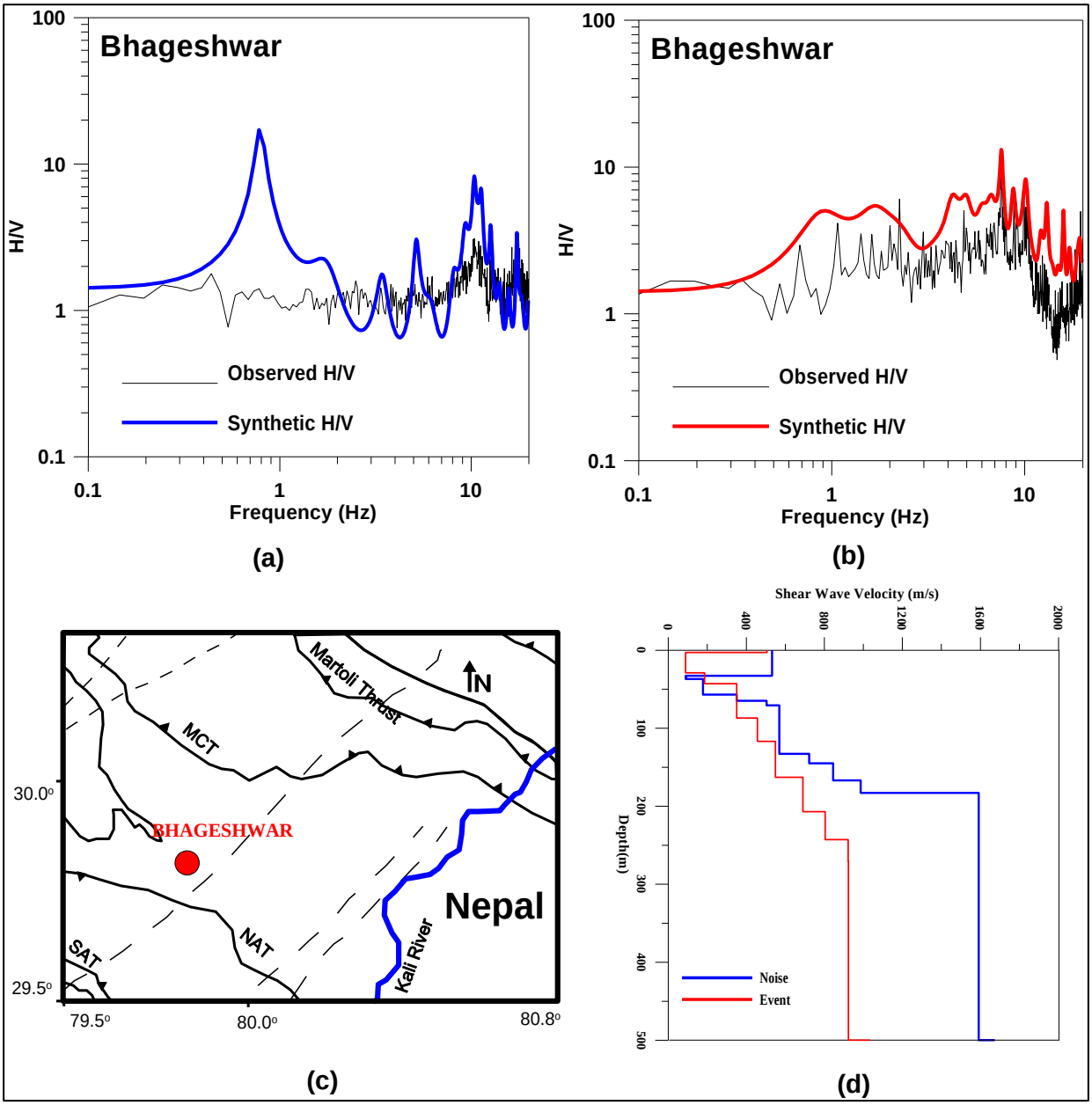

Figure 6.2: The results obtained at Bhageshwar station. Observed H/V showing good match with synthetic H/V using (a) Ambient noise records (b) Strong ground motion records (c) Solid red circle shows the location of recording station. Source of the tectonics of the region is GSI (2000) (d) 1D Shear wave velocity model generated using ambient noise (blue) and strong ground motion (red).

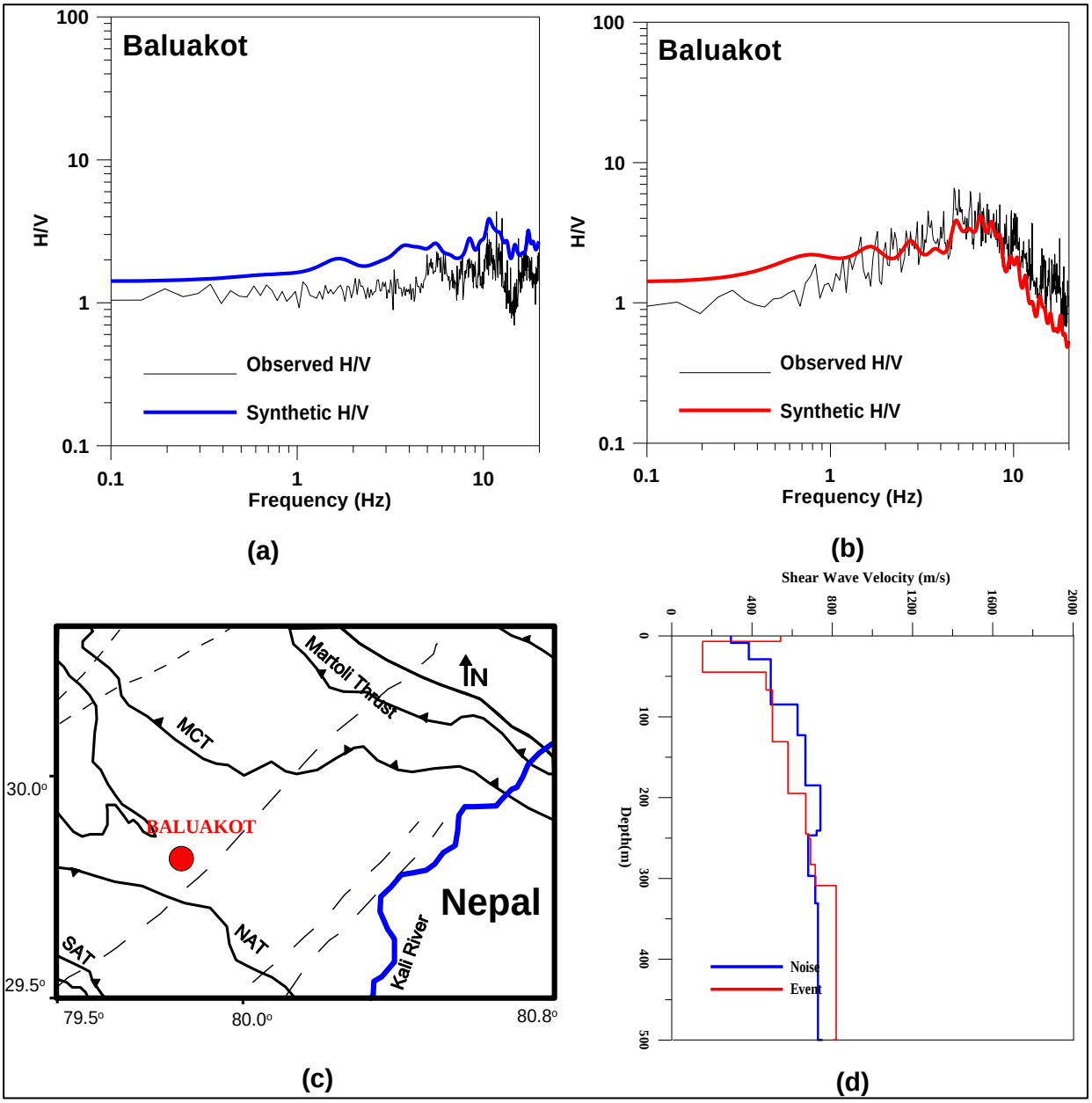

Figure 6.3: The results obtained at Baluakot station. Observed H/V showing good match with synthetic H/V using (a) Ambient noise records (b) Strong ground motion records (c) Solid red circle shows the location of recording station. Source of the tectonics of the region is GSI (2000) (d) 1D Shear wave velocity model generated using ambient noise (blue) and strong ground motion (red).

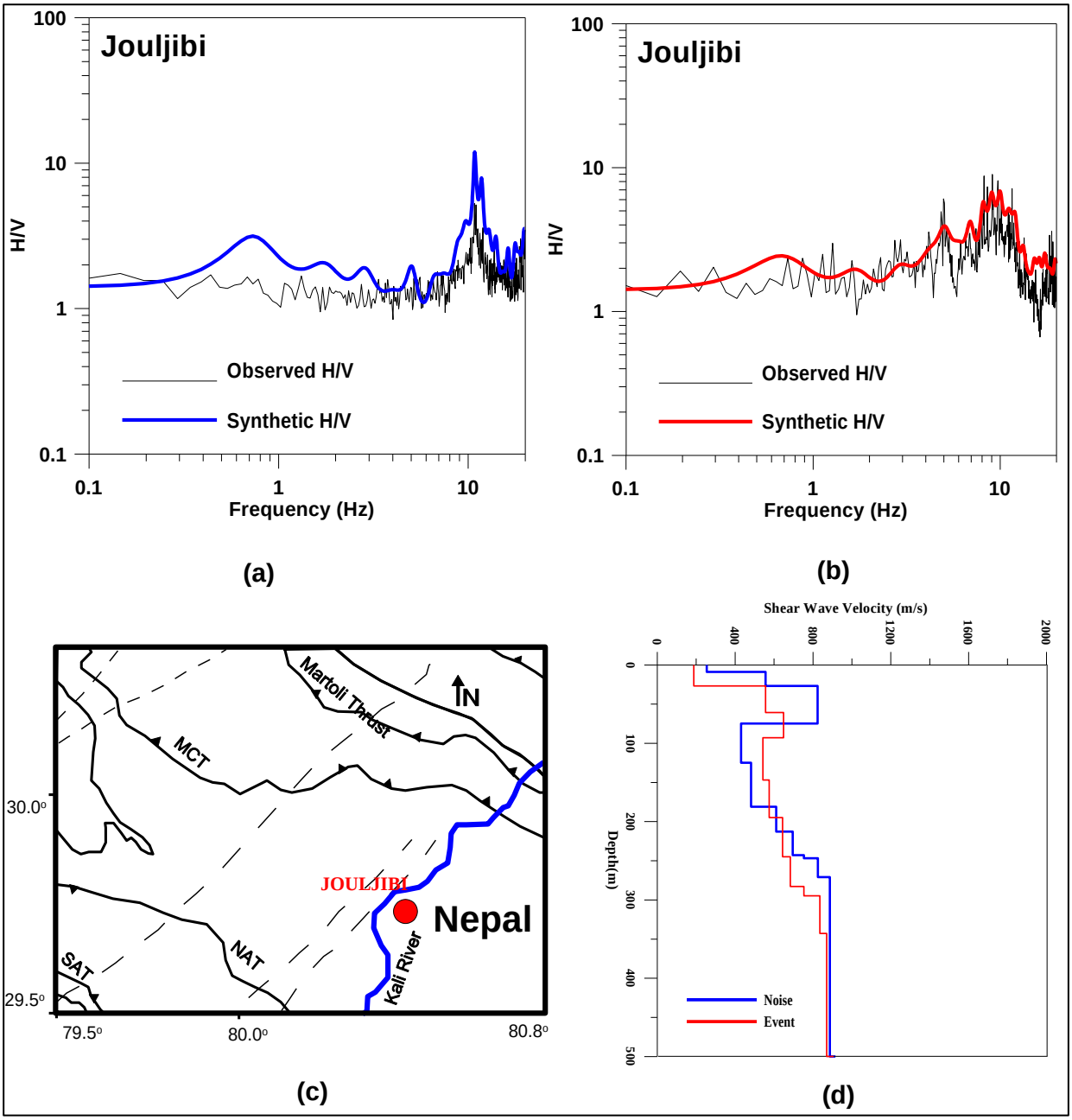

Figure 6.4: The results obtained at Jouljibi station. Observed H/V showing good match with synthetic H/V using (a) Ambient noise records (b) Strong ground motion records (c) Solid red circle shows the location of recording station. Source of the tectonics of the region is GSI (2000) (d) 1D Shear wave velocity model generated using ambient noise (blue) and strong ground motion (red).

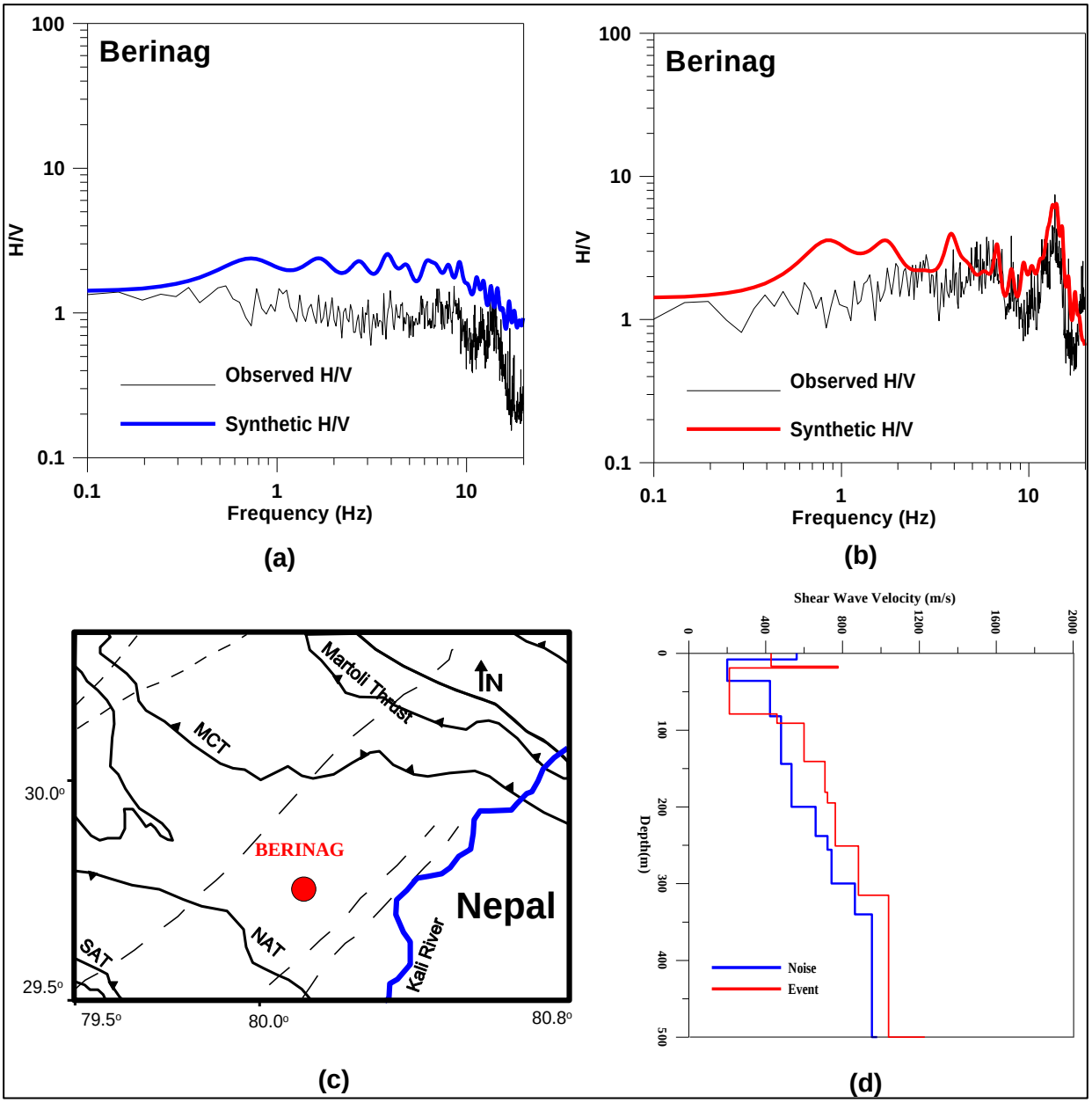

Figure 6.5: The results obtained at Berinag station. Observed H/V showing good match with synthetic H/V using (a) Ambient noise records (b) Strong ground motion records (c) Solid red circle shows the location of recording station. Source of the tectonics of the region is GSI (2000) (d) 1D Shear wave velocity model generated using ambient noise (blue) and strong ground motion (red).

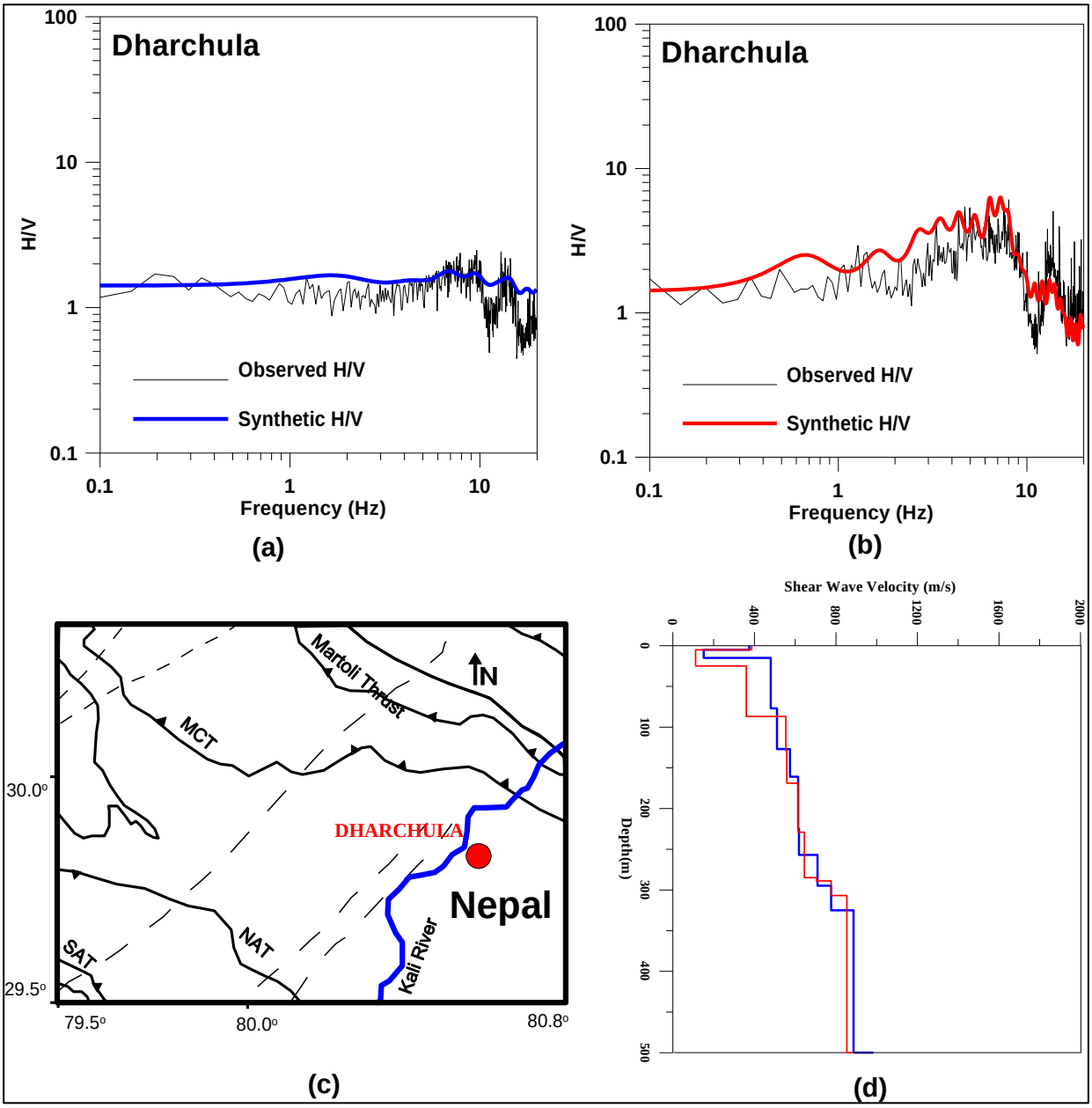

Figure 6.6: The results obtained at Dharchula station. Observed H/V showing good match with synthetic H/V using (a) Ambient noise records (b) Strong ground motion records (c) Solid red circle shows the location of recording station. Source of the tectonics of the region is GSI (2000) (d) 1D Shear wave velocity model generated using ambient noise (blue) and strong ground motion (red).

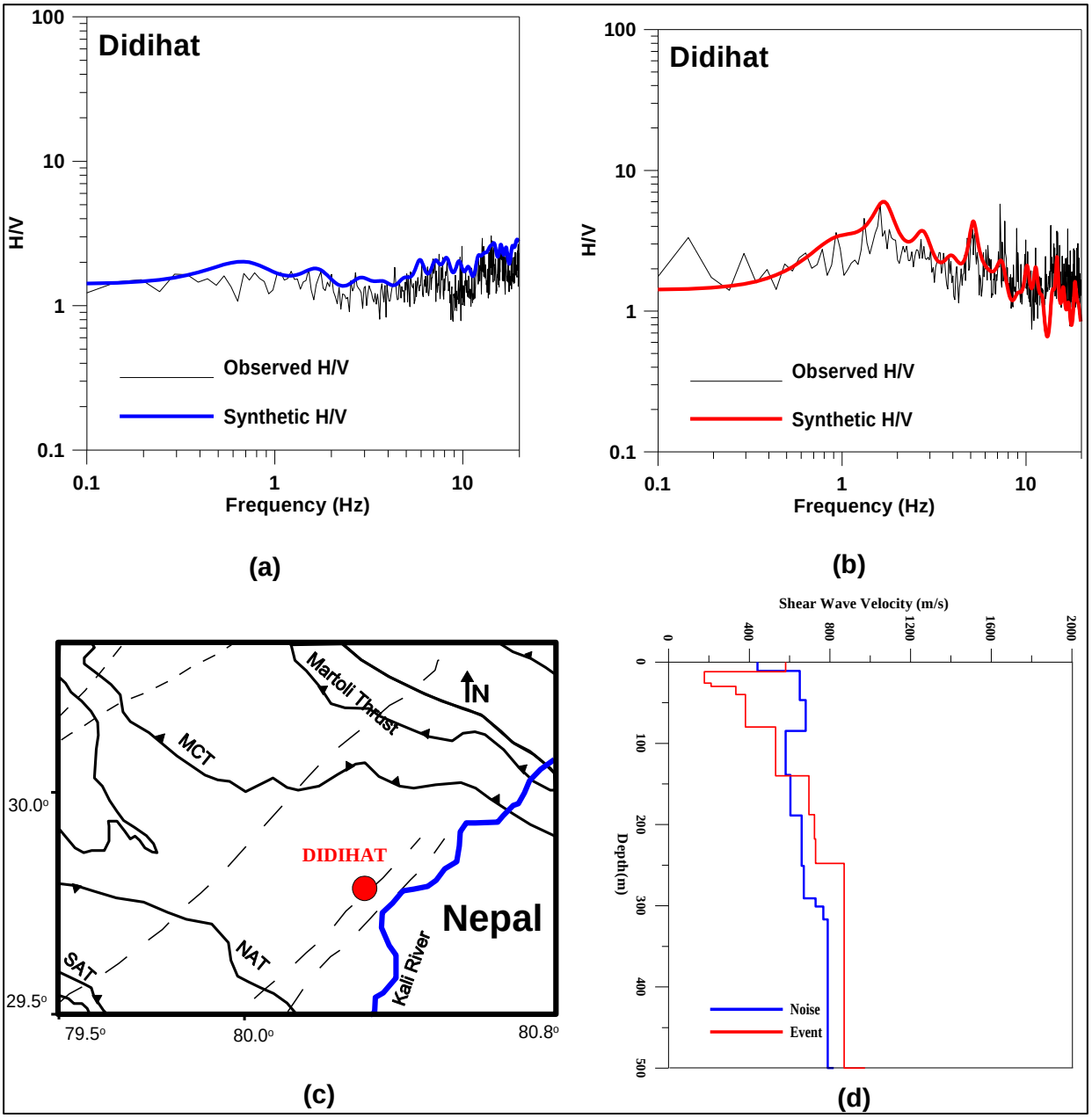

Figure 6.7: The results obtained at Didihat station. Observed H/V showing good match with synthetic H/V using (a) Ambient noise records (b) Strong ground motion records (c) Solid red circle shows the location of recording station. Source of the tectonics of the region is GSI (2000) (d) 1D Shear wave velocity model generated using ambient noise (blue) and strong ground motion (red).

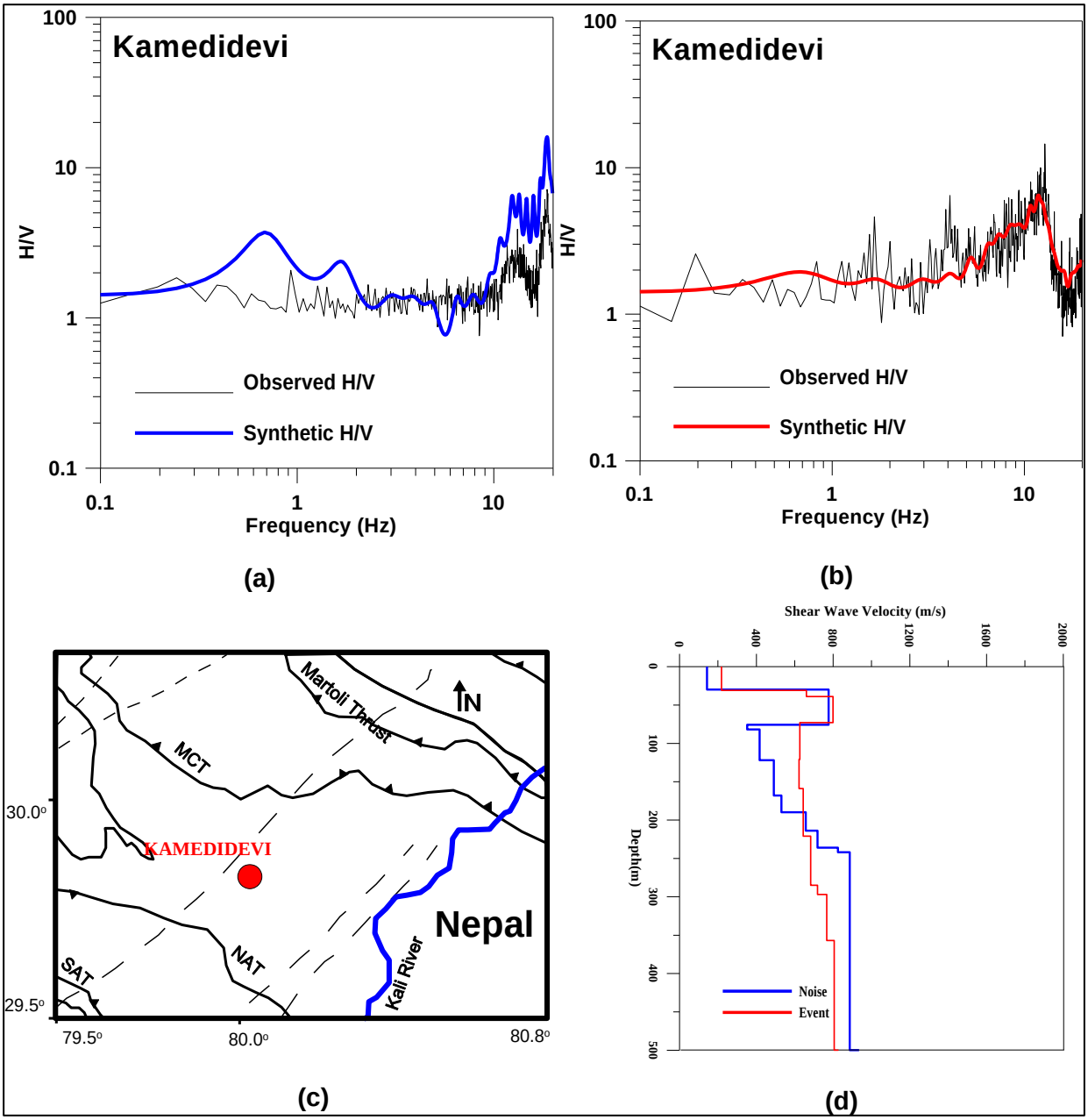

Figure 6.8: The results obtained at Kamedidevi station. Observed H/V showing good match with synthetic H/V using (a) Ambient noise records (b) Strong ground motion records (c) Solid red circle shows the location of recording station. Source of the tectonics of the region is GSI (2000) (d) 1D Shear wave velocity model generated using ambient noise (blue) and strong ground motion (red).

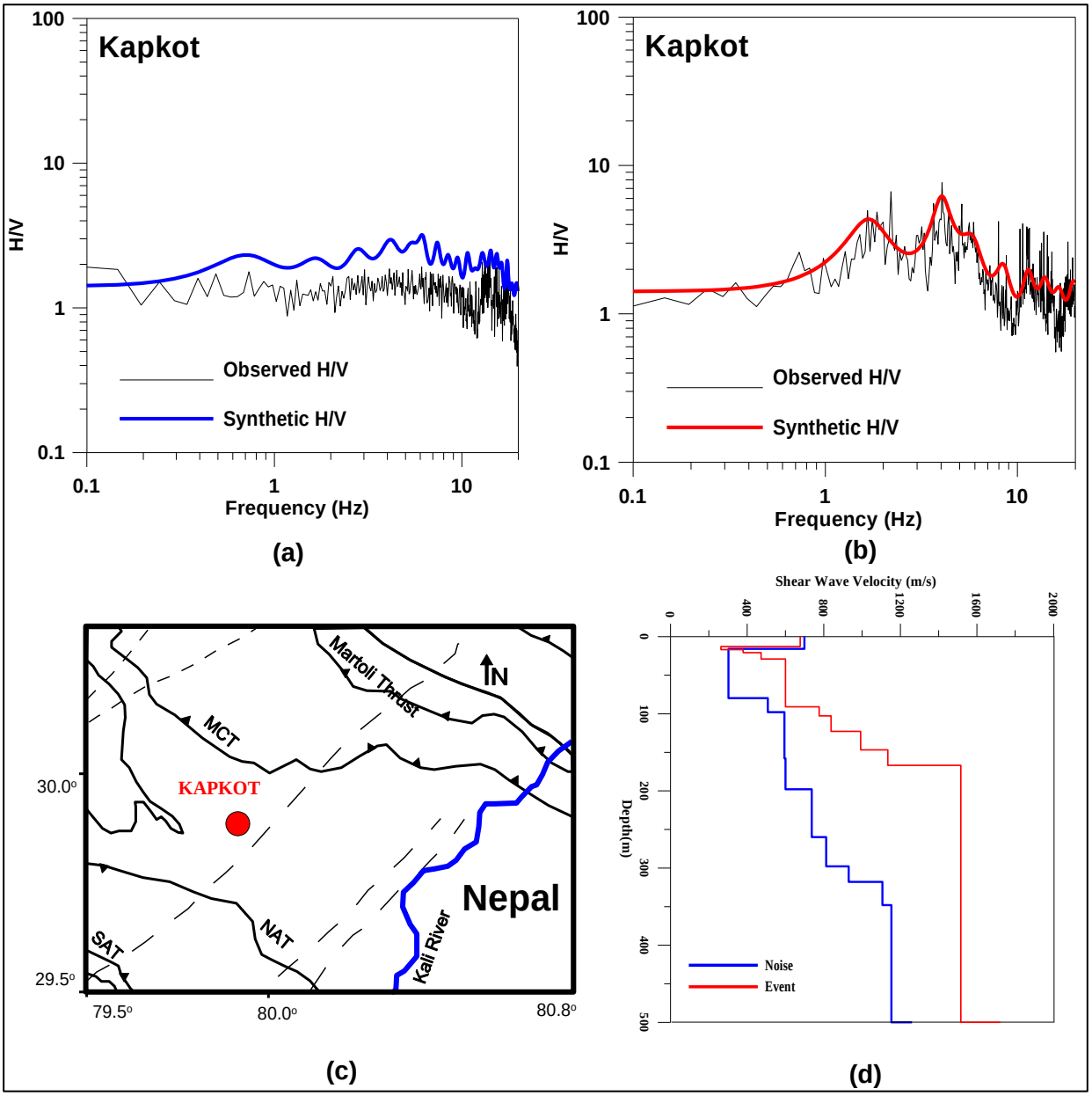

Figure 6.9: The results obtained at Kapkot station. Observed H/V showing good match with synthetic H/V using (a) Ambient noise records (b) Strong ground motion records (c) Solid red circle shows the location of recording station. Source of the tectonics of the region is GSI (2000) (d) 1D Shear wave velocity model generated using ambient noise (blue) and strong ground motion (red).

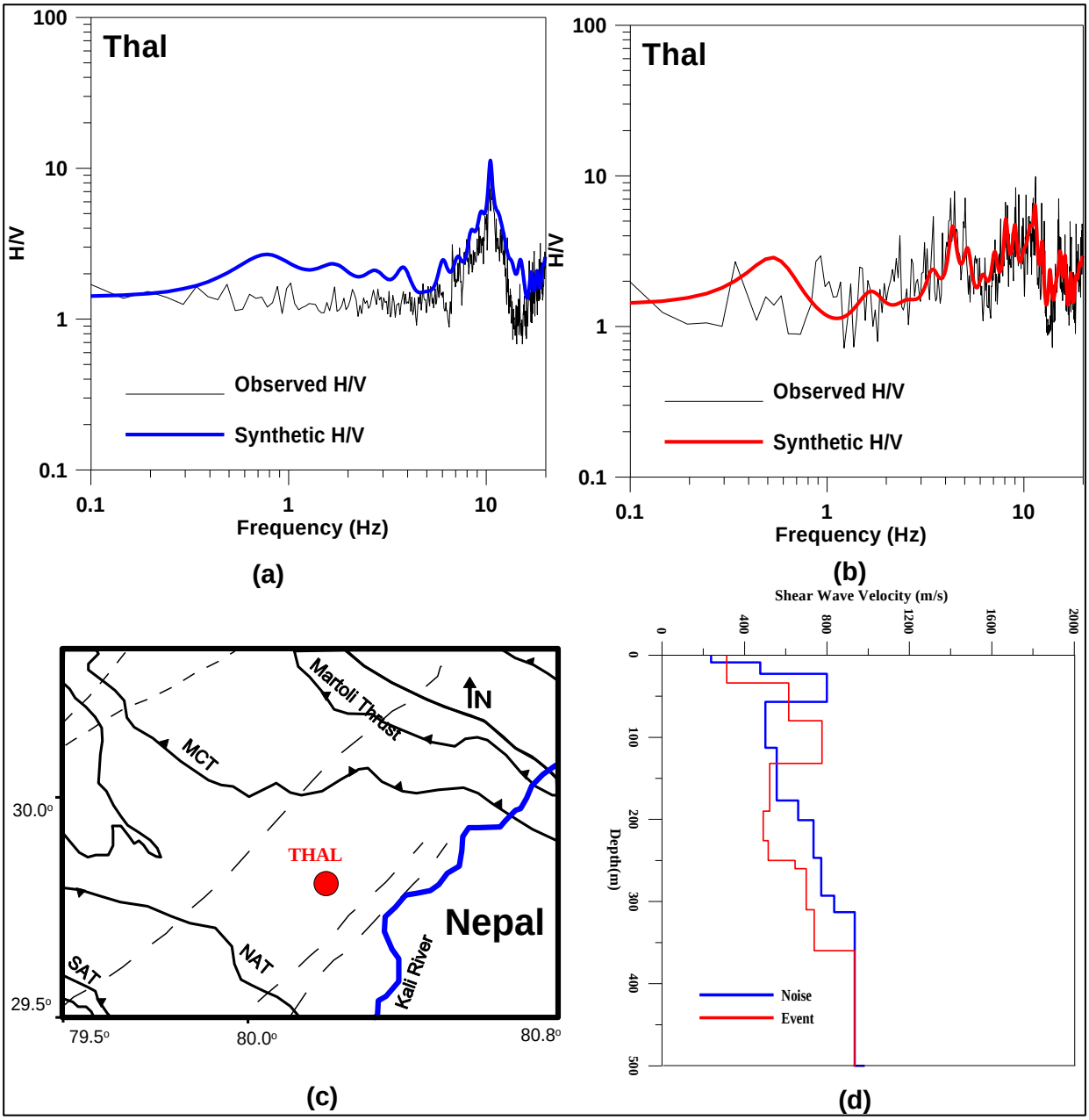

Figure 6.10: The results obtained at Thal station. Observed H/V showing good match with synthetic H/V using (a) Ambient noise records (b) Strong ground motion records (c) Solid red circle shows the location of recording station. Source of the tectonics of the region is GSI (2000) (d) 1D Shear wave velocity model generated using ambient noise (blue) and strong ground motion (red).

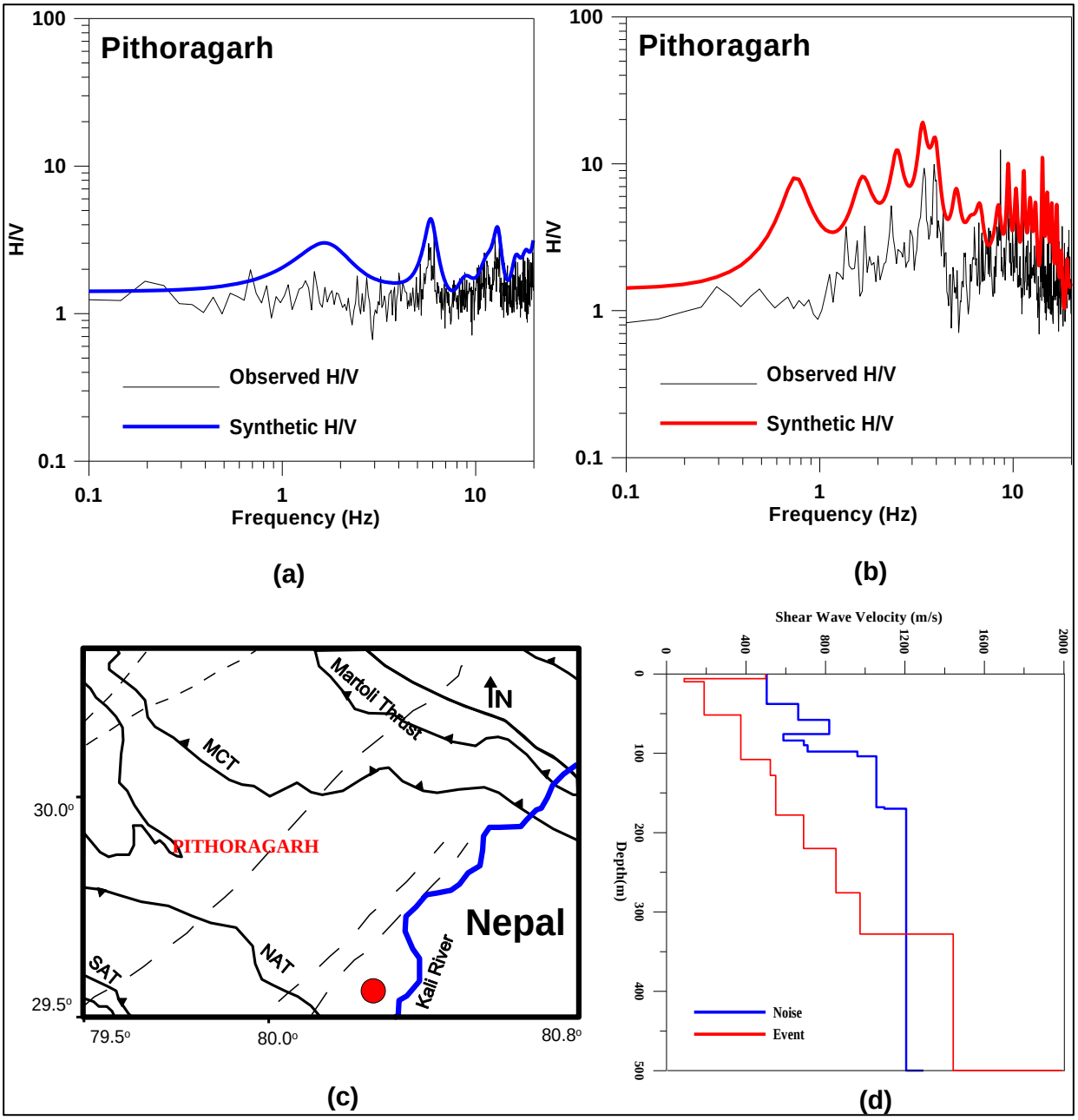

Figure 6.11: The results obtained at Pithoragarh station. Observed H/V showing good match with synthetic H/V using (a) Ambient noise records (b) Strong ground motion records (c) Solid red circle shows the location of recording station. Source of the tectonics of the region is GSI (2000) (d) 1D Shear wave velocity model generated using ambient noise (blue) and strong ground motion (red).

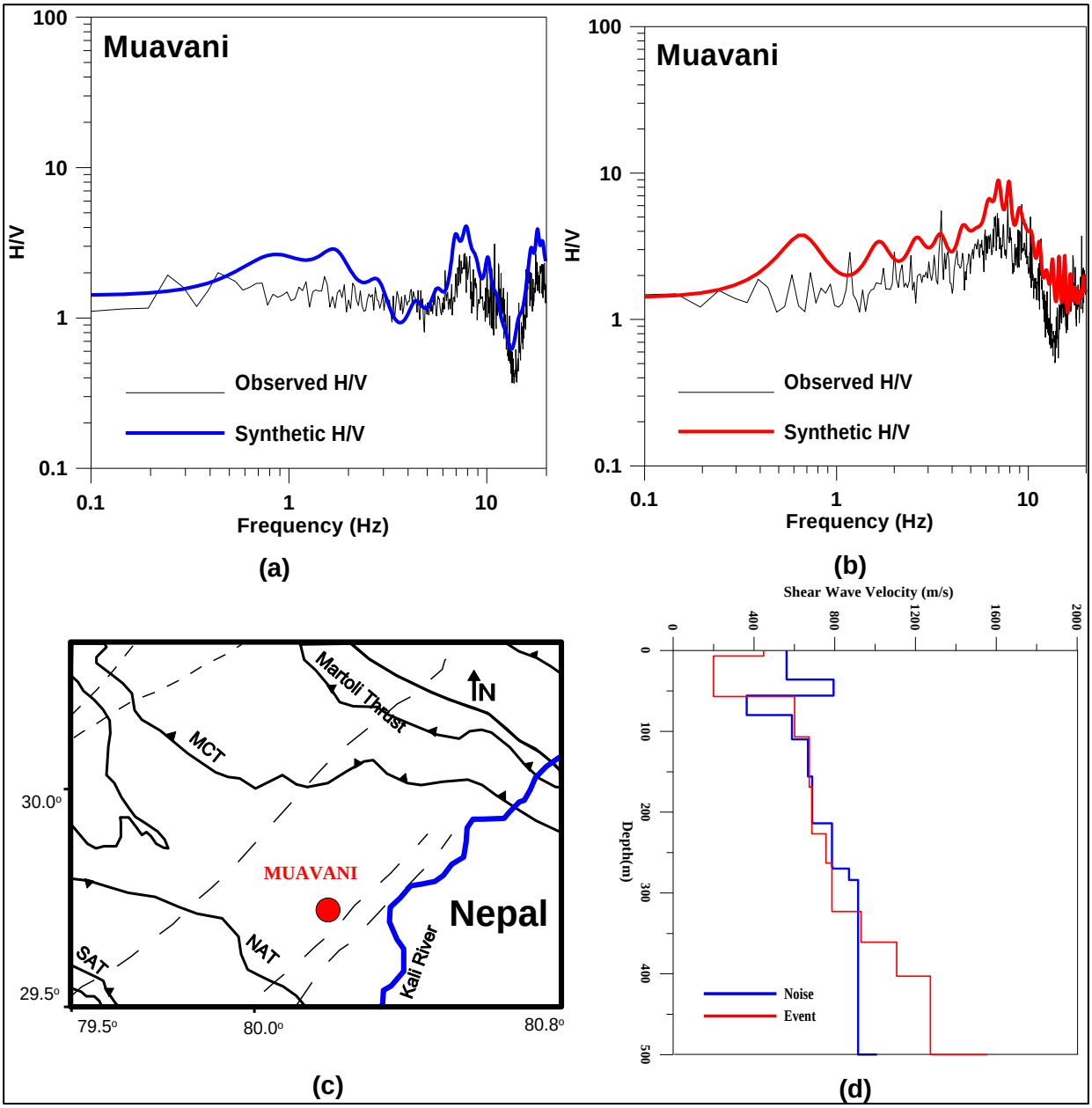

Figure 6.12: The results obtained at Muavani station. Observed H/V showing good match with synthetic H/V using (a) Ambient noise records (b) Strong ground motion records (c) Solid red circle shows the location of recording station. Source of the tectonics of the region is GSI (2000) (d) 1D Shear wave velocity model generated using ambient noise (blue) and strong ground motion (red).

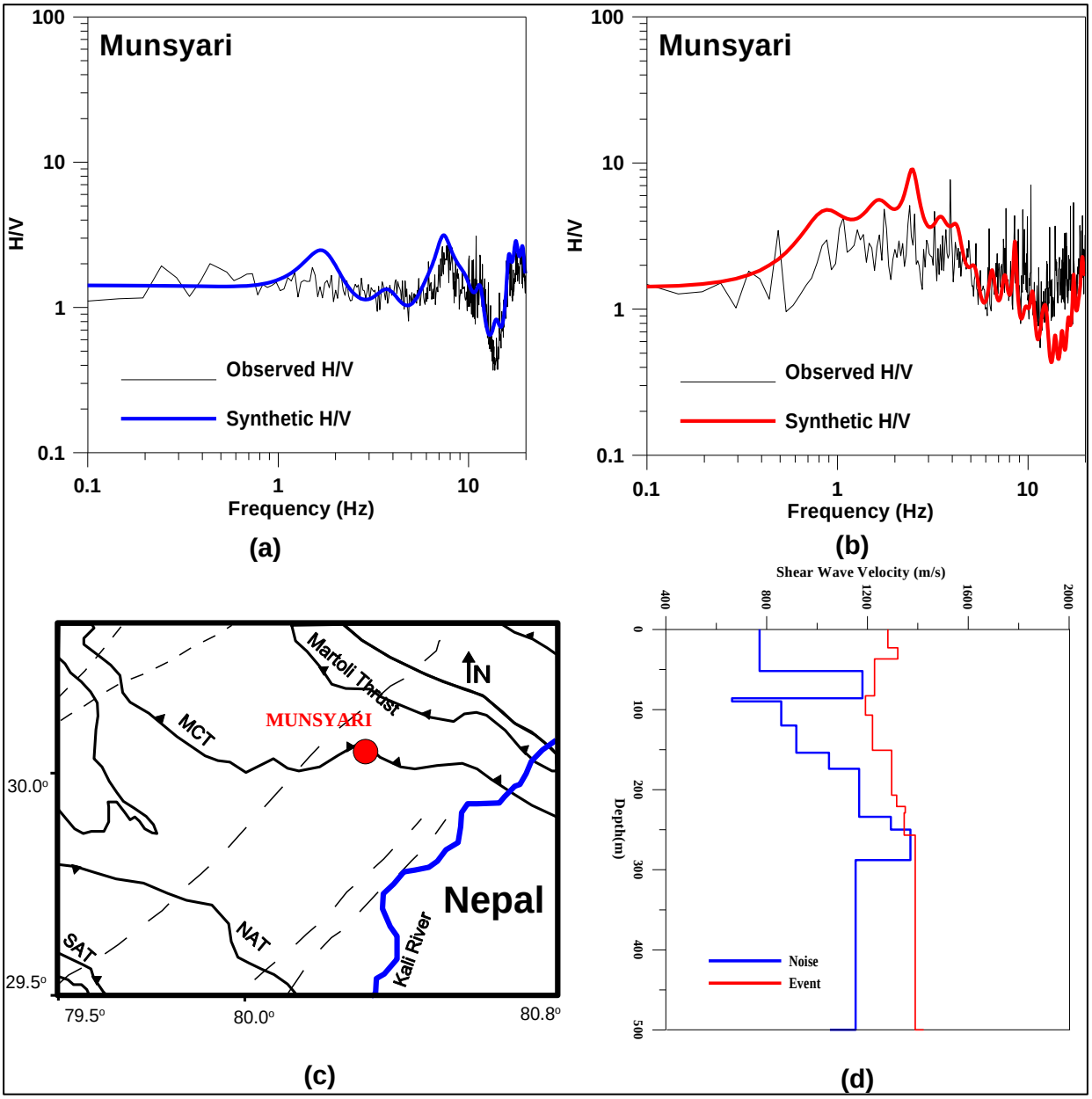

Figure 6.13: The results obtained at Munsyari station. Observed H/V showing good match with synthetic H/V using (a) Ambient noise records (b) Strong ground motion records (c) Solid red circle shows the location of recording station. Source of the tectonics of the region is GSI (2000) (d) 1D Shear wave velocity model generated using ambient noise (blue) and strong ground motion (red).

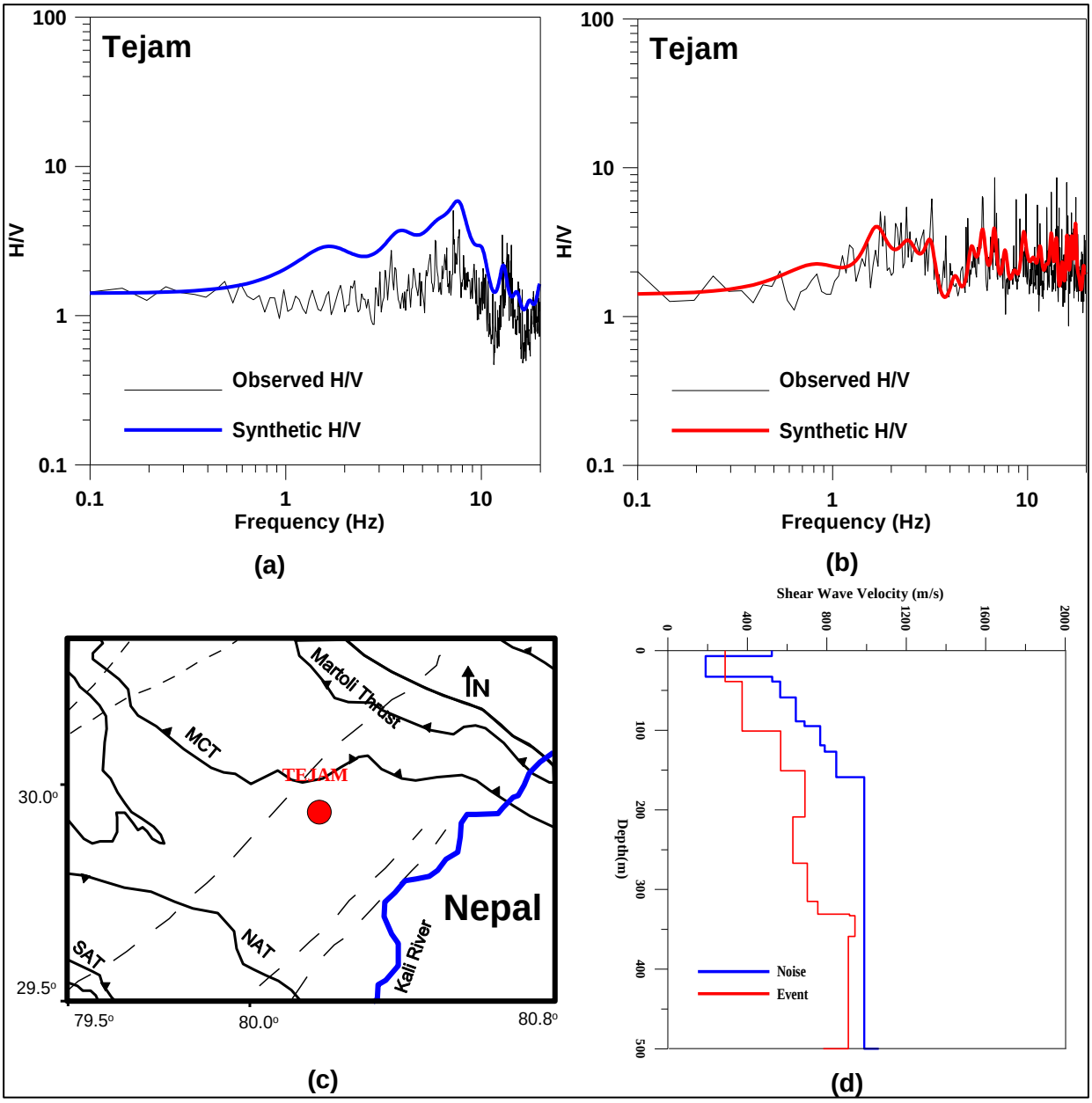

Figure 6.14: The results obtained at Tejam station. Observed H/V showing good match with synthetic H/V using (a) Ambient noise records (b) Strong ground motion records (c) Solid red circle shows the location of recording station. Source of the tectonics of the region is GSI (2000) (d) 1D Shear wave velocity model generated using ambient noise (blue) and strong ground motion (red).

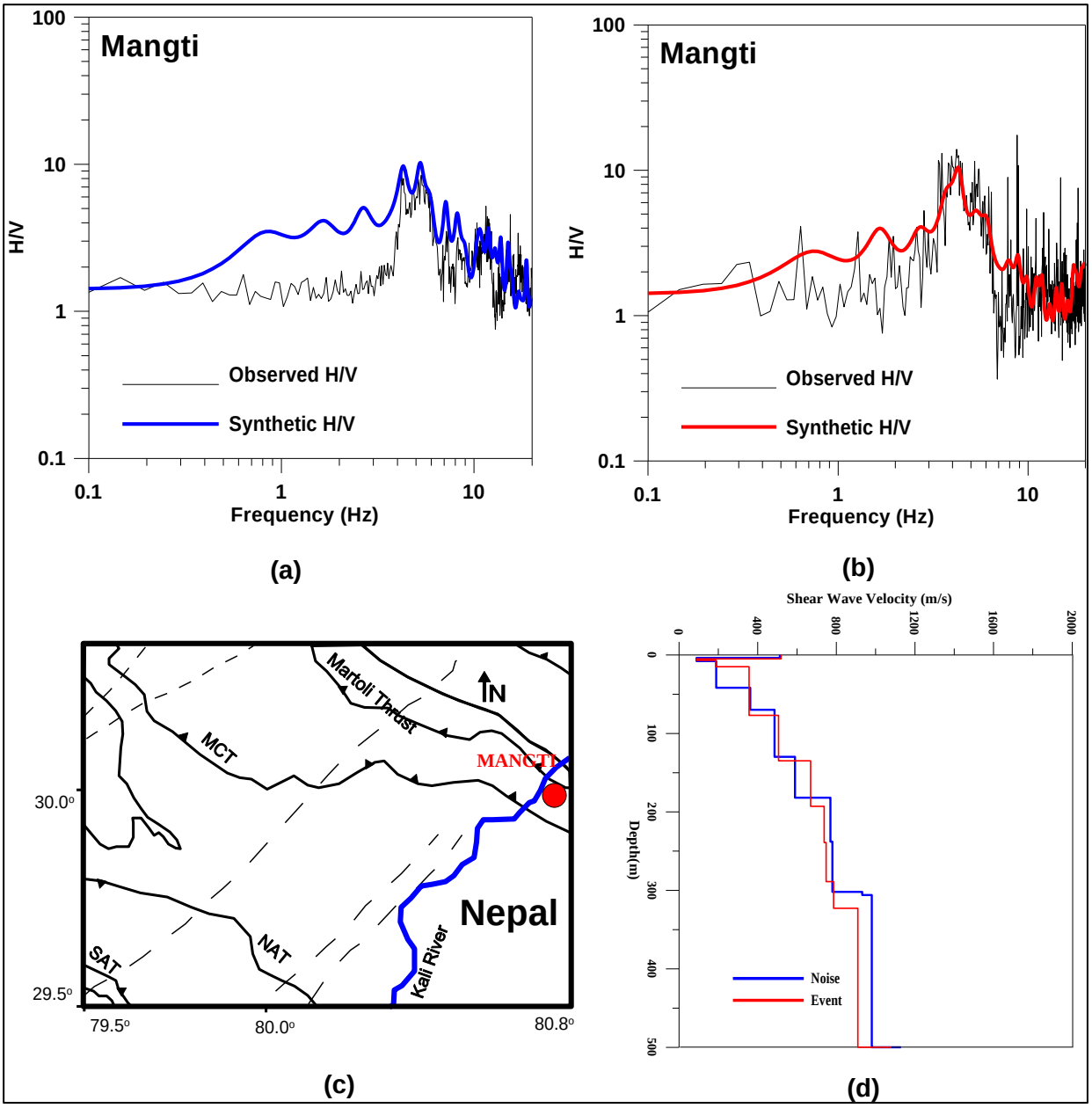

Figure 6.15: The results obtained at Mangti station. Observed H/V showing good match with synthetic H/V using (a) Ambient noise records (b) Strong ground motion records (c) Solid red circle shows the location of recording station. Source of the tectonics of the region is GSI (2000) (d) 1D Shear wave velocity model generated using ambient noise (blue) and strong ground motion (red).

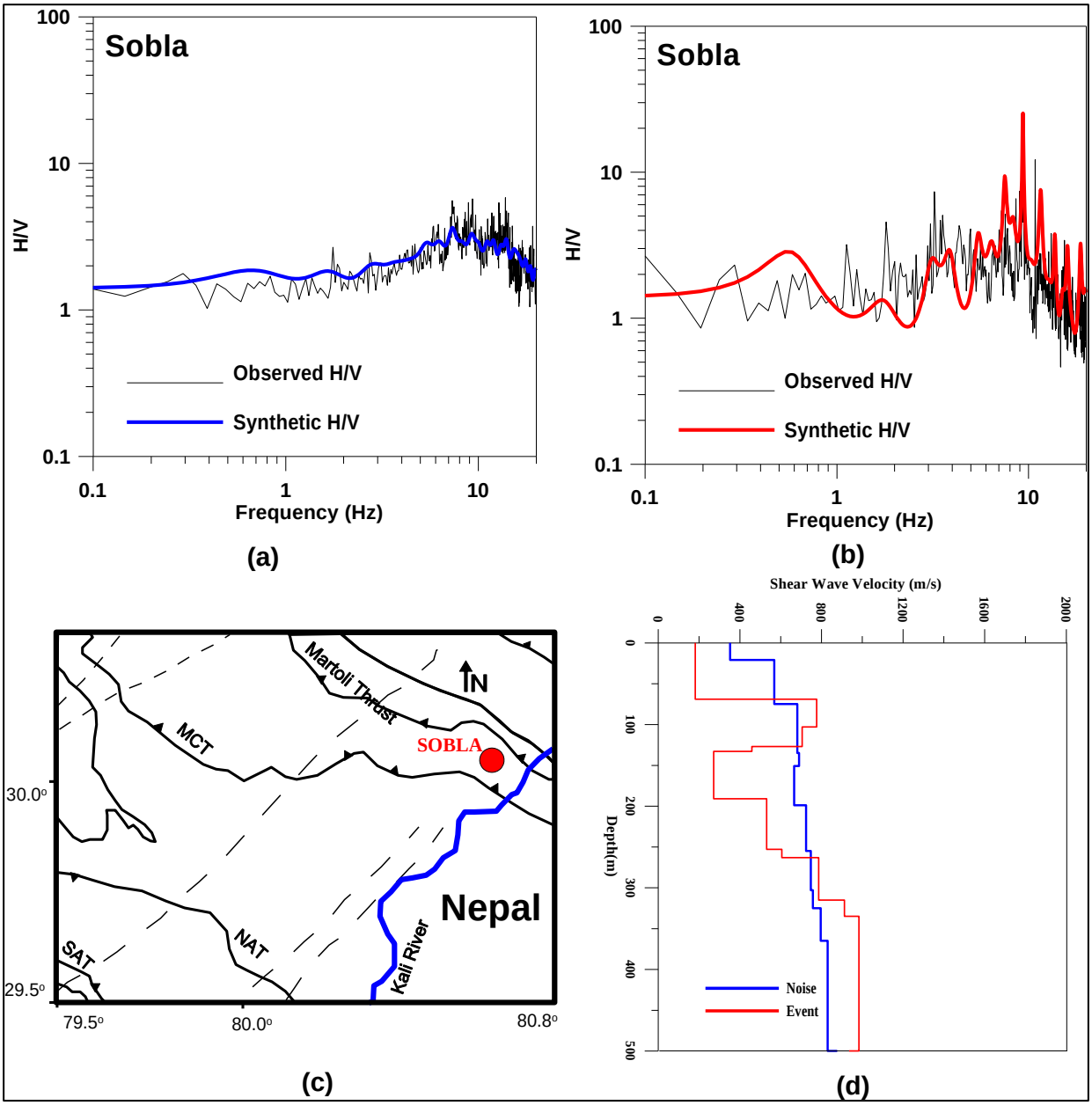

Figure 6.16: The results obtained at Sobla station. Observed H/V showing good match with synthetic H/V using (a) Ambient noise records (b) Strong ground motion records (c) Solid red circle shows the location of recording station. Source of the tectonics of the region is GSI (2000) (d) 1D Shear wave velocity model generated using ambient noise (blue) and strong ground motion (red).

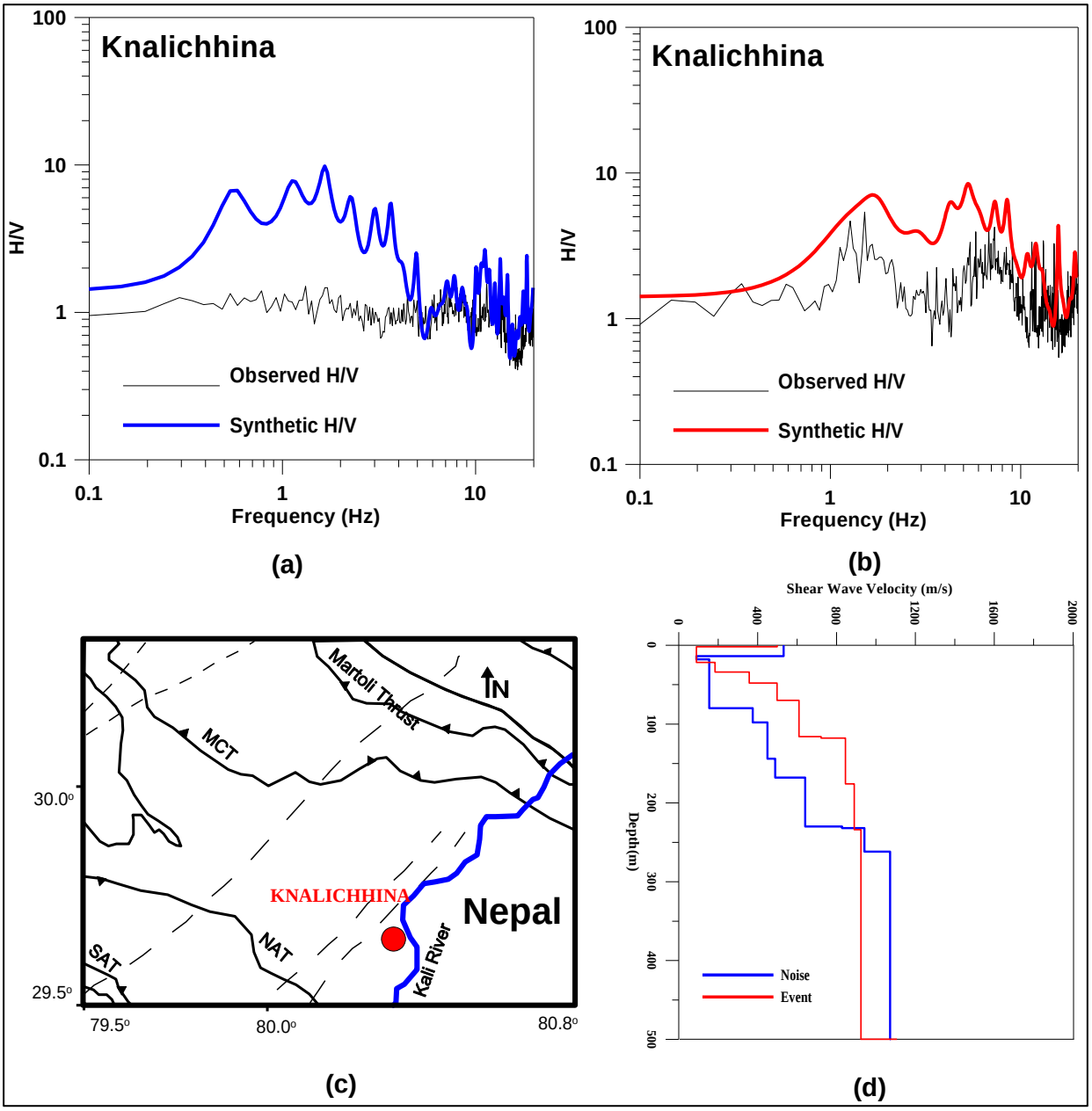

Figure 6.17: The results obtained at Knalichhina station. Observed H/V showing good match with synthetic H/V using (a) Ambient noise records (b) Strong ground motion records (c) Solid red circle shows the location of recording station. Source of the tectonics of the region is GSI (2000) (d) 1D Shear wave velocity model generated using ambient noise (blue) and strong ground motion (red).

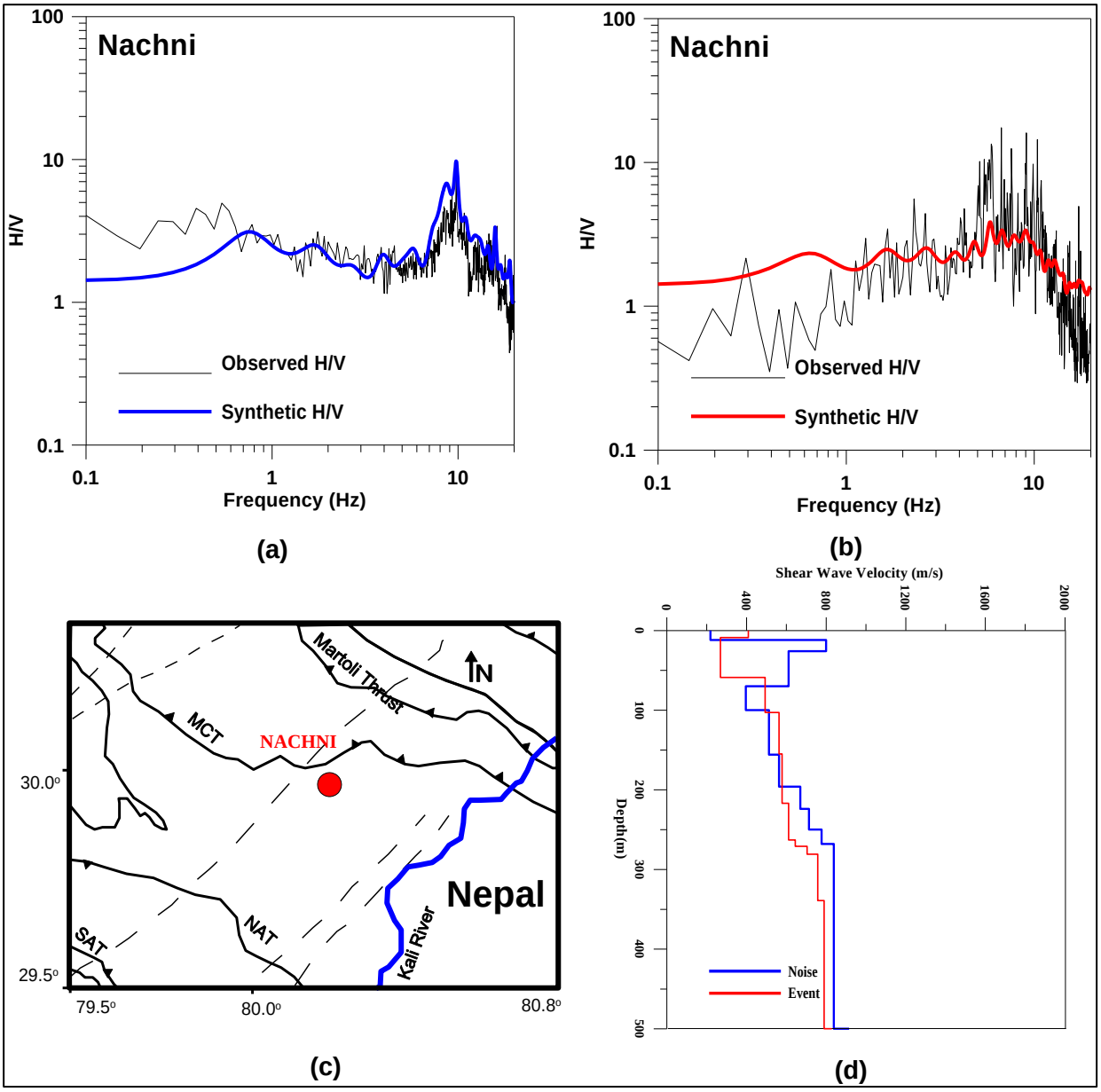

Figure 6.18: The results obtained at Nachni station. Observed H/V showing good match with synthetic H/V using (a) Ambient noise records (b) Strong ground motion records (c) Solid red circle shows the location of recording station. Source of the tectonics of the region is GSI (2000) (d) 1D Shear wave velocity model generated using ambient noise (blue) and strong ground motion (red).

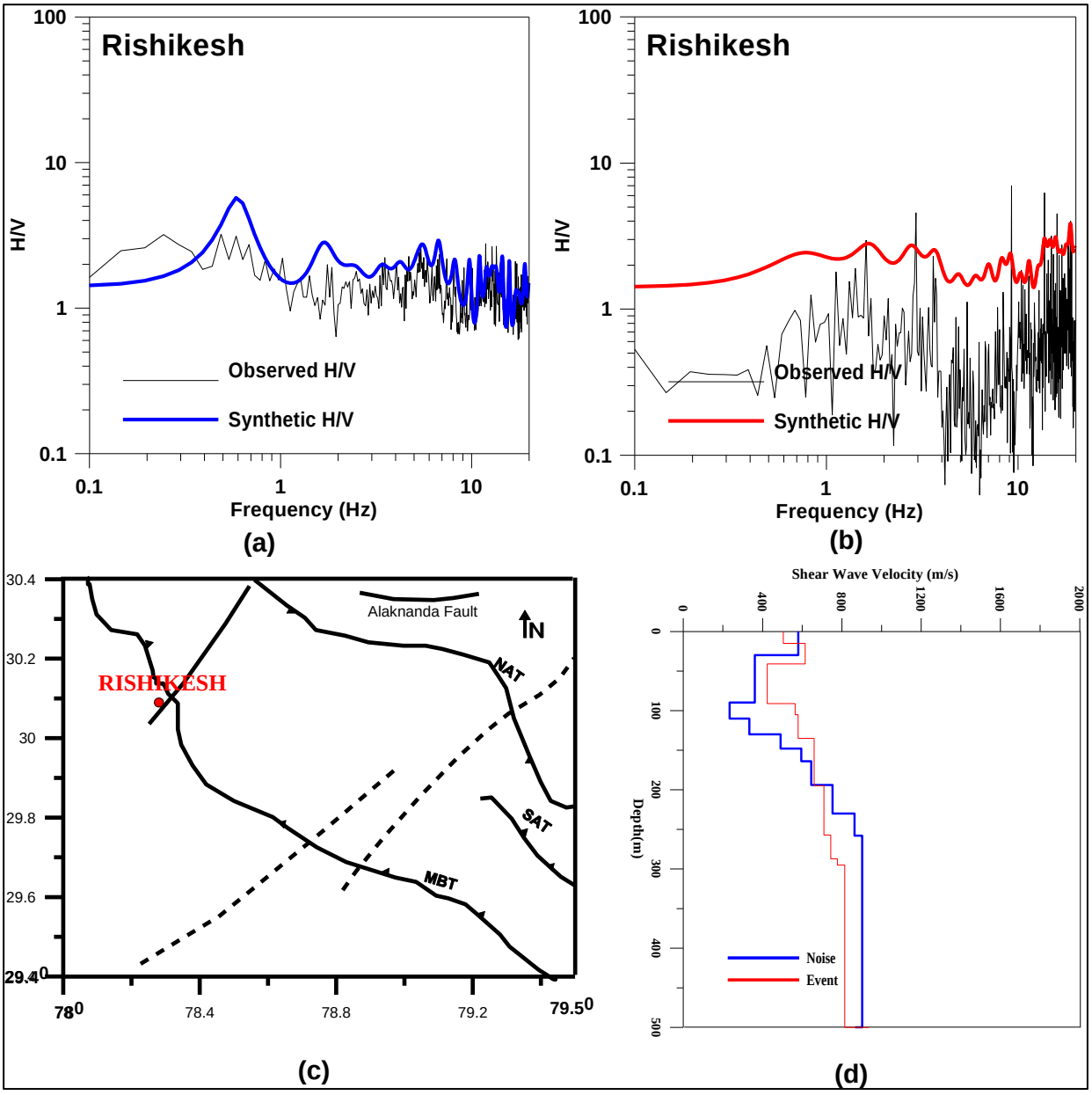

Figure 6.19: The results obtained at Rishikesh station. Observed H/V showing good match with synthetic H/V using (a) Ambient noise records (b) Strong ground motion records (c) Solid red circle shows the location of recording station. Source of the tectonics of the region is GSI (2000) (d) 1D Shear wave velocity model generated using ambient noise (blue) and strong ground motion (red).

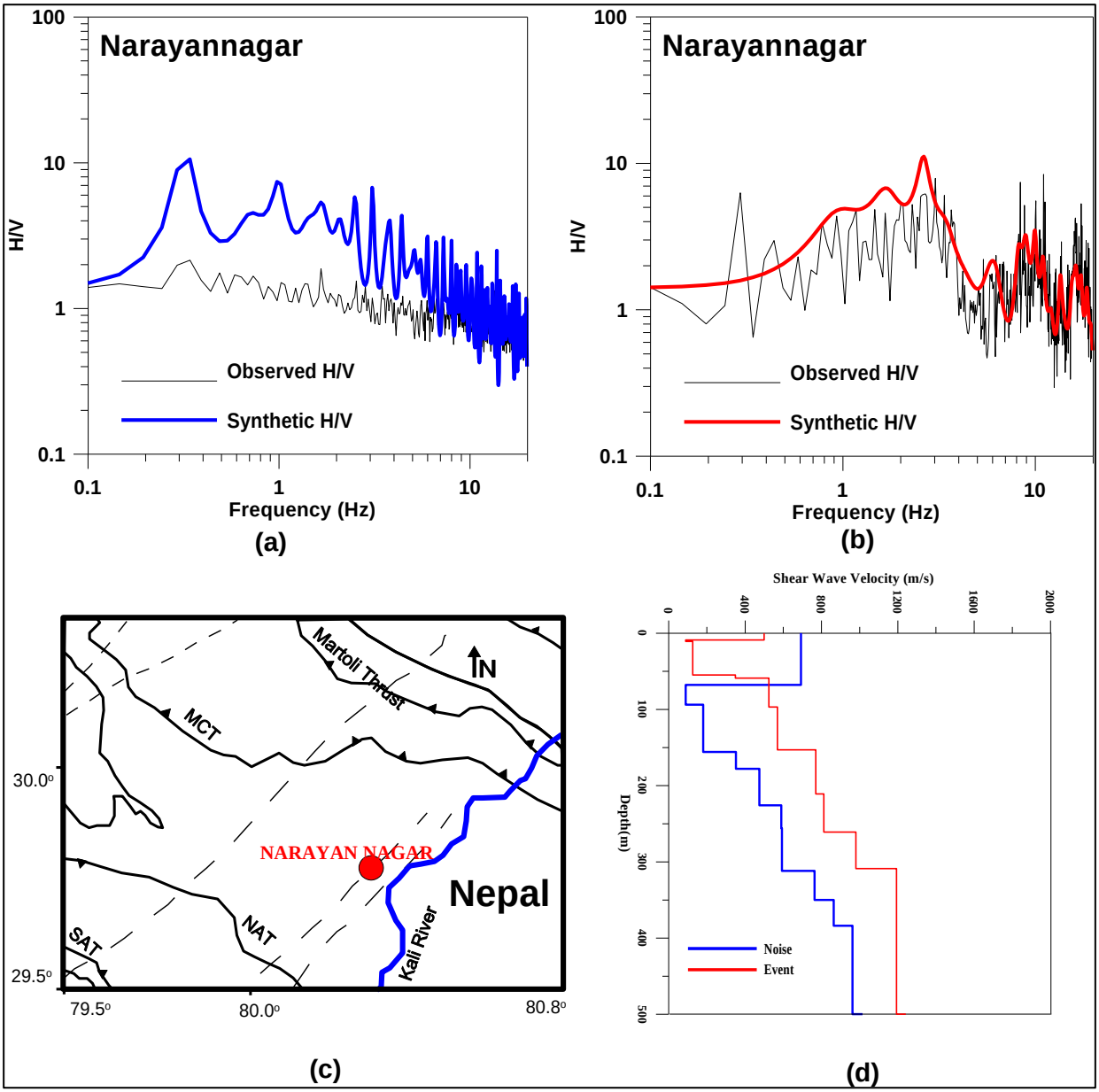

Figure 6.20: The results obtained at Narayannagar station. Observed H/V showing good match with synthetic H/V using (a) Ambient noise records (b) Strong ground motion records (c) Solid red circle shows the location of recording station. Source of the tectonics of the region is GSI (2000) (d) 1D Shear wave velocity model generated using ambient noise (blue) and strong ground motion (red).

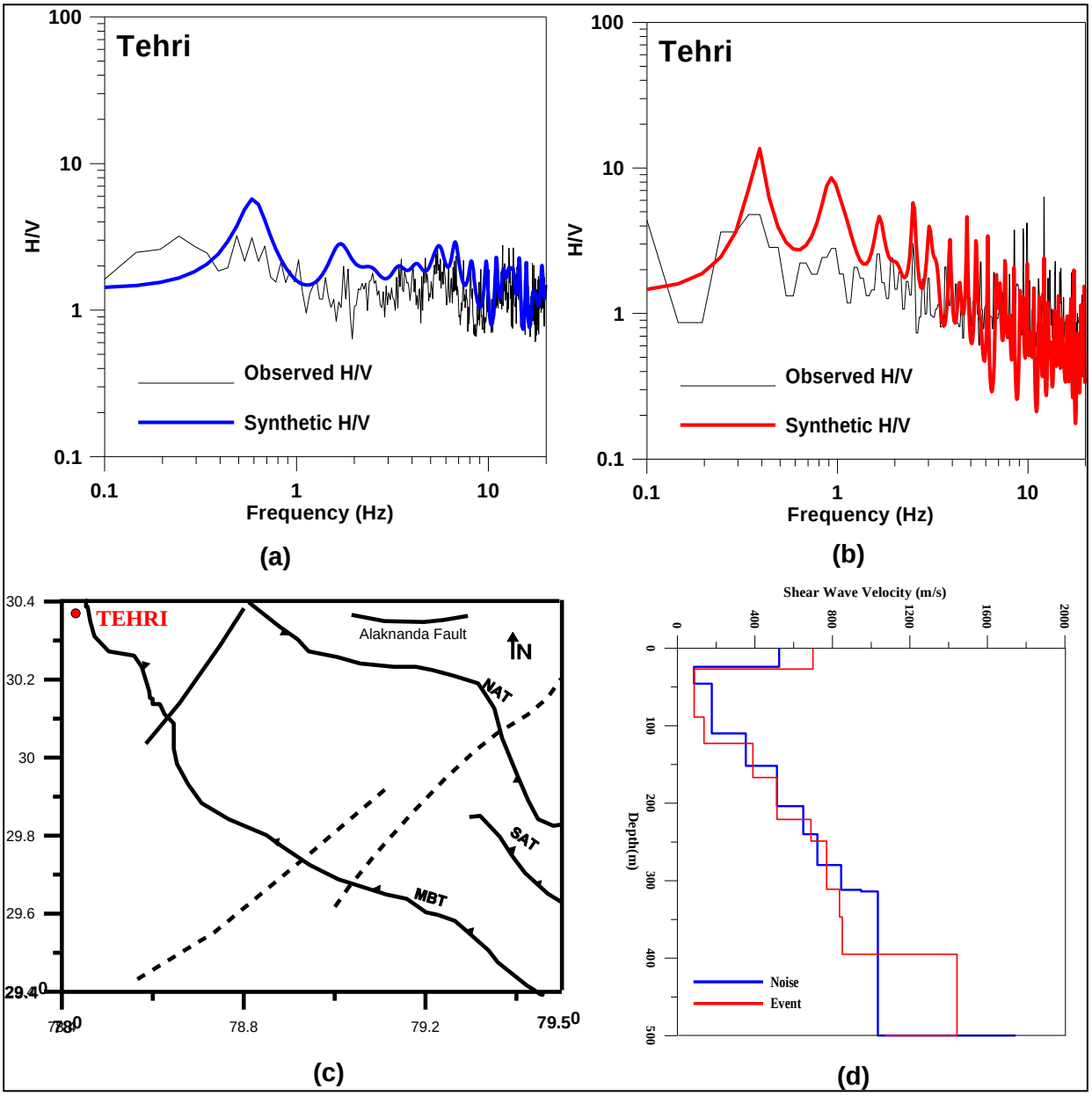

Figure 6.21: The results obtained at Tehri station. Observed H/V showing good match with synthetic H/V using (a) Ambient noise records (b) Strong ground motion records (c) Solid red circle shows the location of recording station. Source of the tectonics of the region is GSI (2000) (d) 1D Shear wave velocity model generated using ambient noise (blue) and strong ground motion (red).

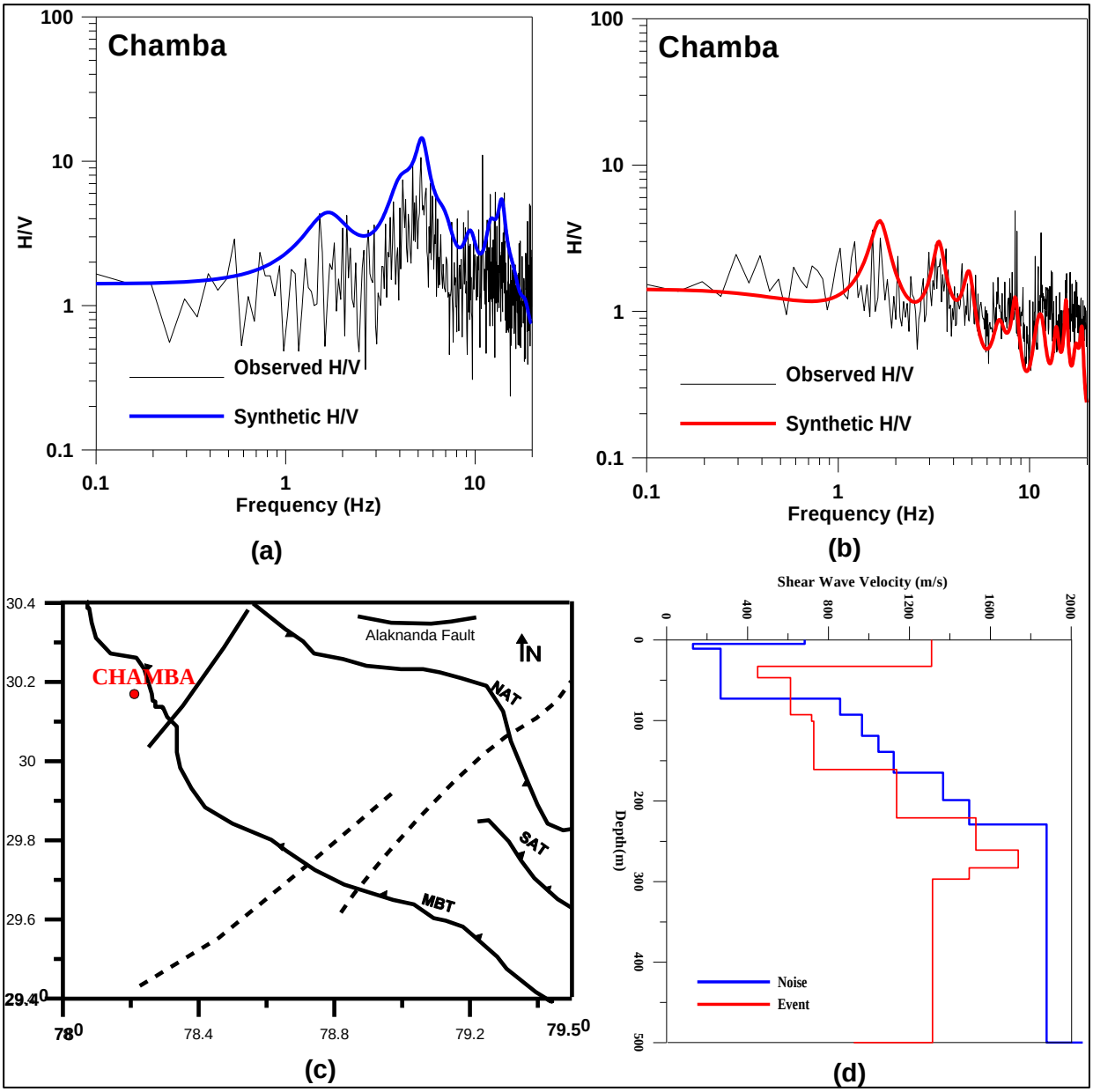

Figure 6.22: The results obtained at Chamba station Observed H/V showing good match with synthetic H/V using (a) Ambient noise records (b) Strong ground motion records (c) Solid red circle shows the location of recording station. Source of the tectonics of the region is GSI (2000) (d) 1D Shear wave velocity model generated using ambient noise (blue) and strong ground motion (red).

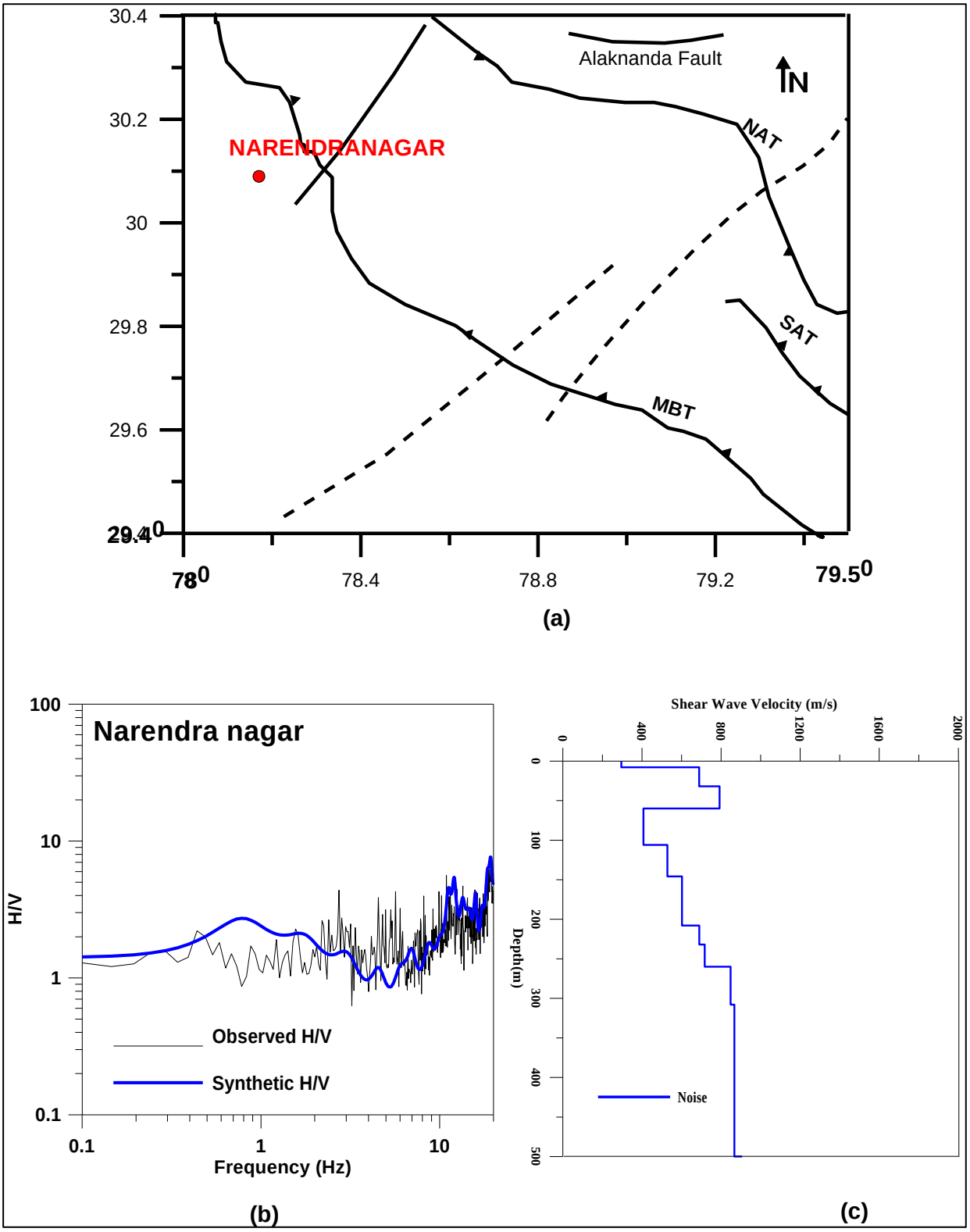

Figure 6.23: The results obtained at Narendra nagar station. (a)Solid red circle shows the location of recording station. Source of the tectonics of the region is GSI (2000) (b) Observed H/V showing good match with synthetic H/V (c) 1D Shear wave velocity model.

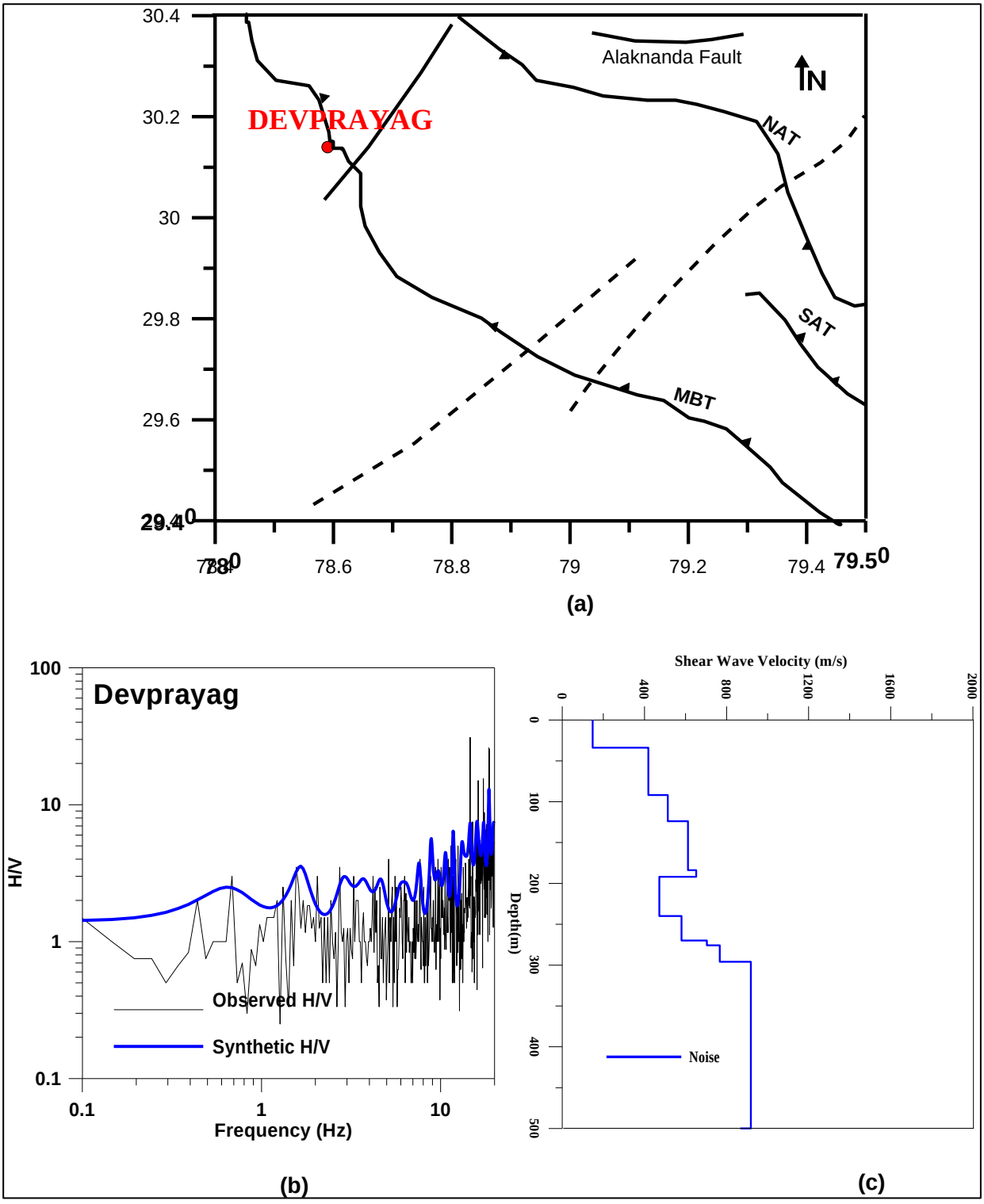

Figure 6.24: The results obtained at Devprayag station. (a)Solid red circle shows the location of recording station. Source of the tectonics of the region is GSI (2000) (b) Observed H/V showing good match with synthetic H/V (c) 1D Shear wave velocity model.

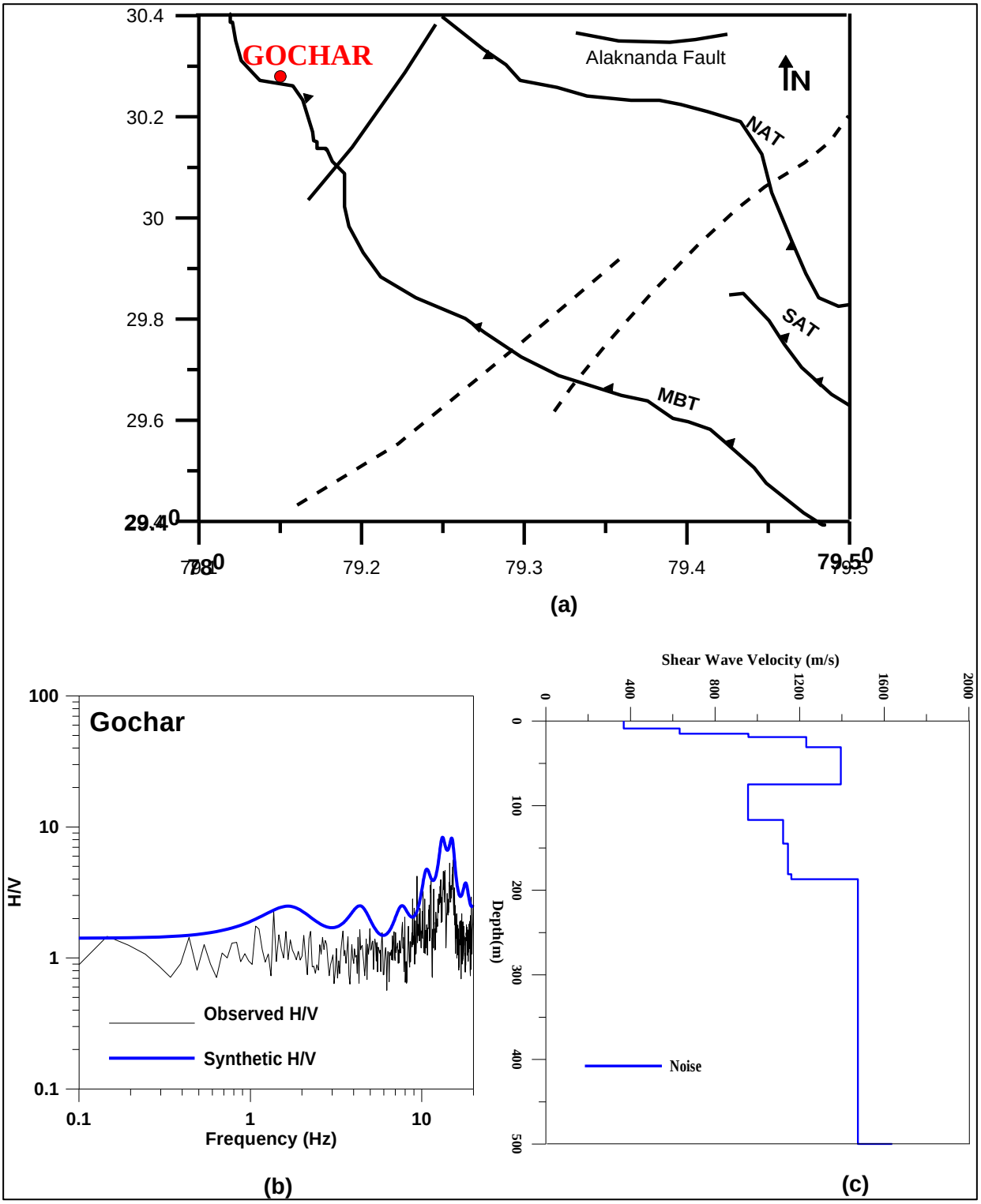

Figure 6.25: The results obtained at Gochar station. (a)Solid red circle shows the location of recording station. Source of the tectonics of the region is GSI (2000) (b) Observed H/V showing good match with synthetic H/V (c) 1D Shear wave velocity model.

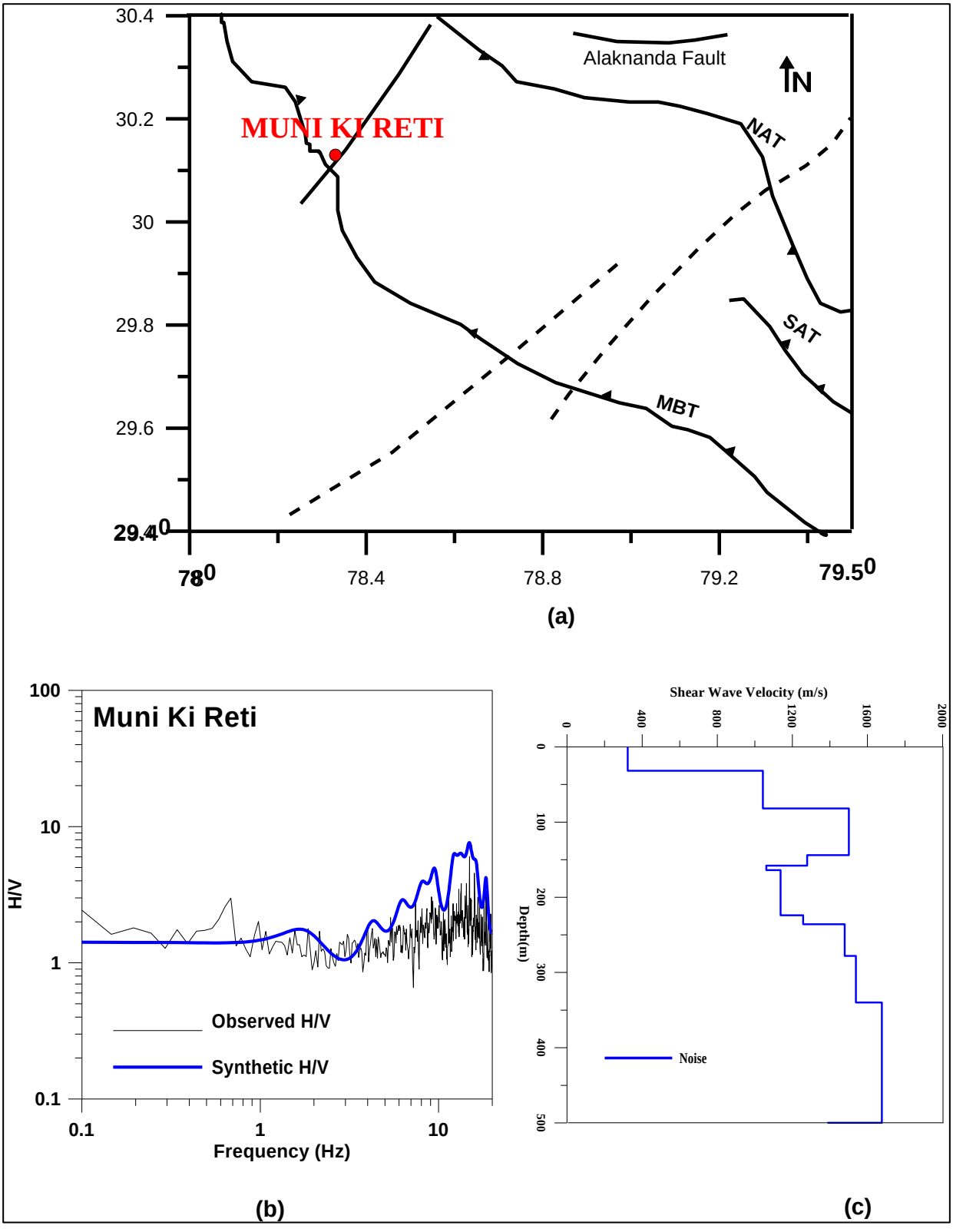

Figure 6.26: The results obtained at Muni ki reti station. (a)Solid red circle shows the location of recording station. Source of the tectonics of the region is GSI (2000) (b) Observed H/V showing good match with synthetic H/V (c) 1D Shear wave velocity model.

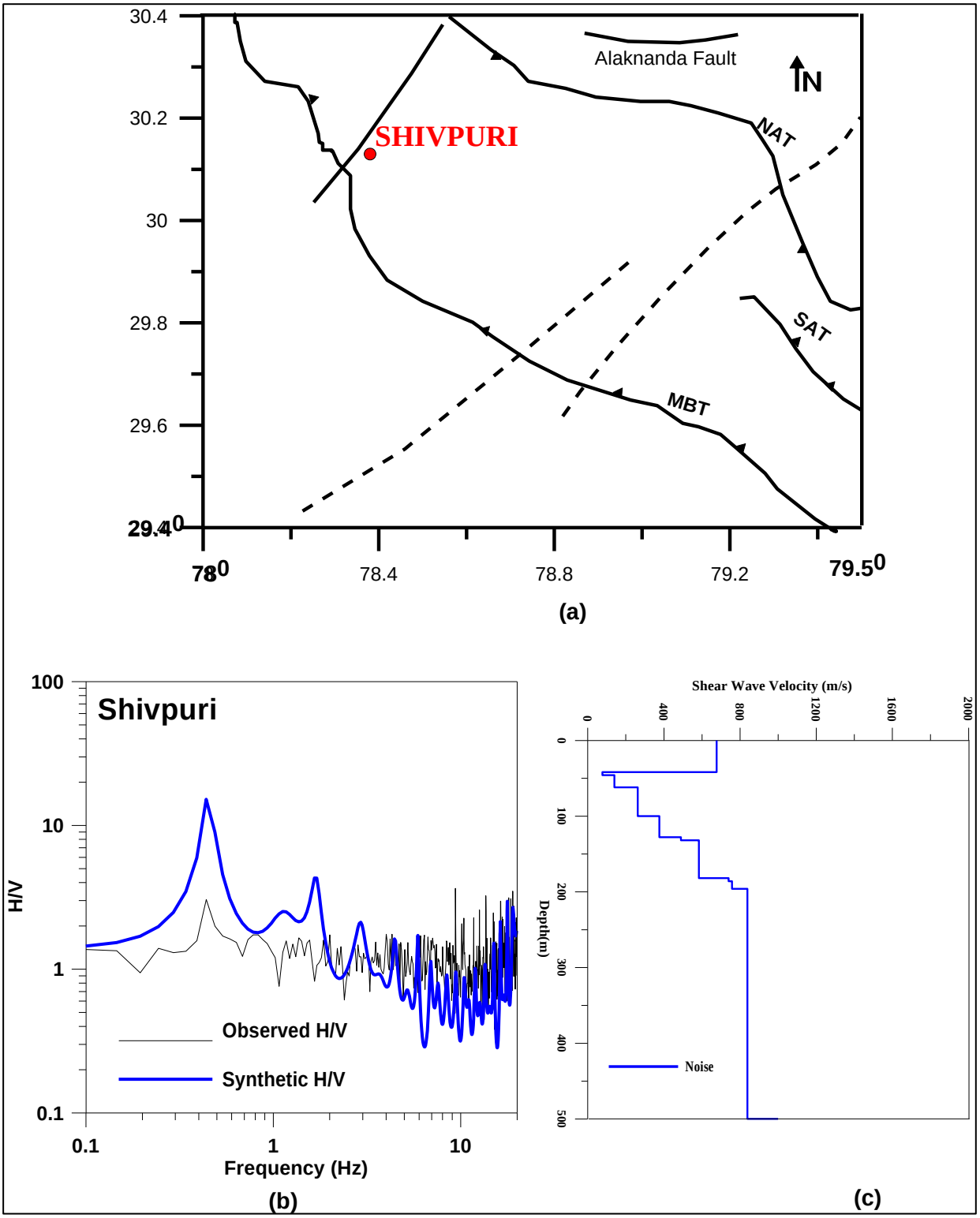

Figure 6.27: The results obtained at Shivpuri station. (a)Solid red circle shows the location of recording station. Source of the tectonics of the region is GSI (2000) (b) Observed H/V showing good match with synthetic H/V (c) 1D Shear wave velocity model.

1D shear wave velocity model estimated at the locations of Kumaon Himalayas and Garhwal Himalayas using ambient noise records are shown in Figure 6.28 and 6.29, respectively.

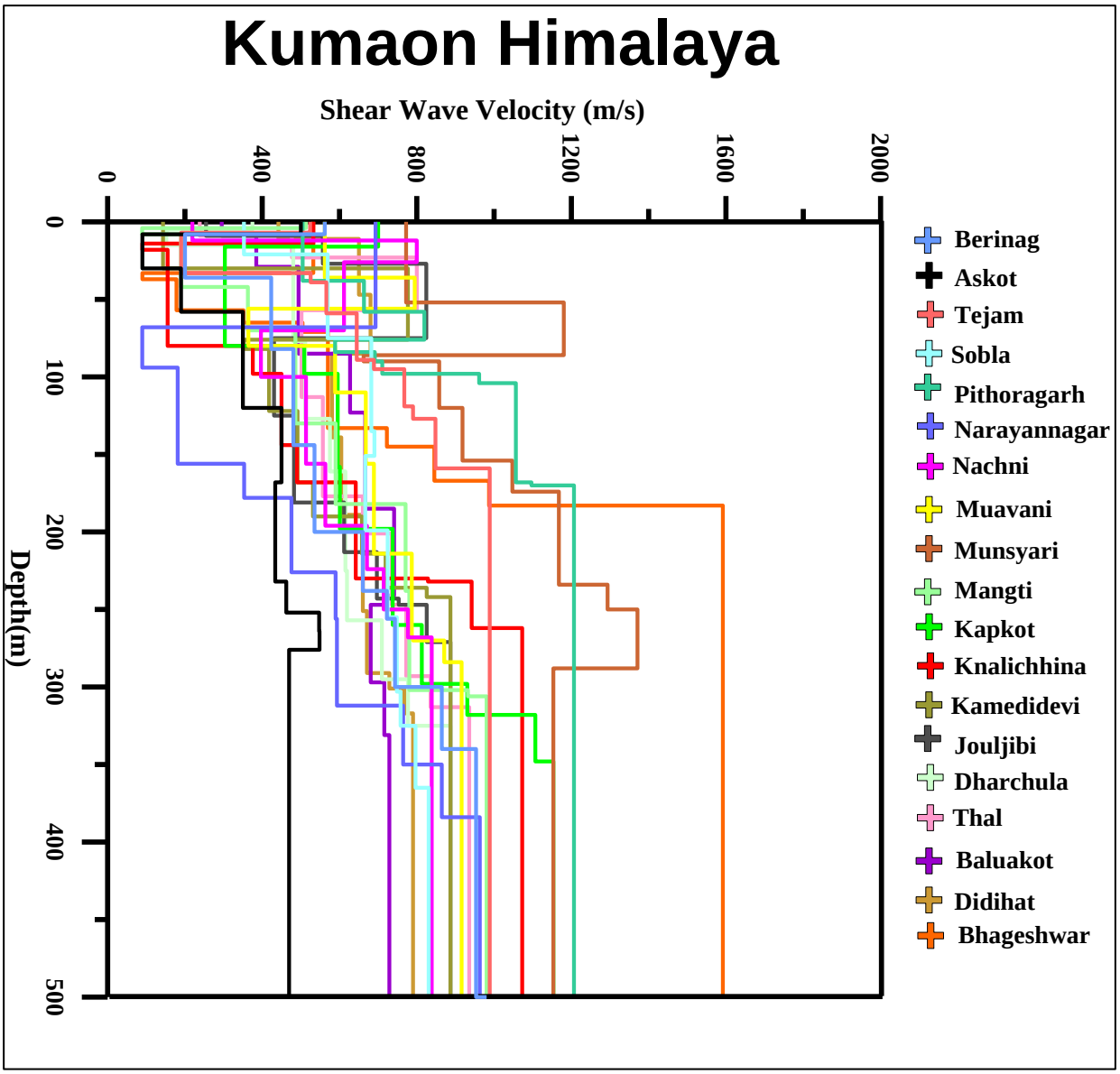

Figure 6.28: 1D shear wave velocity model estimated at the locations of Kumaon Himalayas using ambient noise records.

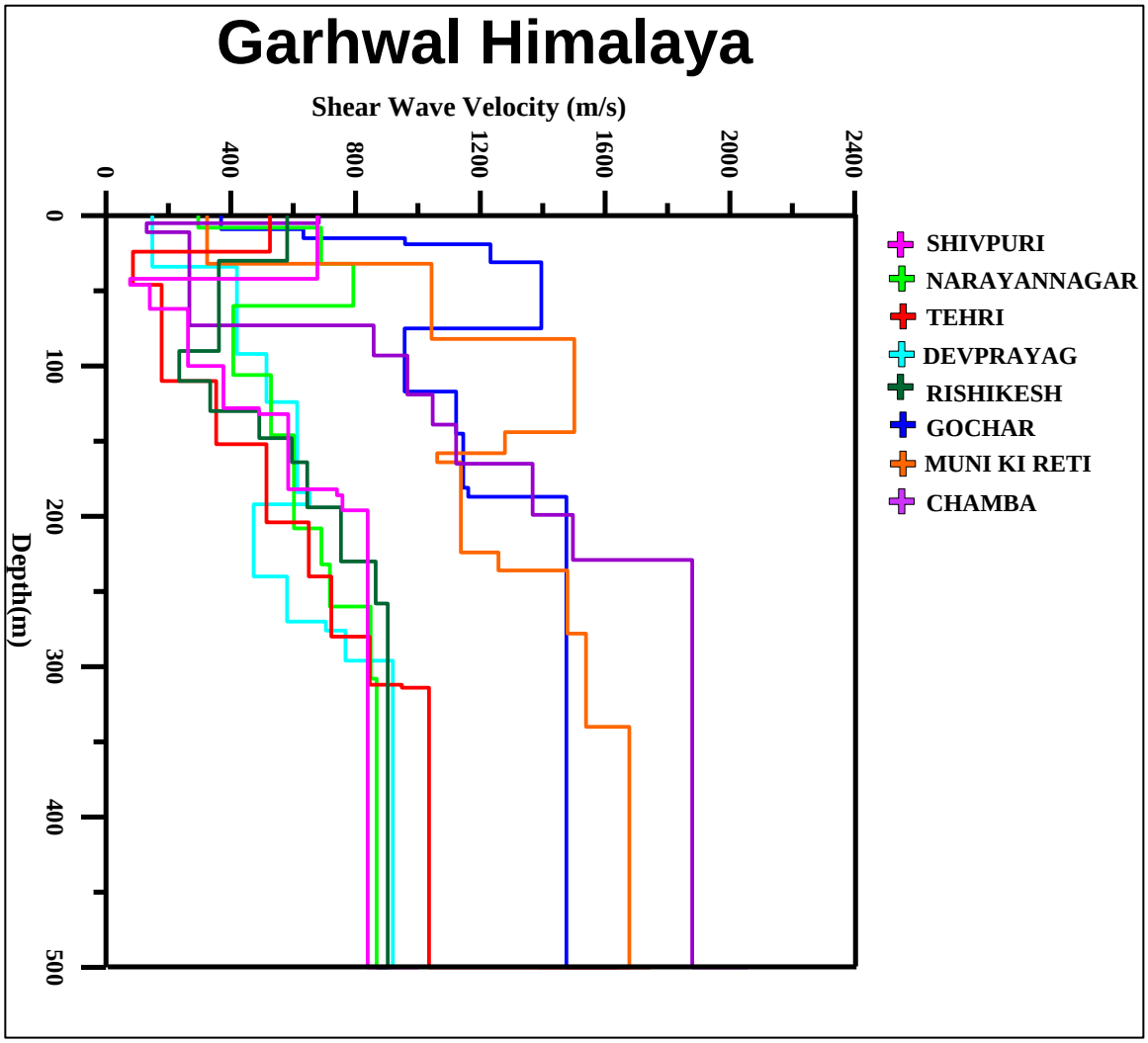

Figure 6.29: 1D shear wave velocity model estimated at the locations of Garhwal Himalayas using ambient noise records.

1D shear wave velocity model estimated at the locations of Kumaon Himalayas and Garhwal Himalayas using strong ground motion records are shown in Figure 6.30 and 6.31, respectively.

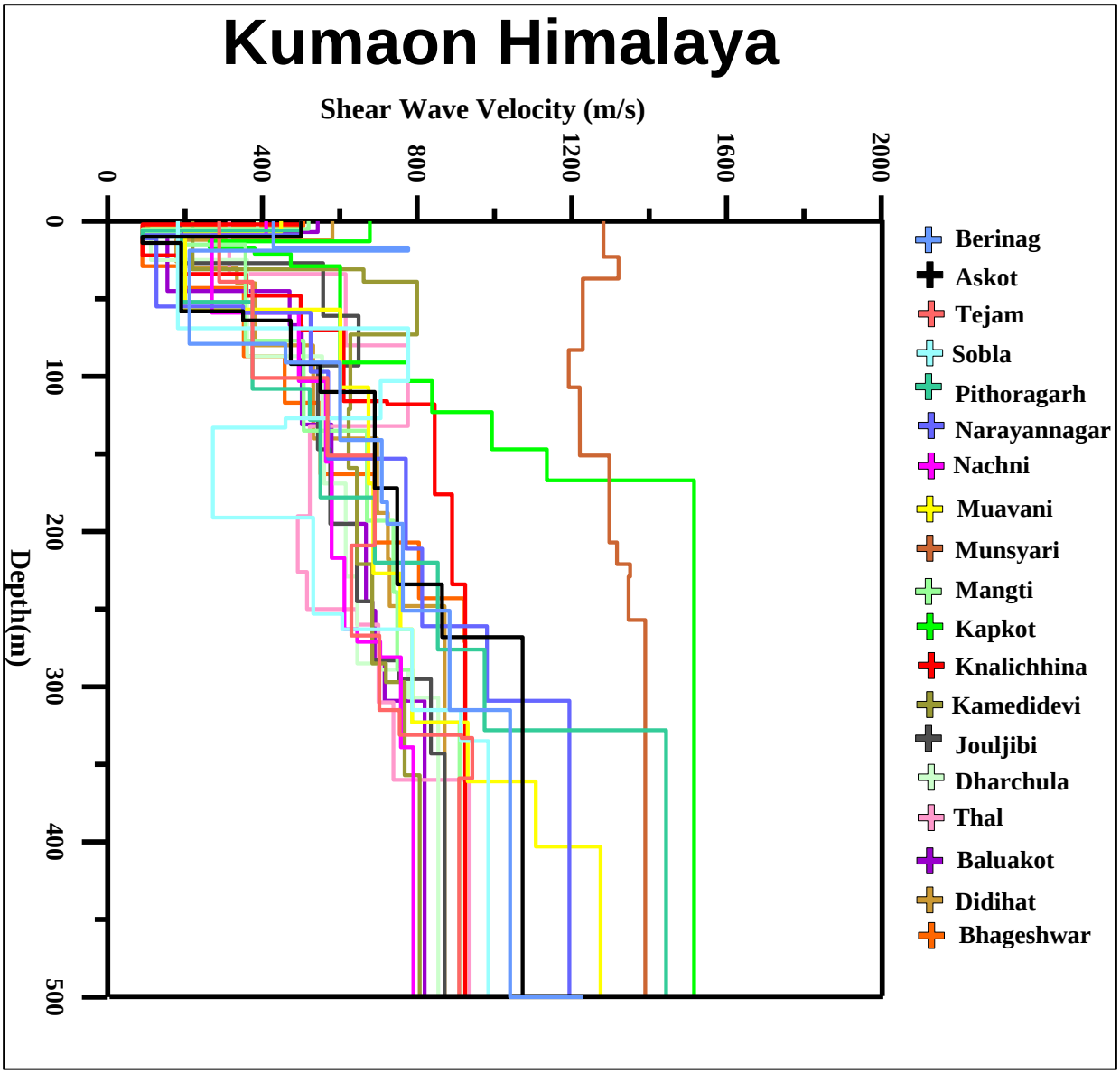

Figure 6.30: 1D shear wave velocity model estimated at the locations of Kumaon Himalayas using strong ground motion data.

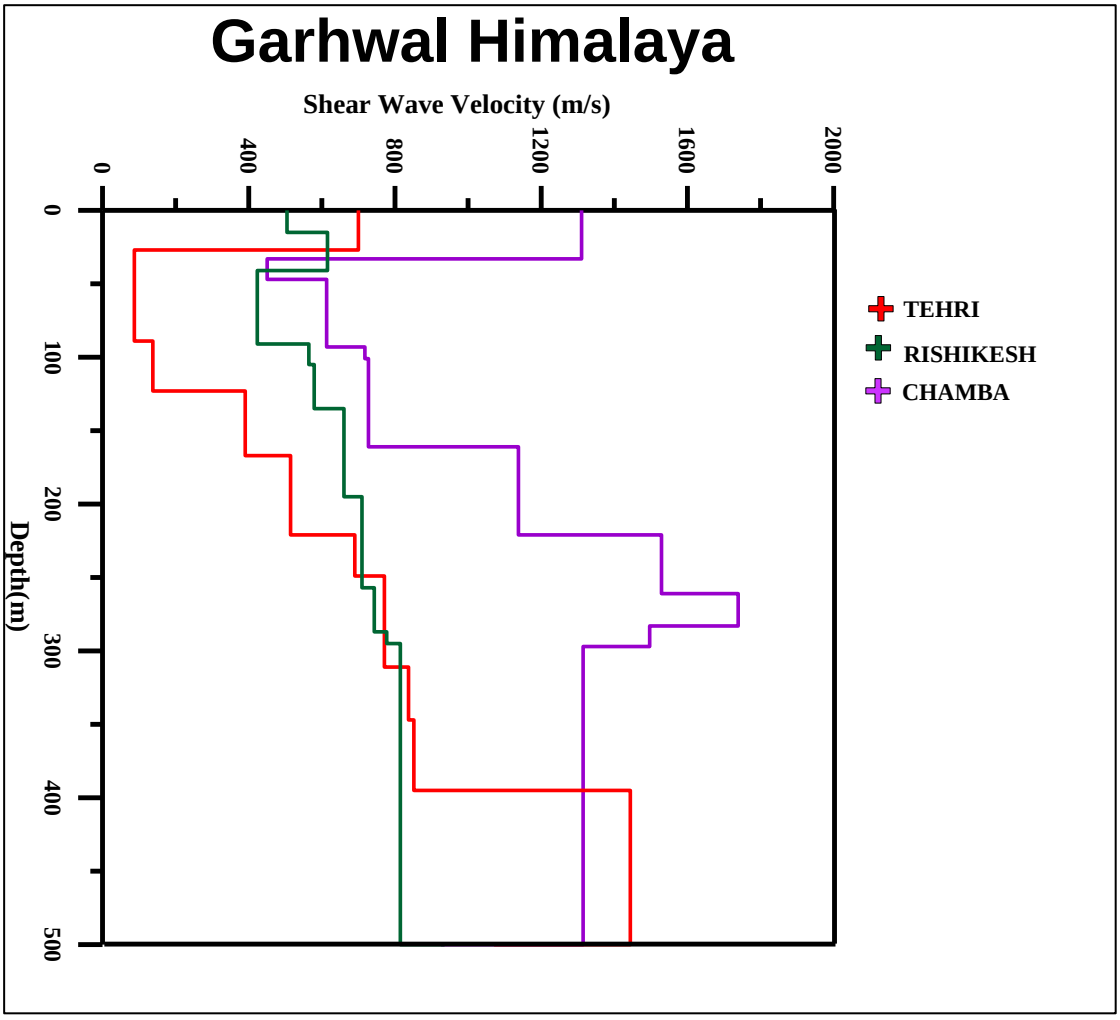

Figure 6.31: 1D shear wave velocity model estimated at the locations of Garhwal Himalayas using strong ground motion data.

It can be observed that the average value of shear wave velocity are approximately matching when estimated using two different methods (b) Non- Reference site method : the horizontal to vertical (H/V) spectral ratio on ambient noise records, and (c) Non- Reference site method : the horizontal to vertical (H/V) spectral ratio on strong ground motion records. The comparison of average shear wave velocity estimated at the various locations of Kumaon and Garhwal Himalayas using strong ground motion records and ambient noise records has been tabulated in Table 6.1. Figure 6.32 shows the plotted values which are mostly in alignment with each other. Average shear velocity has been estimated using equation 3.2.

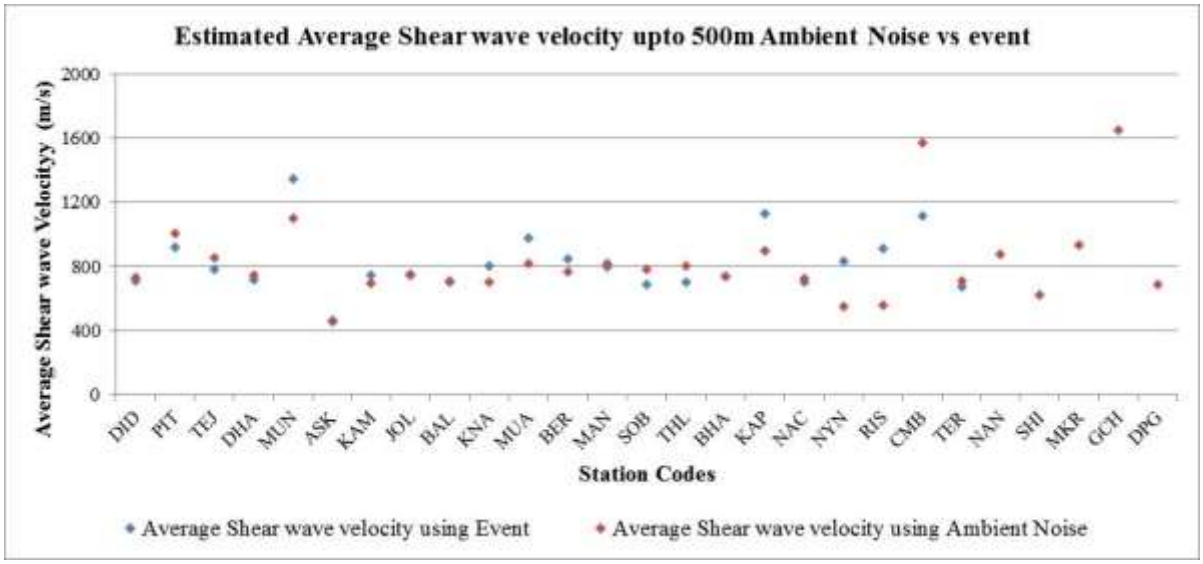

Figure 6.32: The comparison of estimated average shear wave velocity at the various locations of Kumaon and Garhwal Himalayas using strong ground motion records and ambient noise records.

Table 6.1: Comparison of shear wave velocity model estimated at the various locations of Kumaon and Garhwal Himalayas using strong ground motion records and ambient noise records.

Sr. No.	Station Name	Station Code	Vs_{500} Event	Vs_{500} Noise
1	Didihat	DID	711	730
2	Pithoragarh	PIT	915	1003
3	Tejam	TEJ	780	851
4	Dharchula	DHA	717	743
5	Munsyari	MUN	1348	1103
6	Askot	ASK	462	453
7	Kamedidevi	KAM	744	691
8	Jouljibi	JOL	755	742
9	Baluakot	BAL	701	712
10	Knalichhina	KNA	801	704
11	Muavani	MUA	976	814
12	Berinag	BER	844	766
13	Mangti	MAN	792	816
14	Sobla	SOB	689	779
15	Thal	THL	704	801
16	Bhageshwar	BHA	741	734
17	Kapkot	KAP	1131	900
18	Nachni	NAC	698	724
19	Narayan Nagar	NYN	828	549
20	Rishkesh	RIS	913	557
21	Narendra Nagar	NAN	-	874
22	Shivpuri	SHI	-	625
23	Chamba	CMB	1113	1572
24	Tehri	TER	672	712
25	Muni ki reti	MKR	-	929
26	Gochar	GCH	-	1651
27	Devprayag	DPG	-	690

In case of noise records, there is a good match between observed and synthetic curves at shallow depth. The noise records gives better information of near-surface as compared to deeper subsurface because the energy in case of ambient noise records or microtremor records is generated from shallow depths.

Deeper depths are better explored by using strong ground motion records because in such cases, the epicenter locations belong to deeper depths when compared to the epicenter locations of ambient noise records. As a result, the observed H/V curve and synthetic H/V curves obtained from strong ground motion are well matching for both, deeper as well as shallower, depths.

6.4. Conclusion

In this chapter, GA has been used for obtaining shear wave velocity model using of the ambient noise data. Data recorded at twenty two stations located in the Kumaon and Garhwal Himalaya has been used in this study. Site amplification at each station is determined from obtained results of inversion. Phase velocities at a higher frequency gives information about shallow subsurface structures, while the HVSR at a lower frequency (especially at the dominant frequency) gives information about deep subsurface structures.

High shear wave velocity at Chamba and Gochar, in Garhwal Himalayas can be explained by the occurrence of hard and compacted rocks such as quartzite and Phyllites of Jaunsar Group and Garhwal Group and the compacted gravels. High shear wave velocity at Munsyari, Kapkot and Pithoragarh in the Kumaon Himalayas can be explained by the occurrence of hard and compacted rocks such as Phyllites, Dolomite, Quartzite, amphibolites and meta-sedimentary rocks of Tejam Group and Almora Group.

Dharchula, Joljibi, Baluakot and Mangti falls within the velocity range of 701 ms^{-1} to 816 ms^{-1}.This is due to the fact that stations are situated along or nearby river Kali. The softness and water saturation of the alluvial deposits found here are probable causes of this.
The velocity of Mangti is comparatively higher among these stations along river side since it it is situated near MCT and as we go higher up in the Himalaya velocity increases the thickness of top soil layer is found to decrease.

On the basis of average shear wave velocity down to 500 m (V_s), the station Munsyari, Kapkot and Pithoragarh in Kumaon Himalayas and Chamba and Goucher in Garhwal Himalayas, falls in the range of velocity > 1000 ms^{-1} which implies the rock type in these stations is comparatively better for geotechnical basement than other stations.

The two dimensional shear wave velocity profiles at nineteen stations of Kumaon Himalaya and eight stations of Garhwal Himalaya respectively are generated after inverting H/V curves using genetic algorithm for strong ground motion records. Shear wave velocity of Kumaon and Garhwal Himalayas i.e. V_{S500} varies from 462 ms^{-1} to 1348 ms^{-1} respectively. Shear wave velocity of Kumaon and Garhwal Himalayas i.e. V_{S500} varies from 453 ms^{-1} to 1651 ms^{-1} respectively

Chapter – 7

SUMMARY AND CONCLUSIONS

The region of Kumaon and Garhwal Himalayas that has been used for the present research work falls in central Himalayan seismic gap. Despite of high seismicity in the Himalayas, the quantitative study of the amplification of seismic waves is still lacking. Limited database available in the rough and inaccessible terrain of Kumaon and Garhwal region have resulted in limited research work related to the estimation of site amplification. The work presented in the thesis includes several locations in Kumaon and Garhwal Himalayas.

In the present study, the records are analyzed using three different methods: (a) Reference site dependent method : Standard Spectral ratio, (b) Non- Reference site method : the horizontal to vertical (H/V) spectral ratio on ambient noise records, and (c) Non- Reference site method : the horizontal to vertical (H/V) spectral ratio on strong ground motion records.

Present research work is an effort to understand and quantify the shear wave velocity model using strong motion and ambient noise records. Two different techniques are used to generate shear wave velocity models for the region. Due to Urbanization and growth of Himalayas, the study holds immense importance in the said region. However, very few site studies are available for this part of Himalaya. Such studies in this part of Himalaya are required for better assessment of seismic hazard potential of the region.

Propagation of seismic wave through a medium is affected by the three factors viz., source characteristics, travel path and local site effect. The damage distribution during earthquake is strongly controlled by local site conditions of the observing sites. Therefore estimation of site effect is an important task for hazard analysis and subsurface studies. Present research work is an effort to understand and study the site characteristics using earthquake ground motions using strong motion data and ambient noise using micro-tremor data.

7.1 Summary

The area of study, Kumaon and Garhwal Himalayas, for the present research work falls in central seismic gap. This region experienced 294 earthquakes in last few years. However, very few site studies are available for this part of Himalaya. Such studies in this part of Himalaya are required for better assessment of seismic hazard potential of the region. As a

result, using the time-predictable model of the earthquakes, Khattri (1999) estimated the 100 year (beginning the year 1999) probability of occurrence of a great earthquake is 0.52 in the central seismic gap.

Limited database available in the rough and difficult terrain of Kumaon region caused less research work in the area including estimation of site amplification functions. Despite of high seismicity in the Himalayas, the quantitative study of the amplification of seismic waves is still lacking (Srinagesh et al., 2011). The present study is based on new locations in Kumaon and Garhwal Himalayas as compared to previous studies. These studies in this region of Himalaya are essential for better valuation of seismic hazard potential of the region.

In the present analysis, the site amplification functions have been estimated for Kumaon and Garhwal Himalayas using earthquakes and ambient noise data recorded locally at 27 sites from Kumaon and Garhwal region. The HVSR and SSR techniques have been applied on the records to obtain the results. The present study generates shallow shear wave velocity models in Kumaon and Garhwal Himalayas after inversion of H/V curves using genetic algorithm. Later, the results derived from various methods are compared. No such in-depth study has been done in India yet, primarily because data acquisition in the terrains of Kumaon and Garhwal Himalayas is very tough. Following are the sections and methods used in the present research work:

The two dimensional shear wave velocity profiles (V_{s30}) up to 30 m beneath the surface in the Kumaon and Garhwal Himalaya using Multi- channel Surface Wave Analysis (MASW) has been calculated in the present work. MASW technique is a non-destructive method to measure shear wave velocity and is useful to measure shear wave velocity in an urban region. This technique gives a two dimensional shear wave velocity models with depth which can easily be interpreted. Most of the sites were found under class “C” as per NEHRP classification code (BSSC, 2003). Only one site Tejam located in the northern part of Kumaon Himalayas falls under category “E”.

Later in this study, the records are analyzed using three different methods: (a) Non-Reference site method : the horizontal to vertical (H/V) spectral ratio on ambient noise records, (b) Non- Reference site method : the horizontal to vertical (H/V) spectral ratio on strong ground motion records, and (c) Reference site dependent method : Standard Spectral ratio,

We compared the results obtained from HVSR and SSR techniques for the site response characteristics and the estimated results from both the techniques demonstrate close correspondence. The outputs are compared in terms of site amplification functions i.e. amplification level and predominant frequency. It has been found that there is no significant change in the results obtained using two different techniques and three arrangements of datasets. The frequency dependent character of the site response is well constrained using these methods. Thus results are used to constrain the range defined in the study area. It has also been observed that the peak amplification obtained by these two methods for the site under consideration is matching which confirms the reliability of the obtained results.

The site amplification factor varies between 0.23 and 7.91 using HVSR (strong ground motion records) and between 0.3 and 6.01 using HVSR (ambient noise records) among different stations. The estimated predominant frequency using ambient noise records and using strong ground motion data are found to be varying from 8.7 Hz to 11.6 Hz and from 9.8 Hz to 14.5 Hz, respectively.

The initial guess and range of the velocity model is a very important aspect of the study. We found there is a good matching in a many of the cases except a few showing average or poor matching even after many GA runs. The initial and final shear wave velocity models after GA runs at individual stations are shown in Fig 7.1

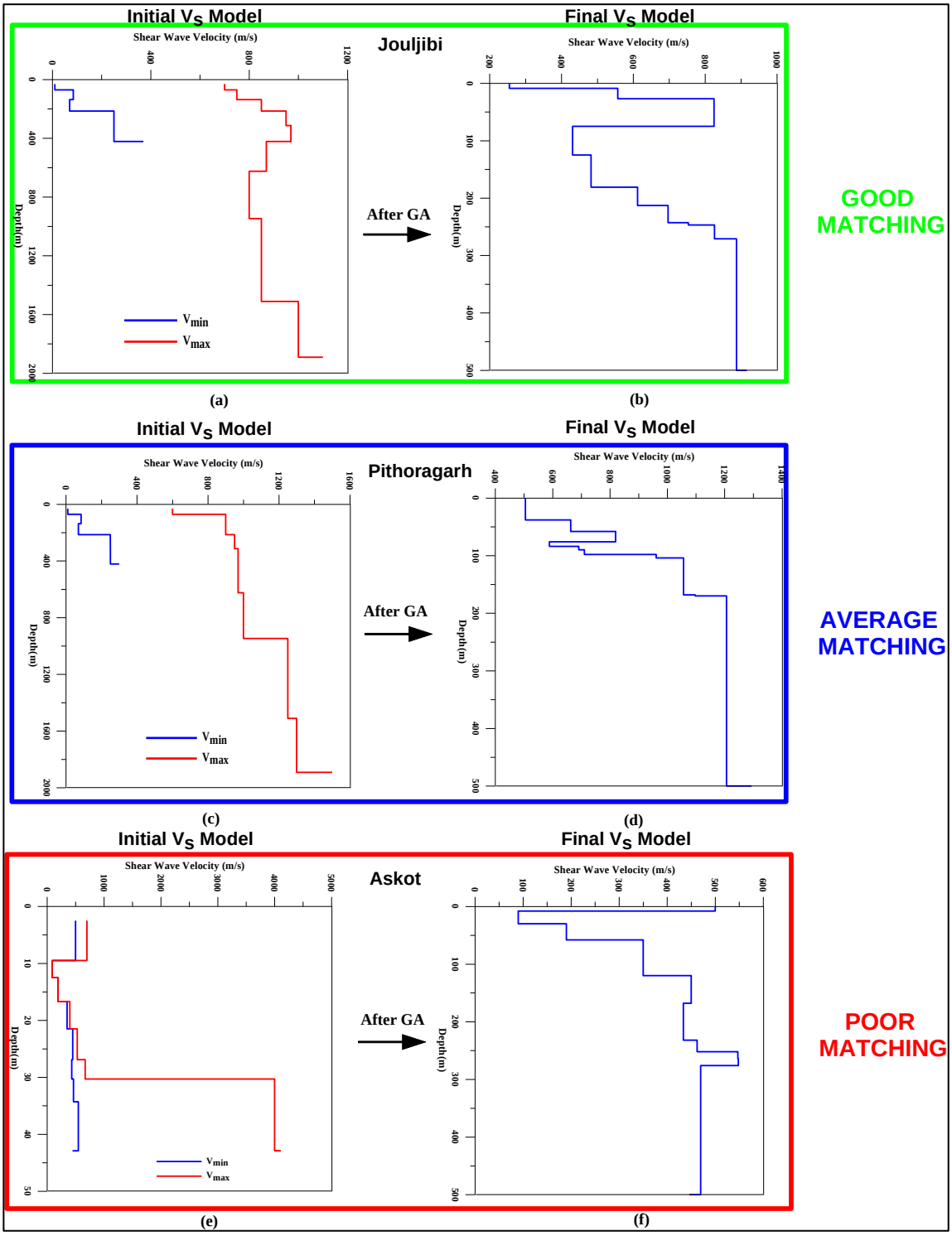

Figure 7.1: The initial and final shear wave velocity models after GA runs at individual stations. Green box shows good matching while blue and red curve boxes show average and poor matching respectively. (a) Jouljibi initial V_s Model (b) Jouljibi final V_s Model (c) Pithoragarh initial V_s Model (d) Pithoragarh final V_s Model (e) Askot initial V_s Model (f) Askot final V_s Model.

7.2 Conclusions

Data recorded at twenty seven stations located in the Kumaon and Garhwal Himalaya has been used in this study.GA has been used for obtaining shear wave velocity model using of the ambient noise data. Site amplification at each station is determined using inversion results. The research work carried out in this thesis revealed that the inversion technique used in this work provides a basic tool to determine detailed shear wave velocity model of the region using microtremor/noise and strong ground motion data. The objectives recognized for the present research work have been fulfilled by determining the shear wave velocity model in the Kumaon and Garhwal Himalayas. Major conclusions of the thesis are listed below:

1. High shear wave velocity at Chamba and Gochar, in Garhwal Himalayas can be explained by the occurrence of hard and compacted rocks such as quartzite and Phyllites of Jaunsar Group and Garhwal Group and the compacted gravels.
2. High shear wave velocity at Munsyari, Kapkot and Pithoragarh in the Kumaon Himalayas can be explained by the occurrence of hard and compacted rocks such as Phyllites, Dolomite, Quartzite, amphibolites and meta-sedimentary rocks of Tejam Group and Almora Group.
3. Dharchula, Joljibi, Baluakot and Mangti falls within the velocity range of 701 ms^{-1} to 816 ms^{-1}.This is due to the fact that stations are situated along or nearby river Kali. The softness and water saturation of the alluvial deposits found here are probable causes of this.
4. The velocity of Mangti is comparatively higher among these stations along river side since it is situated near MCT and as we go higher up in the Himalaya velocity increases the thickness of top soil layer is found to decrease.
5. On the basis of average shear wave velocity down to 500 m (V_s), the station Munsyari, Kapkot and Pithoragarh in Kumaon Himalayas and Chamba and Goucher in Garhwal Himalayas, falls in the range of velocity > 1000 ms^{-1} which implies the rock type in these stations is comparatively better for geotechnical basement than other stations.
6. The site amplification factor varies between 0.23 and 7.91 using HVSR (strong ground motion records) and between 0.3 and 6.01 using HVSR (ambient noise records) among different stations. The estimated predominant frequency using ambient noise records and using strong ground motion data are found to be varying from 8.7 Hz to 11.6 Hz and from 9.8 Hz to 14.5 Hz, respectively.

7. The site amplification functions, including amplitude level and predominant frequency, and shear wave velocity can be utilized in deriving empirical relations for the region, hence seismic hazard analysis.
8. Shear wave velocity structure of Kumaon and Garhwal Himalayas can be employed in various studies related to seismic hazard of the region. Velocity information is also important for simulation of earthquake strong ground motions.
9. MASW technique is a non-destructive method to measure shear wave velocity and is useful to measure shear wave velocity in an urban region. This technique gives a 2D shear wave velocity models with depth which can easily be interpreted.
10. Most of the sites were found under class "C" as per NEHRP classification code (BSSC, 2003). Only one site Tejam located in the northern part of Kumaon Himalayas falls under category "E".
11. The two dimensional shear wave velocity profiles at nineteen stations of Kumaon Himalaya and two stations of Garhwal Himalaya respectively are generated after inverting H/V curves using genetic algorithm for ambient noise records. Shear wave velocity of Kumaon and Garhwal Himalayas i.e. V_{S500} varies from 453 ms^{-1} to 1651 ms^{-1} respectively.
12. The two dimensional shear wave velocity profiles at nineteen stations of Kumaon Himalaya and eight stations of Garhwal Himalaya respectively are generated after inverting H/V curves using genetic algorithm for strong ground motion records. Shear wave velocity of Kumaon and Garhwal Himalayas i.e. V_{S500} varies from 462 ms^{-1} to 1348 ms^{-1} respectively.

7.3 Limitation of Study and Scope of future work

The study was carried out at the scattered locations due to poor accessibility of different locations in the tough terrains of Himalayas. MASW too needs suitably flat regions in this hilly area which is again a challenging situation to accomplish. The other problems encountered during acquisition, processing and analysis can be eliminated with certain precautions and adequate knowledge of the geology of concerned area. In course of this study, it was observed that if recording stations are strategically positioned to be along a line and allowed to record for large time period (allowing the dominance of passive noise), records will have less characteristics of source and more of soil which is of our interest.

The final 1D shear wave velocity structure obtained for each station can be considered accurate as the observed H/V curves are nicely matched with synthetic H/V curves. Deeper depths are better explored by using strong ground motion records because in such cases, the

epicenter locations belong to deeper depths when compared to the ambient noise records. The observed H/V curve and synthetic H/V curves obtained are the combined result from both strong ground motion are well ambient noise records. The results were obtained by iterative inversion algorithm which has given good and reliable results. Results obtained also conform to local geology of the station. A regional or national database can be designed for the benefit of the community which can be utilized in future.

.4 Recommendations

- To verify the MASW results i.e. shear wave velocity model with lithology samples borehole data with core samples may be required.
- More such local measurements at other critical sites like schools and vital infrastructures can be considered using MASW.
- The detailed subsurface mapping can be conducted using other geophysical investigations like Magneto-telluric (MT), Electrical Resistivity Tomography (ERT), Ground Penetrating Radar (GPR), Seismic surveys etc.
- To compare shear wave velocity with depth Standard Penetration Test (SPT) at different locations may be carried out.
- Site characterization study for more locations can be conducted using strong ground motion data.
- More recording stations can be established in Garhwal Himalayas for detailed site characterization studies. Such studies are required for various research works like seismic hazard analysis and attenuation studies which can further help in microzonation studies for Himalayas.

[1] Aki, K., and Richards, P. (1980). *Quantitative Seismology: Theory and Methods*. Volume I. W. H. Freeman, New York. 535 pp.

[2] Anbazhagan, P., and Sitharam, T.G. (2006). Evaluation of Dynamic Properties and Ground Profiles using MASW: Correlation between Vs and N60, *13th symposium of Earthquake Engineering, Indian Institute of Technology, Roorkee,* Paper No. 2008.

[3] Anderson, J.G., Lee, Y., Zeng, Y., and Day, S. (1996). Control of Strong Motion by the Upper 30 Meters, Bulletin of the Seismological Society of America, 86:1749-1759.

[4] Andrews, D. J. (1986). Objective determination of source parameters and similarity of earthquakes of different size. *Earthquake Source Mechanism.*

[5] Ariffin, J., Ismail, M.A.M., Tan, C.G., and Murtadza, N.M.(2015).Site Characterization of Marine Clay Deposits in South Seberang Prai, Penang using Combined Active and Passive Multichannel Analysis of Surface Wave (MASW). *Soft Soil Engineering International Conference 2015 (SEIC2015) IOP Conf. Series: Materials Science and Engineering.*

[6] Aguirre, J., Irikura, K., & Kudo, K. K. (1994). Estimation of strong ground motions on hard rock and soft sediment sites in the Ashigara valley using the empirical green's function method.

[7] Aguirre, J., & Irikura, K. (1997). Nonlinearity, liquefaction, and velocity variation of soft soil layers in Port Island, Kobe, during the Hyogo-ken Nanbu earthquake. *Bulletin of the Seismological society of America*, *87*(5): 1244-1258.

[8] Auden, J. B., & Ghosh, A. M. N. (1934). Preliminary Account of the Earthquake of the 15th January, 1934, in Bihar and Nepal. *Rec. Geol. Surv. India*, *68*(2): 177-293.

[9] Avouac, J. P., and Tapponnier, P. (1993). Kinematic model of active deformation in central Asia. *Geophysical Research Letters*, *20*(10): 895-898.

[10] B.I.S. (2002). Indian standard criteria for earthquake resistant design of structures, IS 1893: (Part 1) 2002, Part 1 General Provisions and Buildings (Fifth Revision), New Delhi: Bureau of Indian Standards.

[11] Banerjee, P., & Bürgmann, R. (2002). Convergence across the northwest Himalaya from GPS measurements. *Geophysical Research Letters*, *29*(13).

[12] Bard, P.Y. (1998). Microtremor measurement: a tool for site effect estimations? *Proc. of the 2nd International Symposium on the Effects of the Surface Geology on Seismic Motion, ESG98, Yokohama, Japan*, 1251–1279.

[13] Bay, F., Fäh, D., Malagnini, L., & Giardini, D. (2003). Spectral shear-wave ground-motion scaling in Switzerland. *Bulletin of the Seismological Society of America*, *93*(1): 414-429.

[14] Berthet, T., Ritz, J. F., Ferry, M., Pelgay, P., Cattin, R., Drukpa, D., and Hetényi, G. (2014). Active tectonics of the eastern Himalaya: New constraints from the first tectonic geomorphology study in southern Bhutan. *Geology*, *42*(5): 427-430.

[15] Bettinelli, P., Avouac, J. P., Flouzat, M., Jouanne, F., Bollinger, L., Willis, P., and Chitrakar, G. R. (2006). Plate motion of India and interseismic strain in the Nepal Himalaya from GPS and DORIS measurements. *Journal of Geodesy*, *80*(8): 567-589.

[16] Bilham R, Gaur VK, Molnar P (2001) Himalayan seismic hazard. Science 293:1442–1444.

[17] Bilham, R., and Ambraseys, N. (2005). Apparent Himalayan slip deficit from the summation of seismic moments for Himalayan earthquakes, 1500–2000. *Current Science*: 1658-1663.

[18] Bilham, R., and Wallace, K. (2005). Future Mw> 8 earthquakes in the Himalaya: implications from the 26 Dec 2004 Mw= 9.0 earthquake on India's eastern plate margin. *Geol. Surv. India Spec. Publ*: *85*, 1-14.

[19] Bilham, R., F. Blume, R. Bendick, and V. K. Gaur (1998). Geodetic constraints on the translation and deformation of India: Implications for future great Himalayan earthquakes, Curr. Sci. 74(3): 213–229.

[20] Boatwright, J., Seekins L. C., and Mueller C. S. (1991).Ground motion amplification in the Marina. *Bulletin of the Seismological Society of America*, 81: 1980–1997.

[21] Bonnefoy-Claudet S., Baize S., Bonilla L. F., Berge-Thierry C., Pasten C., Campos J., Volant P., and Verdugo R. (2008). Site effect evaluation in the basin of Santiago de Chile using ambient noise measurements.176: 925–937.

[22] Boore, D.M. (2004). Can site response be predicted? *J. Earthquake Engineering*, 8: 1-41.

[23] Boore, D. M., and Bommer, J. J. (2005). Processing of strong motion accelerograms: needs, options and consequences. *Soil Dynamic Earthquake Engineering*, 25: 93–115.

[24] Boore, D. M., and Joyner, W. B. (1997). Site amplifications for generic rock sites. *Bulletin of the seismological society of America*, *87*(2): 327-341.

[25] Borcherdt, R. D. (1970). Effects of local geology on ground motion near San Francisco Bay, *Bulletin of the Seismological Society of America*, 60: 29-61.

[26] Borcherdt, R.D. (1994). Estimates of site-dependent response spectra for design (methodology and justification). *Earthquake Spectra,* 10: 617– 653.

[27] Borcherdt, R. D., & Gibbs, J. F. (1976). Effects of local geological conditions in the San Francisco Bay region on ground motions and the intensities of the 1906 earthquake. *Bulletin of the Seismological Society of America*, 66(2): 467-500.

[28] Building and Housing Research Center (2005). Iranian code of practice for seismic resistant design of buildings. Standard no. 2800, 3rd edn. Tehran, Iran.

[29] Building Seismic Safety Council (BSSC FEMA) (2001). NEHRP recommended provision for seismic regulations for new buildings and other structures, part 1. Report FEMA 368, Washington, DC.

[30] Building Seismic Safety Council, (2003). NEHRP Recommended Provisions for seismic Regulations for New buildings and other Structures, Part1: Provisions, FEMA 368, Federal Emergency Management Agency, Washington, D. C.

[31] Bullen, K.E. (1963). An Introduction to the Theory of Seismology, 3rd edition. Cambridge University Press, London.

[32] Cara, M. (1983). Crest-mantle structure inferred from surface waves, in Earthquake: Observation, Theory, and Interpretation, H. Kanamoriand E. Boschi (editors). New York: Elsevier North-Holland, 319-329.

[33] Castellaro, S. (2016). The complementarity of H/V and dispersion curves. *Geophysics*, *81*(6): T323-T338.

[34] Castro, R. R., Mucciarelli, M., Pacor, F., and Petrungaro, C. (1997). S-wave site response using horizontal to vertical spectral ratios. *Bulletin of the Seismological Society of America*, 87: 256-260.

[35] Caldwell, W. B., Klemperer, S. L., Lawrence, J. F., Rai, S. S., & Ashish, A. (2012, December). Geometry of the Main Himalayan Thrust and location of the locking line in the Garhwal Himalaya from receiver function CCP stacking. In AGU Fall Meeting Abstracts.

[36] Chander, R. (1988). Interpretation of observed ground level changes due to the 1905 Kangra earthquake, Northwest Himalaya. *Tectonophysics*, *149*(3-4): 289-298.

[37] Chander, R. (1989). Southern limits of major earthquake ruptures along the Himalaya between longitudes 75 and 90 E. *Tectonophysics*, *170*(1-2): 115-123.

[38] Chander, R., and Gahalaut, V. K. (1995). A simulation of upper crustal stresses for great and moderate thrust earthquakes of the Himalaya. *Proc. Indian Acad. Sci.(Earth Planet. Sci.), 104*(1): 115-129.

[39] Chavez-Garcia, F.J., Sanchez, L.R., and Hatzfield, D. (1996). Topographic site effects and HVSR: a comparison between observations and theory. *Bulletin of the Seismological Society of America*, 86:1559–1573.

[40] Chen, M.H., Wen, K.L., and Loh, C.H.(2003). A study of shear wave velocities for alluvium deposits in south western Taiwan. *Journal of Chinese Institute of Civil and Hydraulic Engineering*, 15:667–77.

[41] Chopra, S., Kumar, D., Rastogi, B. K., Choudhury, P., and Yadav, R. B. S. (2013). Estimation of site amplification functions in Gujarat region, India. *Natural hazards*, *65*(2), 1135-1155.

[42] Chopra, S., Kumar, V., Suthar, A., & Kumar, P. (2012). Modeling of strong ground motions for 1991 Uttarkashi, 1999 Chamoli earthquakes, and a hypothetical great earthquake in Garhwal–Kumaun Himalaya. *Natural hazards*, *64*(2): 1141-1159.

[43] Choudhury, P., Catherine, J. K., Gahalaut, V. K., Chopra, S., Dumka, R., & Roy, K. S. (2013). Post-seismic deformation associated with the 2001 Bhuj earthquake. *Natural hazards*, *65*(2): 1109-1118.

[44] Cloetingh, S., and Wortel, R. (1986). Stress in the Indo-Australian plate. *Tectonophysics*, *132*(1-3): 49-67

[45] Dobry, R., Borcherdt, R.D., Crouse, C.B., Idriss, I.M., Joyner, W.B., Martin, G.R., Power, M.S., Rinne, E.E. and Seed, R.B. (2000). New site coefficients and site classification system used in recent building seismic code provisions. *Earthquake Spectra*, 16: 41 – 67.

[46] Dorman, J., and Ewing, M. (1962). Numerical Inversion of Seismic Surface Wave Dispersion Data and Crust-Mantle Structure in the New York-Pennsylvania Area. *Journal of Geophysical Research*, 16: 5227-5241.

[47] Fa¨h, D., Kind, F., and Giardini, D. (2001). A theoretical investigation of average H/V ratios. *Geophys. J. Int*., 145: 535–549.

[48] Feldl, N., and Bilham, R. (2006). Great Himalayan earthquakes and the Tibetan plateau. Nature, *444*(7116): 65-170.

[49] Field, E. H., and Jacob, K. H. (1993).The theoretical response of sedimentary layers to ambient seismic noise, *Geophys. Res. Lett.* 20: 2925-2928.

[50] Field, E. H., and Jacob, K. H. (1995). A comparison and test of various site-response estimation techniques, including three that are not reference-site dependent. *Bulletin of the seismological society of America*, *85*(4): 1127-1143.

[51] Geological Survey of India, Dasgupta, S., Narula, P. L., Acharyya, S. K., and Banerjee, J. (2000). Seismotectonic atlas of India and its environs. Geological Survey of India.

[52] Gahalaut, V. K., & Chander, R. (1992). On the active tectonics of the Dehra Dun region from observations of ground elevation changes. *J. Geol. Soc. India*, *39*: 61-68.

[53] Gahalaut, V. K., and Chander, R. (1997). Evidence for an earthquake cycle in NW Outer Himalaya near 78 E longitude from precision levelling observations. *Geophysical Research Letters*, *24*(3): 225-228.

[54] Goldberg, D. E., & Deb, K. (1991). A comparative analysis of selection schemes used in genetic algorithms. *Foundations of genetic algorithms*, *1*, 69-93.

[55] Goldberg, D. E. (1989). Genetic algorithms in search, optimization and machine learning: Addison Wesley Publishing Company.

[56] Gupta, S. C., and Kumar, A. (2002). Seismic wave attenuation characteristics of three Indian regions: a comparative study. *Current science*, 82(4): 407-413.

[57] Gupta, S. C., Singh, V. N., and Kumar, A. (1995). Attenuation of coda waves in the Garhwal Himalaya, India. *Physics of the Earth and Planetary Interiors*, *87*(3-4): 247-253.

[58] Harmsen, S. C. (1997). Determination of Site Amplification in the Los Angeles Urban Area from Inversion of Strong-Motion Records. *Bulletin of the Seismological Society of America*, 87: 866-887.

[59] Hartzell, S. H. (1992). Site response estimation from earthquake data. *Bulletin of the Seismological Society of America*, 82:2308-2327.

[60] Haskell, N. A. (1953).The dispersion of surface waves on multilayered media. *Bulletin of the Seismological Society of America*, 17-34.

[61] Haskell, N. A. (1960).Crustal Reflection of Plane SH Waves. *Journal of Geophysical Research*, 65:4147-4150.

[62] Heisey, J. S., Stokoe, K. H., & Meyer, A. H. (1982). Moduli of pavement systems from spectral analysis of surface waves. Transportation research record, 852(22-31):147.

[63] Hetényi, G., Cattin, R., Brunet, F., Bollinger, L., Vergne, J., Nábělek, J. L., and Diament, M. (2007). Density distribution of the India plate beneath the Tibetan plateau:

Geophysical and petrological constraints on the kinetics of lower-crustal eclogitization. *Earth and Planetary Science Letters*, 264(1-2): 226-244.

[64] Hetényi, G., Cattin, R., Berthet, T., Le Moigne, N., Chophel, J., Lechmann, S., and Thinley, K. (2016). Segmentation of the Himalayas as revealed by arc-parallel gravity anomalies. Scientific reports, 6.

[65] Hetényi, G., Cattin, R., Vergne, J., and Nábělek, J. L. (2006). The effective elastic thickness of the India Plate from receiver function imaging, gravity anomalies and thermomechanical modelling. *Geophysical Journal International*, 167(3): 1106-1118.

[66] Horike, M. (1985). Inversion of phase velocity of long-period microtremors to the S-wave-velocity structure down to the basement in urbanized areas. *J. Phys. Earth*, 33: 59–96.

[67] Hough, S.E., Borcherdt, R.D., Friberg, P.A., Busby, R., Field, E.H., and Jacob, K.H. (1990).The role of sediment induced amplification in the collapse of the Nimitz freeway during October 17, 1989 Loma Prieta earthquake. *Nature*, 344: 853-855.

[68] Huang, H. C., & Teng, T. L. (1999). An evaluation on H/V ratio vs. spectral ratio for site-response estimation using the 1994 Northridge earthquake sequences. *Pure and Applied Geophysics*, *156*(4): 631-649.

[69] Ibs-von Seht, M., & Wohlenberg, J. (1999). Microtremor measurements used to map thickness of soft sediments. *Bulletin of the Seismological Society of America*, *89*(1), 250-259.

[70] International Council of Building Officials (ICBO) (1997). Uniform building code (UBC). Whittier, CA.

[71] International Council of Building Officials (ICBO) (2003). International building code (IBC). Whittier, CA.

[72] Irikura, K., & Kawanaka, T. (1980). Characteristics of microtremors on ground with discontinuous underground structure.

[73] Ishihara, K., Ansal, A.M. (1982). Dynamic behavior of soil, soil amplification and soil structure interaction. *Final report for working group D, UNDP/UNESCO project on earthquake risk reduction in the Balkan Region.*

[74] Jarpe, S.P., Cramer, C.H., Tucker, B.E., and Shakal, A.F. (1988). A comparison of observations of ground response to weak and strong motion at Coalinga. *Bulletin of the Seismological Society of America*, 78: 421-427.

[75] Joshi, A. (2006a). Analysis of strong motion data of the Uttarkashi earthquake of 20th October 1991 and the Chamoli earthquake of 28th March 1999 for determining the mid crustal Q value and source parameters. *J Earth Tech*, 43:11–29.

[76] Joshi, A. (2006b). Use of acceleration spectra for determining the frequency dependent attenuation coefficient and source parameters. *Bulletin of the Seismological Society of America*, 96:2165–2180.

[77] Joshi, A. (2007). Inversion of seismic intensity data for the determination of three-dimensional attenuation structures in the central gap region of Himalayas. *Natural Hazards*, *43*(1): 1-22.

[78] Joshi, A., Kumar, P., Mohanty, M., Bansal, A. R., Dimri, V. P., and Chadha, R. K. (2012). Determination of Qβ (f) in Different Parts of Kumaon Himalaya from the Inversion of Spectral Acceleration Data. *Pure and applied geophysics*, *169*(10): 1821-1845.

[79] Joshi, A., Mohanty, M., Bansal, A. R., Dimri, V. P., and Chadha, R. K. (2010). Use of spectral acceleration data for determination of three-dimensional attenuation structure in the Pithoragarh region of Kumaon Himalaya. *Journal of seismology*, *14*(2): 247-272.

[80] Kafka, A. L., and Reiter, E. C. (1987). Dispersion of Rg waves in southeastern Maine: evidence for lateral anisotropy in the shallow crust. *Bulletin of the Seismological Society of America*, 77: 925-941.

[81] Khan, P. K. (2005). Variation in dip-angle of the Indian plate subducting beneath the Burma plate and its tectonic implications. Geosciences Journal, 9(3): 227-234.

[82] Khattri, K. N. (1987). Great earthquakes, seismicity gaps and potential for earthquake disaster along the Himalaya plate boundary. *Tectonophysics*, *138*(1): 79-92.

[83] Khattri, K. N. (1993). Seismic gaps and likelihood of occurrence of larger earthquakes in northern India. *Current science*, 885-888.

[84] Khattri, K. N. (1999). An evaluation of earthquakes hazard and risk in northern India. *Himalayan Geology*, 20(1): 1-46.

[85] Khattri, K. N., and Tyagi, A. K. (1983). Seismicity patterns in the Himalayan plate boundary and identification of the areas of high seismic potential. *Tectonophysics*, 96:281–297.

[86] King, J. L, and B. E. Tucker (1984). Observed variations of earthquake motion across a sediment-filled valley. *Bulletin of the Seismological Society of America*, 74: 137-151.

[87] Klemperer, S. L. (2006). Crustal flow in Tibet: geophysical evidence for the physical state of Tibetan lithosphere, and inferred patterns of active flow. *Geological Society, London, Special Publications*, *268*(1): 39-70.

[88] Kobayashi, R., and Nakanishi, I. (1994). Application of genetic algorithms to focal mechanism determination. *Geophys. Res. Lett*. 21: 729-732.

[89] Konno, K., & Ohmachi, T. (1998). Ground-motion characteristics estimated from spectral ratio between horizontal and vertical components of microtremor. Bulletin of the Seismological Society of America, 88(1): 228-241.

[90] Kudo, K. (1995). Practical estimates of site response. State-of-art report. *Fifth International Conference on Seismic Zonation, Nice, France, III*, 1878-1907.

[91] Kumar, D., Khattri, K.N., Teotia, S.S., and Rai, S.S. (1999). Modelling of accelerograms of two Himalayan earthquakes using a novel semi-empirical method and estimation of accelerograms for a hypothetical great earthquake in the Himalaya. *Curr Sci* , 76:819–830.

[92] Kumar, D., Sarkar, I., Sriram, V., and Khattri, K.N. (2005). Estimation of the source parameters of the Himalaya earthquake of October 19, 1991, average effective shear wave attenuation parameter and local site effects from accelerograms. *Tectonophysics*, 407:1–24.

[93] Kumar, D., Teotia, S. S., & Sriram, V. (2011). Modelling of strong ground motions from 1991 Uttarkashi, India, Earthquake using a hybrid technique. *Pure and applied geophysics*, *168*(10), 1621-1643.

[94] Kumar, P., Joshi, A., and Kumar, A. (2015). Three-Dimensional Attenuation Structure of the Kumaon Himalayas, India, Based on Inversion of Strong Motion Data. *Pure and Applied Geophysics*, *172*(2): 333-358.

[95] Kuo, C.H., Chen C.T., Lin, C.M., Wen, K.L., Huang, J.Y., and Chang S.C. (2016). S-wave velocity structure and site effect parameters derived from microtremor arrays in the Western Plain of Taiwan. *Journal of Asian Earth Sciences*, 128: 27-41.

[96] Kuo, C.H., Cheng, D.S., Hsieh, H.H., Chang, T.M., Chiang, H.J., Lin, C.M. and Wen, K.L. (2009). Comparison of three different methods in investigating shallow shear-wave velocity structures in Ilan, Taiwan. *Soil Dynamics and Earthquake Engineering*, 29: 133–143.

[97] Kuo, C.H., Wen, K.L., Hsieh, H.H., Chang, T.M., Lin, C.M., and Chen, C.T. (2011). Evaluating empirical regression equations for Vs and estimating Vs30 in northeastern Taiwan. *Soil Dynam. Earthquake Eng*. 31 (3): 431–439.

[98] Lachet, C., and Bard, P. Y. (1994). Numerical and theoretical investigations on the possibilities and limitations of the "Nakamura's technique". *J. Phys. Earth*, 42: 377-397.

[99] Lachet, C., Hatzfeld, D., Bard, P. Y., Theodulidis, N., Papaioannou, C., & Savvaidis, A. (1996). Site effects and microzonation in the city of Thessaloniki (Greece) comparison of different approaches. *Bulletin of the Seismological Society of America*, *86*(6): 1692-1703.

[100] Lay, T., & Wallace, T. C. (1995). *Modern global seismology* (Vol. 58). Academic press.

[101] Lermo, J., and Chavez-Garcia, F.J. (1994). Are microtremors useful in site response evaluation? *Bulletin of the Seismological Society of America*, 84: 1350-1364.

[102] Li, A., and Detrick, R. S. (2003). Azimuthal anisotropy and phase velocity beneath Iceland: implication for plume - ridge interaction. *Earth and Planetary Science Letters*, 21:153-165.

[103] Lin, P. S., Chang, C. W., & Chang, W. J. (2004). Characterization of liquefaction resistance in gravelly soil: large hammer penetration test and shear wave velocity approach. *Soil Dynamics and Earthquake Engineering*, *24*(9-10): 675-687.

[104] Lin, C. M., Chang, T. M., Huang, Y. C., Chiang, H. J., Kuo, C. H., & Wen, K. L. (2009). Shallow S-Wave Velocity Structures in the Western Coastal Plain of Taiwan. *Terrestrial, Atmospheric & Oceanic Sciences*, *20*(2).

[105] Liner, C. L. (2012). Elements of seismic dispersion: A somewhat practical guide to frequency dependent phenomena. *Society of Exploration Geophysicists.*.

[106] Lyon-Caen, H., and Molnar, P. (1985). Gravity anomalies, flexure of the Indian plate, and the structure, support and evolution of the Himalaya and Ganga Basin. *Tectonics*, *4*(6): 513-538.

[107] Mahajan, A. K., Slob, S., Ranjan, R., & Sporry, R. Champati Ray P.K., and van Westen C.J. (2007). Seismic microzonation of Dehradun city using geophysical and geotechnical characteristics in the upper 30 m of soil column. *J Seismol*, 11(4), 355-370.

[108] Mandal P, Padhy S, Rastogi BK, Satyanarayana HVS, Kousalya M, Vijayraghavan R, and Srinivasan A (2001) Aftershock activity and frequency-dependent low coda Qc in

the epicentral region of the 1999 Chamoli earthquake of Mw6.4. Pure Appl Geophys 158:1719–1735

[109] Mandal, P., Dutta, U., and Chadha, R.K. (2008). Estimation of site response in the Kachchh seismic zone, Gujarat, India. *Bulletin of the Seismological Society of America*, 98:2559–2566.

[110] Mandal, S., Robinson, D.M., Kohn, M.J., Khanal, S., Das, O., and Bose, S. (2016). Zircon U-Pb ages and Hf isotopes of the Askot klippe, Kumaun, and northwest India: Implications for Paleoproterozoic tectonics, basin evolution and associated metallogeny of the northern Indian cratonic margin. *Tectonics*, 35(4): 965–982.

[111] Middlemiss, C. S. (1910). A revision of the Silurian-Trias sequence in Kashmir.

[112] Miller, R.D., Xia, J., Park, C.B., and Inanov, J.M. (1999). Using MASW to map bedrock in Olathe, Kansas. *Society Exploration Geophysics*, 433-436.

[113] Mitchell, B. (1973). Radiation and attenuation of waves from the southeastern Missouri earthquake of October 21, 1965. *Journal of Geophysical Research*, 78: 886–899.

[114] Mittal, H. (2011). Estimation of ground motion in Delhi.

[115] Mittal, H., and Kumar, A. (2013). Ground motion estimation in Delhi from postulated regional and local earthquakes. *Journal of seismology*, *17*(2): 593-605.

[116] Mogi, K. (1985). Temporal variation of crustal deformation during the days preceding a thrust-type great earthquake—The 1944 Tonankai earthquake of magnitude 8.1, Japan. In *Earthquake Prediction* (pp. 765-780). Birkhäuser, Basel.

[117] Mohanty, W. K., Prakash, R., Suresh, G., Shukla, A. K., Walling, M. Y., and Srivastava, J. P. (2009a). Estimation of coda wave attenuation for the national capital region, Delhi, India using local earthquakes. Pure and Applied Geophysics, 166(3): 429-449.

[118] Molnar, P., & Pandey, M. R. (1989). Rupture zones of great earthquakes in the Himalayan region. Proceedings of the Indian Academy of Sciences-Earth and Planetary Sciences, 98(1): 61-70.

[119] Molnar, P., & England, P. (1990). Late Cenozoic uplift of mountain ranges and global climate change: chicken or egg? Nature, 346(6279): 29-34.

[120] Mooney, H.M., and Bolt, B.A. (1966). Dispersive characteristics of the first three modes for a single surface layer. *Bulletin of the Seismological Society of America*, 56: 43–67.

[121] Mukhopadhyay, S., Sharma, J., Massey, R., and Kayal, J. R. (2008). Lapse-time dependence of coda Q in the source region of the 1999 Chamoli earthquake. *Bulletin of the Seismological Society of America*, *98*(4): 2080-2086.

[122] Mulargia, F., and S. Castellaro (2007). Single-station passive seismic stratigraphy to nearly 2 km depth in sedimentary basins, in the Proc. of the International Union of Geodesy and Geophysics XXIV General Assembly, Perugia, Italy2-13 July 2007.

[123] Mundepi, A. K. (2013). Seismic microzonation study in Doon valley, northwest Himalaya, India. *Journal of the Geological Society of India,* 81(6): 767-773.

[124] Nakamura, Y. (1989). A method for dynamic characteristics estimation of subsurface using microtremor on the ground surface. *Railway Technical Research Institute, Quarterly Reports, 30*(1).

[125] Nakamura, Y. (2000). Clear identification of fundamental idea of Nakamura's technique and its applications. *Proc. of the 12th World Conference on Earthquake Engineering, Auckland, New Zealand*, paper 2656.

[126] Nath, S. K., Vyas, M., Pal, I., and Sengupta, P. (2005). A seismic hazard scenario in the Sikkim Himalaya from seismotectonics, spectral amplification, source parameterization, and spectral attenuation laws using strong motion seismometry. *Journal of Geophysical Research: Solid Earth*, 110(B1).

[127] Nath, S.K., Raj, A., Sharma, J., Thingbaijam, K.K.S., Kumar, A., Nandy, D.R., Yadav, M.K., Dasgupta, S., Majumdar, K., Kayal, J.R., Shukla, A.K., Deb, S.K., Pathak, J., Hazarika, P.J., Paul, D.K., and Bansal, B.K. (2008). Site amplification, Qs and source parametrization in Guwahati region from seismic and geotechnical analysis. *Seismol Res. Lett.,* 79:526–539.

[128] Nath, S.K., Sengupta, P., and Kayal, J.R. (2002). Determination of site response at Garhwal Himalayas from the aftershock sequence of 1999 Chamoli earthquake. *Bulletin of the Seismological Society of America*, 92:1071–1081.

[129] Nath, S.K., Sengupta, P., Sengupta, S., and Chakrabarti, A. (2000). Site response estimation using strong motion network: a step towards microzonation of Sikkim Himalayas, Seismology 2000. *Current Science*, 79:1316–1326.

[130] Nazarian, S., and Stokoe, K. H. (1984). In situ shear wave velocities from spectral analysis of surface waves. Ph.D. dissertation, Univ. of Texas, Austria.

[131] Nazarian, S., Stokoe, K.H. and Hudson, W.R. (1983). Use of spectral analysis of surface wave method for determination of moduli and thickness of pavement. *Transportation Research Record*, 930: 38–45.

[132] Nogoshi, M., and Igarashi, T. (1971). On the amplitude characteristics of microtremor (part 2). *J. Seismol. Soc. Japan*, 24(1), 26-40.

[133] Ordaz, M., & Faccioli, E. (1994). Site response analysis in the valley of Mexico: Selection of input motion and extent of non-linear soil behaviour. *Earthquake engineering & structural dynamics*, *23*(8): 895-908.

[134] Padhy, S. (2009). Inversion of seismogram envelopes using a multiple isotropic scattering model in Garhwal Himalaya. *Bulletin of the Seismological Society of America*, 99(2A): 726-740.

[135] Park, C. B., Miller, R. D., & Xia, J. (1998, January). Imaging dispersion curves of surface waves on multi-channel record. In *1998 SEG Annual Meeting*. Society of Exploration Geophysicists.

[136] Park, C.B., Miller, R.D., and Xia, J. (1999). Multichannel analysis of surface waves (MASW).*Geophysics*, 64: 800–808.

[137] Paul, A., Gupta, S. C., and Pant, C. C. (2003). CODA Q estimates for Kumaun Himalaya. *Journal of Earth System Science*, *112*(4): 569-576.

[138] Pavlenko, O. V., & Irikura, K. (2003). Estimation of nonlinear time-dependent soil behavior in strong ground motion based on vertical array data. *Pure and Applied Geophysics*, *160*(12): 2365-2379.

[139] Prasad, B. R., Klemperer, S. L., Rao, V. V., Tewari, H. C., and Khare, P. (2011). Crustal structure beneath the Sub-Himalayan fold–thrust belt, Kangra recess, northwest India, from seismic reflection profiling: Implications for Late Paleoproterozoic orogenesis and modern earthquake hazard. Earth and Planetary Science Letters, 308(1): 218-228.

[140] Ranjan, R. (2005). Seismic Response Analysis of Dehradun City, India, MSc thesis, Indian Institute of Remote Sensing, *National Remote Sensing Agency, Dehradun Dep. of Space, Govt. of India.*

[141] Richart, F.E., Hall, J.R., and Woods, R.D. (1970). *Vibrations of soils and foundations.* Prentice-Hall, Inc.

[142] Richter, C. F. (1958). Elementaty seismology. Freeman.

[143] Riepl, J., Bard, P.Y., Hatzfeild, D., Papaioannou C., and Nechtschein, S. (1998). Detailed evaluation of site response estimation methods across and along sedimentary valley of Volvi (EURO-SEISTEST). *Bulletin of the Seismological Society of America*, 88:488–502.

[144] Sambridge, M., & Drijkoningen, G. (1992). Genetic algorithms in seismic waveform inversion. Geophysical Journal International, 109(2): 323-342.

[145] Sambridge, M., & Gallagher, K. (1993). Earthquake hypocenter location using genetic algorithms. *Bulletin of the Seismological Society of America*, *83*(5), 1467-1491.

[146] Sandhu, M., Kumar, D., and Teotia, S. S. (2017). Estimation of site amplification functions for the National Capital (Delhi) Region, India. *Natural Hazards*, *85*(1): 171-195.

[147] Setiawan, B., Jaksa, M., Griffith, M., & Love, D. (2016). Analysis of microtremor array measurement using the spatial autocorrelation (SPAC) method across the Adelaide City(Doctoral dissertation, The University of Adelaide).

[148] Satoh, T., Sato, T., & Kawase, H. (1995). Nonlinear behavior of soil sediments identified by using borehole records observed at the Ashigra Valley, Japan. *Bulletin of the Seismological Society of America*, *85*(6): 1821-1834.

[149] Satoh, T., Kawase, H., Iwata, T., Higashi, S., Sato, T., Irikura, K., and Huang, H.C. (2001). S wave velocity structure of the Taichung basin, Taiwan, estimated from array and single-station records of microtremors. *Bulletin of the Seismological Society of America*, 91: 1267–1282.

[150] Satyabala, S. P., and Gupta, H. K. (1996). Is the quiescence of major earthquakes (M≧ 7.5) since 1952 in the Himalaya and northeast India real? *Bulletin of the Seismological Society of America*, *86*(6): 1983-1986.

[151] Satyam, D.N., and Rao, K.S. (2010). Multi-Channel Analysis of Surface Wave (MASW) testing for Dynamic site characterization of Delhi region. *5th International Conference on Recent Advances in Geotechnical Earthquake Engineering and soil dynamics, San Diego, California, I,*327-330.

[152] Sawada, Y., Taga, M., Watanabe, M., Nakamoto, T., Nagumo, H., Kudo, K., & Sasatani, M. (2004). Applicability of microtremor H/V method for KiK-net strong motion observation sites and Nobi plain. *Proceedings of 13th WCEE, paper*, (855).

[153] Seekins, L. C., and Boatwright, J. (1994). Ground motion amplification, geology, and damage from the 1989 Loma Prieta earthquake in the City of San Francisco. *Bulletin of the Seismological Society of America*, 84: 16-30.

[154] Seekins, L.C., Wennerberg, L., Margheriti, L., and Liu, H.P. (1996). Site amplification at five locations in San Francisco, California: a comparison of S Waves, codas, and microtremors. *Bulletin of the Seismological Society of America*, 86: 627-635.

[155] Sen, M. K., and Stoffa, P. L.(1991). Global optimization methods in geophysical inversion.

[156] Seshunarayana, T., and Sundararajan, N. (2004). *Evaluation of 5th Conference and Exposition on Petroleum Geophysics. Hyderabad-2004, India*, 642-646.

[157] Shafiee, A., & Azadi, A. (2007). Shear-wave velocity characteristics of geological units throughout Tehran City, Iran. *Journal of Asian Earth Sciences*, *29*(1), 105-115.

[158] Shafiee, A., Kamalian, M., Jafari, M. K., & Hamzehloo, H. (2011). Ground motion studies for microzonation in Iran. *Natural hazards*, *59*(1), 481-505.

[159] Shakal, A. F., Huang, M. J., & Graizer, V. M. (2004, May). CSMIP Strong motion data processing. *In Proc. Invitational Workshop on Strong Motion Record Processing.*

[160] Shapiro, N. M., & Campillo, M. (2004). Emergence of broadband Rayleigh waves from correlations of the ambient seismic noise. *Geophysical Research Letters*, *31*(7).

[161] Sharma, B., Kumar, D., and Teotia, S.S. (2008). Site amplification factors in Koyna region using coda waves. *J Ind Geophys Union*, 12(4):149–156.

[162] Sharma, J., Chopra, S., & Roy, K. S. (2014). Estimation of Source Parameters, Quality Factor (QS), and Site Characteristics Using Accelerograms: Uttarakhand Himalaya Region Estimation of Source Parameters, QS, and Site Characteristics Using Accelerograms. *Bulletin of the Seismological Society of America*, *104*(1):360-380.

[163] Sheriff, R. E., and Geldart, L. P., 1985, Exploration seismology I: History, theory, and data acquisition: Cambridge Univ. Press

[164] Shima E (1977). On the base rock of Tokyo metropolis. In: 6th world conference on earthquake engineering, 2:161–166

[165] Simons, F. J., Van Der Hilst, R. D., Montagner, J. P., & Zielhuis, A. (2002). Multimode Rayleigh wave inversion for heterogeneity and azimuthal anisotropy of the Australian upper mantle. *Geophysical Journal International*, *151*(3): 738-754.

[166] Singh, S. K., Mohanty, W. K., Bansal, B. K., and Roonwal, G. S. (2002). Ground motion in Delhi from future large/great earthquakes in the central seismic gap of the Himalayan arc. *Bulletin of the Seismological Society of America*, *92*(2): 555-569.

[167] Singh, S. K., Astiz, L., & Havskov, J. (1981). Seismic gaps and recurrence periods of large earthquakes along the Mexican subduction zone: a reexamination. *Bulletin of the Seismological Society of America*, *71*(3): 827-843.

[168] Singh, S.K., Lermo, J., Dominguez, T., Ordaz, M., Espinosa, J.M., and Quass, R., (1988). The Mexico earthquake of September 1985 – a study of seismic waves in the valley of Mexico with reference to a hill zone site. *Earthquake Spectra*, 4: 653-673.

[169] Singh, K. S., Iglesias, A., Garduño, V. H., Quintanar, L., & Ordaz, M. (2012). A source study of the October, 2007 earthquake sequence of Morelia, Mexico and ground-motion estimation from larger earthquakes in the region. *Geofísica internacional*, *51*(1), 73-86.

[170] Singh, S. K., Kumar, A., Suresh, G., Ordaz, M., Pacheco, J. F., Sharma, M. L., , B. K. Bansal, R. S. Dattatrayam, and E. Reinoso, E. (2010). Delhi earthquake of 25 November 2007 (M w 4.1): implications for seismic hazard. *Current Science*, 939-947.

[171] Smith, L.R.B. (1843). Memoir on India earthquakes. *J Asia Soc. Bengal*, 12:1029–1059

[172] Sorkhabi, R. B. and MacFarlane, A. (1999). Himalaya and Tibet: Mountain roots to mountain tops. *Special Paper of the Geological Society of America*, *328*: 1-7.

[173] Sri Ram, V., Kumar, D., and Khattri, K.N. (2005). The Site Amplification Factors in Koyna Region using Coda Waves 1986 Dharamsala earthquake of Himachal Himalaya estimates of source parameters, average intrinsic attenuation and site amplification functions. *Journal of Seismology*, 9: 473-485.

[174] Srinagesh, D., Singh, S. K., Chadha, R. K., Paul, A., Suresh, G., Ordaz, M., and Dattatrayam, R. S. (2011). Amplification of seismic waves in the central Indo-Gangetic basin, India. *Bulletin of the Seismological Society of America*, *101*(5): 2231-2242.

[175] Sriram, V. and Khattri, K.N. (1997). A study of source spectrum, site amplification functions, response spectra, Fourier spectra and peak ground accelerations from the strong ground motion data of the 1991 Uttarkahi earthquake. *Current Science*, 72: 728-740.

[176] Sriram, V., and Khattri, K. N. (1999). Modelling of strong ground motions from Dharmsala earthquake of 1986 (M_b 5.7). *Current Science*, 429-438.

[177] Stoffa, P. L., and Sen, M. K. (1991). Nonlinear multi-parameter optimization using genetic algorithms: Inversion of plane-wave seismograms. *Geophysics*, 56: 1794-1810.

[178] Stokoe, K. H., S. G. Wright, J. A. Bay, and J. M. Roësset, 1994, Characterization of geotechnical sites by SASW method. In: R.D. Woods, Editor, Geophysical Characterization of Sites, ISSMFE Technical Committee #10, Oxford Publishers, New Delhi (1994): 15-25.

[179] Strobbia, C. (2003).Surface wave methods: acquisition, processing and inversion. – Torino. *Politecnico di Torino.*

[180] Thitimakorn, T., and Channoo, S. (2012). Shear Wave Velocity of Soils and NEHRP Site Classification Map of Chiangrai City, Northern Thailand. *Electronic Journal of Geotechnical Engineering*, 17: 2891-2894.

[181] Trivedi, S.S., Rao, K.S., Gupta, K.K., and Rathod, G.W. (2009). Mapping average shear wave velocity for Ahmedabad soil sites: A case study. IGC, Guntur, India.

[182] Tsai, Y.B., and Aki, K. (1969). Simultaneous determination of the seismic moment and attenuation of seismic surface waves. *Bulletin of the Seismological Society of America*, 59: 275–288.

[183] Valdiya, K.S. (1980). Geology of Kumaun Lesser Himalaya, Interim Record: Dehradun. *Wadia Institute of Himalayan Geology*, 289.

[184] Wallace, K., Bilham, R., Blume, F., Gaur, V. K., and Gahalaut, V. (2005). Surface deformation in the region of the 1905 Kangra Mw= 7.8 earthquake in the period 1846–2001. *Geophysical research letters*, *32*(15).

[185] Wen, R., Shi, D., and Ren, Y. (2008). Site Classification based on Geological Genesis and its application. *The 14th World Conference on Earthquake Engineering, Beijing, China*.

[186] Wilson, W., and Vasudevan, K. (1991). Application of the genetic algorithm to residual statics estimation. *Geophys. Res. Lett*. 18: 2181-2184.

[187] Xia N., J., Miller, R. D., and Park, C.B. (1999). Estimation of near-surface shear wave velocity by inversion of Rayleigh waves. *Geophysics*, 64: 691–700.

[188] Xia, J., Miller, R. D., Park, C. B., Hunter, J. A., Harris, J. B., & Ivanov, J. (2002). Comparing shear-wave velocity profiles inverted from multichannel surface wave with borehole measurements. *Soil dynamics and earthquake engineering*, *22*(3): 181-190.

[189] Yamanaka, H., and Ishida, H. (1996). Application of Genetic Algorithms to an Inversion of Surface-Wave Dispersion Data. *Bulletin of the Seismological Society of America*, 86: 436-444.

[190] Yeats, R. S., and Thakur, V. C. (1998). Reassessment of earthquake hazard based on a fault-bend fold model of the Himalayan plate-boundary fault. *Current Science, 74*(3): 230-233.

[191] Zare, M., Bard, P.Y. and Ghafory, A.M. (1999). Site categorization for Iranian strong motion network. *Soil Dynamic Earthquake Engineering*, 18:101–123.

[192] Zhang, W. B., Xie, L. L., & Guo, M. Z. (2001). Estimation on site-amplification from different methods using strong motion data obtained in Tangshan, China. *Acta Seismologica Sinica*, *14*(6): 642-653.

[193] Zhou, R., Tajima, F., & Stoffa, P. L. (1995). Earthquake source parameter determination using genetic algorithms. *Geophysical Research Letters*, *22*(4), 517-520.

[194] Zhang, Z., and Klemperer, S. (2010). Crustal structure of the Tethyan Himalaya, southern Tibet: new constraints from old wide-angle seismic data. Geophysical Journal International, 181(3): 1247-1260.

[195] Zhao, J. X., Irikura, K., Zhang, J., Fukushima, Y., Somerville, P. G., Saiki, T., & Takahashi, T. (2004, August). Site classification for strong-motion stations in Japan using H/V response spectral ratio. In *13th World Conference of Earthquake Engineering*.

Websites used:

www.ndma.gov.in